Modelling Hypertrophy in Dystrophic Cardiomyocytes

Morten Ritso

A thesis submitted for the degree of Doctor of Philosophy

Institute of Genetic Medicine

Newcastle University

November 2015

Author's Declaration

This thesis is submitted for the degree of Doctor of Philosophy at Newcastle University. I, Morten Ritso, declare that the work described here is my own, unless where clearly acknowledged and stated otherwise. I certify that I have not submitted any of the material in this thesis for a degree qualification at this or any other university.

Abstract

Duchenne Muscular Dystrophy (DMD) is an X-linked disorder, caused by mutations in the *DMD* gene. This gene encodes dystrophin, a structural protein that links the sarcomere to the extracellular matrix via a trans-membrane protein complex. In the absence of dystrophin the associated glycoprotein complex fails to assemble, leading to sarcolemmal instability, impaired ion handling, skeletal muscle wasting and fibrosis. Patients become non-ambulant in their teens and seldom live past their third decade. Cardiac failure is one of the leading causes of death. The heart initially compensates for reduced functional capacity by becoming hypertrophic, but eventually becomes fibrotic and develops dilated cardiomyopathy.

Several proposed therapies have now reached clinical trial phase, but there is still no cure available for all DMD patients. Some of these therapies target skeletal muscle better than the heart. Sample availability restricts research into cardiac mechanisms of disease and testing treatments. This thesis presents a model that can potentially be used as an *in vitro* outcome measure for testing DMD therapies. Cardiomyocytes isolated from hearts collected from the DMD mouse model (mdx) embryos became larger than control mouse embryo-derived cardiomyocytes in response to serum starvation in culture. Control and mdx cardiomyocytes were collected at five time-points of serum starvation and RNA-Seq was performed on the samples to identify pathways responsible for this hypertrophic response observed in dystrophic cells.

Several pharmacological compounds as well as a proposed gene therapy method were trialled for their ability to reduce the hypertrophic response. Serum starved cardiomyocytes from mdx mouse embryos were transduced with adeno-associated viruses containing a gene construct expressing a functional internally truncated version of dystrophin. The viral rescue therapy and some pharmacological compounds significantly reduced the dystrophic hypertrophy caused by serum starvation. This model of mdx cardiomyocyte hypertrophy could therefore be used for testing therapies in pre-clinical trials.

Dedication

This thesis is dedicated to Duchenne Muscular Dystrophy patients.

Acknowledgements

First I would like to thank my supervisors Hanns Lochmüller, Chris Denning and Steve Laval for giving me the opportunity to take on this project and supporting me all the way through my PhD.

I could not have done all of this work without the contributions and support from members of the John Walton Muscular Dystrophy Research Centre and the Institute of Genetic Medicine, past and present. Thank you to my PhD progress assessors Judith Goodship and Lyle Armstrong, as well as Kate Bushby, Volker Straub and Gavin Richardson for your expert advice. Louise Jørgensen and Tewes Tralau, you are inspirational researchers and I will always remember your invaluable guidance. Alison Blain and Rita Barresi, thank you for helping me establish the cardiomyocyte isolation technique. Tom Slater, Elizabeth Roberts, Sophie Wright and Stephanie Carr, thank you for your contributions to optimising the cardiomyocyte model. Helmut Blum, my time in Munich was a great experience, thank you to your team for making me feel welcome and teaching me most of what I know about RNA-Seq analysis, special thanks to Stefan Krebs, Alex Graf and Andrea Klanner for your contributions to this work. Thank you Liz Greally and FGU staff for all your help with animal work and Volker Straub for allowing me to conduct my animal work under his project licence, Lisa Hodgson and Alex Laude for your help with microscopy, Oliver Müller's team in Heidelberg for the AAVs, Rebecca Dodds for helping with qRT-PCRs, Johannes Hönekopp for advice on statistics. Thanks Andrew Best, Jon Ingledew, Mojgan Reza, Juliane Müller, Debbie Hicks, Anna Sarkozy, Ann Marie Hynes, Dean Hallam and Lorraine Eley for always having my back.

Mum, dad and Valter, thank you for always pushing me to try harder. Vello, Maire, Kristiina and the Zambonins, I appreciate you having been as caring and welcoming. Kristjan, Karin, Reio, Mart, Tanel, Luke and Phoebe, thanks for your immeasurable support. Eia and Jim, I now have even more appreciation towards your work.

Jess, even from half the world away you made sure I never felt alone. I could not have completed this without you having been there for me every step of the way.

This work was funded by the Medical Research Council UK and Aktion Benni & Co E.V.

Table of Contents

List of Figures

List of Tables

List of Abbreviations

2OMePS	2'-*O*-methyl phosphorothioate oligoribonucleotide
AAV	Adeno-associated virus
AC	Adenylyl Cyclase
ACE	Angiotensin converting enzyme
Akt	Protein kinase B
Ang	Angiotensin
ANGPTL4	Angiopoietin-like 4
ANP	Atrial natriuretic protein
AON	Antisense oligonucleotide
ASCII	American standard code for information interchange
AT_1R	Angiotensin receptor type 1
ATP	Adenosine triphosphate
BAD	Bcl-2 associated death promoter
βAR	Beta-adrenergic receptor
BL/10	C57BL/10 mouse model
BMD	Becker muscular dystrophy
BMP	Bone morphogenic protein
BNP	Brain/B-type/ventricular natriuretic peptide
bp	Base pairs
BSA	Bovine serum albumin
CaMK	Calmodulin-dependent kinase
Ca_V1	L-type calcium channel / dihydropyridine receptor
CBS	Cardiomyocyte buffer solution
CGM	Cardiomyocyte growth medium
cGMP	Cyclic guanosine monophosphate
CK	Creatine kinase
CMV	Cytomegalovirus
DAPI	4',6-diamidino-2-phenylindole
DGC	Dystrophin glycoprotein complex
dH_2O	Distilled water
dko	Dystrophin and utrophin double knockout mouse model
DMD	Duchenne muscular dystrophy
DMEM	Dulbecco's modified Eagle's medium
DMSO	Dimethyl sulfoxide

DNA	Deoxyribonucleic acid
E17.5	Mouse embryos at day 17.5 of gestation period
ECL	Enhanced chemiluminescence
ECM	Extracellular matrix
EDTA	Ethylenediaminetetraacetic acid
eNOS	Endothelial nitric oxide synthase
ERK	Extracellular signal-regulated kinase
ESC	Embryonic Stem Cells
FACS	Fluorescence-activated cell sorting
FBS	Foetal bovine serum
FC	Fold change
FDR	False discovery rate
FGP	Foetal gene program
FHF	First heart field
GC	Guanylyl cyclase
GCR	Glucocorticoid receptor
gDNA	Genomic DNA
GO	Gene ontology
GOI	Gene of interest
GRMD	Golden retriever muscular dystrophy model
HGF	Hepatocyte growth factor
HIF-1	Hypoxia-inducible factor 1
HISAT	Hierarchical indexing for spliced alignment of transcripts
HKG	Housekeeping gene
HRP	Horseradish peroxidase
HS	Horse serum
ICC	Immunocytochemistry
IFNγ	Interferon gamma
IκBα	Inhibitor of kappa B alpha
Immorto	CBA;B10-Tg($H2K^b$-tsA58)6Kio/Crl mice
iNOS	Inducible nitric oxide synthase
IP_3	Inositol triphosphate
iPSC	Induced pluripotent stem cells
JNK	c-Jun N-terminal kinase
kbp	Kilobase pairs

KEGG	Kyoto Encyclopedia of Genes and Genomes
LDS	Lithium dodecyl sulphate
Log2FC	Base 2 logarithm fold change
Log_{10}	Base 10 logarithm
LUT	Look-up table
MAPK	Mitogen-activated protein kinase
mdx	C57BL/10ScSn-Dmd^{mdx} mouse model
µDys	Micro-dystrophin
MEF2	Myocyte enhancer factor 2
MES	2-(N-morpholino)ethanesulfonic acid
MeSH	Medical Subject Headings
MHC	Myosin heavy chain
miRNA	Micro ribonucleic acid
MISO	Mixture of isoforms
MLC	Myosin light chain
MMP	Matrix metalloproteinase
MOI	Multiplicity of Infection
MRF	Myogenic regulatory factor
mTOR	Mammalian target of rapamycin
MYH6	Skeletal myosin heavy chain
NADH	Nicotinamide adenine dinucleotide
NCBI	National Centre for Biotechnology Information
NCX	Sodium calcium exchanger
NDUFA4L2	Ubiquinone 1 alpha subcomplex 4-like 2
NFAT	Nuclear factor of activated T-cells
NFκB	Nuclear factor kappa B
NFW	Nuclease-free water
NGS	Next generation sequencing
NHE	Sodium hydrogen exchanger
nNOS	Neuronal nitric oxide synthase
NO	Nitric oxide
NPR	Natriuretic peptide receptor
NS	Non-significant
NTC	No template control
NVC	No virus control

ORAI	Calcium release-activated calcium channel
P2RX7	Purinergic receptor P2X ligand-gated ion channel 7
PBS	Phosphate buffered saline
PCA	Principal component analysis
PCR	Polymerase chain reaction
PDE5	cGMP-specific phosphodiesterase type 5
PEG	Polyethylene glycol
PFA	Paraformaldehyde
PI3K	Phosphatidylinositide 3-kinase
PKA	Protein kinase A
PKG	Protein kinase G
PLB	Protein lysis buffer
PLC	Phospholipase C
PLN	Phospholamban
PMCA	Plasma membrane Ca^{2+}-transporting ATPase
PMO	Phosphorodiamidate morpholino oligomer
PPARδ	Peroxisome proliferator-activated receptor δ
PTB	Protein transfer buffer
qRT-PCR	Quantitative real-time polymerase chain reaction
RA	Retinoic acid
RIN	RNA integrity number
RIPA	Radioimmunoprecipitation assay buffer
rLog	Regularised logarithmic transformation
RNA	Ribonucleic acid
RNA-Seq	Whole transcriptome shotgun sequencing
ROS	Reactive oxygen species
RT-PCR	Reverse transcription polymerase chain reaction
RyR	Ryanodine receptor
SD	Standard deviation
SDS-PAGE	Sodium dodecyl sulphate polyacrylamide gel electrophoresis
SEM	Standard error of the mean
SERCA	Sarcoplasmic reticulum luminal Ca2+-ATPase
SFCGM	Serum-free cardiomyocyte growth medium
SHR	Second heart field
SHH	Sonic hedgehog

SLRP	Small leucine-rich proteoglycan
SOCE	Store-operated calcium entry
SOD3	Superoxide dismutase 3
SOTA	Self-organising tree algorithm
SR	Sarcoplasmic reticulum
SRF	Serum response factor
SSCGM	Serum-starvation cardiomyocyte medium
STIM	Stromal interaction molecule
SV40	Simian vacuolating virus SV40
TAE	Tris acetic acid EDTA buffer
TBS	Tris buffered saline
TBST	Tris buffered saline with Tween20
TE	Tris-EDTA buffer
TGFβ	Transforming growth factor beta
TIMP	Tissue Inhibitor of metalloproteinase
Tm	Melting temperature
TRPC	Canonical transient receptor potential channel
TWEAK	Tumour necrosis factor-like weak inducer of apoptosis
VEGF	Vascular endothelial growth factor
VEGFR	Vascular endothelial growth factor receptor
vg	Viral genomes

Chapter 1. Introduction

1.1 Mesoderm to Muscle

Embryogenesis is a remarkable progressive event that entails cell division from fertilisation resulting in the formation of three germ layers – ectoderm, endoderm and mesoderm – and subsequent development of a foetus. The three germ layers each give rise to specific parts of the human body. Skeletal, cardiac and smooth muscle are all derived from mesoderm in a progressive manner depending on spatial orientation and signalling cascades (Yin et al., 2013; Xin et al., 2013).

1.1.1 Heart Development

The heart is an essential organ that pumps blood to other tissues in the body and it is the first organ to form in vertebrates (Buckingham et al., 2005). Fate-mapping analyses in various models such as zebrafish, frogs, chick embryos and mice have helped to establish cardiac development. Two distinct mesoderm-derived progenitor cell populations form different parts of the heart. The first (or primary) heart field (FHF) contributes mostly towards atrial and left ventricular development (Evans et al., 2010), whilst the second (or secondary) heart field (SHF) forms most of the right ventricle and outflow tract, along with the conduction system (Van Vliet et al., 2012). The pharyngeal mesoderm, which is the origin of the SHF, also forms head muscles (Tzahor & Evans, 2011). At 6.5 days post coitum (E6.5) in mouse embryo development cardiac progenitors become a distinct population (Lyons, 1996). The cardiac crescent of heart fields forms a contractile heart tube by E8.0, which then loops at E8.5 and forms cardiac chambers by E10.5 (Watanabe & Buckingham, 2010). Septation and valve formation by the E15 stage marks the completion of heart development in mouse embryos (Xin et al., 2013).

Sonic hedgehog (SHH), retinoic acid (RA) and Wnt/β-catenin signalling are essential for initially maintaining the proliferative and undifferentiated state of cardiac progenitor cells (Evans et al., 2010). However, SHH and the non-canonical Wnt signalling pathway later also drive differentiation in the SHF (Rochais et al., 2009). The earliest currently known pre-cardiac progenitor marker is the mesoderm posterior 1 homolog *Mesp1* (Van Vliet et al., 2012). It is expressed at different times in mouse FHF and SHF, with an overlap at E6.75, but not all *Mesp1* positive cells express the same downstream genes and may therefore require other signalling molecules to determine their fate (Lescroart et al., 2014). *Mesp1* drives the Islet1 gene *Isl1* expression, which marks proliferating undifferentiated cardiac progenitors (Evans et al., 2010) and together with bone morphogenic protein (BMP) induces pharyngeal mesoderm commitment to the SHF (Tzahor & Evans, 2011).

GATA4 and *Nkx2.5* are central cardiac commitment markers expressed in both heart fields (Van Vliet et al., 2012; Xin et al., 2013) and along with BMP and serum response factor (SRF) regulate gene expression initialising cardiac beating (Evans et al., 2010). *Isl1* downregulation and induction of *Tbx5* expression are only associated with the FHF cells (Sirbu et al., 2008), marking left ventricular determination as well as contributing cells towards atrial myocyte formation (Buckingham et al., 2005; Van Vliet et al., 2012). RA is upstream of *Tbx5* (Sirbu et al., 2008), which together with GATA4, *Nkx2.5* and *Tbx20* (expressed in the right ventricle) regulates the separation of the two ventricles by inducing growth of the septum (Takeuchi et al., 2003). *Tbx1* expression in the SHF commits cells to outflow tract development, leading to the formation of both the aorta and pulmonary artery (Buckingham et al., 2005); Rochais et al., 2009). Some neural crest cells infiltrate the forming heart and contribute to the development of the aorta and other big vessels connecting the heart with the rest of the vascular system (Watanabe & Buckingham, 2010; Fishman & Chien, 1997). Heart field contributions to the developing heart are summarised in figure 1.1.

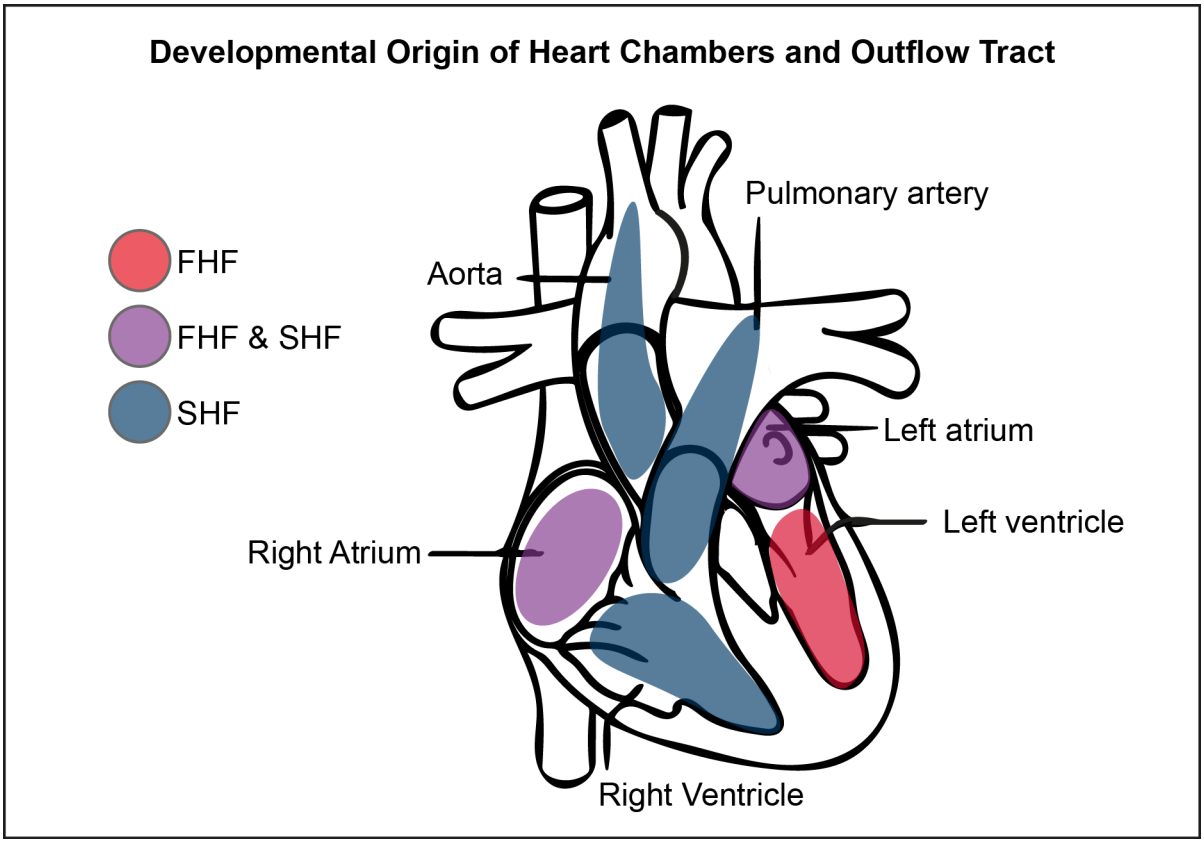

Figure 1.1. Developmental origin of cells giving rise to heart structure. The mammalian heart is a four chamber organ formed from two mesodermal progenitor cell populations called the first and second heart field (FHF and SHF). The SHF forms the right ventricle, the outflow tract and contributes towards atrial development. The FHF forms the left ventricle and also contributes towards atrial development. This image was adapted from Xin et al. (2013).

1.1.2 Skeletal Muscle Development

Skeletal muscle development, except in the head (Tzahor & Evans, 2011), is dependent on signals that are passed from the neural tube and notochord to paraxial mesoderm condensations called somites (figure 1.2 A). These signals trigger the ventromedial and dorsal parts of somites to differentiate into the sclerotome and dermomyotome, respectively (figure 1.2 B). The dermomyotome bows ventrally at both epaxial and hypaxial ends to form the myotome (figure 1.2 C). At sites of limb buds hypaxial dermomyotome cells migrate and populate the forming limbs with myogenic precursor cells (MPC) (figure 1.2 D) (Bailey et al., 2001).

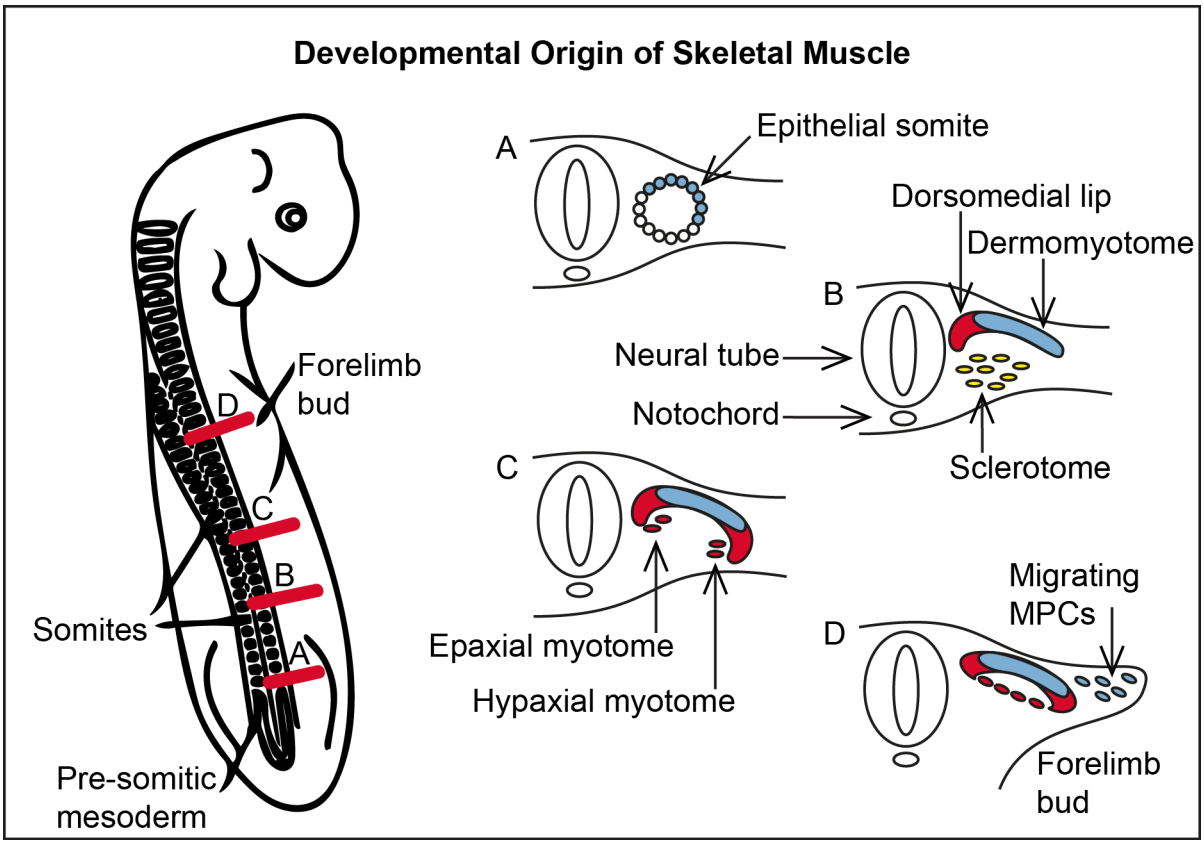

Figure 1.2. Skeletal muscle formation in chick embryos. (A) Epithelial somites are formed from the pre-somitic mesoderm. (B) These somites differentiate into the dermomyotome and sclerotome. Signal molecules from the neural tube and notochord induce myotome differentiation at the dorsomedial lip. (C) Epaxial and hypaxial myotome formation at both ends of the dermomyotome. (D) Migration of myogenic precursor cells (MPC) to the forelimb bud. This image was adapted from Bailey et al. (2001).

The neural tube and notochord launch an important cross-talk system that influences somite differentiation. SHH from the notochord induces sclerotome formation (Fan et al., 1995) whilst Wnt signalling from the neural tube and surface ectoderm initiate dermomyotome formation. Combined SHH and Wnt signalling promotes dermomyotomal expression of paired box protein Pax3, which is a potent myogenic transcription factor acting upstream of myogenic regulatory factor (MRF) genes (Maroto et al., 1997). Pax3-positive cells act as pioneers of myotome formation establishing the ventral migration at both epaxial and hypaxial ends of the dermomyotome (Goulding et al., 1994).

Cells in the myotome exhibit rapid onset of MRF gene expression and subsequent myogenesis through four basic helix-loop-helix MRFs: Myf5, Mrf4, MyoD and myogenin (Bismuth & Relaix, 2010). Although signalling factor expression hierarchy varies in tissues during development and regeneration, most frequently myogenin is the terminal MRF to be expressed and can be used as a marker for cells that have committed to myotube formation (Parker et al., 2003). Myomaker is a recently discovered membrane protein expressed in myoblasts during fusion with myotubes and subsequently downregulated, which means that it is one of the final markers of myoblast commitment to fusion (Millay et al., 2013).

BMP-4 secretion from the lateral plate mesoderm inhibits myogenesis. Concomitant SHH and Wnt signalling activates BMP4 antagonist noggin, which explains why hypaxial dermomyotome exhibits delayed myotome formation in comparison to the epaxial end (Reshef et al., 1998). However, this delay is a pivotal mechanism in myogenesis as it ensures the survival of a small population of $Pax3^+$ MPCs that migrate out of the dermomyotome and into forming limb buds eventually giving rise to $Pax7^+$ adult skeletal muscle-specific stem cells (Amthor et al., 1998; Gros et al., 2005) widely known as satellite cells (Mauro, 1961). BMP signalling's continuing significant role in satellite cell population maintenance and differentiation during muscle regeneration cycles has also recently been shown (Ono et al., 2011). An overview of signalling pathways in myogenesis is depicted in figure 1.3.

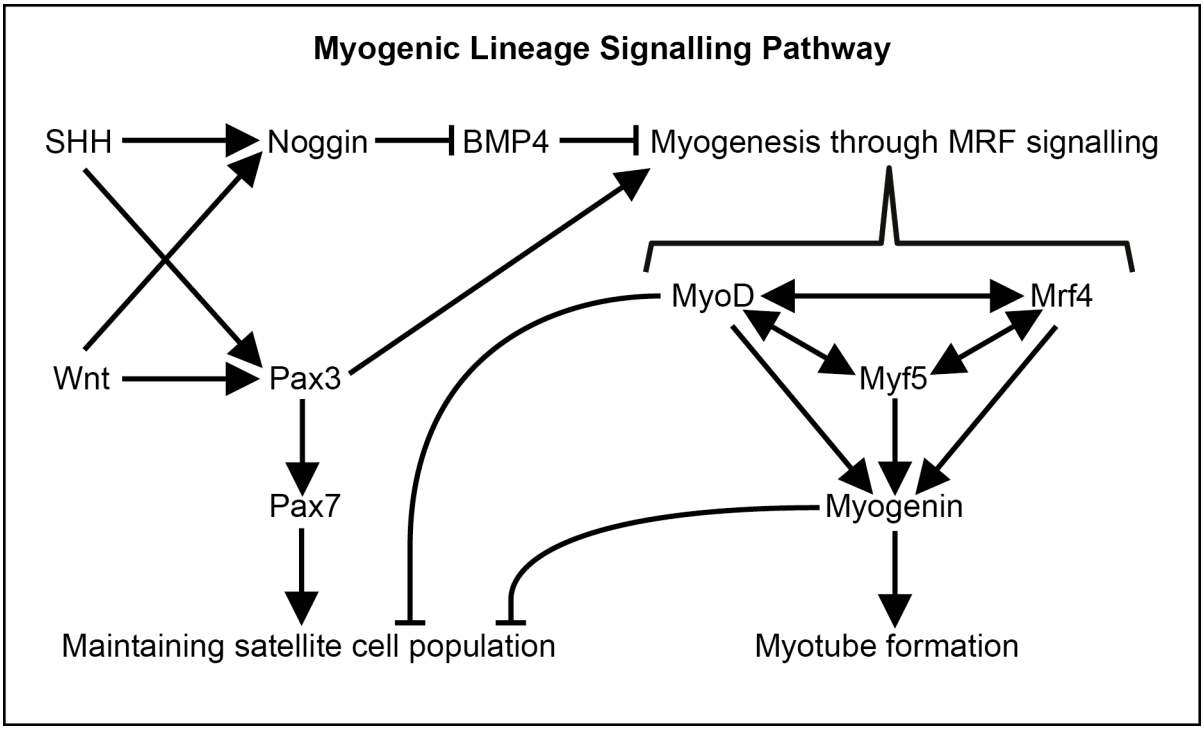

Figure 1.3. The myogenic lineage signalling pathway. SHH and Wnt crosstalk induces Pax3 and noggin synthesis. Pax3 regulates myogenesis through myogenic regulator factor (MRF) cross-talk signalling, which is inhibited by bone morphogenic protein 4 (BMP4). Noggin, in turn, inhibits BMP4 and therefore indirectly facilitates myogenic differentiation. Pax7 – expressed downstream and in parallel with Pax3 – maintains the satellite cell population. MyoD marks commitment to myogenesis and its expression in satellite cells induces differentiation. Myogenin is the furthest down the myogenic pathway out of MRFs and is considered a marker of complete myoblast commitment to differentiation and fusion into myotubes.

1.1.3 Satellite Cells and Muscle Regeneration

In their quiescent state satellite cells are located between the basal lamina and the sarcolemma of muscle fibres. They have been characterised as $Pax7^+$ M-cadherin$^+$ $CD34^+$, yet $MyoD^-$ cells (Zammit et al., 2006). Pax7 expression restricts satellite cells from differentiating down the haematopoietic lineage (Seale et al., 2000) and despite some success in generating skeletal muscle from the haematopoietic lineage (Corbel et al., 2003; Camargo et al., 2003) it has been shown that even whilst $CD45^+$ cells are inherent to skeletal muscle, they do not significantly contribute to the satellite cell pool, which is directly descended from the central dermomyotome (Sherwood et al., 2004; Gros et al., 2005).

Satellite cells can become activated by weight or shear forces due to trauma or exercise. These forces causes nitric oxide (NO) release from the neuronal form of NO synthase (nNOS), associated with the focal adhesion dystrophin glycoprotein complex (DGC) in muscle fibres (Garbincius & Michele, 2015). The DGC links sarcoplasmic F-actin with the extracellular matrix essentially working as a structural damage inhibitor increasing sarcolemmal stability (Rando, 2001). During normal muscle contraction and relaxation cycles NO fluctuations do not affect satellite cells (Wozniak & Anderson, 2007). When fibres are damaged in response to physical exercise, or when sarcolemmal stability is compromised, nNOS causes a sharp rise in NO levels (Baldelli et al., 2014). An increase in NO also causes satellite cell activation through hepatocyte growth factor (HGF) release and its subsequent binding to c-Met receptor, which is an early satellite cell activation gene (Le Grand & Rudnicki, 2007). Concomitantly the mitogen activated protein kinase (MAPK) signalling pathway is activated by microenvironment-secreted FGFs and sphingosin-1-phosphate (Nagata et al., 2006). All of these events orchestrate an exodus of satellite cells from their niche through delamination and cause rapid cell division to repair the damaged muscle fibres.

Myf5 signalling plays a pivotal role in muscle differentiation. It is controlled upstream by the Pax3/7 pathway and acts on par and upstream – depending on tissue – with MyoD (Dumont et al., 2015). As previously described the interaction of MRFs Myf5, MyoD and Mrf4 expression in muscle precursor cells represents commitment to differentiation and is gradually superseded by myogenin expression, which marks terminal differentiation. Subsequently various muscle specific genes are expressed in myotubes and myofibres, such as desmin and the DGC constituents marking the end of the muscle regeneration cycle (Zammit et al., 2006).

1.2 Duchenne Muscular Dystrophy

Mutations in the genes encoding DGC constituents causing negligible or non-functional protein expression can destabilise the protein complex and as a result compromise sarcolemmal integrity as well as signalling pathways (Sandonà & Betto, 2009). Consequently, these mutations often cause various forms of muscular dystrophies. Duchenne Muscular Dystrophy (DMD) is a recessive X-linked genetic disorder. It was first described by Guillaume Duchenne in 1861 and is caused by the more than 7,000 determined mutations (Bladen et al., 2015) in the *DMD* gene expressing dystrophin. The extraordinarily large number of mutations recorded can be attributed to the length of the *DMD* gene. These 2.4Mb located at locus Xp21 and comprising 79 exons give rise to several isoforms of dystrophin, some of which are ubiquitously expressed, some are tissue specific, particularly in skeletal muscle (Ferlini et al., 2013). Full-length dystrophin, essential for both skeletal and cardiac muscle function, is a 427kDa protein, translated from 14kb mRNA (Scott et al., 2002). The incidence of DMD is from around 1/3,600 to 1/6,000 male births (Bushby et al., 2010a).

Several animal models are available for DMD research and have considerably helped to understand pathological mechanisms of the disease and test potential therapies. The C57BL/10ScSn-Dmd^{mdx} (mdx) mouse model (Bulfield et al., 1984) and the golden retriever muscular dystrophy dog (GRMD) model (Cooper et al., 1988) are most widely used, but there are also other model organisms available, such as the *sapje* fish (Bassett & Currie, 2004) and the dystrophic pig (Klymiuk et al., 2013).

1.2.1 The Dystrophin-associated Glycoprotein Complex

Dystrophin protects the sarcolemma of muscle fibres from shear force damage, acting in the DGC as a 'spring' that links fibre actin cytoskeleton with the extracellular matrix and basal lamina (Petrof et al., 1993). Calponin homology domains at dystrophin's N-terminal region interact with sarcomeric F-actin (Stone et al., 2005; Cohn, 2005). The middle part dystrophin, also called the rod domain, consists of spectrin-like repeats (Duan, 2011). The WW and EF hand domains at the C-terminal region accommodate interactions with β-dystroglycan (Chung & Campanelli, 1999). The latter is located on the sarcolemma and is linked to the extracellular matrix via laminins bound to heavily glycosylated α-dystroglycan (figure 1.4) (Cohn et al., 2002).

DGC formation is hampered by loss of function or absence of dystrophin and the underlying causative mutations have varying effects on expression of dystrophin (Birnkrant et al., 2010). DMD patients are diagnosed around the age of five when it becomes apparent that their physical abilities are lagging behind compared to their peers (Bushby et al., 2010a). Lacking DGC protection, the sarcolemma becomes fragile and lipid bilayer lesions visible with electron microscopy (Mokri & Engel, 1975) occur, triggering three key proposed pathological pathways, which are also hypothesised to interact with each other.

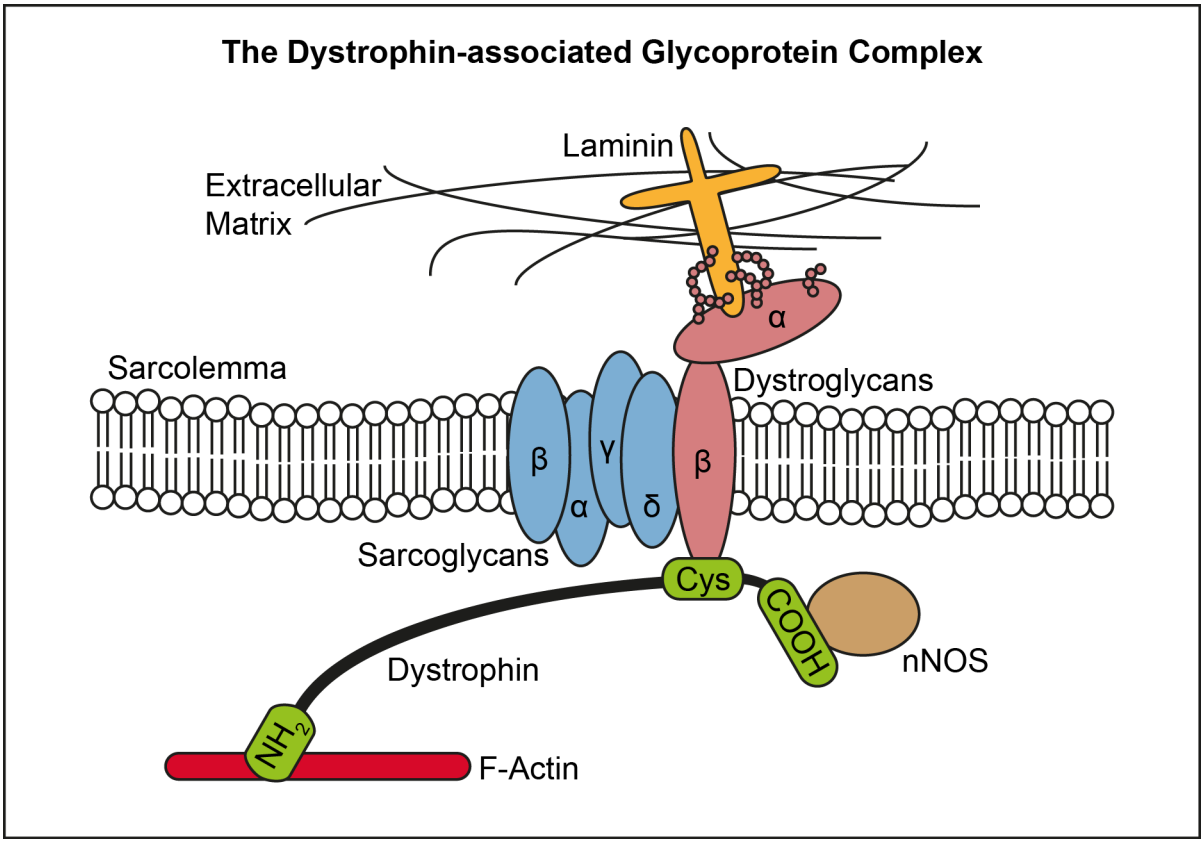

Figure 1.4. The dystrophin-associated glycoprotein complex. Dystrophin acts as a shock absorber by linking the muscle sarcomere to the extracellular matrix. It is bound to sarcomeric F-actin at its N-terminus (NH_2) and transmembrane protein β-dystroglycan at a cysteine-rich domain (Cys) close to its C-terminus (COOH), where dystrophin is associated with nNOS. β-dystroglycan is bound to the sarcoglycan complex as well as α-dystroglycan on the extracellular side of the sarcolemma. Heavy glycosylation of α-dystroglycan is required for laminin binding and association with extracellular matrix proteins. In Duchenne muscular dystrophy absence of dystrophin also causes mislocalisation of nNOS, sarco- and dystroglycans, leading to sarcolemmal fragility. This image has been adapted from Cohn (2005).

1.2.2 Skeletal Muscle Pathology

The first of these pathological pathways is release of signals for satellite cell activation. Consequently, the inherent satellite stem cell population proliferates and some daughter cells committed to differentiation down the myogenic lineage fuse with damaged fibres to repair the sarcolemma (Wang et al., 2014). Other differentiating cells can fuse with one another to form and extend *de novo* myotubes. Despite initial success with repairing injured tissue this regeneration cycle is thought to be overpowered as the satellite cell population becomes depleted over time due to the magnitude of damage (Wallace & Mcnally, 2009).

The second proposed pathway is caused by the rapid rise of sarcoplasmic Ca^{2+} via damage-induced sarcolemmal lesions (Bodensteiner & Engel, 1978) and stretch-activated channels (Iwata et al., 2003). This triggers an intrinsic dysferlin-mediated membrane repair mechanism to be activated, attracting cytoplasmic vesicles and transporting them to the sarcolemma (Chiu et al., 2009). However, Ca^{2+} influx also affects mitochondrial function (Vandebrouck et al., 2006), increases reactive oxygen species (ROS) production (Whitehead et al., 2006) and activates calcium-dependent proteolytic enzymes, which over time cause much more damage to muscle fibres (Alderton & Steinhardt, 2000). Lesions in the sarcolemma also cause leaking of various proteins, such as creatine kinase (CK). Highly elevated CK in blood serum is used as a diagnostic test for several muscle diseases (Ozawa et al., 1999).

The third pathological theory is mediated by free radicals. As previously mentioned, NO is imperative for satellite cell recruitment to sites of injury (Yin et al., 2013). With impaired DGC formation nNOS is also displaced from the sarcolemma (Kobayashi et al., 2008). As a result, NO levels are lower, hindering the process of mopping up free radicals that damage muscle fibres and attract inflammatory cells (Messina et al., 2006) (Whitehead et al., 2006). Additionally, nNOS competes for arginine with arginase, which produces pro-fibrotic agents in type M2a macrophages (Wehling-Henricks et al., 2010). Co-culture of myoblasts and macrophages has shown a delay in myoblast differentiation (Merly et al., 1999). Hence, reduced nNOS function can also hasten replacement of necrotic fibres with fatty tissue.

1.2.3 Cardiac Pathology

Cardiac failure is one of the primary causes of death in DMD (Romfh & Mcnally, 2010). Lack of dystrophin destabilises the highly specialised environment of muscle fibres, resulting in a range of associated proteins being mislocalised from their niche, ultimately compromising signalling pathways as well as structural integrity (Townsend et al., 2011). DMD patients mostly develop rapidly progressing dilated cardiac myopathy (Williams & Allen, 2007).

Pathology in dystrophic hearts is caused by a disruption in the various signalling pathways, illustrated in figure 1.5. Mechanical stress in cardiomyocytes – exacerbated by lack of dystrophin – leads to various stimuli capable of instigating hypertrophy, such as angiotensin (Ang) release from internal stores (Zou et al., 2002). Depending on the direction of sarcomere addition as a response to hypertrophic signals cardiomyocytes can either undergo concentric (increased width) or eccentric (increased length) hypertrophy (Frey et al., 2004; Maillet et al., 2013). Cardiac hypertrophy is not necessarily detrimental *per se*, as in the case of exercise-induced temporary hypertrophy (Barry et al., 2008), but prolonged exposure to permissive stimuli and an underlying compromised signalling environment in dystrophic cardiac tissue provoke pathological consequences (Taigen et al., 2000).

Angiotensin-converting enzyme (ACE) generates AngII as a response to mechanical stress and its effect is mediated by AngII receptor type 1 (AT_1R), activating MAPK pathways (Schlüter & Wenzel, 2008). MAPKs are capable of increasing protein synthesis (Zou et al., 2002), as well as increasing intracellular reactive oxygen species (ROS) levels – causing a nuclear factor kappa B ($NF\kappa B$) mediated hypertrophic response – and triggering apoptosis via c-Jun N-terminal kinase (JNK) (Schlüter & Wenzel, 2008). An alternative pathway for MAPK-induced hypertrophy is mediated by integrins (ITG) as a result of mechanical stretch (Zou et al., 2002) (Kuppuswamy et al., 1997). Both ITG and AngII activation of MAPKs cause cardiac hypertrophy directly via interaction with myocyte enhancer factor 2 (MEF2) and indirectly by the ROS-$NF\kappa B$ stimulating effect on stretch-activated Ca^{2+} channels on the cell membrane and by reducing calcineurin autoinhibition, leading to the potentiation of MAPK effect on MEF2 (Schlüter & Wenzel, 2008; Gaspar-Pereira et al., 2012).

Lack of dystrophin also causes nNOS mislocalisation in cardiac tissue (Garbincius & Michele, 2015), which leads to lower NO levels and compromises ROS clearance (Booz, 2005). NO activates soluble guanylyl cyclase (GC) receptors, which produce cyclic guanosine monophosphate (cGMP) (Zois et al., 2014). cGMP sequentially regulates hypertrophy by improving the function of cGMP-dependent protein kinase G (PKG), which in turn inhibits voltage-gated L-type calcium channels (Ca_V1) (Barry et al., 2008). PKG also inhibits Na^+/H^+ exchanger 1 (NHE) function (Frey et al., 2004), consequently aiding Na^+/Ca^{2+} exchanger (NCX) function (Bkaily et al., 2015).

Ultimately both of these actions of cGMP lower intracellular Ca^{2+} concentration ($[Ca^{2+}]_i$). Reduced NO therefore leads to an increase in Ca^{2+}, which feeds back to increased hypertrophy as a result of augmented calcineurin activity and subsequent nuclear factor of activated T-cells (NFAT) mediated gene activation (Enwere et al., 2014; Liu et al., 2012). On the other hand, β-adrenergic receptor (βAR) activation can lead to calcineurin-dependent apoptotic commitment by dephosphorylation of the Bcl-2 associated death promoter (BAD) (Wang et al., 1999; Saito et al., 2000). For this reason, despite the option of inhibiting calcineurin's pro-hypertrophic activity with Cyclosporine A, it is important to maintain some NFAT and calcineurin activity to permit apoptosis of cardiomyocytes (Zou et al., 2002; Frey et al., 2004).

Intracellular Ca^{2+} activates ryanodine receptors (RyR) on the sarcoplasmic reticulum (SR) causing a positive feedback loop, releasing more Ca^{2+} from SR stores, consequently exacerbating the pathological environment, especially in mdx mice, where expression of RyRs is upregulated (Williams & Allen, 2007; Yamaguchi et al., 2011). Intracellular Ca^{2+} additionally activates calmodulin-dependent kinases (CaMK), leading to MEF2 induced cardiac hypertrophy (Frey et al., 2004; Konno et al., 2010), mentioned before. CaMK may have this effect by modulating the MEF2 activation domain resulting in the potentiation of its activation by MAPK (Lu et al., 2000). Cardiac SR luminal Ca^{2+}-ATPase (SERCA) is one of the major proteins responsible for mopping up intracellular Ca^{2+}, storing it in the SR. SERCA is inhibited by dephosphorylated phospholamban (PLN) (Haghighi et al., 2014). β-AR activation leads to PLN phosphorylation and a consequent increase in SERCA activity (MacLennan & Kranias, 2003). However, blocking β-ARs and the concomitant PLN inhibition is counteracted by increased SERCA expression (Barry et al., 2008).

A pathway attenuating hypertrophic response in cardiomyocytes is GATA4-mediated expression and release of atrial and brain natriuretic peptides (ANP and BNP), which form a negative feedback loop for various cellular signals (Gardner et al., 2007). Natriuretic peptides are activated by furin cleavage (Ichiki et al., 2013) and their response is mediated by natriuretic peptide receptors (NPR). NPRA and NPRB are GCs, generating anti-hypertrophic cGMP and also inhibiting the MAPK pathway (Zois et al., 2014; Schlüter & Wenzel, 2008).

Corticosteroids are prescribed to DMD patients in order to combat their muscle phenotype (Bushby et al., 2009). Glucocorticoid receptors (GCR) reside in the cytoplasm in their inactivated state, but once bound by corticosteroids they translocate to the nucleus where they inhibit NFκB function (Rao et al., 2011). Consequently, corticosteroids have an anti-hypertrophic as well as an anti-apoptotic effect on cardiomyocytes (Ren et al., 2012). A signalling system regulated by the tumour necrosis factor-like weak inducer of apoptosis (TWEAK) and its receptor Fn14 has been discovered to be playing a role in skeletal muscle wasting (Bhatnagar & Kumar, 2012), and cardiac hypertrophy (Ren & Sui, 2012). This TWEAK-Fn14 signalling system is capable of activating NFκB signalling (Enwere et al., 2014) and therefore could also be inhibited by steroids.

P2X purinoreceptor 7 (P2RX7) is upregulated in mdx mouse myoblasts (Young et al., 2012). As a response to extracellular adenosine triphosphate (ATP), P2X7Rs open a pore permeable to Ca^{2+} and consequently cause a rise in $[Ca^{2+}]_i$ (Sinadinos et al., 2015), which plays a big role in disease progression. Although purinergic receptors are primarily associated with an augmented immunological response in DMD (Jiang et al., 2005; Young et al., 2015), it has also been shown that P2RX7 is expressed in caveolin-1 deficient mouse atrial cardiomyocytes (Barth et al., 2010). Considering the drastic P2RX7 upregulation observed in mdx myoblasts it may also be the case for cardiomyocytes. Involvement of this pathway in DMD cardiac tissue pathology needs to be elucidated.

A group of markers for pathological cardiac hypertrophy have been identified and named the foetal gene program (FGP) (Taegtmeyer et al., 2010). In addition to the aforementioned onset of ANP and BNP expression, a switch in the adult heart myosin heavy chain (MHC) composition, whereby MHCα expression is gradually replaced by MHCβ expression, is characteristic for FGP activation (Rajabi et al., 2007). Similarly a shift from cardiac α-actin expression to skeletal α-actin preference in cardiomyocytes is also an indicator of FGP initiation (Rajabi et al., 2007; Taegtmeyer et al., 2010). All of these are markers of hypertrophy that deserve to be investigated for potential effector treatment targets.

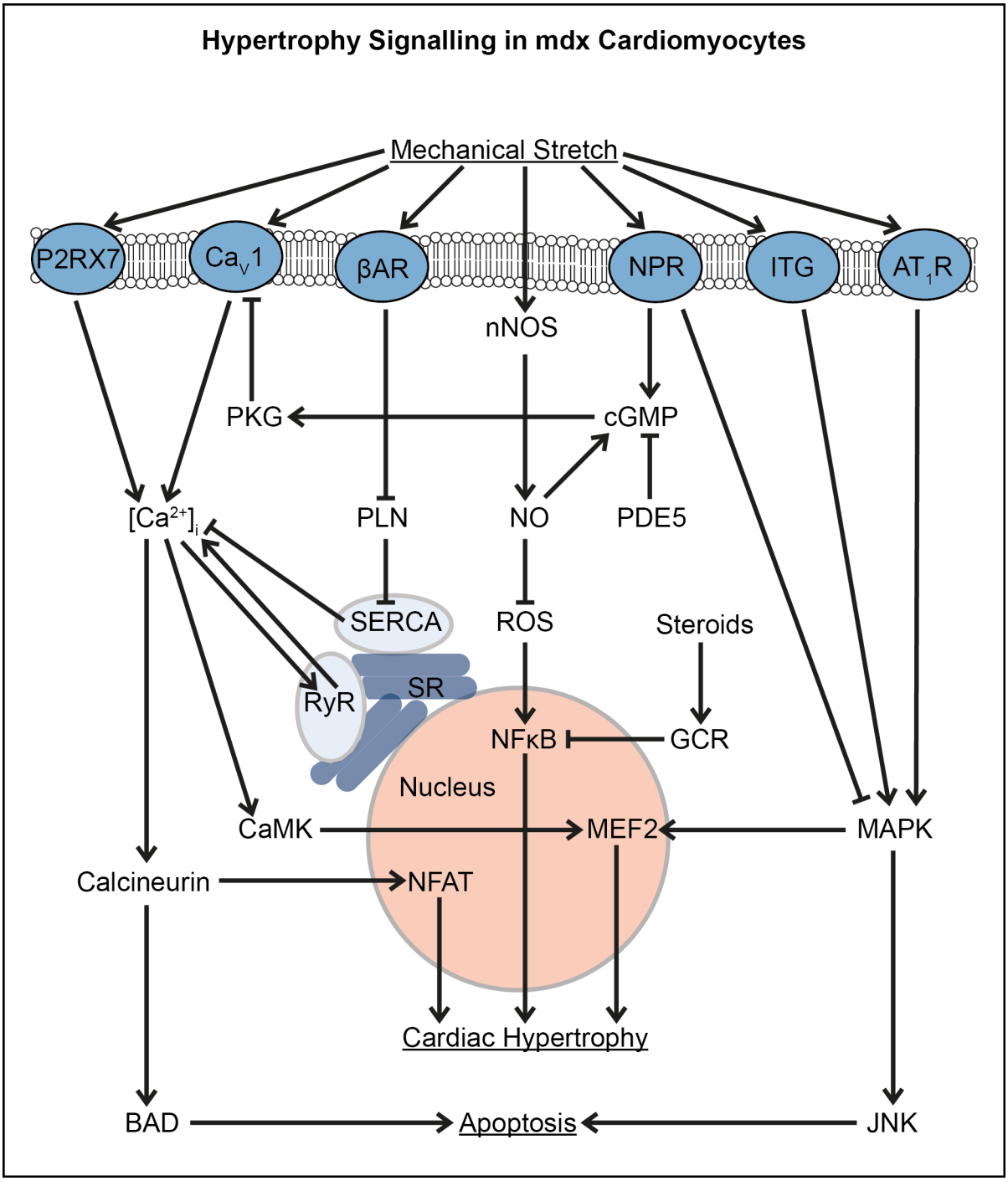
Hypertrophy Signalling in mdx Cardiomyocytes
Mechanical Stretch
P2RX7
Ca_V1
βAR
NPR
ITG
AT_1R
nNOS
PKG
cGMP
$[Ca^{2+}]_i$
PLN
NO
PDE5
SERCA
ROS
Steroids
SR
RyR
NFκB
GCR
Nucleus
CaMK
MEF2
MAPK
Calcineurin
NFAT
Cardiac Hypertrophy
BAD
Apoptosis
JNK

Figure 1.5. Pathological pathways in mdx cardiomyocytes. Mechanical stretch causes activation of signalling cascades leading to activation of several cross-talking pathways. Purinergic receptors (P2RX7) and voltage-gated (Ca_V1) channels cause Ca^{2+} influx to the sarcoplasm. β-adrenergic receptors (βAR) can inhibit phospholamban (PLN) inactivation of sarcoplasmic reticulum luminal Ca^{2+} ATPase (SERCA), which together with ryanodine receptors (RyR) regulates sarcoplasmic reticulum (SR) Ca^{2+} storage. Elevated intracellular Ca^{2+} leads to calmodulin-dependent kinase (CaMK) and calcineurin activation, both leading to a hypertrophic response via myocyte enhancer factor 2 (MEF2) and nuclear factor of activated T-cells (NFAT) activation, respectively. Calcineurin can cause the onset of apoptosis via the Bcl2-associated death promoter (BAD). Integrin (ITG) and angiotensin type 1 receptor (AT_1R) activation can trigger mitogen activated protein kinase (MAPK) signalling, which in turn leads to cardiac hypertrophy via MEF2 and apoptosis via c-Jun N-terminal kinase (JNK) activation. Both the MAPK pathway and Ca_V1 can be inhibited by natriuretic peptide receptors (NPR) A and B. Neuronal nitric oxide synthase (nNOS) can also mediate the same Ca_V1 inactivation pathway through nitric oxide (NO) activated cyclic guanosine monophosphate (cGMP) production and subsequent protein kinase G (PKG) activation, which in turn inhibits Ca_V1 function. NO also aids reactive oxygen species (ROS) clearance. The latter is responsible for triggering nuclear factor kappa B (NFκB) mediated cardiac hypertrophy. Corticosteroid treatment can activate glucocorticoid receptors (GCR) that translocate to the nucleus and inhibit NFκB signalling. Phosphodiesterase 5 (PDE5) breaks down cGMP and is therefore also a therapeutic target in DMD.

1.3 Clinical Aspects and Management of DMD

Expanding fibrotic infiltration in Duchenne patients causes progressive muscle weakness and wasting primarily in large muscles of the upper and lower limbs leading to loss of ambulation by early teens (Yiu & Kornberg, 2015). Lack of dystrophin also affects cardiac tissue with large-scale fibrosis leading to ventricular hypertrophy to compensate loss of function. Subsequent wall thinning, however, results in dilated cardiomyopathy (Romfh & Mcnally, 2010). Deterioration of intercostal muscles and the diaphragm often forces patients to require nocturnal ventilation to compensate reduced lung function. Respiratory and cardiac failure are the primary causes of mortality in the patient cohort (Wehling-Henricks et al., 2010). Extensive aplasia also involves paraspinal muscles, affecting posture, resulting in the development of scoliosis, especially once patients are wheelchair-bound. Surgical correction of the spine needs to be performed before pulmonary and cardiac function is compromised and carefully performed by experienced specialists due to an increased anaesthetic risk (Alman et al., 2004). As an anomaly some laryngeal and extra-ocular muscles are spared in DMD (Sussman, 2002; Smythe, 2009). These sparing phenomena are under strong scientific scrutiny as they could elucidate further intricacies of muscle regeneration as well as potential rescue therapies. Interestingly laryngeal and extra-ocular muscles are not derived from the dermomyotome, but from the pharyngeal mesoderm instead, which is the same source as the FHF (Tzahor & Evans, 2011).

One potential explanation for their sparing could be that extra-ocular as well as specific laryngeal muscles are mostly composed of slow-twitch fibres, which are less severely damaged by routine contractions (Smythe, 2009). Furthermore, it has been shown that fast-twitch fibres can be rescued to some extent in mdx mice using β-adrenergic agonists (Gehrig et al., 2010). This suggests there may also be a therapeutic effect in humans, but so far on the contrary β-blockers have been identified to have more effect on alleviating cardiac symptoms in DMD patients (Jefferies et al., 2005). Corticosteroids are the only currently available treatment prescribed for decelerating disease progression (Strober, 2006). There are several side-effects associated with steroid treatment including weight gain, coupled with height restriction, delayed puberty and reduced bone mineral content. Recent meetings of specialists have, however, concluded that despite the side-effects the overall benefits in terms of prolonging ambulation, improving skeletal and pulmonary

muscle function as well as delaying scoliosis significantly outweigh the disadvantages, which can be tackled with further alternative medication (Bianchi et al., 2011).

Dietary supplements for increasing muscle strength - creatine monohydrate (Tarnopolsky & Martin, 1999) - and reduction of fibre necrosis via upregulation of nNOS with L-arginine (Voisin et al., 2005), combined with reduced fat and sugar uptake have also been investigated as potential options to improve muscle function and control steroid-associated risks. In fact, L-arginine transporter function and expression were found to be considerably elevated in dystrophic mouse hearts, providing L-arginine as an alternative to reduced NO levels for GC activation and cardioprotection (Ramachandran et al., 2012). Furthermore, phosphodiesterase type 5 (PDE5) breaks down cGMP, dampening its signalling potential and the downstream cardioprotective effect (Kobayashi et al., 2008). Sildenafil, an inhibitor of PDE5 was therefore explored as a potential DMD therapeutic in a clinical trial, but unfortunately did not show cardiac improvement and the trial was terminated before completion (Leung et al., 2014).

It has been suggested that a small decrease in muscle strength can cause a much greater reduction in function (Beenakker et al., 2005). Therefore, even a modest delay in disease progression can significantly benefit the patient's quality of life. Patient care and standardisation of disease management have recently been targeted as important factors for improving patient well-being as well as a starting point for recruiting patients in clinical trials for novel rescue therapies (Bushby et al., 2009; Mayhew et al., 2011).

1.4 Proposed Therapies for DMD

Several rescue therapies for DMD are currently in clinical trials, but some target skeletal muscle more efficiently than cardiac tissue (Betts et al., 2015). Recovery in skeletal muscle may escalate the cardiac phenotype as a result of increased activity in patients and therefore it is essential to target cardiac muscle in therapeutic approaches (Duan, 2006).

Due to the large number of varying mutations in the *DMD* gene patients with mutations in dystrophin exhibit a spectrum of disease severity. Some mutations – such as in-frame deletions – in the *DMD* gene cause a milder phenotype, termed Becker Muscular Dystrophy (BMD). These patients mostly become symptomatic in adulthood and general progression of the disease is significantly slower as a result of partial salvation of dystrophin function (Bushby et al., 1991). Some of these patients with large open reading frame deletions only present with mild symptoms in late adulthood (Ferreiro et al., 2009). These cases have inspired the rationale behind some rescue therapies for DMD.

1.4.1 Gene Delivery Therapy

One option to alleviate symptoms in DMD patients is to use Becker patient genetic data for developing smaller forms of the DMD gene expressing functional variants of the dystrophin protein. Several groups have created mini- and micro-Dystrophin (often referred to as mDys and µDys) constructs (figure 1.6) to restore functional dystrophin expression in affected tissues (Moisset et al., 1998; Fabb et al., 2002). However, screening these variants for efficacy has been a time-consuming process that often requires costly *in vivo* testing in animal models as well as specialist knowledge and licenses for viral production and transduction (Wang et al., 2007). Time- and cost-efficient *in vitro* methods have been developed for faster screening of dystrophin variants through means of CK release measurements as a result of exposing cells to hypo-osmotic stress (Jørgensen et al., 2009). Although beneficial for determining efficacy in dystrophic mouse myoblasts, this method does not elucidate any systemic response complications that may arise (Wang et al., 2007), nor has it been tested in cardiomyocytes.

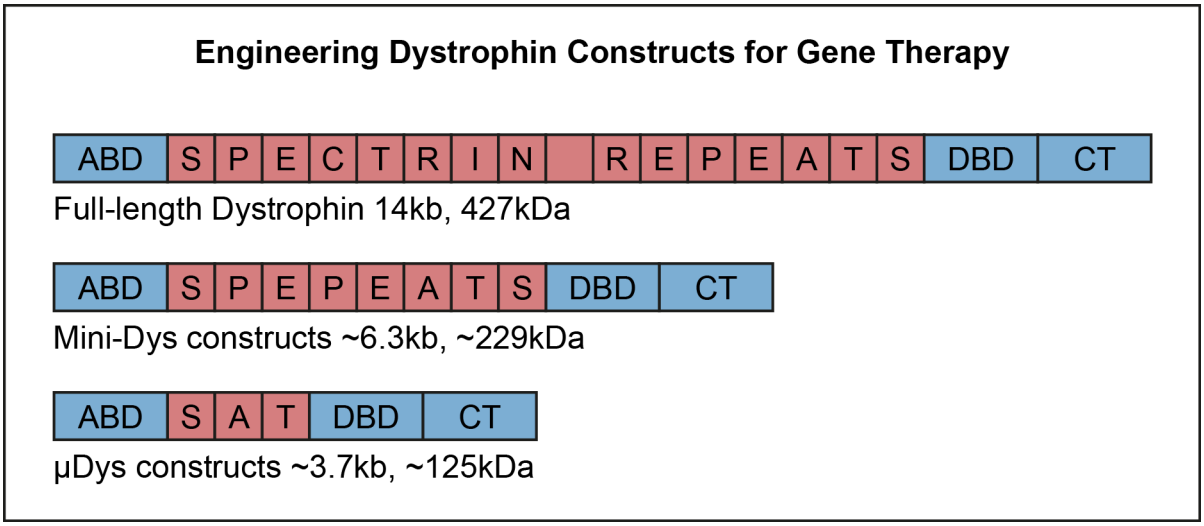

Figure 1.6. Engineering dystrophin constructs for gene therapy. Viral vectors have a restricted packaging capacity and most prospective therapeutic vectors cannot fit the full-length dystrophin gene. For this purpose, based on Becker muscular dystrophy patient mutations, smaller mini- and micro-dystrophin constructs have been developed to allow packaging and delivery with viral vectors. This image was adapted from Fabb et al. (2002), the depicted µDys construct is reported in Jørgensen et al. (2009).

Differentiation of fibroblasts into myogenic cells for diagnostic and *in vitro* experimental purposes has successfully been achieved by adenoviral transduction of MyoD (Roest et al., 1996). This method has also been proposed as an *ex vivo* therapeutic approach to compensate the diminishing satellite cell population in DMD (Lattanzi et al., 1998). Whilst using adenoviruses allows effective transduction of various genetic material it is not the safest approach, despite overriding the immune system by *ex vivo* transduction and screening for viral incorporation before transplantation.

New generations of lentiviruses and adeno-associated viruses (AAV) may be a solution, but their capsid size restricts the genetic material they can fit. Using mini-Dys and µDys constructs, developed on the basis of less pathogenic mutations in BMD patients, offers an invaluable tool for viral rescue therapies for DMD (Trollet et al., 2009; Falzarano et al., 2015). Out of these two viral vectors AAVs have been determined to be significantly safer, because they are not pathogenic in humans and result in markedly extended transgene expression (Zincarelli et al., 2008). Furthermore, AAV insertion sites are episomal over 99% of the time (Kay, 2011) and

show varying tissue tropism in different serotypes, which can be further modified by capsid mutagenesis (Yu et al., 2009; Michelfelder et al., 2011).

AAVs have a single-stranded genome and can package around 4.7kb of genetic material when their own replication genes (*rep* and *cap*) have been removed. This free space is flanked by inverted terminal loops at either end of the DNA strand (Hastie & Samulski, 2015). The conversion of single-stranded genetic material is often the rate-determining step in AAV transduction and although self-complementary vectors have been produced, for the purposes of DMD treatment maximal space is required to reintroduce dystrophin in a most functional form as possible (Tang et al., 2010). In addition to packaging capacity, another draw-back of AAVs is the lack of muscle-specific gene delivery. Expression of the DMD gene specifically in skeletal and cardiac muscle is essential as development of an immune response is higher when dystrophin is introduced elsewhere in the body (Hartigan-O'Connor et al., 2001). Myosin heavy- and light chain promoters are currently most promising for delivery to both heart and skeletal muscle and avoiding non-specific delivery (Salva et al., 2007; Schinkel et al., 2012).

Previous studies employing viral vectors have shown that even whilst a smaller construct of dystrophin driven by a muscle-specific promoter ameliorates the phenotype in fast-twitch fibres in mdx mice, it is ineffective in restoring diaphragm and cardiac tissue function (Dunant et al., 2003). It may be hypothesised that by restoring fast-twitch fibre function in humans, ambulation is also prolonged, hindering degeneration of the diaphragm through a reduced probability of developing scoliosis. However, this is nevertheless only a delay in phenotypic development. Augmented cardiac deterioration has been observed in mdx mice where only skeletal muscle function is therapeutically rescued (Townsend et al., 2008). This study correlates with pathology observed in defective dystrophin-induced X-linked dilated cardiomyopathy patients, where dystrophin is definitively only lost in the myocardium (Cohen, 2004). Hence, it is pivotal to reiterate that both skeletal and cardiac muscle must be targeted when developing therapies for DMD. Promising results have been reported with highly cardiac-specific transduction in δ-sarcoglycan knockout mice (Goehringer et al., 2009), which have a more prominent cardiac phenotype. Delivery of μDys with AAVs to mdx mouse heart, effective construct expression and functional restoration has also been published (Schinkel et al., 2012). These results are encouraging for

being used in combination with other rescue therapies to successfully target both skeletal and cardiac muscle.

AAVs exhibit varying tissue specificity, which can be augmented with capsid and promoter engineering (Nance & Duan, 2015). Hence, AAVs may be most suitable for gene therapy, potentially ensuring a balanced recovery in both skeletal and cardiac muscle (Duan, 2006). The recent approval from the European Medicines Agency for the use of an AAV-based therapy against lipoprotein lipase deficiency also improves the outlook for approval of other applications of AAVs in clinical trials (Ylä-Herttuala, 2012). However, utilising AAV vectors for DMD treatment will need to overcome a reporting of an immune response towards the introduced construct in clinical trials (Mendell et al., 2012).

1.4.2 Antisense Oligonucleotides

Another BMD-inspired method employs antisense oligonucleotides (AON) to artificially induce alternative splicing, removing out-of-frame exons and consequently restoring the dystrophin gene's reading frame (figure 1.7) with the overall size of the protein being smaller compared to wild-type. AONs have been shown to be successful at restoring dystrophin expression, and most importantly restore localisation of the DGC constituents to the sarcolemma in mdx mice (Gebski et al., 2003; Vitiello et al., 2008). There are ongoing multi-centre clinical trials with phosphorodiamidate morpholino oligomer (PMO) (Kinali et al., 2009; Cirak et al., 2011) as well as Prosensa's (now acquired by GlaxoSmithKlein) 2'-*O*-methyl phosphorothioate oligoribonucleotide (2OMePS), which are both designed to skip exon 51 in dystrophin mRNA to restore the reading frame and thus allow a shorter variant of the protein to be expressed (Goemans et al., 2011). Preliminary clinical data for the 2OMePS (Voit et al., 2014) and PMO (Mendell et al., 2013) compounds showed some improvement in DMD patients but require further and larger cohort studies.

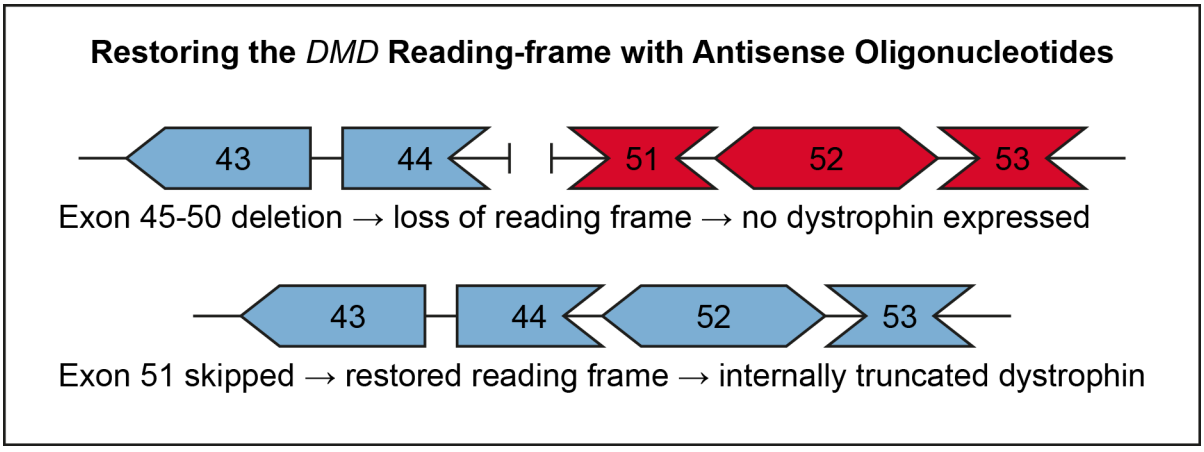

Figure 1.7 Exon skipping as a therapeutic option to restore dystrophin expression. In this illustrated example, a large deletion of the *DMD* gene exons 45-50 results in an acceptor codon (one nucleotide missing from a codon) both at the end of exon 44 and the start of exon 51, leading to reading frame disruption. When exon 51 is skipped with antisense oligonucleotides then exon 52 donates an overhanging nucleotide to the acceptor codon at the end of exon 44 and the reading frame is restored. This leads to internally truncated, but functional, dystrophin expression. The image is adapted from Aartsma-Rus & van Ommen (2009).

Unfortunately, exon 51 skipping by these compounds can only restore dystrophin expression in roughly 13% of DMD patients (Aartsma-Rus & van Ommen, 2009) and this is the biggest group of patients that could be treated with one compound. Overall, exon skipping may eventually help up to 83% of all DMD patients, requiring development of several compounds specific for mutations that only a small number of patients have (Bushby et al., 2009). In essence, exon skipping therapy is moving closer to personalised medicine and consequently there will be evident implications on the price of these drugs. It must also be noted that disparities between cardiac and skeletal muscle rescue have been observed in the efficacy of PMOs with higher dystrophin expression in skeletal muscle (Wu et al., 2010; Betts et al., 2015). For these reasons, improved compounds are now emerging and being investigated in animal models for exon skipping, such as tricyclo-DNA oligomers (Goyenvalle et al., 2015) and peptide-conjugated PMOs (Wu et al., 2014).

1.4.3 Stop Codon Read-through

Calcium channel blocking has also been noted as a potential rescue therapy for DMD. It has been observed that transient receptor potential canonical (TRPC) channel 3 induction can result in muscular dystrophy development in mice (Millay et al., 2009). Streptomycin has been shown to be able to block these stretch-activated channels and accordingly reduce internal calcium levels in guinea pigs (Gannier et al., 1994). This effect was investigated in mdx mice, which were treated *in utero* and until adulthood. The study concluded that initial improvements in mice were overshadowed by rapid progression of the disease in late adulthood with no effect on the diaphragm or cardiac tissue and, in fact, significant worsening of pathology in the heart (Jørgensen et al., 2011). It was hypothesised that one of the reasons for an initial improvement in 6 week old pups may have been due to streptomycin's potential of reading through premature stop codons (Welch et al., 2007). However, results for that time-point showed that there was no dystrophin expression in TA muscle. Elucidation of calcium channel blocking as a potential rescue therapy will need to be further investigated.

Atalauren is a drug also capable of premature stop codon read-through (Hamed, 2006). It was used for clinical trials as a therapeutic agent for cystic fibrosis (Wilschanski et al., 2011), but regrettably Ataluren clinical trials with nonsense mutation DMD patients were initially discontinued as no significant improvement was seen in the primary outcome measure, despite a slight improvement in the low-dose cohort (Muntoni & Wood, 2011). Further clinical studies have since been completed (Bushby et al., 2014), and it is now conditionally approved by the European Medicines Agency for use in DMD patients under the trade-name Translarna (Haas et al., 2015). However, this drug would only be applicable to about 15% of DMD patients (Bushby et al., 2009), which highlights the need for developing a universal therapy for DMD that would equally restore dystrophin expression in both cardiac and skeletal muscle.

1.4.4 Cell Therapy

Myoblasts can be isolated from muscle tissue at a high purity (Blanco-Bose et al., 2001), but have a restricted capacity for proliferation. Satellite cells are found at a relatively low abundance of 2-5% *in situ* (Figeac et al., 2007), readily differentiate into myoblasts *ex vivo* and, hence, also become senescent after activation and onset of MyoD expression when cultured (Hawke & Garry, 2001).

Technical advances have improved satellite cell yields from muscle tissue samples on the basis of transcription factor (Pax3, Pax7) and cell surface marker (CD34, SM/C-2.6) expression (Fukada et al., 2004; Montarras et al., 2005). Although myoblasts and satellite cells can routinely be used for *in vitro* experiments and have successfully been used to repopulate muscle in mouse models, these isolation methods will unfortunately not be able to produce sufficient quantities of cells for therapeutic purposes (Pleasure, 2011). Erythropoietin signalling has been shown to delay myogenin expression *in vivo*, thus inducing transplanted myoblast proliferation and incorporation to muscle fibres in mdx mice (Jia et al., 2009). This suggests cells that express erythropoietin may have more success in repopulating damaged tissues.

Muscle side population cells have been investigated as a potential resource for transplantation. These cells express haematopoietic stem cell markers Sca-1 and to a lesser extent CD45, they do not become activated or differentiate down the myogenic lineage *in vitro*, but have been shown to differentiate into myocytes and satellite cells when used for transplantation in mice (Asakura et al., 2002). However, recent results indicated that muscle side population cells derived from dystrophic mouse muscle fail to go down the myogenic lineage and instead become adipogenic (Penton et al., 2013).

Pericytes, derived from microvasculature in muscle tissue, are another type of precursor cells that have been scrutinised and tested as a source of cells for myogenic regeneration. These cells express proteoglycans and alkaline phosphatase that allow them to be relatively easily isolated and purified. Human pericytes from adipose tissue increase the life-span of utrophin and dystrophin double knock-out (dko) mice when injected intraperitoneally (Valadares et al., 2014). Pericytes have also previously been shown to incorporate into myotubes in mice. These cells may

be closely related to the mesoangioblast population due to their same origin in the vasculature (Dellavalle et al., 2007).

Mesoangioblasts have been used as a cell therapy method to restore DGC formation and localisation to the sarcolemma in the α-sarcoglycanopathy mouse model (Sampaolesi et al., 2003). That research group used the same intra-arterial administration method to restore dystrophin expression in the golden retriever dog model of DMD (GRMD) (Sampaolesi et al., 2006). These *in vivo* experiments showed great potential especially as there were no significant immune reaction noted and the phenotype was alleviated in GRDM. However, a clinical trial of HLA-matched donor mesoangioblast intra-arterial injection into DMD patient limbs did not stop disease progression (Cossu et al., 2015).

Farini et al. (2009) have successfully rescued dystrophin expression in CD133-positive endothelial circulating progenitor cells with better results than haematopoietic-lineage derived stem cells. These cells have also been used in a phase I clinical trial, where neovascularisation was observed in DMD patients after autologous cells had been corrected and reintroduced. There was a shift in the fibre types as well from slow- to fast-twitch fibres (Torrente et al., 2007). However, immunological aspects of introducing stem cell therapies in clinic and a lack of significant increase in muscle strength in patients caused concern (Lodi et al., 2011). Furthermore there could always be immunological consequences to introducing dystrophin to the patients' fibres as was seen in the previously mentioned AAV trial (Mendell et al., 2012).

Conditionally immortalised CBA;B10-Tg(H2K^{b}-tsA58)6Kio/Crl (Immorto) mouse-derived heterozygous Immorto-mdx mouse cell lines can provide a near infinite resource of myoblast cells for *in vitro* experiments and are applicable for transplantation as the immortalising large T antigen from simian vacuolating virus (SV40) is thermo-labile and rapidly degrades at 37ºC (Jat et al., 1991) (Morgan et al., 1994). Whilst these cells are available from the mdx mouse model, they cannot be derived from humans and therefore are only useful for proof-of-concept animal studies. Nevertheless, these cells bring down the number of animals needed for tissue and cell harvesting for conducting experiments and improved models with no tumorigenicity upon transplantation are now available (Muses et al., 2011). The T

antigen inhibits p53 function, allowing these cells to exit the G1 stage and proliferate. It has been suggested that p53 interacts with MyoD to induce muscle CK transcription (Tamir & Bengal, 1998) and as such could compromise any results for rescue therapies that employ CK release as an outcome measure. However, as mentioned above, the T antigen is thermolabile and therefore would not compromise p53 function at the conventional 37ºC cell culture temperature.

In conditionally immortalised atrial HL-1 cells the T antigen is expressed under the ANP promoter, which makes its expression localised and cardiomyocyte-specific, reducing contaminating cells during the cell isolation process (White et al., 2004). Whilst these cells are more easily obtained than through conventional cardiac cell isolation procedures, they still remain only an animal-model tool for DMD research considering ventricles are more severely affected in DMD. A mouse strain has been developed that expresses the T antigen under the *Nkx2.5* promoter, where it is also controlled by a Cre-lox system (Rybkin et al., 2003). Although this provides a more suitable model for DMD research as it would be possible to obtain a ventricular cell line when crossed with the mdx mouse, it would still only be a resource for animal studies and the urgent need for human alternatives remains.

1.4.5 Stem Cell Models for DMD Research into Therapies

Pluripotent stem cells, capable of differentiating into most cell types, are a promising resource for testing various rescue therapies as they are essentially a self-replenishing resource of cells. Until recently stem cell research has been hindered by ethical concern. Many scientists initially anticipated blastocyst-derived embryonic stem cell (ESC) lines to be an essential resource for conducting *in vitro* experiments (Thomson et al., 1998). After wide press coverage and public opposition further development of these resources was restricted by legislation in many countries. The destruction of a fertilised egg for research purposes – sacrificing a person in the making – was the major ethical counter-argument for using human embryo-derived cell lines. Furthermore, a series of publications were retracted when serious allegations of fraud and abuse were brought to light in a research group working on human oocytes and cloning (Cyranoski, 2009). Fortunately, recent developments in the field of stem cell research have led to several alternative methods – with less significant ethical concerns – having been established for pluripotent cell line creation.

Shinya Yamanaka's research group has paved the way for deriving pluripotent stem cells by transducing fibroblasts with specific transcription factors (in the initial journal articles with *Oct3/4, Sox2, Klf4* and *c-Myc*) to reprogram mouse (Takahashi & Yamanaka, 2006) and a year later human (Takahashi et al., 2007) cells into induced pluripotent stem cells (iPSC), revolutionising stem cell research. There are no ethical concerns related to perishing embryos in this process, which meant countries where legislation was hampering developments in this field now had a legitimate alternative to proceed with their research. However, despite the scientific and legal reasoning for allowing iPSC production a survey showed that iPSCs only had a marginally higher public approval rate in the US compared to *in vitro* fertilisation-derived ESCs (Evans & Kelley, 2011).

C-Myc's tumorigenicity was noted at the very start and although other transcription factors were used to replace it, there remained no alternative that would have kept the success rate as high. Nevertheless, several suggestions for optimising the methods and making the process safer have now been published. *Glis1* was recently reported to be an appropriate substitute for *c-Myc* (Maekawa et al., 2011). Lithium has been shown to increase reprogramming efficiency by also affecting epigenetics

(Wang et al., 2011). Integration site specificity has been tackled by using transcription activator-like effector nucleases (Hockemeyer et al., 2011). Better determination of appropriate markers to select truly reprogrammed cells has decreased subjectivity and technical demand (Chan et al., 2009). Biotinylated viral capsids (Nesbeth et al., 2006) used with other combinations of transcription factors such as *Oct4*, *Sox2*, *Nanog* and *Lin28* as well as marker expression selection significantly speeds up the process (Dick et al., 2011).

There has been a myriad of publications on reprogramming somatic cells to generate cells belonging to different lineages. It has been possible to generate hepatocyte-like cells (Sekiya & Suzuki, 2011; Huang et al., 2011), neuronal cells (Pang et al., 2011) as well as patient-specific cardiomyocytes (Carvajal-Vergara et al., 2010). DMD patient-specific cardiomyocytes have now been generated and used as a model to test rescue therapies (Dick et al., 2013). Due to the continual nature of transcription factor regulation in myogenesis, it has taken considerably longer to establish a replicable protocol for myogenic cell derivation from iPSC, but recently published results (Shelton et al., 2015; Chal et al., 2015) have paved the way for DMD iPSC-derived satellite cell and skeletal muscle derivation, enhancing DMD researchers' toolbox with human models for *in vitro* trials.

1.5 Statement of Aims

This thesis introduces an *in vitro* mdx cardiomyocyte hypertrophy model. It is pivotal to determine which pathways are involved in this process in order to fully understand the mechanisms of cardiac remodelling in dystrophic hearts and to test therapeutic targets to ensure the model can be used for *in vitro* studies. The aims of the three results chapters in this thesis were as follows.

- To establish a model of mdx mouse cardiomyocyte hypertrophy for modelling the dystrophic heart in an *in vitro* setting.
- To identify signalling pathways and mechanisms of hypertrophy responsible for changes in mdx cardiomyocyte size in response to serum starvation.
- To investigate the efficacy of therapeutic compounds and AAV-mediated μDys transduction at reducing serum-induced mdx cardiomyocyte hypertrophy.

Chapter 2. Materials and Methods

2.1 Consumables and Equipment

Item	Product Code	Supplier
0.05% Trypsin-EDTA	25300096	Gibco
0.2ml PCR tube	I1402-4308	Starlab
1.5ml microfuge tube	211-2610	VWR
1.5ml microfuge tube screw-cap	716261	Greiner
1000µl pipette filter tips	S1122-1830	Starlab
100mm petri dishes	734-2321	VWR
10ml serological pipettes	86.1254.001	Sarstedt
10µl pipette filter tips	S1121-3810	Starlab
13mm⌀ No.1 cover glasses	ECN 631-1578	VWR
15ml centrifuge tubes	430766	Corning
1kb DNA ladder	G571A	Promega
200µl pipette filter tips	S1120-8810	Starlab
20µl pipette filter tips	S1120-1810	Starlab
24-well plates	734-2325	VWR
25ml serological pipettes	86.1685.001	Sarstedt
3-8% Tris-Acetate NuPAGE gels	EA0378BOX	Invitrogen
384-well PCR plate	785290	Greiner
4-12% Bis-Tris NuPAGE gels	NP0321BOX	Invitrogen
50ml centrifuge tubes	430829	Corning
50ml serological pipettes	86.1689.001	Sarstedt
50ml syringes without needles	SYR6212	SLS
5ml serological pipettes	86.1689.001	Sarstedt
60mm petri dishes	734-2318	VWR
8-channel spectrophotometer	ND-8000	NanoDrop
96-well PCR plates	E1403-5200	Starlab
ab15277 anti-dystrophin antibody	ab15277	Abcam
Acetic acid	A6283-1L	Sigma
Acrodisc 0.2µm sterile filter	514-4126	Pall/VWR
Agarose	NBS-AG500	NBS Biologicals
Agarose gel electrophoresis tanks	1704405	Bio-Rad
Agfa X-ray film	AGF1824G	Vet Direct

Alexa Fluor 488 goat anti-mouse IgG	A11001	Invitrogen
Alexa Fluor 488 goat anti-rabbit IgG	A11008	Invitrogen
Alexa Fluor 594 goat anti-mouse IgG	A11005	Invitrogen
Alexa Fluor 594 phalloidin	A12381	Invitrogen
Anti-α-actinin antibody	A7811-.2ML	Sigma
Antioxidant solution	NP0005	Invitrogen
Autoclave	RS232	Astell
Autoclave tape	817-0118	VWR
β1AR (V-19) antibody	sc-568	Santa Cruz
β-mercaptoethanol	31350010	Life Technologies
Bicinchoninic acid kit	BCA1-1KT	Sigma
Bioanalyzer 2100	G2940CA	Agilent
Blue/orange 6x loading dye	G190A	Promega
Bovine serum albumin	A3294-50G	Sigma
Camera BW	AxioCam HRc	Zeiss
Camera RGB	DS-Fi2	Nikon
Captopril	C4042-5G	Sigma
cDNA reverse transcription kit	4368814	App’d Biosystems
Cell scraper 220mm fixed blade	CC7600-0220	Starlab
Chloroform	C2432-1L	Sigma
Class 1 airflow cabinet	Hera guard	Heraeus
Class 2 airflow cabinet	Hera safe	Heraeus
Collagen from calf skin	C8919-20ML	Sigma
Collagenase type II	17101-015	Gibco
cOmplete protease inhibitor tablets	05892791001	Roche
DEPC-treated water	AM9906	Ambion
Dexamethasone	D4902-25MG	Sigma
Digital graphic printer	UP-D897	Sony
Dimethyl sulfoxide (DMSO)	D-8779	Sigma
Dulbecco's modified Eagle medium	41966052	Gibco
EDTA	E5134-500G	Sigma
Encore RNA-Seq Multiplex System	0312-32	NuGen
Enhanced chemiluminescence kit	RPN2232	Amersham
Ethanol	20821.330	VWR
Film developer	SRX-101A	Konica

Film developer cassette	RPN11643	Amersham
Fine scales	BD BH 110	Denver
Foetal bovine serum (FBS)	EU-000-F	SLI
Freezer -80°	U725	NB Scientific
Fridge/freezer -20°	KGV36VW32G	Bosch
GelDoc-It Imaging System	GelDoc-It310	UVP
Glucose	G8270-100G	Sigma
Glycine	G8898-1KG	Sigma
Goat anti-mouse IgG HRP conjugate	G21040	Invitrogen
Goat anti-rabbit IgG HRP conjugate	G21234	Invitrogen
Haemocytometer	680030	Marienfeld
Heat sealer	23/2696	Hulme Martin
Heater magnetic stir block	101N0052	Fisher
HEPES	H3375-100G	Sigma
HiMark Pre-stained protein standards	LC5699	Invitrogen
HiSeq 1500	HiSeq1500	Illumina
Horse serum (HS)	26050088	Gibco
HotStarTaq DNA polymerase	203205	Qiagen
Hsp90ab1 KiCqStart primers	M_Hsp90ab1_1	Sigma
Hybond PVDF membrane	RPN303F	GE Healthcare
Hydrochloric acid	84436-1L	Sigma
Incubator	Hera cell 240	Heraeus
Insulin syringe with needle	613-4897	VWR
Interferon gamma (IFNγ)	PMC4031	Invitrogen
Isopropanol	20842.330	VWR
KCl potassium chloride	P9541-500G	Sigma
Lab Armor beads	A1254301	Life Technologies
LDS sample buffer	NP0007	Invitrogen
Lens tissue	2105-841	Whatman
MANDRA1 anti-dystrophin antibody	ab7164	Abcam
Medium 199	31150-022	Gibco
MES SDS protein gel running buffer	NP0002	Invitrogen
Methanol	20846.326	VWR
Metoprolol tartrate	M5391-10G	Sigma
$MgSO_4$ magnesium sulphate	208094-500G-D	Sigma

Microfuge	5415D	Eppendorf
Microscope confocal	A1R	Nikon
Microscope filter DAPI	FS02	Zeiss
Microscope filter GFP	FS13	Zeiss
Microscope filter Rhodamine	FS15	Zeiss
Microscope inverted fluorescence	AxioVert200M	Zeiss
Microscope inverted light	AE20	Motic
Microwave oven	KOR-8A0R	Daewoo
Milk powder	93327	Marvel
Mounting medium with DAPI	H-1200	Vectorlabs
NaCl sodium chloride	S9888-5KG	Sigma
NaH_2PO_4	S9638-500G	Sigma
NaOH	S5881-500G	Sigma
NCL-DYS1 anti-dystrophin antibody	NCL-DYS1-S	Novocastra/Leica
NCL-Hamlet anti-dysferlin antibody	Hamlet-CE	Novocastra/Leica
NHE inhibitor KR-33028	KR-33028	Peacock Pharma
Nitrile gloves	112-2755	VWR
Novex Mini-gel PAGE tanks	120801-2839	Invitrogen
Nuclease-free water (NFW)	AM9937	Ambion
Objective CFI Plan Apochromat 20x	VC 20x/0.75	Nikon
Objective CFI Plan Fluor 10x	DL-10x F/0.3	Nikon
Objective Plan Neofluar 10x	10x/0.3	Zeiss
Objective Plan Neofluar 20x	20x/0.5	Zeiss
Oregon Green 488 phalloidin	O7466	Invitrogen
p-ERK (E-4) antibody	sc-7383	Santa Cruz
P2RX7 inhibitor A804598	A804598	Tocris
Parafilm	PM-999	Pechiney
Paraformaldehyde	P6148-1KG	Sigma
Pasteur pipettes 230mm	612-1702	VWR
PBS tablets	18912-014	Gibco
PCR thermocycler	LabCycler	Sensoquest
PCR plate adhesive sealing sheets	AB-0558	Thermo
Penicillin/Streptomycin	15070063	Gibco
pH meter	HI 2210	Hanna
Phenol:chloroform:isoamyl alcohol	15593031	Ambion

Phosphate buffered saline solution	20012068	Gibco
Plate reader Infinite	F200	Tecan
Plate reader Multiskan	354	Ascent
Polyethylene glycol (PEG) 400	91893-250ML-F	Sigma
PowerPac HC	1645052	Bio-Rad
Prednisolone tablets	6565/0914	Sovereign
Proteinase K	1964372	Roche
qRT-PCR plate thermocycler	QuantStudio7	App'd Biosystems
Refrigerated centrifuge	5804R	Eppendorf
Refrigerated centrifuge	5810R	Eppendorf
RIPA buffer	10230544	Thermo
RNAClean XP	A63987	Agencourt
RNase Zap	AM9780	Ambion
RNase-free DNase set	79254	Qiagen
RNeasy Mini kit	74104	Qiagen
Rotor	A-4-44	Eppendorf
Rotor	F45-30-11	Eppendorf
Rotor	A-4-62	Eppendorf
SafeView nucleic acid stain	NBS-SV1	NBS Biologicals
Sample reducing agent	NP0009	Invitrogen
Scales	HL-200i	A&D
Scalpels no.22	REF0508	Swann-Morton
SeeBlue Plus2 protein standards	LC5925	Invitrogen
SimplyBlue SafeStain	LC6060	Invitrogen
Sleeve protector	113-0718	VWR
Sodium dodecyl sulphate (SDS)	L3771-500G	Sigma
SYBR Green JumpStart Taq	S4438-500RXN	Sigma
T25 flasks	734-2311	VWR
Tissue homogeniser	9001273	Qiagen
Tissue ruptor probes	990890	Qiagen
Tpt1 KiCqStart SYBR Green primers	M_Tpt1_1	Sigma
Tris-Acetate protein gel running buffer	LA0041	Invitrogen
Triton X-100	T8787-50ML	Sigma
Trizma base	T1503-1KG	Sigma
TRIzol	15596026	Ambion

Trypsin 2.5%	15090-046	Gibco
Tween 20	P9416-100ML	Sigma
Ultrapure water system	D11901	Thermo
Virkon	A01302780	Dupont
Water bath	JB Aqua 18 Plus	Grant
Western blot transfer tanks	1703930	Bio-Rad
Zymo-Spin columns	C1004-50	Zymo Research

2.2 Solutions

Phosphate buffered saline (PBS)

· PBS tablets	2
· dH_2O	1000ml

4% (w/V) paraformaldehyde (PFA) in PBS

· dH_2O	500ml
· PBS tablets	2
· NaOH	3 pellets
· PFA	40g
· pH adjusted with NaOH	7.4
· dH_2O	to 1000ml

Tris buffered saline (TBS) 10x

· Trizma base	60.5g
· NaCl	87.6g
· pH adjusted with HCl	7.5

0.5% (V/V) Tween 20 in TBS

· TBS 10x	100ml
· dH_2O	899.5ml
· Tween 20	500µl

4% (w/V) bovine serum albumin (BSA) in TBST

· BSA	2g
· TBST	to 50ml

DNA digestion buffer

· Tris HCl	50mM
· EDTA	100mM
· NaCl	100mM
· Sodium dodecyl sulphate (SDS)	1%(w/V)
· pH	8

Tris-EDTA (TE) buffer

- Tris 10mM
- EDTA 1mM
- pH 7.4

Tris acetic acid EDTA (TAE) buffer

- Tris 400mM
- EDTA 10mM
- Acetic acid 11.4% (V/V)
- pH (with Trizma base and acetic acid) 7.6

Collagen solution

- dH_2O 179ml
- Acetic acid 1ml
- Sterilisation with 0.2µm filtration
- Collagen from calf skin (see consumables) 20ml
- stored at 4°C

Cardiomyocyte buffer solution (CBS)

- 1M NaCl 116.35ml
- 1M HEPES 20ml
- 1M NaH2PO4 1ml
- 1M KCl 5.366ml
- 833mM MgSO4 1ml
- 1M NaOH 8.28ml
- dH_2O 848ml
- pH 7.4

Cardiomyocyte enzyme solution (CES)

- CBS 99ml
- 1M glucose 540µl
- Collagenase type II (240U/mg) 33.3mg
- Sterilisation with 0.2µm filtration
- 2.5% trypsin added after first isolation step 1% (V/V)

Cardiomyocyte growth medium (CGM)

- Dulbecco's modified Eagle's medium (DMEM) 340ml
- Medium 199 85ml
- Foetal bovine serum (FBS) 25ml
- Horse serum (HS) 50ml
- Penicillin/Streptomycin 100x 5ml
- stored at 4°C

Immorto-CGM (ICGM)

- Dulbecco's modified Eagle's medium (DMEM) 340ml
- Medium 199 85ml
- FBS 25ml
- Horse serum (HS) 50ml
- Penicillin/Streptomycin 100x 5ml
- Interferon-gamma (IFNγ) 15µg
- stored at 4°C

Serum-free CGM (SFCGM)

- Dulbecco's modified Eagle's medium (DMEM) 34ml
- Medium 199 8.5ml
- Penicillin/Streptomycin 100x 430µl
- stored at 4°C

Serum starvation CGM (SSCGM)

- Dulbecco's modified Eagle's medium (DMEM) 34ml
- Medium 199 8.5ml
- FBS 430µl
- Penicillin/Streptomycin 100x 430µl

Protein lysis buffer (PLB)

- RIPA buffer 10ml
- cOmplete ULTRA protease inhibitor tablet 1

Tris-Acetate protein running buffer

- Tris-Acetate protein running buffer (20x) 35ml
- dH_2O 665ml

MES SDS protein running buffer

- MES SDS protein running buffer (20x) 35ml
- dH_2O 665ml

Western blotting protein transfer buffer (PTB)

- Trizma base 3.03g
- Glycine 14.4g
- dH_2O to 800ml
- Methanol 200ml

5% milk powder blocking solution

- Instant dried skimmed milk powder 5g
- TBST to 100ml

PVDF membrane protein stripping buffer

- 50mM β-mercaptoethanol 7.8ml
- SDS 20g
- Trizma base 7.57g

2.3 Genotyping Mice

All animal work was conducted following Home Office guidelines under Professor Volker Straub's project licence 60/4137. C57BL/10 (BL/10), C57BL/10ScSn-Dmd^{mdx} (mdx) and CBA;B10-Tg(H2K^{b}-tsA58)6Kio/Crl (Immorto) mouse breeders were set up by Elizabeth Greally (laboratory technician) personal licence number 60/10222).

Ear biopsies were taken from progeny of Immorto mice bred with BL/10 or mdx mice and collected into 1.5ml microfuge tubes. 500μl of DNA digestion buffer and 12.5μ of proteinase K (0.5mg/ml final concentration) were added to the biopsies. These samples were incubated at 50°C overnight.

The following day 700μl of phenol/chloroform/isoamyl alcohol was added to each sample, the tubes were shaken until white precipitate formed and centrifuged at 14,000rpm for 5min. The top phase solution from each sample was transferred into fresh microfuge tubes and 1ml of ethanol was added. The tubes were inverted and incubated at -80°C for 2h. Post-incubation the samples were centrifuged at 4°C, 14,000rpm for 20min. Supernatants were discarded and pellets resuspended in 1ml of 75% ethanol 25% dH_2O solution, precooled to -20°C. Tubes were centrifuged at 4°C, 8,000rpm for 5min, the supernatant discarded and pellets air dried at ambient temperature for 30min. Dried pellets were resuspended in 100μl TE buffer and DNA quantified with a spectrophotometer and the samples were stored at -20°C.

A mastermix was prepared of polymerase chain reaction (PCR) reagents following the manufacturers' guidelines (Qiagen HotStarTaq DNA polymerase), using the following primers (Yang et al., 2000):
Immorto forward primer: 5'-AGC GCT TGT GTC GCC ATT GTA TTC-3'
Immorto reverse primer: 5'-GTC ACA CCA CAG AAG TAA GGT TCC-3'

The thermocycler was programmed according to the polymerase kit instructions with the annealing temperature set to 58°C. A 1% (w/V) agarose solution in TAE buffer was prepared and microwaved to solubilise the agarose. The solution was allowed to cool, 10μl of SafeView stain was added, the gel poured and allowed to set for 30min. 2μl of loading dye was added to 10μl of each sample's PCR product and loaded onto the agarose gel along with a 1kbp reference DNA ladder. The DNA samples were

separated according to size with a constant voltage electrical current for 30min at 100V. The gel was imaged under ultraviolet light. Mouse DNA positive for the Immorto construct yielded a 1kbp band.

2.4 Collagen-coated Plastics

Tissue culture vessels used for plating and pre-plating cardiomyocytes were all coated with collagen. Collagen solution was added at 100µl/cm^2 and incubated at ambient temperature overnight. On the following day the collagen solution was collected and stored at 4°C along with the remaining stock solution. Coated tissue culture vessels were washed with autoclaved distilled water and left to air dry in a class 2 tissue culture cabinet. Once dried, the coated vessels were stored in a sterile plastic bag at ambient temperature for up to a month.

2.5 Cardiomyocyte Isolation

The cardiomyocyte isolation protocol was adapted from Sreejit et al. (2008) with help and advice from Rita Barresi (lecturer) and Alison Blain (post doctoral associate). Female mice from breeding pairs and trios were checked for post-coital vaginal plugs daily. Mice were sacrificed using Schedule I procedures, embryos at gestation period day 17.5 (E17.5) extracted and stunned by incubating in CBS on a petri dish on ice. A mid-abdominal incision was made with dissection scissors and the heart removed after bisecting the rib cage along the cranio-caudal axis. All collected hearts from one litter were collected into one 15ml centrifugation tube containing 8ml of CBS, pre-cooled on ice (figure 2.1).

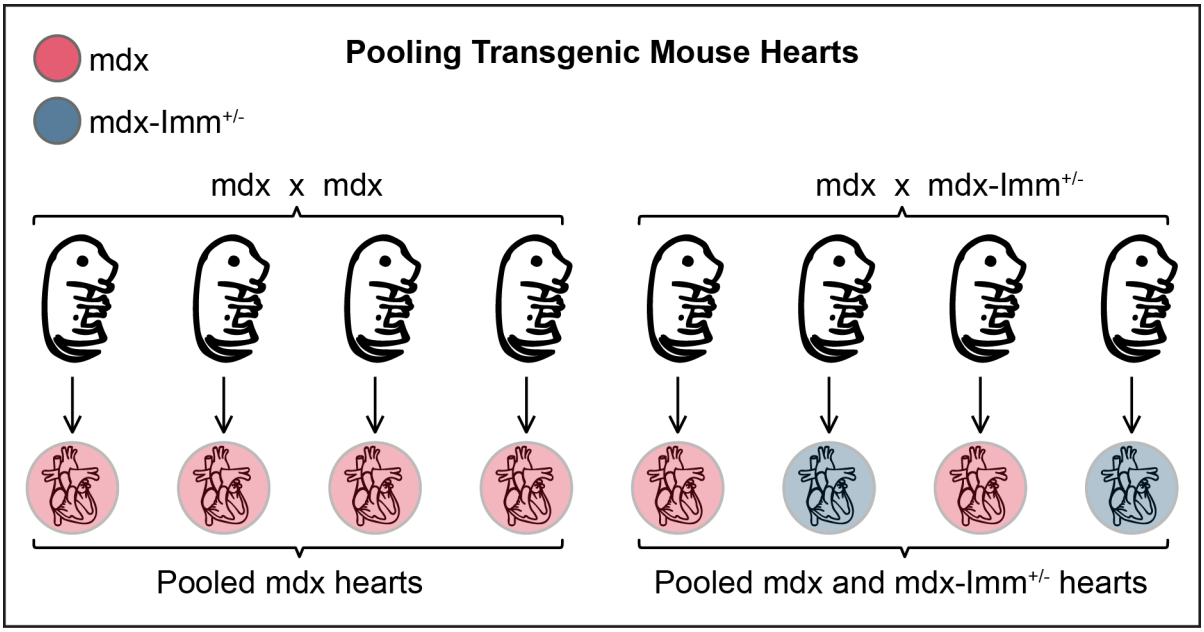

Figure 2.1. Pooling transgenic mouse embryo hearts for isolating cardiomyocytes. Hearts from male and female E17.5 embryos from dystrophic mdx mouse breeding pairs were pooled. When mdx and mdx-Immorto$^{+/-}$ mice were crossed all hearts from both male and female E17.5 embryos were still pooled together regardless of their genotype.

The hearts were decanted into a 6mm petri dish, gently squeezed with forceps to eject any residual coagulated blood, major vessels were removed and remaining cardiac tissue cut into ~1mm sized fragments with a scalpel. All fragments were subsequently transferred into 5ml CES without trypsin in a 15ml centrifugation tube, pre-heated to 37°C. The fragments were incubated at 37°C for 10min in a water bath. Tissue fragments were allowed to settle to the bottom of the tube and the supernatant was discarded.

8ml of fresh CES with trypsin was added to the heart fragments and the tube incubated for 30min at 37°C, tilting the tube ten times every 10min. At the end of the incubation the tissue fragments were allowed to settle to the bottom of the tube and the supernatant was collected into a 15ml centrifugation tube, which was subsequently centrifuged at 1,200g for 5min at 15°C. Fresh CES was added to the heart fragments and the tube incubated in the water bath at 37°C. The centrifuged supernatant was discarded and the recovered cell pellet resuspended in 1ml of FBS, pre-cooled to 4°C. The resuspended cells were stored at 4°C for the duration of the subsequent incubation steps.

The residual tissue was subjected to another three 30min incubation steps following the procedure above, or more in case all the tissue had not dissociated, with collecting the cell-rich CES at the end of each step into the tube containing cells in FBS. Following the centrifugation at the end of the last incubation step the cell pellet was resuspended in 5ml of CGM. The cell suspension was transferred into a collagen-coated T25 flask and incubated at 37°C for 2h. The cardiomyocyte-enriched supernatant CGM was collected and centrifuged at 1,200g for 5min at 23°C. The pelleted cells were counted on a haemocytometer and dispensed onto collagen-coated tissue culture vessels as required in experiments described below.

Isolated primary cardiomyocytes were dispensed onto 24-well plates. For immunocytochemistry the density was ~$1.2x10^5$ cells per well. For RNA and protein extraction the cell density was ~$5x10^5$. Plated cells were cultured at 37°C for 48h under 5% CO_2, followed by two PBS washes and serum starvation with either SFCGM or SSCGM for 24h to 96h at 37°C under 5% CO_2. A specific number of wells were designated for PFA-fixing, or RNA and protein extraction at each of the five serum starvation time-points: 0h, 24h, 48h, 72h and 96h.

2.6 Immunocytochemistry (ICC)

Following the initial 48h incubation in CGM, all cells were washed twice with PBS for 5min and the growth medium and wash solution discarded. The wells containing cells for 24h, 48h, 72h and 96h of serum starvation were replenished with SFCGM or SSCGM and incubated at 37°C. The control 0h cells were PFA-fixed as described below. The medium on cells remaining in culture was discarded and replenished every 24h with further wells fixed for staining.

Cells were fixed at the appropriate time-point with 4% PFA in PBS over 15min at ambient temperature in a fume cupboard, followed by one 5min wash with PBS and a second 5min wash with TBS. The cardiomyocytes were subsequently permeabilised with 0.5% Triton X-100 in TBS for 10min, followed by two 5min washes with TBS. 4% BSA (w/V) in TBST was used for blocking non-specific protein binding sites, at room temperature for 30min. Primary antibodies were dissolved in 4% BSA in TBST and staining was performed overnight at 4°C. The cells were washed twice for 5min with TBST. The secondary antibody and phalloidin (both prepared in 4% BSA in TBST) staining was conducted at room temperature for 1h, protected from light. The

cardiomyocytes were washed twice for 5min with TBST and once with dH_2O, mounted under a coverslip in Vectashield medium containing DAPI and stored at 4°C until imaging. Antibody dilutions for ICC were: mouse monoclonal anti-α-actinin 1/800, mouse monoclonal MANDRA1 anti-dystrophin 1/100, rabbit polyclonal ab15277 anti-dystrophin 1/100, Alexa Fluor 488 goat anti-mouse 1/500, Alexa Fluor 594 goat anti-mouse 1/500, Alexa Fluor 488 goat anti-rabbit 488 1/500. Oregon Green conjugated phalloidin and Alexa Fluor 594 conjugated phalloidin were both used at a 1/300 dilution.

2.7 Microscopy

Imaging was conducted on two microscopes. The Zeiss Axiovert 200M inverted fluorescence microscope was used with an AxioCam HRc monochrome camera, FS 02 (DAPI), FS 13 (GFP) and FS15 (Rhodamine) filters, Plan Apocromat 10x/0.45 Ph1 and LD Achroplan 20x/0.4 Ph2 objectives. The Nikon A1R confocal microscope was used with a Galvano scanner, Nikon DS-Fi2 RGB camera, 405nm, 488nm and 561nm lasers, as well as CFI Plan Fluor DL-10x F/0.3 Ph1 and CFI Plan Apochromat VC 20x/0.75 objectives. All exposure times, gain and offset values were maintained at constant values within each compared set of experiments.

Original zvi and nd2 files were retained with the relevant metadata. Prior to image analysis, brightness and contrast adjustments were only made on images acquired on the Zeiss Axiovert 200M to aid visual detection of α-actinin positive cell boundaries. For display purposes look-up table (LUT) adjustments were made on images and kept constant in all compared images within a sample set. Scale bars were added onto final versions of exported tiff images. All figures with ICC images have been compiled using Adobe Photoshop CC and Adobe Illustrator CC, without any alterations performed in Adobe software.

2.8 Area and Volume Measurements

All area measurements of images acquired on the Zeiss Axiovert 200M were either acquired manually on the AxioVision LE software or automated on the Perkin Elmer Volocity software package, using the signal from the α-actinin antibody binding. All volume measurements were obtained by three-dimensional construction of Z-stack images, acquired on the Nikon A1R confocal microscope and analysed in Volocity in the same manner as area measurements. In both cases cells that were multinucleated or touching the side of the image were removed from the final analysed dataset. Area measurements of images acquired on the Nikon A1R confocal microscope were performed using the Nikon Elements 4.0 software area recognition function employing the α-actinin channel signal. All area and volume measurements were transferred to Microsoft Excel for statistical and further analyses.

2.9 RNA Extraction

BL/10 and mdx adult mouse hearts were surgically removed from mice culled following Schedule 1 procedures. The hearts were chopped with a scalpel and tissue pieces homogenised with disposable tissue ruptor probes in 1ml Trizol. Cells in the tissue homogenate were lysed by aspiration with insulin syringes. A 300μl aliquot of each cell lysate in Trizol was transferred into individual screw-cap microfuge tubes and used for subsequent RNA extraction steps. The remaining 700μl of each sample was stored at -80°C.

300μl aliquots of heart tissue samples in Trizol were centrifuged at 12,000rpm for 10min at 4°C and the supernatant transferred to a fresh screw-cap 1.5ml microfuge tube. 50μl of chloroform was added to each sample and the tubes were vigorously shaken for 15s, incubated at ambient temperature for 3min and centrifuged at 12,000rpm for 15min at 4°C. The resulting transparent top layer was transferred to a fresh 1.5ml microfuge tube and RNA was precipitated by mixing with 125μl of isopropanol over a 10min incubation at ambient temperature. The samples were subsequently centrifuged at 12,000rpm for 10min at 4°C and the supernatant discarded. The RNA pellet was washed with 1ml 70% ethanol in DEPC-treated H_2O, pre-cooled to -20°C. The tubes were centrifuged at 7,500g for 5min at 4°C, the supernatant discarded and the pellet air-dried at ambient temperature. The RNA

pellets were ultimately dissolved in 25µl of DEPC-treated H_2O and quantified using the Agilent 2100 Bioanalyzer or the Thermo NanoDrop 8000 following manufacturers' instructions.

For qRT-PCR experiments the Qiagen RNeasy Mini Kit was used to extract RNA from cardiomyocytes, following manufacturers' guidelines. At the relevant collection time-point, cardiomyocytes in 24-well plates were washed twice with PBS and scraped in 350µl buffer RLT, supplemented with 350µl of 70% ethanol in 30% nuclease-free water (NFW) and the 700µl sample solution was transferred to spin columns. The columns were centrifuged at 8,000g for 15sec, flow-through discarded, 350µl of buffer RW1 added to each column, followed by centrifugation at 8,000g for 15sec. The flow-through was discarded and an on-column 15min DNase I digest performed. 350µl of buffer RW1 was added to each column, a centrifugation step at 8,000g for 15sec performed and the flow-through discarded. 500µl of buffer RPE was added and the columns centrifuged at 8,000g for 15sec. Another 500µl RPE was added and the columns centrifuged at 8,000g for 2min. The flow-through was discarded and columns were dried by centrifugation at maximum speed for 1min. The columns were placed into 1.5ml screw-cap microfuge tubes and two elution steps with 15µl of NFW and 15sec centrifugation at 8,000g performed. BL/10 and mdx heart tissue RNA samples obtained through Trizol extraction were also purified and DNase-treated using the RNeasy Mini Kit. All RNA samples were quantified using a NanoDrop spectrophotometer and samples were stored at -80°C.

2.10 RNA-Seq

For whole transcriptome shotgun sequencing (RNA-Seq) experiments, at the relevant collection time-point, cardiomyocytes in 24-well plates were washed twice with PBS and detached in 300µl of Trizol using a cell-scraper. Detached cells were transferred into an individual 1.5ml screw-cap microfuge tubes. Three biological replicates of BL/10 and mdx cardiomyocytes at each time-point were shipped to Helmut Blum's research group in Munich for RNA-Seq.

Andrea Klanner (laboratory technician in Helmut Blum's research group) performed all the following steps in this paragraph. RNA was extracted using Zymo-Spin columns, quantification and quality control performed using an Agilent Bioanalyzer 2100. The lowest RNA integrity number (RIN) value accepted for continuing

experiments with a given sample was 8. RNA samples were DNase-treated, reverse transcriptase first strand and second strand cDNA synthesised. The DNA samples were fragmented with sonication, purification performed with RNAClean XP beads, adapter sequences ligated with an Encore Complete RNA-Seq Library Multiplexing system for multiplexing the samples and strand-specific sequence libraries generated.

Stefan Krebs (post doctoral associate in Helmut Blum's research group) split the samples intro two groups, and each group was analysed on a separate Illumina HiSeq 1500 lane. Duplicate single-end reads were obtained and used for subsequent bioinformatics analyses.

The sequencing results were uploaded onto a Galaxy next-generation sequencing analysis web portal (Goecks et al., 2010). Samples were demultiplexed based on their reference sequences and fastqsanger files analysed with FastQC for quality control (Andrews, 2010) in a Linux server using command-line execution. TopHat2 (Kim et al., 2013) was used in Galaxy to generate bam files by aligning sequences from each sample to the University of California Santa Cruz mm10 reference mouse genome, specifying the single-end data type and using gene annotations. The latter was required to ensure short intronic inclusions were not causing sequences to be dropped. Generated bam files were viewed in the Integrative Genomics Viewer (IGV) software (Thorvaldsdóttir et al., 2013) and used with HTSeq (Anders et al., 2015) to determine individual counts of gene expression for each sample. The feature type parameter in HTSeq analysis was set to "exon", the attribute used as feature identification was set to "gene_id", the detection mode was set to "intersection-strict" and strand specificity was selected. Alex Graf (post doctoral associate in Helmut Blum's research group) wrote an R programming environment (Ihaka & Gentleman, 1996) script for differential gene expression analysis with DeSeq2 package (Love et al., 2014).

Databases of differentially expressed gene comparisons and individual gene fold change (FC) values were generated in Microsoft Excel. Gene ontology was performed with DAVID (Huang et al., 2009) online software and Genomatix software, which uses a PubMed literature mining algorithm for associating genes with each other (Frisch et al., 2009).

2.11 Quantitative Real-time PCR

Reverse transcription PCR (RT-PCR) was performed with an Applied Biosystems kit, following manufacturers' guidelines. 10μl of each sample RNA template was added to 10μl of the reaction mastermix for reverse transcribing cDNA. The thermocycler was programmed as follows:

Step 1) 10min at 25°C;

Step 2) 120min at 37°C;

Step 3) 5min at 85°C;

Step 4) ∞ at 4°C.

Samples were diluted with 180μl of NFW, split into 50μl aliquots and stored at -20°C.

Quantitative real-time PCR (qRT-PCR) primers were designed using the National Centre for Biotechnology Information (NCBI) gene search tool for each mouse gene of interest (GOI), picking the NM number link followed from the mRNA and protein section and primers picked based on the following parameters: PCR product size 80-200bp, minimal primer melting temperature (Tm) 58°C, maximal Tm 62°C, maximal ΔTm 2°C and compulsion of exon junction span. Primer pairs were chosen based on their GC content (preferably between 50%-60%) and the ΔTm less than 1°C where possible. Genes, such as *Vegfa* had several transcript and primers were designed to pick up all of the possible transcripts. Predesigned housekeeping gene (HKG) *Tpt1* and *Hsp90ab1* primers were ordered from Sigma-Aldrich. Sequences of these primer pairs were not reported here due to proprietary reasons. The following designed primer sequences were ordered from Eurofins MWG Biotech:

Pln forward primer: 5'-TTC CTG CGT AAC AGG TCT CC-3'

Pln reverse primer: 5'-TCC ATT ATG CCA GGA AGG CA-3'

Ndufa4l2 forward primer: 5'-AAA AGA CAC CCT GGG CTC ATC-3'

Ndufa4l2 reverse primer: 5'-GGC AAG TCG CAG CAA GTA GA-3'

Fmod forward primer: 5'-AGG GCA ACA GGA TCA ATG AGT T-3'

Fmod reverse primer: 5'-GAT CTC GTT CCC ATC CAG GC-3'

Nppb forward primer: 5'-TTT GGG CTG TAA CGC ACT GA-3'

Nppb reverse primer: 5'-AAG AGA CCC AGG CAG AGT CA-3'

Vegfa forward primer: 5'-TGC GGA TCA AAC CTC ACC AA-3'

Vegfa reverse primer: 5'-TGT CTT TCT TTG GTC TGC ATT CAC-3'

Primer specificity was tested using end-point PCR (following protocol described in section 2.3) for their amplification capacity from DNase-treated RNA samples and reverse transcribed cDNA templates. Only those primer pairs were used for qRT-PCR, which showed a product at the correct anticipated size and only in the cDNA amplification reactions.

The SYBR Green JumpStart Taq ReadyMix kit was used for qRT-PCR experiments following manufacturers' instructions. All samples were run in triplicate and with 4 biological replicates for each mdx and BL/10 cardiomyocyte serum starvation time-point. BL/10 and mdx heart tissue cDNA samples were also run in triplicate for each gene of interest and the HKGs. Each reaction consisted on 5μl of SYBR green mix, 0.1μl ROX reference dye, 1.9μl of NFW, 0.5μl of the forward primer, 0.5μl of the reverse primer and 2μl of cDNA template or NFW for no-template control (NTC) reactions. Reactions were prepared in a class 1 laminar flow cabinet and loaded onto 384-well plates, sealed with an adhesive sheet and centrifuged for 2min at 1,200g. The QuantStudio7 thermocycler was set up to quantify primer product amplification using the ΔΔCt method, SYBR green chemistry and ROX as the reference dye. The following cycling parameters were used:
Step 1) 2min 50°C for sample warm-up;
Step 2) 10min 95°C for initial denaturation;
Step 3) 15sec 95°C for denaturation;
Step 4) 1min 60°C for annealing, extension and fluorescence reads;
Step 5) Steps 3 and 4 were repeated for another 39 cycles, followed by:
Step 6) 15sec 95°C for denaturation
Step 7) 1min 60°C for annealing and extension
Step 8) gradual temperature rise at 0.05°C/sec to 95°C for melt curve data.

Results were recorded on the QuantStudio software and exported into Microsoft Excel for further analyses. Samples with more than one melt curve peak were omitted. Outliers were omitted in sample triplicates where the Ct value range exceeded 1 unit. Remaining Ct values were used to calculate the mean value for each individual sample and gene combination. ΔCt values for each sample were determined by subtracting the HKG Ct value from the GOI Ct value, i.e. ΔCt = Ct(GOI) – Ct(HKG). ΔΔCt was determined for each sample comparison within a set

of ΔCt expression values for a GOI, i.e. ΔΔCt = ΔCt(sample1) – ΔCt(sample2). These values represented the relative expression base 2 logarithm fold change (Log_2FC) in gene expression. Nominal relative expression FC values were determined by taking 2 to the power of the negative value of ΔΔCt, i.e. $FC = 2^{-\Delta\Delta Ct}$.

Tpt1 and *Hsp90ab1* primer pair efficiency was assessed by creating a scatter plot of their qRT-PCR Ct values against the base 10 logarithm (Log_{10}) of the sample RNA concentrations reverse transcribed for cDNA template. A line of best fit was drawn in Microsoft Excel and the slope of the curve used to calculate efficiency values from the following formula: Efficiency=10^(-1/slope).

2.12 Protein Extraction and Western Blotting

Cardiomyocytes in a 24-well plate well were washed twice with PBS. The cells were detached in 100µl of PLB with a cell-scraper and transferred into a 1.5ml screw-cap microfuge tube. The well was washed with a further 100µl of PLB and the wash solution also transferred to the same microfuge tube. The cells were lysed by repeated aspiration with an insulin syringe. Protein content of primary cells was quantified using the BCA assay, following manufacturer's instructions and diluting samples as appropriate to obtain absorbance values lying within the range of the standard curve. A standard curve was plotted alongside each quantification experiment with standards run in triplicate and samples in duplicate. Two absorbance values were obtained at both 550nm and 570nm on a Thermo Multiskan Ascent or Tecan plate reader. The raw absorbance values were normalised against a baseline average from three blank wells (containing PLB) and the measures from both wavelengths combined to get an average absorbance value for each standard and sample. The standard curve was plotted as a linear line of best fit on a scatter plot of average standard measures in Microsoft Excel. The standard curve equation was subsequently employed to determine the protein content of each sample by incorporating sample average absorbance measures into the equation. Samples were stored at -20°C.

Samples were diluted to the lowest concentration in a given set of samples by adding the appropriate volume of lysis buffer, LDS and reducing agent. Pre-cast protein gels were run at 180V for 1h. Bis-Tris NuPAGE polyacrylamide gels and MES buffer with SeeBlue Plus2 standards were used when proteins smaller than 100kDa were

detected. Tris-Acetate NuPAGE gels and buffers with HiMark standards were used for detecting proteins larger than 100kDa. Protein was transferred from polyacrylamide gels onto PVDF membranes at 350mA constant current in a Bio-Rad transfer chamber, surrounded by ice, filled with 1l PTB pre-cooled to -10°C. SimplyBlue SafeStain was used as a protein loading control. Gels were washed three times with dH_2O, stained with SimplyBlue SafeStain for 1h and washed twice with dH_2O, for 1h and overnight at ambient temperature, prior to imaging.

Membranes were washed three times for 10min with TBST, blocked with 5% milk powder in TBST for 1h at ambient temperature and probed with primary antibodies dissolved in 5% milk powder in TBST overnight at 4°C. The membranes were subsequently washed three times with TBST and probed with secondary antibodies conjugated with horseradish peroxidase (HRP) dissolved in 5% milk powder in TBST for 1h at ambient temperature. Before imaging the membranes were washed three times for 10min with TBST. Antibody dilutions for Western blotting were: mouse monoclonal NCL-DYS1 anti-dystrophin 1/250, mouse monoclonal anti-phospho-ERK 1/100, rabbit polyclonal anti-β_1AR 1/100, mouse monoclonal Hamlet anti-dysferlin 1/100, rabbit polyclonal ab15277 anti-dystrophin 1/300, HRP conjugated goat anti-mouse 1/5,000 and HRP conjugated goat anti-rabbit 1/5,000.

Immunoblotted membranes were then transferred into a darkroom, incubated with ECL kit reagents for 5min at ambient temperature and light signal detected in a developer cassette using X-ray film.

Protein band intensities were quantified in ImageJ software by drawing identical rectangular regions of interest around bands in each lane, then drawing a line under the signal peak and using the wand tool to determine the area under the peak curve. Microsoft Excel was used to normalise protein expression to skeletal myosin heavy chain (MHC) signal on SimplyBlue stained polyacrylamide gel images. The average intensity of all MHC bands was determined and expression coefficient values determined by dividing individual band intensities to the average value. The coefficients were used to multiply protein of interest band intensities to get a normalised vale. Contrast and brightness of bands was only adjusted for display purposes in Adobe Photoshop CC, but not before image analysis had been completed.

2.13 Drug Treatment

Cardiomyocyte drug treatment was started at 24h of serum starvation and the therapeutic agent was replenished in SFCGM or SSCGM (specified in each individual experiment in results chapters) every 24h until the final time-point at 96h of serum starvation. Only 96h serum starvation time-point cells were analysed. The drugs trialled for their ability to reduce hypertrophy of embryonic mdx mouse cardiomyocytes were prednisolone 10μg/ml – 100pg/ml, dexamethasone 20μg/ml – 200ng/ml (ethanol was required as the solubilising vehicle at 2% - 0.02% V/V corresponding to the drug concentrations), metoprolol 5mg/ml – 5ng/ml, captopril 100μg/ml – 10ng/ml, A804598 1μM – 10pM (dimethyl sulfoxide was required as the solubilising vehicle at either 0.01% - 0.0000001% or 10% - 0.00001% V/V corresponding to the drug concentrations and specified in section 5.7) and KR-33028 100μM – 10nM (polyethylene glycol was required as the solubilising vehicle at 0.85% - 0.000085% V/V corresponding to the drug concentrations).

2.14 Viral Transduction

A set of AAV vectors with naturally occurring serotypes expressing eGFP as a marker gene or μDys as a therapeutic gene were kindly provided by Dr. Oliver Müller from Heidelberg University.

Cells were transduced at various multiplicity of infection (MOI) values, calculated as added viral genomes (vg) divided by the number of cells in culture. The appropriate volume of AAV stock solution was added directly to mdx cardiomyocytes in SSCGM medium at 24h of serum starvation. Cells were cultured for a further 72h to the final 96h of serum starvation time-point and then analysed for either size or protein expression with assays detailed above or as follows.

AAV construct expression in mdx cardiomyocytes transduced with eGFP was determined by imaging live cells in culture on the AxioVert200 every 24h up to 120h post-transduction. End-point eGFP expression was analysed in ICC stained cells imaged on the Nikon A1R and analysed in Nikon Elements 4.0. AAV construct expression in mdx cardiomyocytes transduced with μDys was determined by imaging ICC stained cells on the Nikon A1R and analysed in Nikon Elements 4.0, or by protein extraction and Western blotting with the ab15277 anti-dystrophin antibody.

2.15 Statistical Analyses

All statistical analyses were performed in Microsoft Excel. Area and volume measurement comparisons from samples were analysed with one-tail Student's t-test. Skedasticity of data was assessed by Levene's test, conducted by determining the absolute difference from sample average for each data point within the sample, followed by a single factor analysis of variance comparison of the absolute difference measures of the two samples of interest. The heteroskedasticity cut-off in Levene's test was p-value<0.05. Student's test significance cut-offs were p-value<0.05 for *, p-value<0.01 for ** and p-value<0.001 for ***. Standard deviation of the sample was used to calculate standard error of the mean values, used for displaying error bars in figures.

For cardiomyocyte size correlation testing, BL/10 and mdx cardiomyocyte average area measurements were plotted against corresponding volume measurements at given time-points of serum starvation. The line of best fit was drawn and the r^2 values displayed. The Pearson's product-moment correlation coefficients (r values) from BL/10 and mdx datasets were compared against critical r values at three levels of significance: 5%, 1% and 0.1%. The null hypothesis for the test stated that there was no difference between the samples. Determined r values that were lower than the critical r values allowed rejecting the null-hypothesis at the given level of significance and therefore concluding that there was significant correlation between the two compared parameters.

Pearson's chi-squared test was used to assess differences in protein expression between BL/10 and mdx cardiomyocytes. Normalised BL/10 protein sample band intensities were used as the expected values and mdx cardiomyocyte results as the observed values.

Chapter 3. Modelling Cardiac Hypertrophy with Primary Dystrophic Mouse Cardiomyocytes.

3.1 Introduction and Aims

Many DMD rescue and treatment therapies currently in clinical trials do not target the heart as successfully as skeletal muscle. This is due to cardiac tissue being much harder to access, and there is also a limited number of *in vitro* cardiac models for testing therapies in early development. For example, phosphodiesterase 5 (PDE5) inhibitors (Witting et al., 2014; Leung et al., 2014), peptide-conjugated phosporodiamidate morpholino oligonucleotides (PPMO) (Betts et al., 2015) and improved viral vectors (Schinkel et al., 2012) could all have been tested with an *in vitro* functional cardiomyocyte-based assay before costly *in vivo* experiments were commenced.

This chapter aims to develop a technology that models the phenotype of the dystrophic heart in an *in vitro* setting.

3.2 Overview of the Technique

In preliminary experiments, cardiomyocytes were isolated from the hearts of mouse neonates and embryos using an enzyme digest. Cell yields from embryo-derived cardiomyocytes were higher and those cardiomyocytes adhered more readily to collagen-coated plastic. Though the heart predominantly consists of contracting cardiomyocytes (Maillet et al., 2013), the resulting primary cell population was found to be heterogeneous, with fibroblast-like cells being the main other cell type. Pre-plating on collagen-coated vessels for 2h was identified as the necessary duration to enrich the primary cell population for cardiomyocytes prior to plating the cells remaining in suspension onto multi-well dishes (collaborative experiment with MRes student Tom Slater).

A standardised protocol was designed, where hearts were collected from embryos at day 17.5 of gestation (E17.5). This fixed age of mouse embryos was chosen because by E15 the murine heart is fully formed (S. M. Evans et al., 2010; Xin et al., 2013) and the chosen timing within the gestation time-line was not too close to the female birthing. A fixed day was chosen to obtain consistent results, minimising any potential effect of remaining developmental changes during rodent gestation. A time-line in figure 3.1 depicts the standardised experimental set-up. Cardiomyocytes were initially cultured for 48h in high-serum CGM, followed by a change to serum starvation CGM and maintained in culture for a further 96h. Cells were fed with fresh medium every 24h.

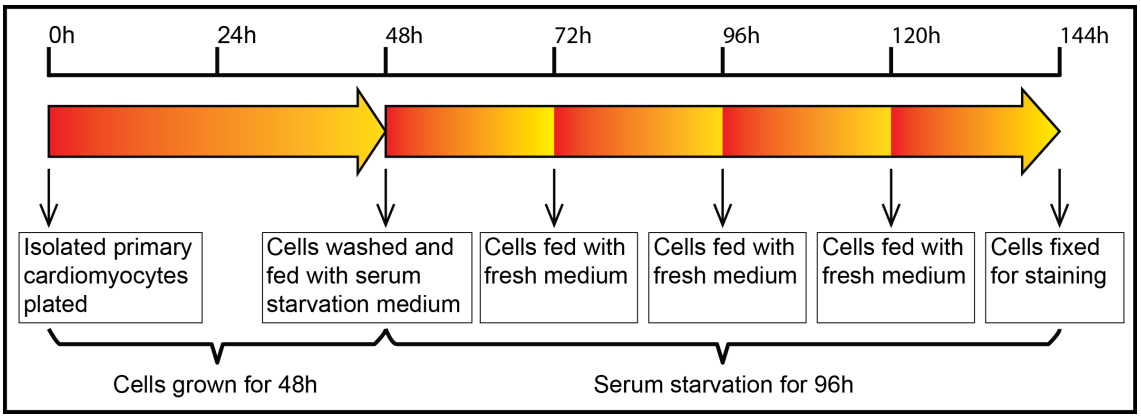

Figure 3.1. The time-course of primary cardiomyocyte culture. Cells were cultured in serum-rich growth medium for 48h, followed by serum starvation for 96h, feeding with fresh medium every 24h.

3.3 Establishing a Conditionally Immortalised Primary Cardiomyocyte Cell-line

The number of cells obtained from each experiment was dependent on the number of embryos in the contributing litter. Consequently, experimental design was limited by litter size as well as subject to biological variability between litters. This puts limitations on the ability to replicate observations due to the large numbers of timed matings required to overcome variability. As an alternative to the culture of primary cardiomyocytes, attempts were made to isolate an immortalised cardiomyocyte cell line culture. Transgenic CBA;B10-Tg(H2K^{b}-tsA58)6Kio/Crl mice (Immorto mice) on a C57BL/10 background (Jat et al., 1991) harbour a construct expressed under the mouse major histocompatibility complex class I gene (*H2K^{b}*) promoter expressing tsA58, a thermolabile mutant region of the simian vacuolating virus 40 (SV40) large and small tumour antigens, capable of immortalising cells under permissive conditions *in vitro*. These two permissive conditions were induction of tsA58 construct expression by supplementing culture medium with interferon gamma (IFNγ), which induces expression from the *H2K^{b}* gene promoter, and incubation at 33°C to avoid inactivation of the thermolabile tumour antigen products.

A visual summary of mouse breeding procedures to obtain mdx-Immorto mice is presented in figure 3.2. Parental transgenic male C57BL/10::H-2K^{b}-tsA58$^{+/-}$ (BL/10-Immorto) mice, heterozygous for the Immorto construct, were crossed with homozygous C57BL/10ScSn-Dmd^{mdx} (mdx) female mice. Half of the resulting F1 male progeny in the litters from this crossing were hemizygous for the dystrophin mutation and also hemizygous for the conditionally immortalising construct (mdx^{-}::H-2K^{b}-tsA58$^{+/-}$). Presence of the tsA58 construct was confirmed with PCR and agarose gel electrophoresis (figure 3.3), where DNA from mice heterozygous for the Immorto-construct yielded a 1kbp band. The F1 male mdx-Immorto mice were subsequently crossed with homozygous mdx female mice. The resulting F2 progeny were all homozygous for the mdx mutation and, in proportions predicted by Mendelian genetics, half the litters were heterozygous for the presence of tsA58 (figure 3.2).

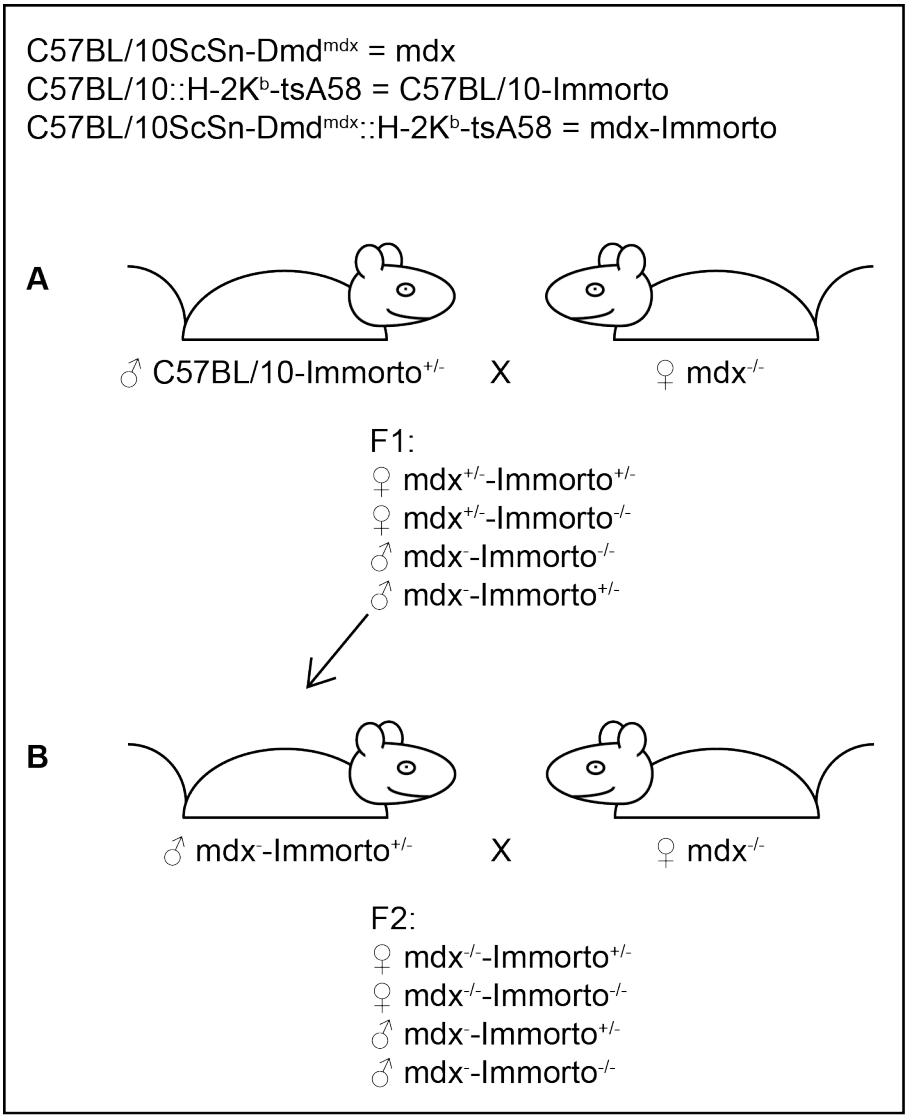

Figure 3.2. Deriving mdx::H-2K^{b}-tsA58$^{+/-}$ mice. Male heterozygous Immorto-mice on the BL/10 background were crossed with mdx female mice. Male F1 progeny heterozygous Immorto-mice were crossed again with mdx female mice and F2 embryos used for cardiomyocyte isolation.

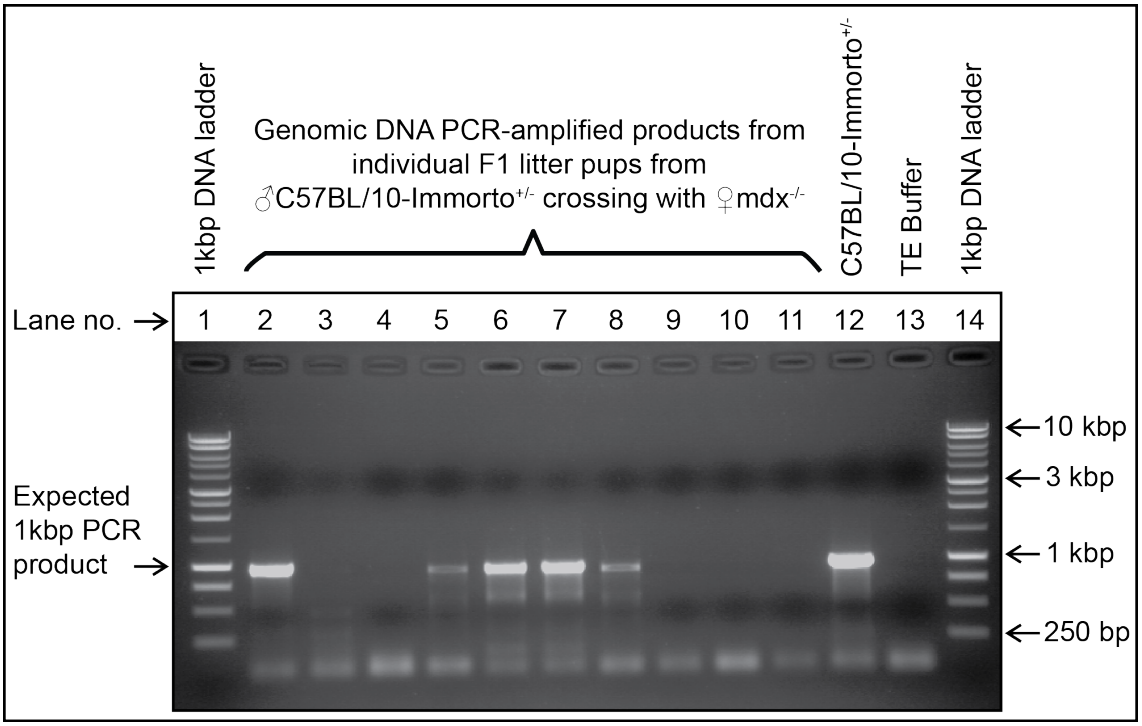

Figure 3.3. Genotyping for the Immorto-construct with agarose gel electrophoresis. PCR products of gDNA obtained from F1 progeny in lanes 2-11. Samples in lanes 2, 5, 6, 7 and 8 yielded a 1kbp DNA band, which indicates those pups were heterozygous for the immorto construct. Lanes 1 and 14 were loaded with a marker containing DNA fragments of known size, lane 12 contains gDNA from a C57BL/10-Immorto$^{+/-}$ mouse as a positive control for amplification of the 1kbp product and lane 13 contains TEB as a no-template negative control.

Cardiomyocytes were isolated from the embryos of pregnant mice from the F2 generation (figure 3.2). 50% of the embryos derived from these crosses were predicted to be Immorto positive, conditionally immortalised cardiomyocytes were anticipated to outgrow tsA58-negative cells and therefore embryo genotyping was unnecessary. These cells were maintained and observed to proliferate when cultured under permissive conditions. However, once trypsinised, the cardiomyocytes failed to re-adhere to collagen-coated tissue culture vessels.

Furthermore, fibroblasts proliferated much more rapidly and were readherent post-passaging, overgrowing cardiomyocytes over time. For these reasons clonal selection was never performed on mdx-Immorto cardiomyocytes and consequently, each subsequent experiment is restricted to cells obtained from the hearts of one biological litter with a mixed population of male and female embryonic cells.

3.4 Inducing a Hypertrophic Response in Primary Embryonic Cardiomyocytes with SFCGM

3.4.1 Area of Primary Cardiomyocytes Cultured in SFCGM

An endothelin-driven hypertrophic response was initially envisaged as a necessity when designing the experimental model (Fujioka et al., 2006). Cardiomyocytes were cultured in CGM for 48h, at which point the medium was discarded, cells were rinsed with PBS and fresh serum-free CGM (SFCGM) added. Knocking out serum content from the medium avoided any undesirable inhibitory effects or interactions stemming from factors in sera interacting with endothelin and treatment compounds. Initial 24h incubation prior to drug treatment was included in the protocol to allow cardiomyocytes to get accustomed to serum starvation. Observations of untreated mdx cardiomyocytes revealed that by 96h of serum starvation the cells were spontaneously becoming larger and it was therefore hypothesised that serum starvation triggered a hypertrophic response in mdx cardiomyocytes even without pharmacological induction of hypertrophy, illustrated in figure 3.4.

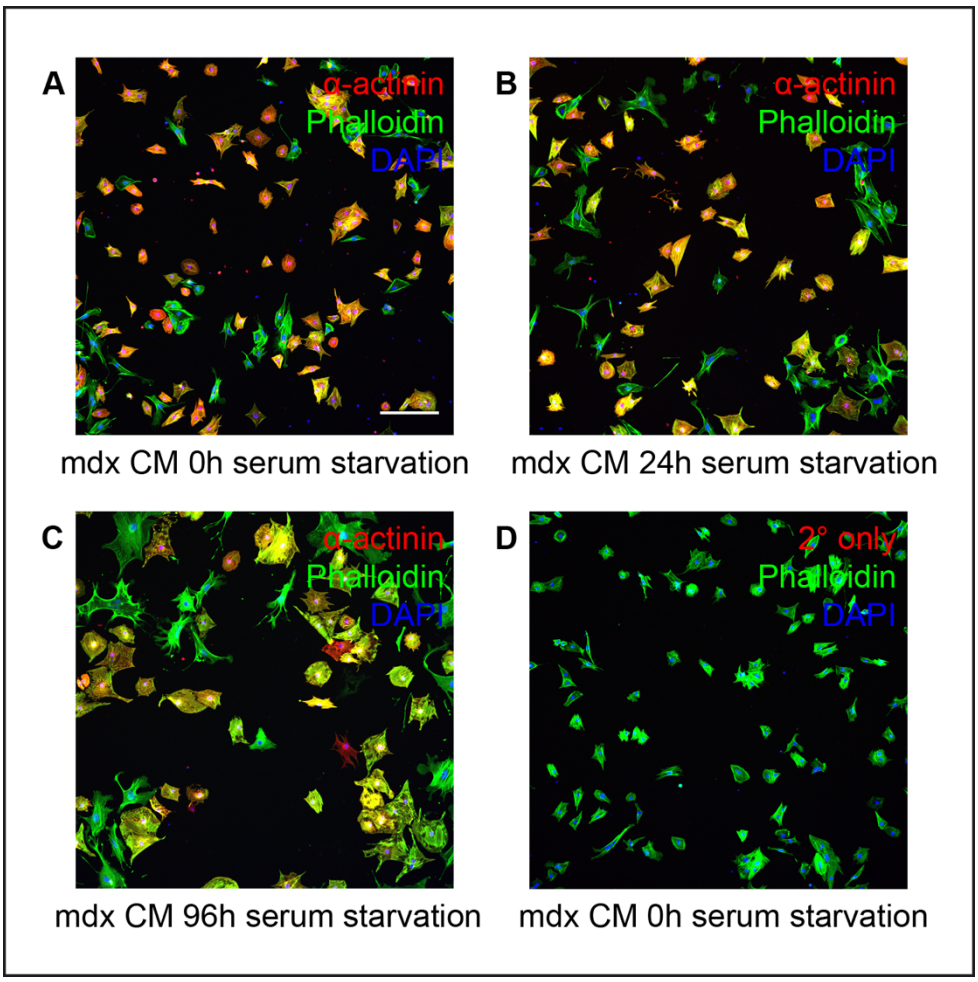

Figure 3.4. Primary mdx mouse E17.5-derived cardiomyocytes. Cells at 0h (A), 24h (B) and 96h (C) of serum starvation were stained with Alexa Fluor 594 and α-actinin in red, as well as Oregon Green-conjugated phalloidin in green and nuclei with DAPI in blue. Phalloidin binds to F-actin in the cytoskeleton of all cells, whereas α-actinin specifically stains muscle cells, here cardiomyocytes. Panel D depicts cells at 0h serum starvation and is a no primary anti-α-actinin antibody control. The scale bar in panel A represents 200μm and applies to all four panels.

Primary cardiomyocyte size was quantified by manually measuring the area of cells expressing α-actinin, detected by immunocytochemistry (ICC), in AxioVision LE software (figure 3.5). These area measurements were subsequently compared to BL/10 control mouse cardiomyocyte data, also obtained following the same serum starvation and ICC protocol.

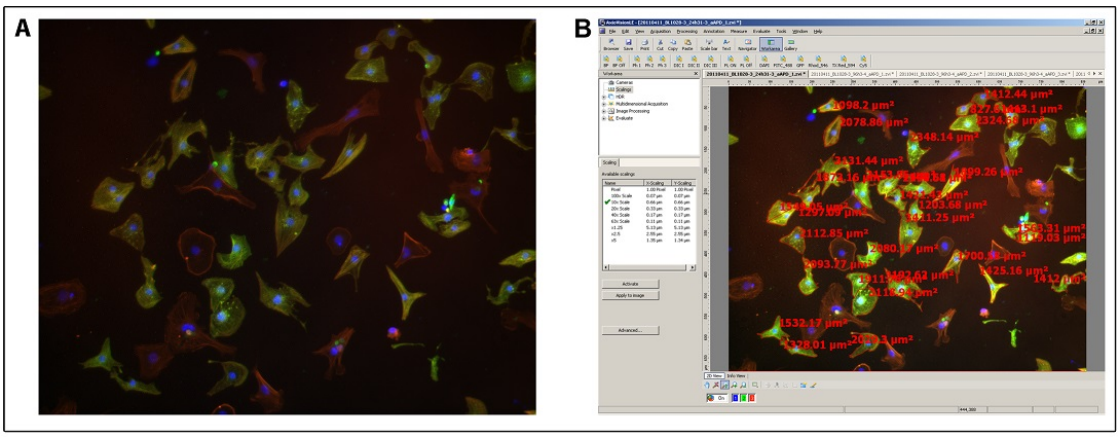

Figure 3.5. Measuring the area of cardiomyocytes with AxioVision LE software. (A) Cardiomyocytes were stained with α-actinin in green; all cells were stained with Alexa Fluor 594-conjugated phalloidin in red and nuclei with DAPI in blue. (B) Area measurements of cells were obtained by manually drawing boundaries around individual cells.

The results of this comparison between mdx and BL/10 cardiomyocytes are illustrated in figure 3.6. Cardiomyocytes from BL/10 mouse embryos did not show a distinguishable response to serum starvation, with the difference in the change in average size at 24h and 96h of serum starvation being a slight reduction of 45μm^2 from 1,890μm^2 at 24h (n=32) to 1,845μm^2 by 96h (n= 24; p=0.426; one-tailed Student's t-test). Cardiomyocytes from mdx embryos increased in size by 1.5-fold between 24h and 96h of serum starvation, gaining 835μm^2 in area from 1,659μm^2 at 24h (n=20) to 2,494μm^2 at the 96h time-point (n=23; p<0.05; one-tailed Student's t-test).

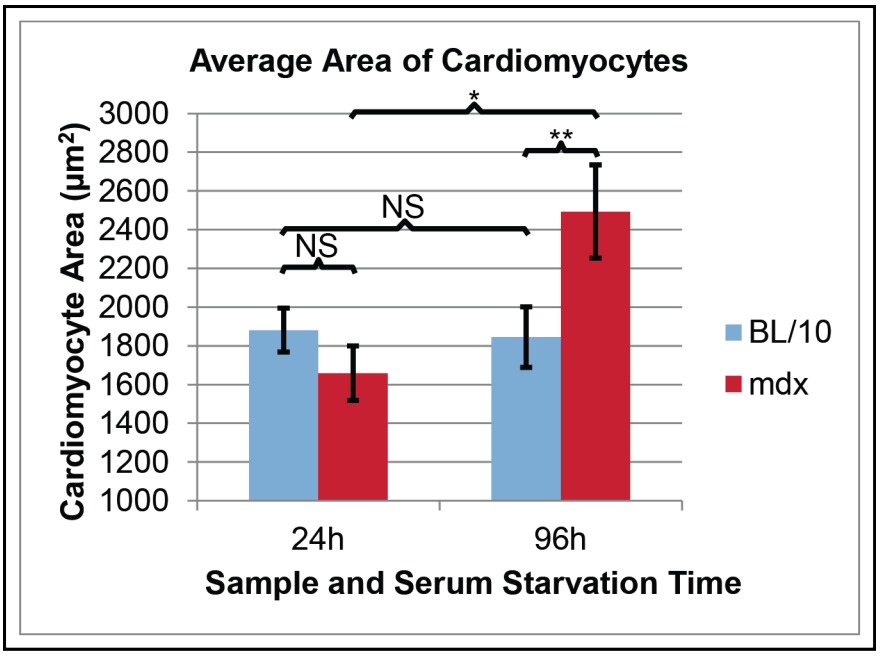

Figure 3.6. The average area of cardiomyocytes at 24h and 96h of serum starvation with SFCGM. BL/10 cardiomyocytes were unaffected by serum starvation, in contrast to mdx cardiomyocytes, which showed a significantly increase in size. Error bars represent SEM, NS = Non-significant, * = p-value<0.05, ** = p-value<0.01.

Levene's test revealed that three of the four possible comparisons between the data sets could be considered homoskedastic (with indistinguishable variance; table 3.1) while one comparison was heteroskedastic (with higher variance observed in the mdx 96h cell areas than mdx 24h). Student's t-test analyses appropriate to variance type revealed that mdx cardiomyocytes serum starved for 96h were significantly larger than both, mdx cells serum starved for 24h (p<0.05) and BL/10 cells serum starved for 96h (p<0.01). The difference between BL/10 24h and 96h serum starved cells, as well as BL/10 24h and mdx 24h serum starved cells did not reach statistical significance. These comparisons are summarised in table 3.1.

Comparison	Levene's Test p-value	Variance	t-test p-value
BL/10 24h v BL/10 96h	0.6669	Equal	0.4257
mdx 24h v mdx 96h	0.0346	Unequal	0.0025
BL/10 24h v mdx 24h	0.9100	Equal	0.1125
BL/10 96h v mdx 96h	0.0793	Equal	0.0139

Table 3.1. Statistical analyses of serum starved cardiomyocyte area measurements. A Levene's test p-value less than 0.05 was necessary to deem variance between two sets of data unequal. Skedasticity of data was taken into consideration when performing t-tests.

Binning data points into 1,000μm^2 data ranges and calculating the percentage of cells falling within the boundaries of each bin demonstrated a shift in cell area distribution in mdx cardiomyocyte size from 24h to 96h of serum starvation. This distribution shift was not replicated in control cells, thus confirming the physiological difference in dystrophic cardiomyocytes (figure 3.7).

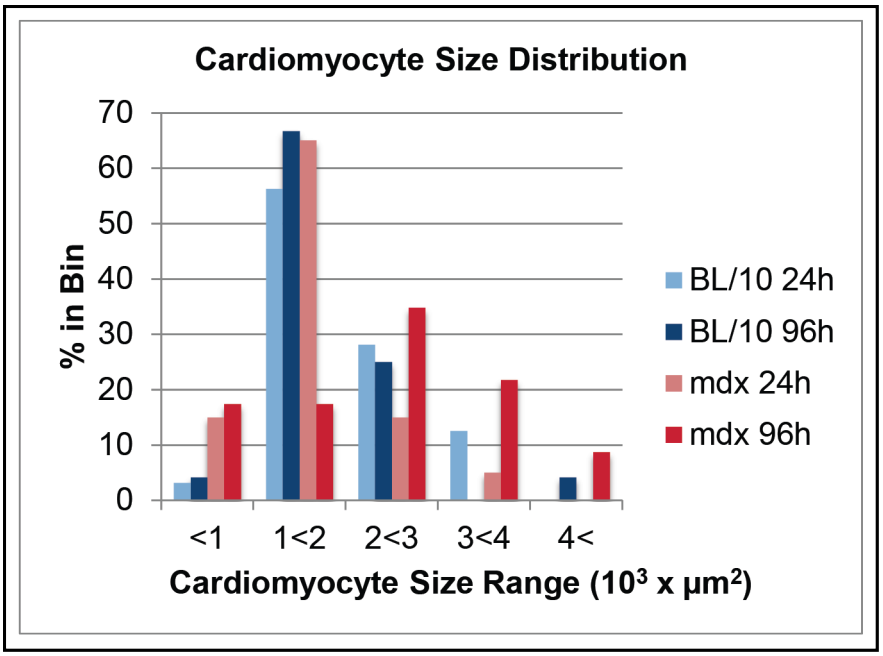

Figure 3.7. Distribution of control and dystrophic cardiomyocyte area. A distribution shift from smaller to larger cells across the serum starvation time course was evident in mdx E17.5-derived cardiomyocytes, but not in control cells.

3.4.2 Volume of Cardiomyocytes Cultured in SFCGM

BL/10 and mdx cardiomyocyte volume was subsequently quantified by acquiring Z-stack images on a confocal microscope and semi-automated analysis using Volocity software to measure cell volume. A screen-shot of the software masking cells positive for α-actinin staining is shown in figure 3.8.

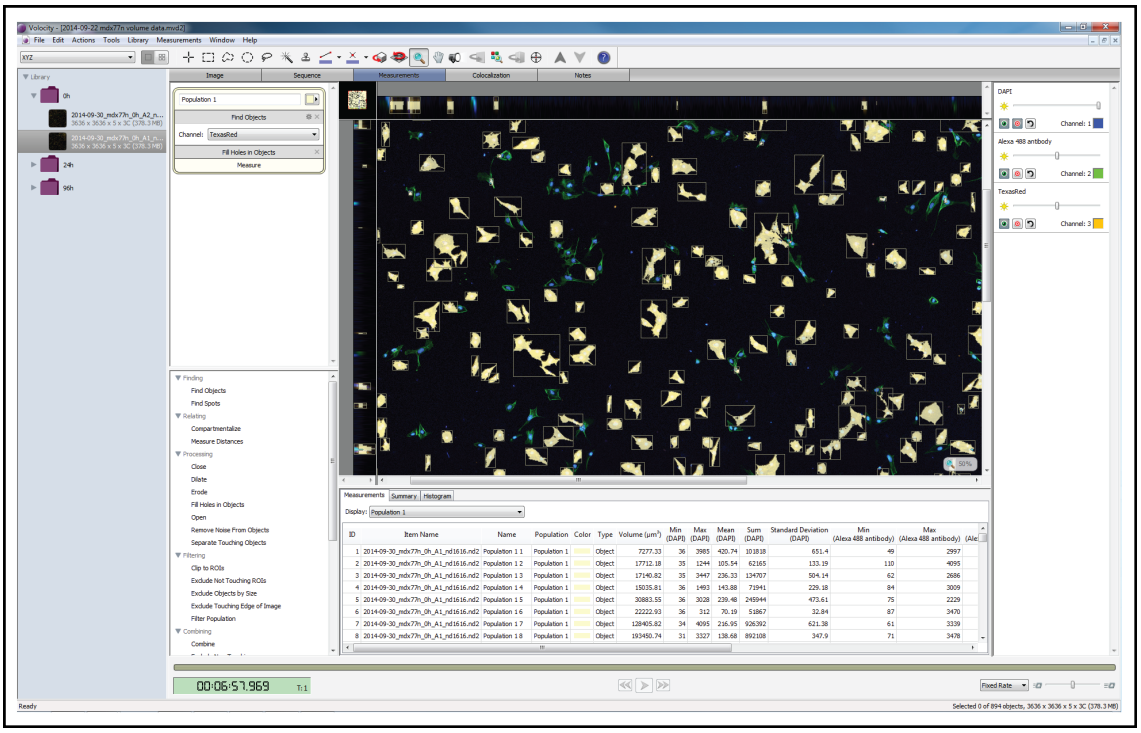

Figure 3.8. Using Volocity for semi-automatic quantification of cardiomyocyte volume. Cardiomyocytes were automatically detected by the “Find Objects” function, detecting cells positive for α-actinin staining, here gated in beige. Objects with multiple or no nuclei, detected with DAPI staining in blue, were manually omitted from the analysis.

Three litters of BL/10 embryos and six litters of mdx embryos were used to isolate primary cardiomyocytes. BSc student Sophie Wright performed the volume measurement image analysis for one of the BL/10 and three of the mdx biological replicates. MRes student Elizabeth Roberts performed the volume analysis for the other two BL/10 and three of the mdx biological replicates. Figure 3.9 depicts the mean value of average volume measurements from biological replicates at each time-point. BL/10 cardiomyocytes were on average 5,000μm^3 smaller by 96h serum starvation (49,000μm^3; n=1,174), in comparison to the 24h time-point (54,000μm^3; n=1,223), but this reduction was non-significant. Cardiomyocytes from mdx embryos,

on the other hand, became significantly larger, by 1.5-fold from an average of 66,000μm^3 at 24h of serum starvation (n=1,197) to 99,000μm^3 by 96h of serum starvation (n=826). All of the compared datasets showed equal variance when compared with Levene's test set to $p<0.05$ stringency for detecting heteroskedasticity. The statistical data from volume measurements are summarised in table 3.2 and the results complemented the hypertrophic trends displayed in area measurements.

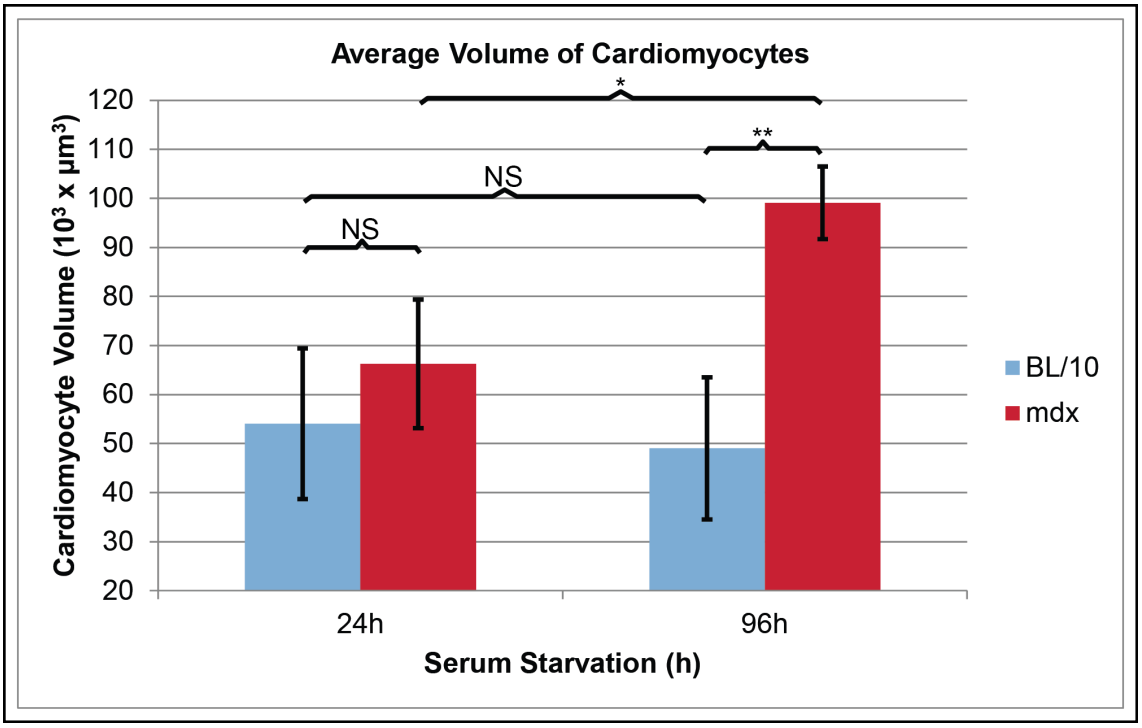

Figure 3.9. The average volume of cardiomyocytes at 24h and 96h of serum starvation with SFCGM. BL/10 cardiomyocyte volume remained similar throughout the course of serum starvation, contrary to mdx cardiomyocytes, which significantly gained in size. Error bars represent SEM, NS = Non-significant, * = p-value<0.05, ** = p-value<0.01.

Comparison	Levene's Test p-value	Variance	t-test p-value
BL/10 24h v BL/10 96h	0.9591	Equal	0.4116
mdx 24h v mdx 96h	0.2832	Equal	0.0270
BL/10 24h v mdx 24h	0.7029	Equal	0.2955
BL/10 96h v mdx 96h	0.4472	Equal	0.0051

Table 3.2. Statistical analyses of serum starved cardiomyocyte volume measurement comparisons. A Levene's test p-value of less than 0.05 was necessary to deem variance between two sets of data unequal. Skedasticity of data was taken into consideration when performing t-tests.

3.5 Dystrophin Expression in E17.5-derived Cardiomyocytes

It was subsequently determined whether dystrophin was expressed in E17.5-derived BL/10 cardiomyocytes. ICC was used to detect dystrophin protein expression with MANDRA1 and ab15277 primary antibodies. MANDRA1 detection gave inconsistent results with very faint halos of positive signal surrounding some cells, shown with an arrow in panel A of figure 3.10. This signal was obtained only at maximum laser power and 130V gain and most of the cardiomyocytes showed punctate cytosolic signal, which was also faintly visible as a background hue in the no-primary-antibody control image, taken with the same acquisition parameters (panel B in figure 3.10). Contrastingly, the ab15277 antibody only detected nuclear signal for dystrophin, both in cardiomyocytes (also positive for α-actinin signal), shown with arrowheads in panel C of figure 3.10, and other cells (negative for α-actinin signal) in the same culture sample. The nuclear signal, however, was not present in the control sample (panel D, figure 3.10).

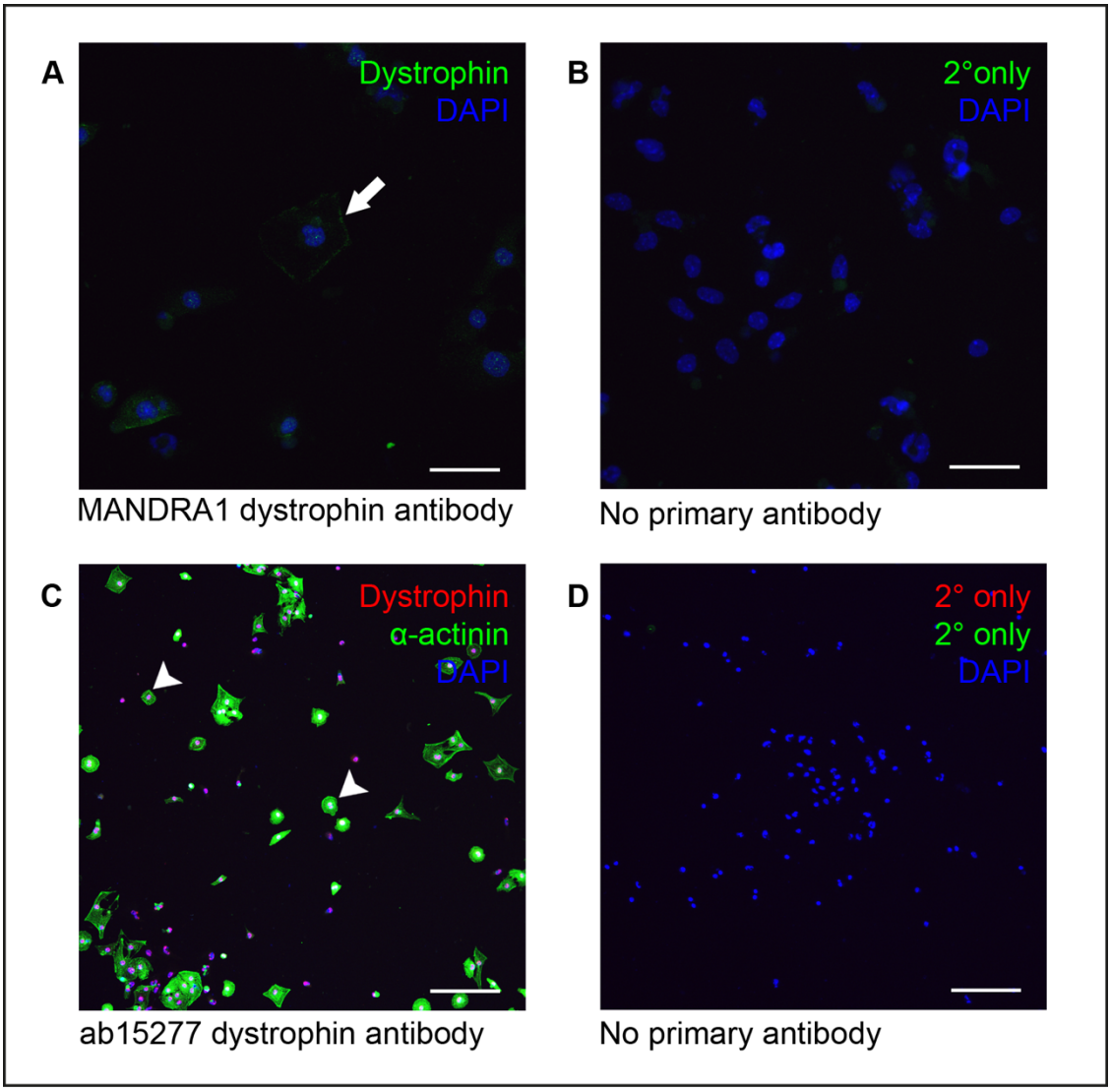

Figure 3.10. Dystrophin signal in ICC images of BL/10 E17.5 cardiomyocytes. Panel A shows dystrophin expression in BL/10 cardiomyocytes with MANDRA1 signal in green, indicated by an arrow, and panel B is the corresponding control image where no primary antibody was used. Panel C depicts cardiomyocytes stained with α-actinin, in green, and ab15277 signal for dystrophin in red. The arrowheads indicate cardiomyocytes showing nuclear dystrophin staining, not present in the corresponding no primary antibody control image in panel D. Nuclei were detected in all images with DAPI, in blue. In panels A and B scale bars represent 50μm, in panels C and D 200μm.

Protein lysates from mdx and BL/10 cardiomyocytes at each 24h time-point of serum starvation were prepared. A total of five samples (0h, 24h, 48h, 72h and 96h following serum starvation) for BL/10 and mdx were used for a Western blot, probed with NCL-Dys1 primary antibody against dystrophin. The results are shown in figure 3.11 and confirm that BL/10 E17.5-derived cardiomyocytes express dystrophin throughout the serum starvation time-course, whilst mdx cardiomyocyte lysates do not show detectable dystrophin protein.

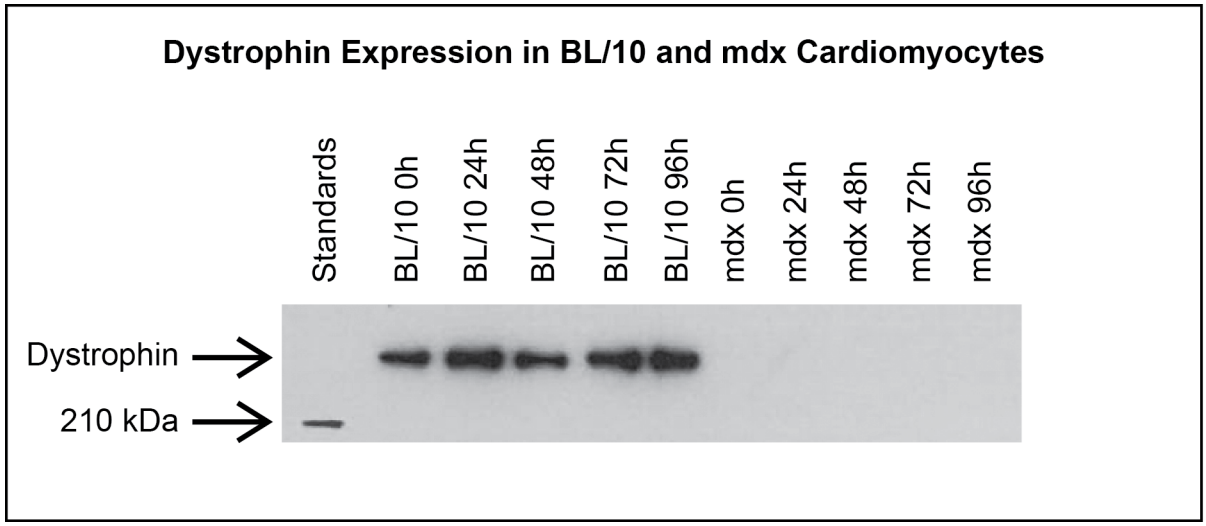

Figure 3.11. Detecting dystrophin expression by Western blotting with NCL-Dys1 antibody. The expected band for dystrophin (in the range of 427kDa) is visible in BL/10 cardiomyocyte samples in lanes 2-6 and remains constant throughout the serum starvation time-course, whilst mdx E17.5-derived cardiomyocytes (lanes 7-11) do not express dystrophin.

3.6 Optimising Image Analysis and Serum Starvation

3.6.1 Semi-automation of Area Measurements Using Nikon Elements Software

The analysis process of cardiomyocyte ICC images was semi-automated with NIS-Elements software. A signal threshold-based algorithm automatically drew boundaries around events targeted by a mouse cursor click. The area from within each boundary was identified and added to a list of measured data reads in the software, illustrated in figure 3.12.

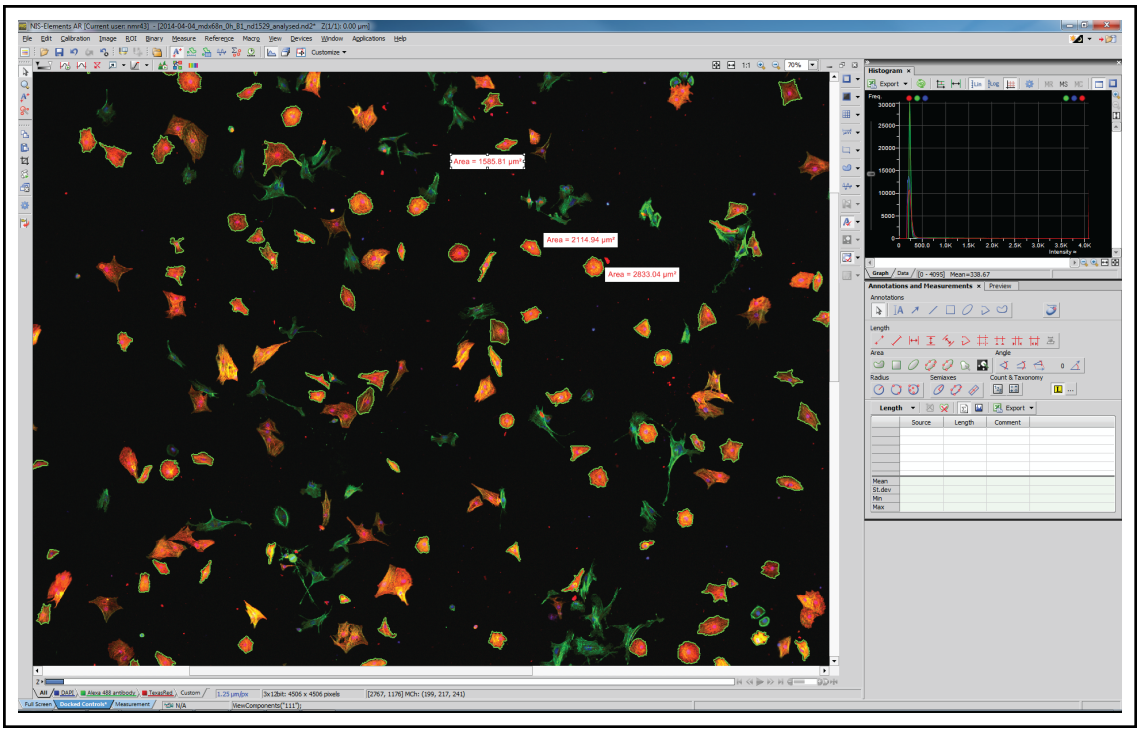

Figure 3.12. Semi-automation of cardiomyocyte area measurements with NIS-Elements. Cardiomyocytes were identified by α-actinin signal, here in red. The area of each cell was automatically detected in response to a mouse cursor click that triggered a boundary to be drawn around the cell, based on a signal threshold algorithm. For illustrative purposes three information boxes have been included in this figure, showing individual area reads for the adjacent cardiomyocytes.

3.6.2 Effect of 1% FBS in Serum Starvation Medium

It was observed that a large number of cells were not surviving the complete omission of serum from CGM. The medium was therefore supplemented with 1% FBS (SSCGM) in order to improve cell survival. Comparative BL/10 and mdx cardiomyocyte culture experiments were performed to assess the effect of complete serum omission (SFCGM), low serum presence (SSCGM) and full serum (CGM) on cell size, summarised in figure 3.13 and the corresponding statistics shown in table 3.3. The BL/10 cell isolation yielded enough cardiomyocytes to investigate intermediate time-points for all three culture media (0h n=1,231; SFCGM 24h n=353, 48h n=98, 72h n=62, 96h n=76; SSCGM 24h n=531, 48h n=321, 72h n=806, 96h n=523; CGM 24h n=775, 48h n=305, 72h n=550, 96h n=418), whilst there were only enough mdx cardiomyocytes for 0h, 24h and 96h samples (0h n=226; SFCGM 24h n=154, 96h n=85; SSCGM 24h n=159, 96h n=78; CGM 24h n=175, 96h n=94).

Both control and dystrophic cardiomyocytes showed improved survival and became larger when cultured in NCGM, accompanied by an increased fibroblast expansion rate and presence in the culture. This outcome was anticipated, due to increased availability of nutrients. However, for the purpose of therapeutic treatment of the hypertrophic response seen in mdx cardiomyocytes, serum presence was undesirable and culture in the full serum content CGM was not further explored. 96h culture in SSCGM caused BL/10 cardiomyocytes to become significantly larger than equivalent cells cultured in SFCGM. In contrast, mdx cardiomyocyte survival was improved, but the average area was not significantly affected by changing SFCGM to SSCGM. However, the BL/10 cardiomyocytes cultured in this experiment also showed a significant increase in area when serum starved both with SFCGM and SSCGM, a finding that contradicted with previous results.

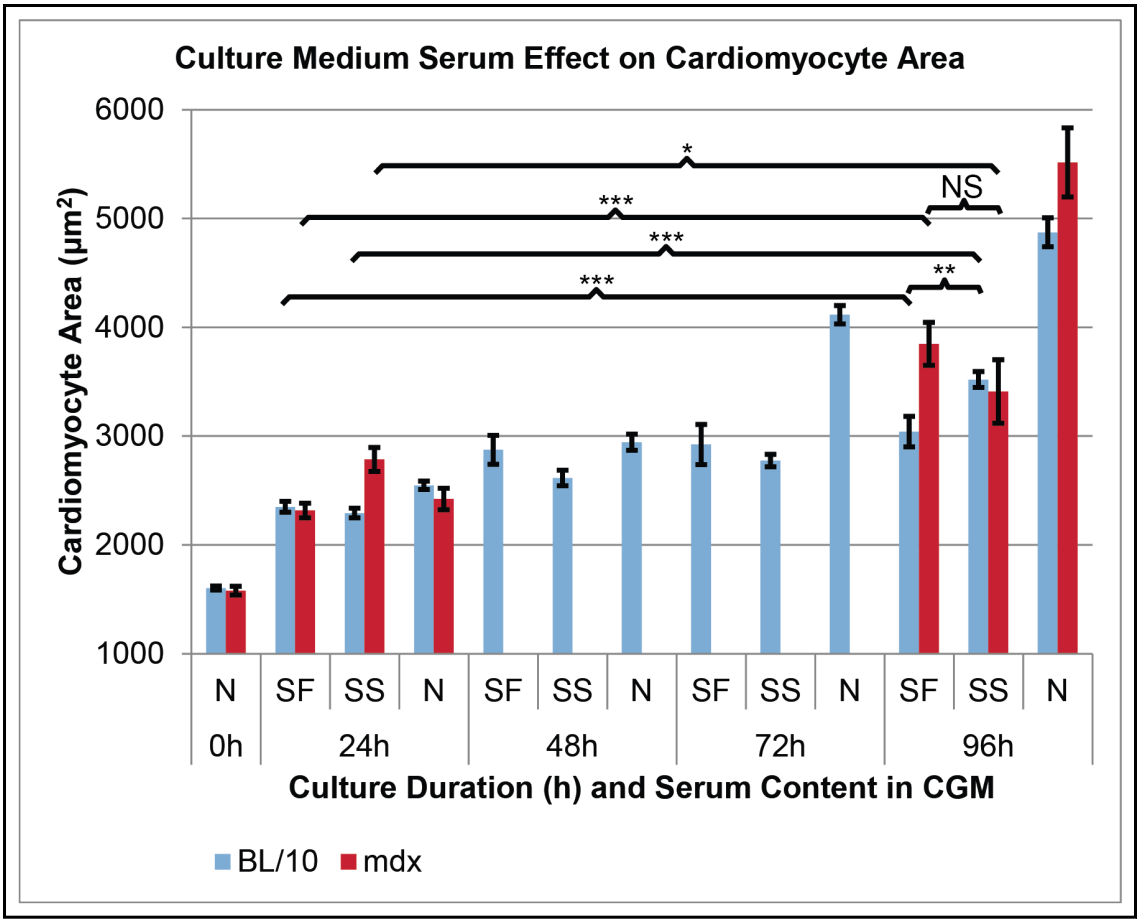

Figure 3.13. The effect of CGM serum content on cardiomyocyte area. BL/10 and mdx cardiomyocytes were cultured in SFCGM (SF), SSCGM (SS) and CGM (N) and the average area value determined. Error bars represent SEM, NS = Non-significant, * = p-value<0.05, ** = p-value<0.01, *** = p-value<0.001.

Comparison	Levene's Test p-value	Variance	t-test p-value
BL/10 24h SF v BL/10 96h SF	0.000465839	Unequal	5.96575E-06
BL/10 24h SS v BL/10 96h SS	2.03152E-16	Unequal	9.16971E-43
mdx 24h SF v mdx 96h SF	9.15309E-09	Unequal	2.28576E-11
mdx 24h SS v mdx 96h SS	8.65022E-05	Unequal	0.023747657
BL/10 96h SF v BL/10 96h SS	0.051731444	Equal	0.007666469
mdx 96h SF v mdx 96h SS	0.084729137	Equal	0.104364852

Table 3.3. Statistical analyses of cultured cardiomyocyte area measurements. A Levene's test p-value less than 0.05 was necessary to deem variance between two sets of data unequal. Skedasticity of data was taken into consideration when performing t-tests.

3.6.3 Correlation between Cardiomyocyte Area and Volume Data

A study was conducted to verify the correlation between volume and area measurements in C57BL/10 and mdx cardiomyocytes. Six biological replicates of BL/10 cardiomyocytes at each of the five time-points – 0h (n_{Area}=3,513; n_{Vol}=2,071), 24h (n_{Area}=2,594; n_{Vol}=1,467), 48h (n_{Area}=2,263; n_{Vol}=1,252), 72h (n_{Area}=1,788; n_{Vol}=1,111) and 96h (n_{Area}=1,704; n_{Vol}=1,034) of serum starvation – were used to acquire area and volume measurements. Three biological replicates of mdx cardiomyocyte populations at each of three time-points – 0h (n_{Area}=1,698; n_{Vol}=1,593), 24h (n_{Area}=1,946; n_{Vol}=1,224) and 96h (n_{Area}=2,249; n_{Vol}=1,028) of serum starvation – and two replicates at each of 48h (n_{Area}=541; n_{Vol}=344) and 72h (n_{Area}=493; n_{Vol}=288) of serum starvation time-points were used for acquiring volume and area measurements. Comparative analysis of Pearson product-moment correlation coefficients from SSCGM-treated control and dystrophic cells demonstrated a significant correlation between area and volume measurements in dystrophic, but not control cardiomyocytes (figure 3.14 and table 3.4).

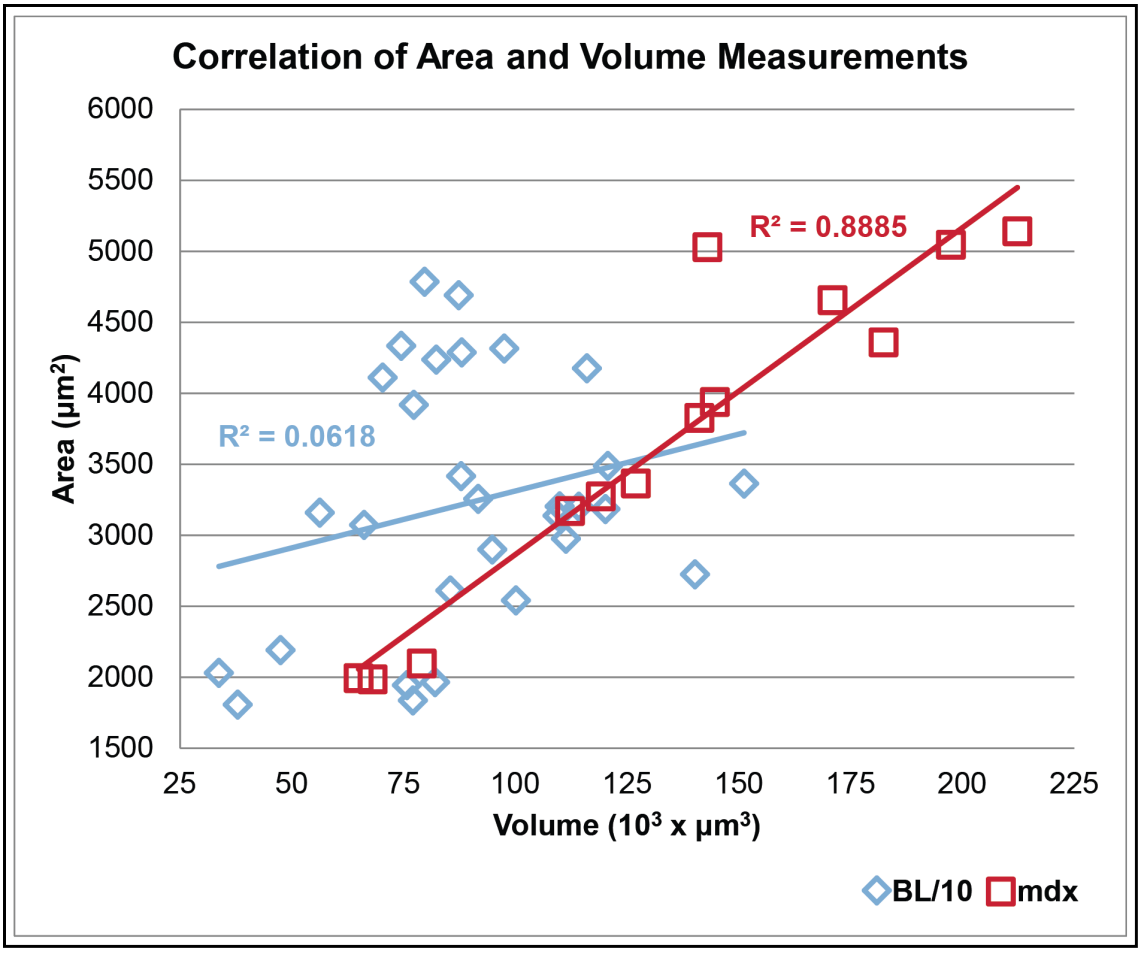

Figure 3.14. Correlation plots of BL/10 and mdx cardiomyocyte area against volume. Each data point represents the area and volume measurements from the same sample at a specific time-point of serum starvation.

Sample	r Value	n	Deg. of F	Critical Value p=0.05	Critical Value p=0.01	Critical Value p=0.001	Reject H_0
mdx	0.94262	13	11	0.553	0.684	0.801	Yes
BL/10	0.24869	30	28	0.361	0.463	0.57	No

Table 3.4. Correlation analysis of BL/10 and mdx cardiomyocyte area and volume measurements. Dystrophic mdx cardiomyocytes showed a significant positive correlation between increasing area and volume measurements ($p<0.001$=***). Control BL/10 cardiomyocytes showed a statistically non-significant positive correlation between size increases in area and volume measurements.

3.7 Large-Scale Serum Starvation Study

In order to ensure the model was robust, thirteen biological replicates of BL/10 and ten of mdx cardiomyocytes were used for area measurements. Out of the thirteen BL/10 replicates three had enough data for 0h, 24h and 96h time-points, ten had measurements at all five serum starvation time-points – 0h, 24h, 48h, 72h and 96h. Out of the ten mdx replicates five had data for the same three time-points and the other five for all time-points.

Volume measurements were also obtained from six of the BL/10 biological replicates, at all five time-points of serum starvation. One of the mdx replicates was used to obtain 0h, 24h and 96h serum starvation volume measurements, whilst another two were used for acquiring data from all five serum starvation time-points. These samples were also used for the correlation study in figure 3.14.

3.7.1 Comparison of Combined Area and Volume Data

The mean values of averaged cardiomyocyte size at each time-point of serum starvation were obtained to avoid biological replicates with larger population sizes having a disproportionate weight on overall results. Both area and volume measurements are compared and summarised in figure 3.15. On average mdx cardiomyocytes increased in area from 2,870μm^2 at 24h of serum starvation to 4,070μm^2 at 96h, which equates to a nominal change of 1,200μm^2 and a 1.4-fold increase in size (BL/10 0h n=8,216; BL/10 24h n=6,284; BL/10 48h n=3,331; BL/10 72h n=3,378; BL/10 96h n=4063; mdx 0h n=7,726; mdx 24h n=5,624; mdx 48h n=2,858; mdx 72h n=1,847; mdx 96h n=5,112). The equivalent volume data showed a nominal increase of 65,000μm^3 and a 1.5-fold increase of mdx cardiomyocyte size from 119,000μm^3 at 24h to 184,000μm^3 at 96h of serum starvation (n numbers equivalent to those stated in sub-section 3.6.3).

In area measurements mdx cardiomyocytes were only significantly larger than BL/10 cardiomyocytes at 72h ($p<0.05$) of serum starvation. The average volume of mdx cardiomyocytes was significantly greater at 72h ($p<0.001$) and 96h ($p<0.01$), but non-significantly larger at 0h, 24h and 48h of serum starvation. The statistical analyses of these datasets are summarised in table 3.5.

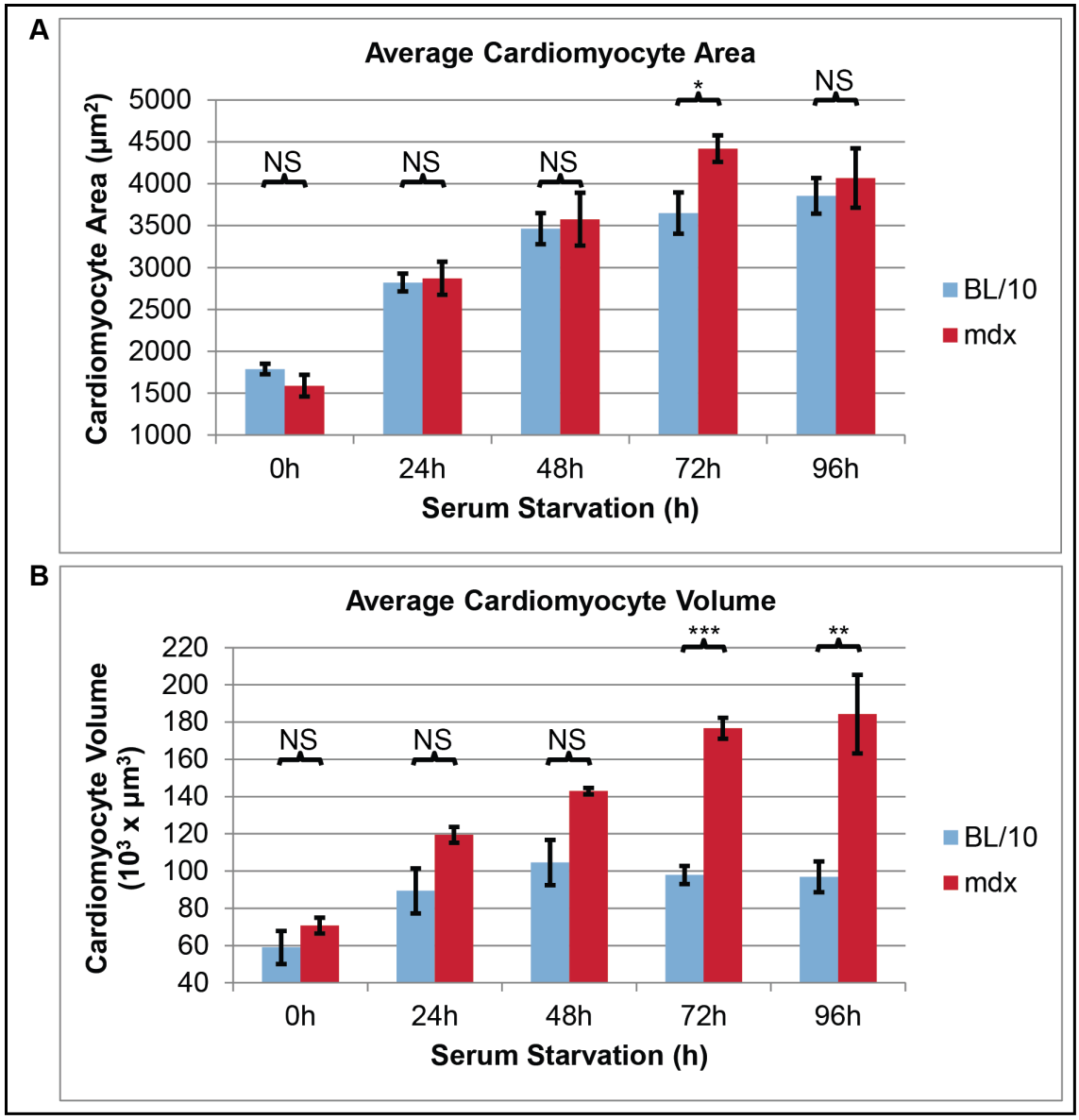

Figure 3.15. Average area and volume of BL/10 and mdx cardiomyocytes across the serum starvation time-scale. One-tail Student's t-tests were performed, taking sample variance into consideration. Error bars represent SEM, NS = Non-significant, * = p-value<0.05, ** = p-value<0.01, *** = p-value<0.001.

Measurement	Comparison	Levene's Test p-value	Variance	t-test p-value
Area	BL/10 0h v mdx 0h	0.17586204	Equal	0.0748
Area	BL/10 24h v mdx 24h	0.220130292	Equal	0.4069
Area	BL/10 48h v mdx 48h	0.914752501	Equal	0.3724
Area	BL/10 72h v mdx 72h	0.006473062	Unequal	0.0101
Area	BL/10 96h v mdx 96h	0.258105054	Equal	0.2984
Volume	BL/10 0h v mdx 0h	0.003326526	Unequal	0.1374
Volume	BL/10 24h v mdx 24h	0.218634779	Equal	0.0676
Volume	BL/10 48h v mdx 48h	0.125922308	Equal	0.0676
Volume	BL/10 72h v mdx 72h	0.314641411	Equal	0.0001
Volume	BL/10 96h v mdx 96h	0.152576297	Equal	0.0010

Table 3.5. Statistical analyses of serum starved cardiomyocyte area and volume measurement comparisons. A Levene's test p-value less than 0.05 was necessary to deem variance between two sets of data unequal. Skedasticity of data was taken into consideration when performing t-tests.

3.7.2 Combined Area Data Distribution

Cardiomyocyte area measurements were binned into 48 size range bins, increasing at 250μm^2 per bin from 0<250μm^2 as the lowest bin range to events above 12,000μm^2 as the highest bin. Biological replicate data at each time-point were individually binned and the relative frequency of events falling into bins independently determined. The mean of biological replicate frequency values in bins were calculated and plotted as line graphs for time-points of serum starvation (figure 3.16). The distribution of BL/10 and mdx cardiomyocyte area measurements was fairly similar. Longer serum starvation caused the distribution to spread out, the frequency peak to shrink and shift towards higher value range bins in both BL/10 and mdx cardiomyocyte samples.

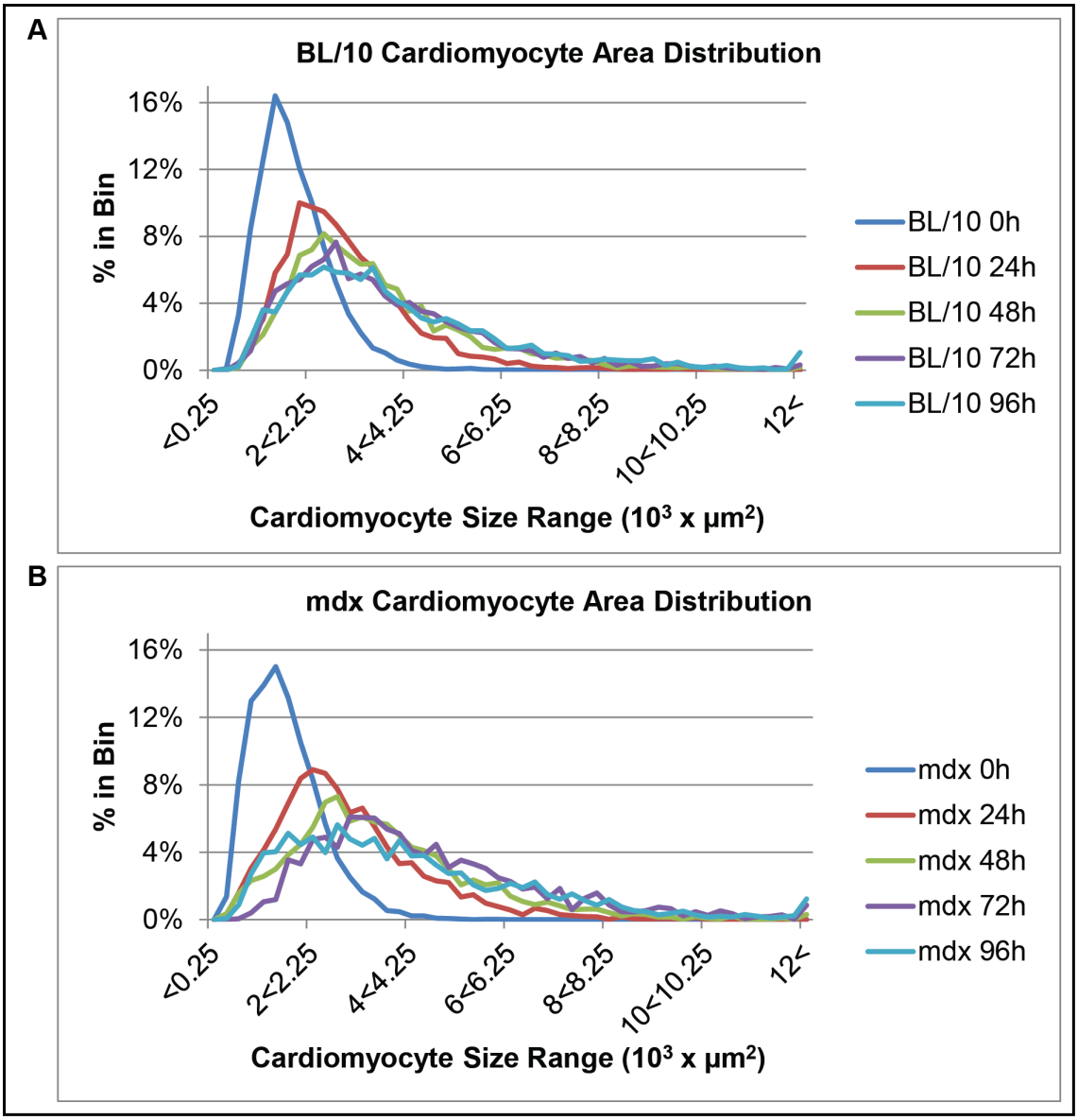

Figure 3.16. BL/10 and mdx cardiomyocyte area measurement data distribution. Area measurements of BL/10 and mdx serum starved cardiomyocytes were binned into size ranges and the relative frequencies determined for each biological replicate. Mean frequencies were calculated and plotted for each serum starvation time-point for both BL/10 (A) and mdx (B) samples. With increasing serum starvation time the distribution peaks spread across the size range bins and shifted towards higher ranges.

3.7.3 Combined Volume Data Distribution

Cardiomyocyte volume measurements were also binned into 48 size range bins, increasing in 10,000μm^3 increments per bin from 0<10,000μm3 as the lowest bin range and above 480,000μm^3 as the highest bin. The relative frequencies were calculated in the same way as for area measurements and the mean values for each time-point plotted for both BL/10 and mdx cardiomyocytes. The distribution of BL/10 and mdx volume data differed drastically. While both showed spreading out of the data and lowering peak frequency values with increasing serum starvation time, the differences in mdx samples were much greater (figure 3.17). There was a clear shift in volume distribution from 0h to 24h of serum starvation in both, BL/10 and mdx, cardiomyocyte populations, but whilst the mdx distribution plots continued to shift towards larger bin ranges with increasing serum starvation duration, BL/10 samples contrasted by remaining more or less constant in the same place as the 24h plot. These data supplement the significant increase in mdx cardiomyocyte average volume as opposed to BL/10 data and further illustrate the differences between control and dystrophic cardiomyocytes.

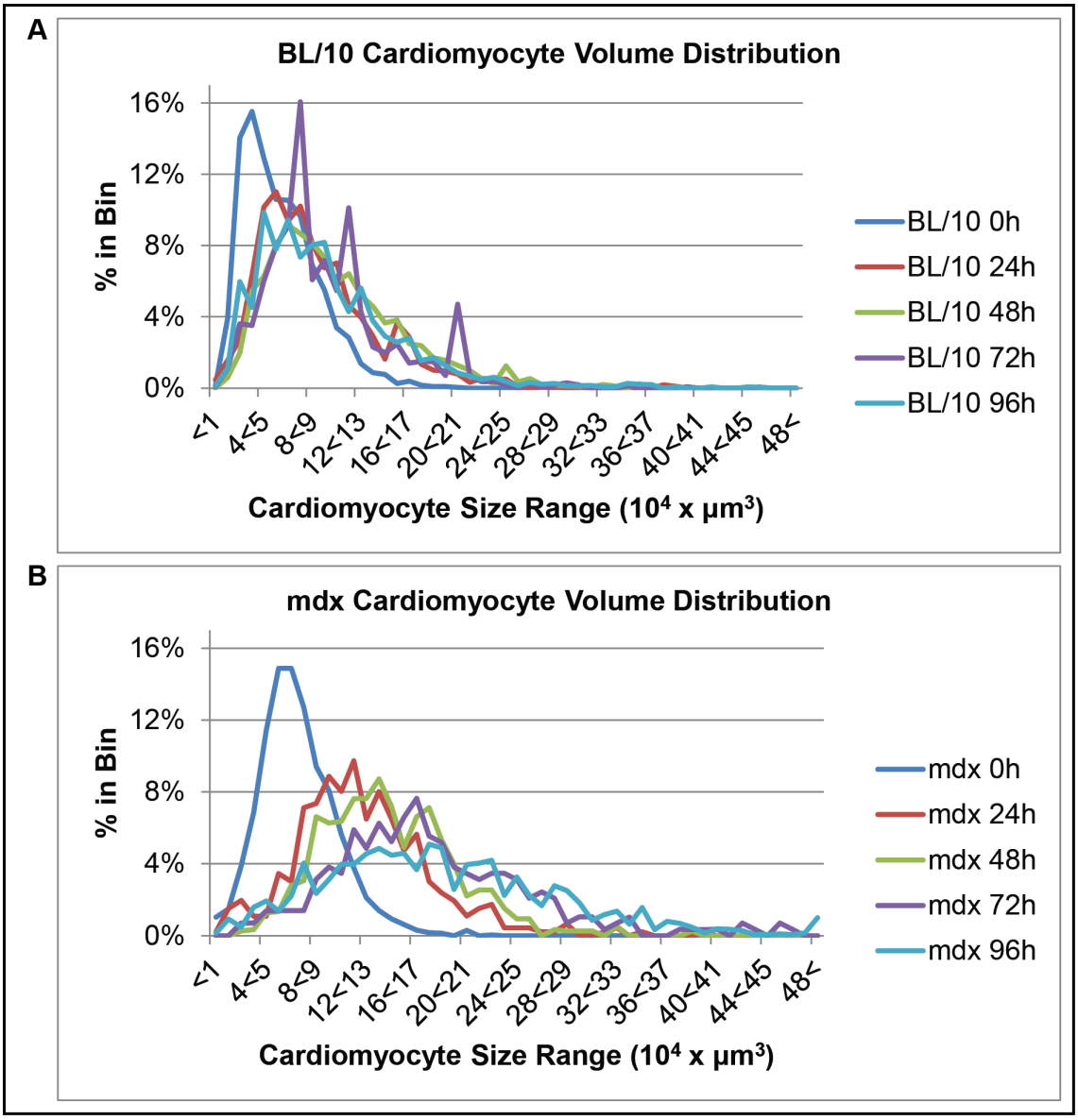

Figure 3.17. BL/10 and mdx cardiomyocyte volume measurement data distribution. Volume measurements of BL/10 and mdx serum starved cardiomyocytes were binned into size ranges and the relative frequencies determined for each biological replicate. Mean frequencies were subsequently calculated and plotted for each serum starvation time-point for both BL/10 (A) and mdx (B) samples. An increase in serum starvation time caused both BL/10 and mdx cardiomyocytes to become larger and thus spread the mean frequency plots out, reducing the nominal peak frequency value and shifting it towards larger bin ranges. This trend was augmented throughout the serum starvation time-course in mdx cardiomyocyte volume data, but not in BL/10 samples, where an initial shift within the first 24h of serum starvation did not continue to magnify.

3.8 Discussion

The primary mouse E17.5-derived cardiomyocyte serum starvation protocol was developed to provide an outcome measure for testing novel therapies aimed at rescuing the cardiac phenotype of DMD. The technique was optimised in several ways to reduce variables and increase consistency in the model, allowing it to be used to assess differences between control BL/10 and dystrophic mdx cardiomyocytes. It was concluded that, in response to serum starvation, mdx cardiomyocytes became significantly larger than BL/10 cardiomyocytes.

3.8.1 Establishing Conditionally Immortalised Cardiomyocyte Cell Lines

Previous attempts to use SV40-based conditional immortalisation to develop cardiomyocyte cell lines have only yielded one widely published cell line that can be passaged *in vitro* and recovered after freezing (White et al., 2004). The HL-1 cells have been derived from AT-1 cells, where the SV40 tumour antigen is expressed under the ANP promoter. AT-1 cells are atrial cardiomyocytes, derived from atrial tumours, and early attempts to produce such cardiac-specific transgenic models were met with disappointing results, such as tumorigenesis and arrhythmias due to the tumour antigen expression (Field, 1988). In the context of DMD it is pivotal to use ventricular or both ventricular and atrial cardiomyocytes for testing therapeutics. This is due to the DMD phenotype being more severe in ventricular muscle. Hence, it was not considered an optimal choice to develop conditionally immortalised cardiomyocyte cell lines from crossing mdx mice with the mice which AT-1 cells originated from. Rybkin et al. (2003) developed an Nkx2.5 promoter-driven large T antigen ventricular tumour-derived cell line. Despite these cells displaying voltage-dependent contractile potential, they did not fully differentiate and did not consistently maintain contractile properties when electrically stimulated.

Consequently, the Immorto-mouse described in this chapter – with an $H2K^b$ promoter-driven tsA58 construct – was chosen to generate a model by crossing with mdx mice. The primary cells isolated from embryo hearts were universally conditionally immortalised and thus also allowed both ventricular and atrial cardiomyocytes to be extracted and cultured. However, much like previous attempts to establish cardiac immortalised cell lines, it was cell adhesion post-trypsinising and freezing that remained an issue for passaging these cardiomyocytes. Various freezing media and a multi-step detachment protocol (Maltsev et al., 1994) were

tested to solve these issues, but with little success. Therefore, establishing a conditionally immortalised mdx cardiomyocyte cell line from mdx-Immorto mouse embryo hearts was not pursued any further.

3.8.2 Differences in BL/10 and mdx Mouse Cardiomyocyte Response to Serum Starvation

Preliminary data from cardiomyocytes serum starved with SFCGM implied that mdx cardiomyocytes became larger in area when compared to control cardiomyocytes. It was subsequently confirmed that the cells were not becoming flatter in culture and gained in size when volume measurements from Z-stack images were acquired and compared between dystrophic and control cells. However, when serum starved with SSCGM, subsequent comparison of the two types of cardiomyocytes revealed that BL/10 cardiomyocytes were gaining size in area measurements, whilst the volume of these cells did not catch up in the same way.

These opposing results in two types of measurements indicated that the control cardiomyocytes were becoming flatter in adherent culture, whilst mdx cardiomyocytes were increasing in size in three dimensions. The correlation (figure 3.14 and table 3.4) as well as size distribution studies (figures 3.16 and 3.17) supported this conclusion. BL/10 cardiomyocyte area and volume measurements did not show a significant positive correlation and therefore cells that were becoming larger in area were not necessarily increasing in volume, whilst mdx cardiomyocyte area and volume measurements displayed a strongly significant positive correlation. There was also a clear difference in the distribution of area and volume measurements when BL/10 and mdx cardiomyocyte data were compared. The changes in cardiomyocyte size distribution were similar in area measurements, whilst mdx cardiomyocytes presented a clear shift towards higher size, observed in both the bin with highest counts and general spread of data across a wider range of larger size bins.

3.8.3 Further Optimisation, Functional Studies and Translating the Technique to Human Cardiomyocytes

Despite the limitations of experimental design due to small cell numbers per biological replicate, it would be interesting to see if atrial or ventricular cells were more likely to become hypertrophic and whether removing either from the cultured population affected the remaining cells' response to serum starvation. Atrial cardiomyocytes have a strong contribution to ANP-led hypertrophic signalling (Zois et al., 2014) and therefore specifically enriching the population for cells of ventricular origin may have significant effects on the hypertrophic response. A better idea of whether specifically ANP-signalling was going to be an important factor in the hypertrophic response was established when analysing data from gene expression studies, discussed in more detail in chapter 4.

Fluorescence-activated cell sorting (FACS) may have helped to purify the cardiomyocyte population even further in comparison to pre-plating. However, removing myofibroblasts altogether from the heterogeneous population of primary cells may have had effects on the hypertrophic response of the cardiomyocytes (Kamo et al., 2015). It can also be argued that a low presence of contaminating cell types in cardiomyocyte culture may be beneficial for cell survival and pivotal for maintaining contractile interactions (Parodi & Kuhn, 2014).

Several research groups have derived DMD patient iPSC lines. Some of these have also been differentiated into cardiomyocytes and used for testing various rescue therapies (Dick et al., 2013; Lin et al., 2015). Taking into consideration the recorded effects of choosing the tissue of origin for cells to be reprogrammed into iPSCs, the epigenetic memory of fibroblasts (the most prevalently reprogrammed cell type) may not allow for as close of a comparison in cardiomyocyte hypertrophy between iPSC-derived and primary cardiomyocytes (Lee et al., 2014) (Dixit & Katare, 2015). Accordingly, data on DMD patient iPSC-derived cardiomyocyte hypertrophic response to serum starvation will be much anticipated in order to establish any differences from mouse E17.5-derived cardiomyocytes. Should human cardiomyocytes show a similar response to serum starvation then the model could be improved by not only allowing therapeutic testing in human cells, but also by introducing a limitless supply of biological replicate cardiomyocytes.

Considering this platform was developed as an outcome measure for therapies it was concluded that mdx cardiomyocyte area measurements were subsequently to be used for rescue therapy studies. The reasons for this were that although the relative size increase from 24h to 96h of serum starvation dropped from 1.5-fold in SFCGM-induced hypertrophy to 1.4-fold in SSCGM-induced hypertrophy, the nominal difference increased from 850μm^2 to 1,200μm^2, respectively.

It was encouraging to witness a wider nominal area change margin emerge between the 24h and 96h serum starvation time-points, because these were deemed the start and end-point for assessing efficacy of therapeutics. A wider margin in nominal values therefore improved the sensitivity of this model, improving interpretation of subtler changes in cardiomyocyte size in response to therapies, witnessed in some of the therapeutic compound trials in chapter 5.

3.8.4 Potential for an mdx Cardiomyocyte-based Model in Research

As briefly mentioned in the introduction section of this chapter, several potential therapeutic avenues for DMD treatment could be tested using this model. There is an increasing range of PPMO compounds constantly being developed and tested for their efficacy (Betts et al., 2012; Betts et al., 2015). A screen using this hypertrophy model to test delivery to cardiac cells *in vitro* may improve the work-flow of testing therapeutic potential of the new chemical variations.

When discussing the much-anticipated, but discouraging results from the sildenafil clinical trials it was noted that tadalafil may exhibit higher specificity towards PDE5 inhibition (Leung et al., 2014). In fact, it has been reported that tadalafil improves Z-disc organisation in dystrophic hearts (De Arcangelis et al., 2015) in a similar way reported in sildenafil treatment of hypertensive dogs (Bishu et al., 2011). These results could be replicated in the mdx cardiomyocyte model and would also elucidate the compounds' functional effect on hypertrophy. Testing both tadalafil as well as sildenafil using the mdx cardiomyocyte model may give an answer not only to any differences in compound efficacy, but also to any differences between therapeutic assessment in an early symptomatic environment as opposed to adult individuals. The two sildenafil clinical trials (Leung et al., 2014; Witting et al., 2014) showed no significant effect on the cardiac phenotype, but only recruited adult patients with progressed heart disease or BMD patients who have a milder and slowly progressing phenotype. Hypertrophy studies in mdx cardiomyocytes utilising this model may therefore provide results for assessment of therapeutic potential in an earlier pathological setting.

Many viral vectors are being optimised for delivery of gene therapy to DMD patients and some have reached clinical trial phase. Improved skeletal muscle *in vitro* testing techniques have been published (Jørgensen et al., 2009), but an *in vitro* model for fast screening in a cardiac setting is also required. The potential of this mdx cardiomyocyte hypertrophy model as a method for viral vector delivery is assessed and discussed in chapter 5 of this thesis.

Chapter 4. RNA-Seq Analysis of Cardiomyocytes

4.1 Introduction and Aims

Current developments in understanding the DMD cardiac pathology are limited due to lack of tissue availability and appropriate models. The plummeting cost of sequencing over the past decade has made whole transcriptome studies in rare diseases more attainable and cost-effective, helping to identify disease causing genes and phenotype progression mechanisms (Wang et al., 2013; Jia et al., 2013; Lin et al., 2015).

This chapter aims to identify signalling pathways and mechanisms of hypertrophy responsible for changes in the size of mdx cardiomyocytes in response to serum starvation.

4.2 Overview of the Experimental Setup

BL/10 and mdx cardiomyocytes were isolated from E17.5 hearts and cells were collected for RNA extraction at five time-points following serum starvation: 0h, 24h, 48h, 72h and 96h. The time-line of the experimental design for RNA collection is summarised in figure 4.1.

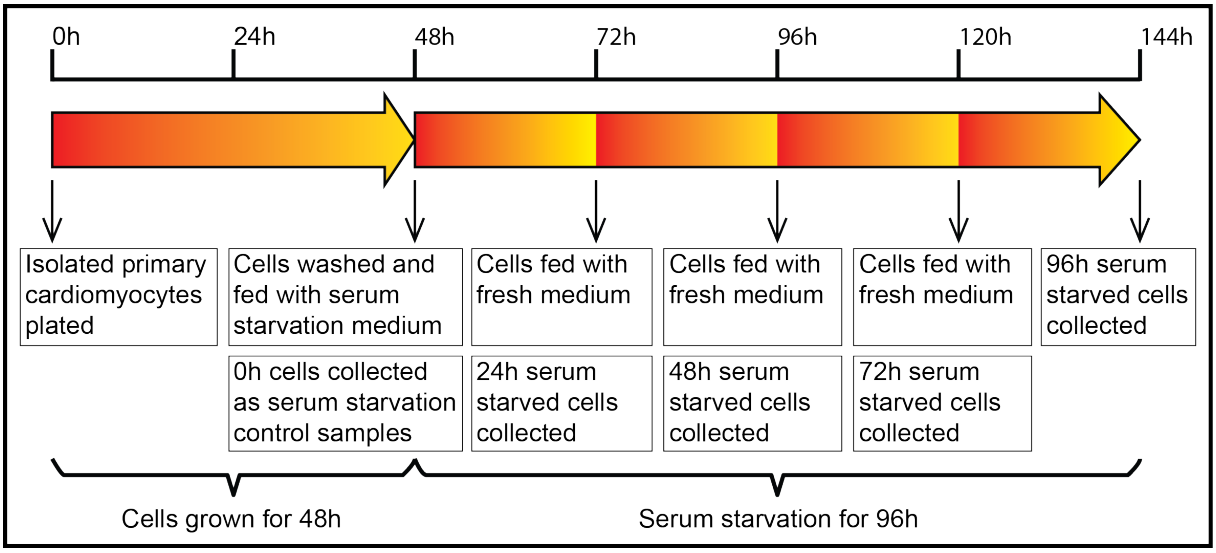

Figure 4.1. Experimental time-course of primary cardiomyocyte RNA sample collection. Cells were cultured in serum-rich growth medium for 48h, followed by serum starvation for 96h, feeding with fresh medium every 24h. Cells were harvested for RNA extraction at the start of and at each of the subsequent 24h time-point of serum starvation.

Three biological replicates of BL/10 and mdx samples were collected in Trizol at each time-point and shipped to Helmut Blum's research group for RNA-Seq analysis. Andrea Klanner (laboratory technician in Helmut Blum's research group) extracted RNA and performed quality control analysis on the samples using an Agilent 2100 Bioanalyser, data from which is summarised in table 4.1 and figure 4.2. The RNA integrity number (RIN) value cut-off for including samples in further analyses was 8. Three of the thirty analysed samples showed RNA degradation and RIN values below 8. All three belonged to the same BL/10 biological replicate (named B56) and were the 48h, 72h and 96h time-point of the same biological replicate. All five time-point samples of the B56 biological replicate were excluded from subsequent experimental procedures. After cDNA synthesis and fragmentation, unique barcodes were added to each set of fragmented DNA samples. Samples were combined and Stefan Krebs (post doctoral associate in Helmut Blum's research group) performed the sequencing on an Illumina HiSeq 1500.

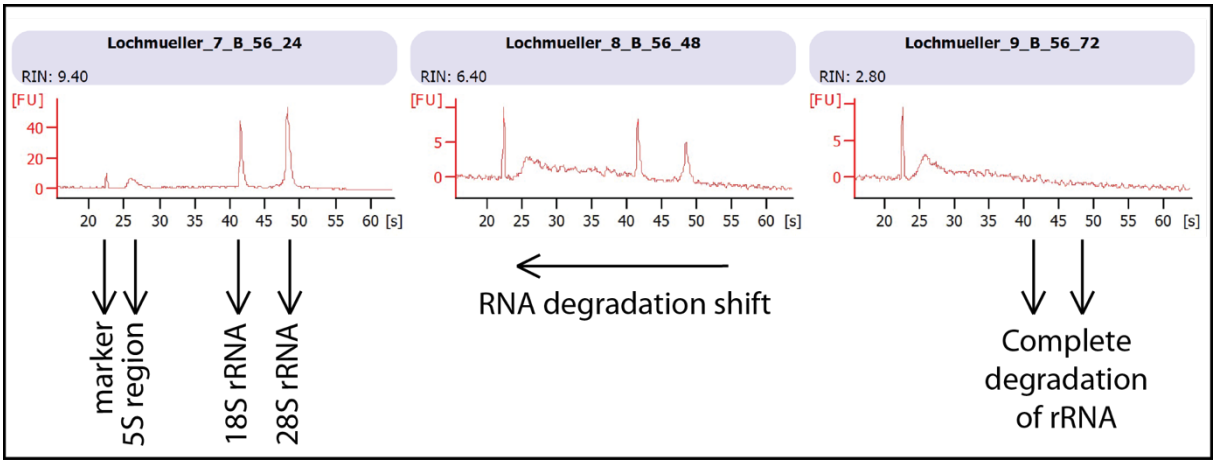

Figure 4.2. RNA quality control on Agilent 2100 Bioanalyzer. The y-axis on the graphs represents fluorescence units and the x-axis shows elution time in seconds. RIN stands for RNA integrity number and rRNA is ribosomal RNA. Samples indicating RNA degradation were omitted from subsequent experiments.

Sample	Mouse strain	Time-point	Illumina Barcode Sequence	[RNA] ng/µl	RIN	QC	% Mapped
B53 0h	BL/10	0h	AAGGGA	98	9.5	Pass	46.7
B53 24h	BL/10	24h	GGATGT	82	10	Pass	66.9
B53 48h	BL/10	48h	AAGGGA	52	9.6	Pass	56.0
B53 72h	BL/10	72h	GGATGT	65	9.8	Pass	58.1
B53 96h	BL/10	96h	CCTTCA	57	9.7	Pass	56.1
B56 0h	BL/10	0h	N/A	143	9	Pass	N/A
B56 24h	BL/10	24h	N/A	94	9.4	Pass	N/A
B56 48h	BL/10	48h	N/A	48	6.4	Fail	N/A
B56 72h	BL/10	72h	N/A	32	2.8	Fail	N/A
B56 96h	BL/10	96h	N/A	32	2.9	Fail	N/A
B57 0h	BL/10	0h	CCTTCA	122	9.6	Pass	61.0
B57 24h	BL/10	24h	TTCGCT	131	9.9	Pass	59.5
B57 48h	BL/10	48h	GGACCC	109	8.9	Pass	61.1
B57 72h	BL/10	72h	TTCGCT	95	8.8	Pass	42.0
B57 96h	BL/10	96h	ACACGA	74	8.2	Pass	44.0
m68 0h	mdx	0h	GGACCC	129	9.1	Pass	44.7
m68 24h	mdx	24h	TTCAGC	102	9.8	Pass	54.7
m68 48h	mdx	48h	ACACGA	119	9.5	Pass	47.1
m68 72h	mdx	72h	CACACA	100	9.7	Pass	59.7
m68 96h	mdx	96h	CACACA	105	9.6	Pass	62.5
m70 0h	mdx	0h	GTGTTA	157	9.7	Pass	40.0
m70 24h	mdx	24h	GTGTTA	144	10	Pass	58.8
m70 48h	mdx	48h	TTCAGC	140	9.6	Pass	54.5
m70 72h	mdx	72h	AAGACG	165	9.9	Pass	43.4
m70 96h	mdx	96h	TGTGAA	141	9.8	Pass	58.2
m71 0h	mdx	0h	AAGACG	151	9.4	Pass	47.6
m71 24h	mdx	24h	CCTCGG	167	9.6	Pass	61.8
m71 48h	mdx	48h	CCTCGG	125	9	Pass	56.3
m71 72h	mdx	72h	TGTGAA	102	8.2	Pass	59.2
m71 96h	mdx	96h	ACAAAC	98	8.2	Pass	49.8

Table 4.1. Quality control and DNA barcode adaptors for RNA-Seq samples. BL/10 and mdx cardiomyocyte RNA was quantified and analysed on the Agilent 2100 Bioanalyser. Each sample's cDNA fragments were tagged with six nucleotide reference sequence adaptors for multiplexed runs on Illumina HiSeq 1500.

4.3 RNA-Seq Data Analysis

Sequencing data from Illumina HiSeq 1500 was uploaded to Galaxy next-generation sequencing analysis web portal (Goecks et al., 2010) and demultiplexed based on reference sequences detailed in table 4.1. The resulting fastqsanger files were analysed with the FastQC quality control package (Andrews, 2010). Results were visualised in html format summary files. All samples gave high quality sequences (above 28) per base sequence analysis with none of the sequences flagged as poor quality (figure 4.3). Sequence trimming was therefore unnecessary (Kroll et al., 2014).

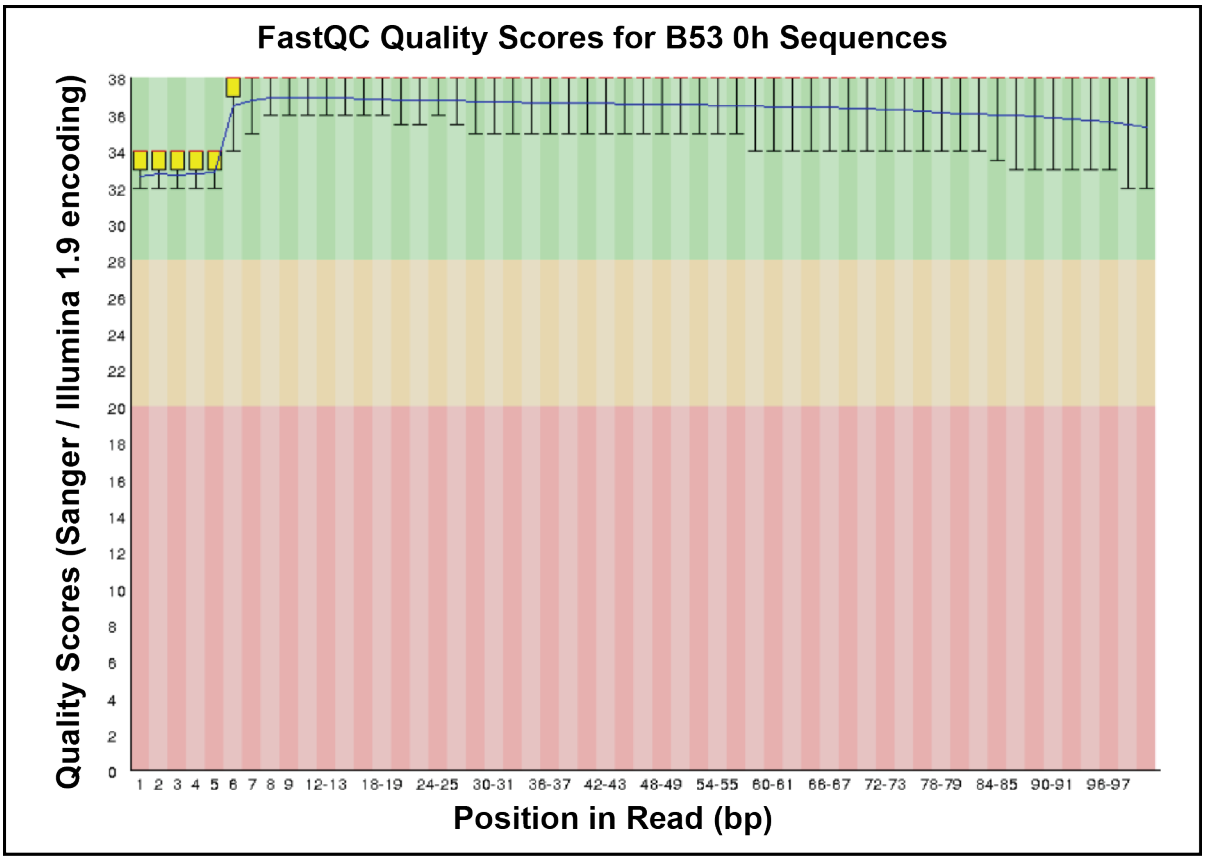

Figure 4.3 FastQC base quality analysis of B53 0h sample sequences. This graph showed a typical pattern for sequences from RNA-Seq runs with the first six bases having a lower median quality value (red line in the yellow boxes), representing the six base adapter sequences. The declining quality further along the sequence is typical for Illumina sequencing platform results. The whiskers in these (representing 90% of the data) plots were also showing very high quality in most reads.

All fastqsanger files were individually aligned to the mm10 reference mouse genome with TopHat2 (Kim et al., 2013) in Galaxy. Resulting bam files were visualised in Integrative Genomics Viewer (IGV) software (Thorvaldsdóttir et al., 2013) and the single nucleotide C->T mutation in exon 23 of the *Dmd* gene in mdx mouse samples confirmed (figure 4.4) (Sicinski et al., 1989). Alignment summary files from TopHat2 runs gave information about the proportion of sequences mapped from each sample, the lowest value was 40% and highest 66.9% (table 4.1).

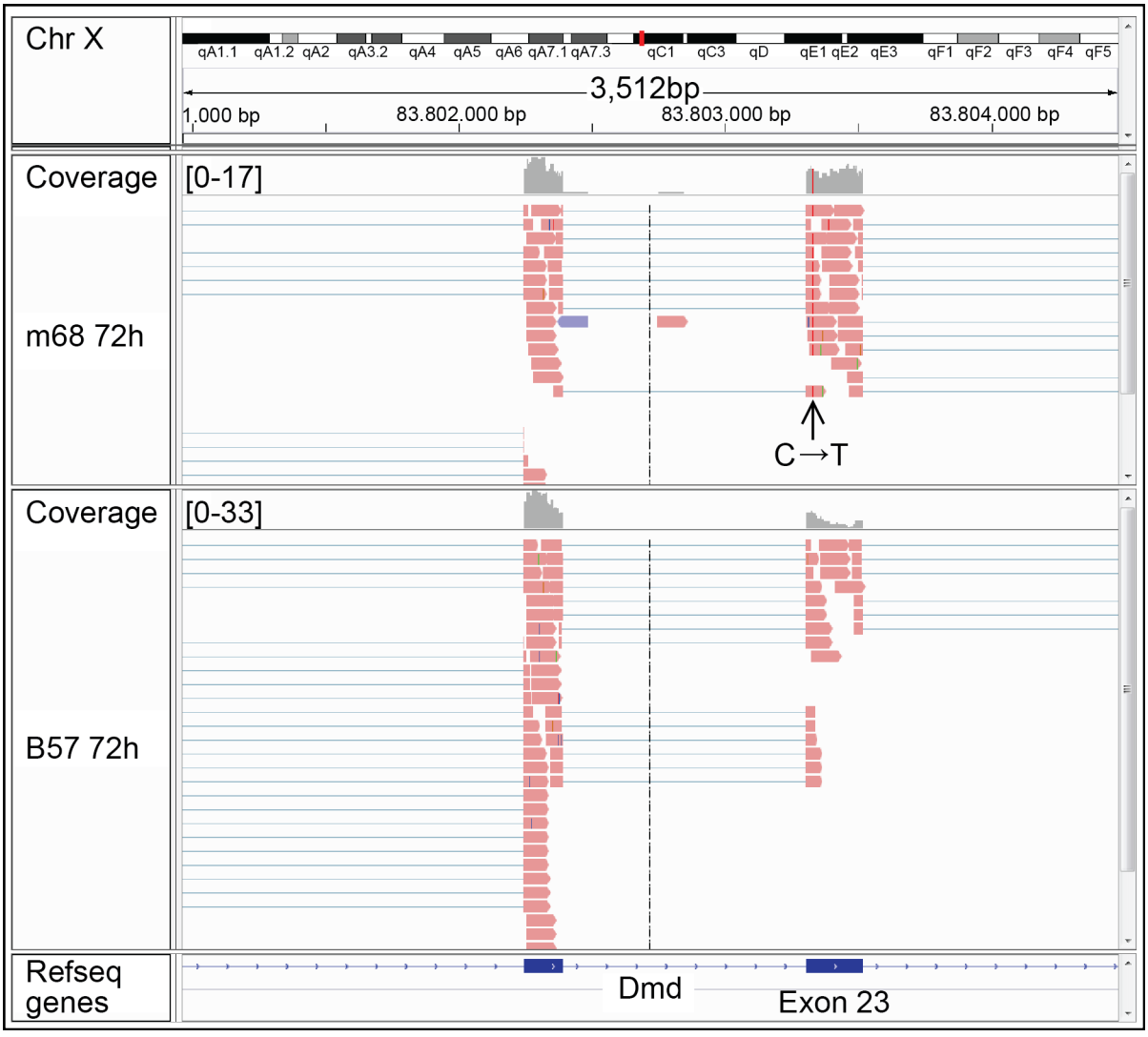

Figure 4.4 Visualising aligned sequencing data in IGV. The m68 72h sample .bam file was viewed in IGV software to visualise the mdx mouse point mutation in the *Dmd* gene.

Individual counts of gene expression were determined from TopHat2 accepted hits files for each sample. This was again performed in Galaxy, using the HTSeq package (Anders et al., 2015). The read count files were used to draw data saturation plots for each sample (figure 4.5) in order to assess completeness of data. All of the samples were considered to have yielded high quality data based on the overall number of mapped reads and the level of transcripts above the set 10x coverage. Most sample plots reached a plateau stage where additional reads had a reduced impact on improving coverage. Therefore, all samples were included in differential gene expression analyses.

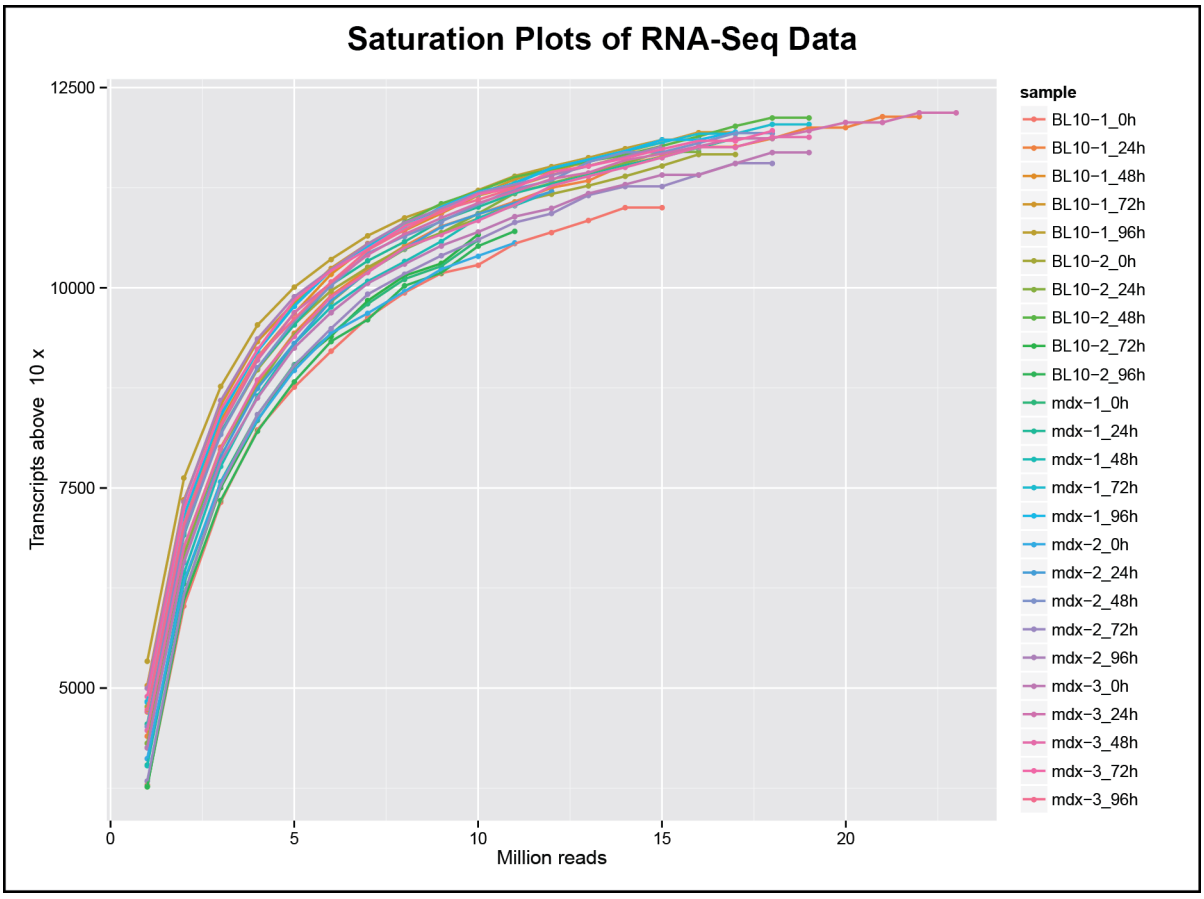

Figure 4.5. BL/10 and mdx cardiomyocyte RNA-Seq sample gene count saturation plots. This graph illustrates how each subsequent bin of 1 million sequence reads on the x-axis cumulatively increased the number of genes covered above a set threshold of transcripts (here minimum of 10) on the y-axis. All sample plots were expected to plateau beyond a certain number of reads. A failed sample would not have shown an exponential increase at the start, reached a comparable level of coverage along the y-axis (sequences not mapped or poor quality), or would have shown a short curve along the x-axis (not enough reads sequenced). Samples from these sequencing replicates all showed similar saturation curves and were therefore included in differential gene expression analyses.

4.4 Differential Gene Expression

An R programming environment (Ihaka & Gentleman, 1996) script to analyse differential gene expression with DeSeq2 package (Love et al., 2014) was written by Alex Graf (post doctoral associate in Helmut Blum's research group). Read count tab-delimited files from HTSeq were used as input data and the script was customised to allow selection of input samples to identify differentially expressed genes from a range of comparisons (summarised in table 4.2) in regularised logarithmic (rLog) transformation expression data, at a false discovery rate (FDR) of 0.05, based on Benjamini-Hochberg correction adjusted p-values (Benjamini & Hochberg, 1995). The output format for quantifying gene expression changes was in base 2 logarithm fold change (Log_2FC) format. In addition to comparisons based on contrasting one factor at a time, a multi-factor analysis was performed with DeSeq2 to identify genes that were differentially expressed when accounting for both sample type (BL/10 to mdx) and the effect of serum starvation (0h to 24h, to 48h, to 72h, to 96h). This multi-factor method therefore provided a two-dimensional analysis, which gave a list of genes with altered expression patterns in dystrophic cardiomyocytes across the serum starvation time-course.

4.4.1 Quality Control of Differential Gene Expression Data

Scripts invoked DeSeq2 to perform sample quality control in each of the comparisons. Principal component analysis (PCA) was conducted on sample sets in each comparison. These plots, some of which are shown in figure 4.6, revealed that it was not possible to separate genotype clusters when all BL/10 and mdx samples were analysed together on a two variance scale (figure 4.6 A). However, when samples from each time-point were compared then BL/10 and mdx samples formed distinct groups with no overlap between each other, indicating that genotype samples clustered together based on their gene expression variance measures.

Figure 4.6. Principal component analyses of BL/10 and mdx cardiomyocyte samples. Axes of the graphs show the two strongest dimensions of variance, and where each plotted sample lies on those scales. Samples with closer clustering showed greater similarity than those more distant from each other. (A) The comparison of all BL/10 and mdx samples did not allow separation of sample populations from each other based on genotype. However, comparison of biological replicates from the strains at individual time-points (B-F) allowed distinct separation of samples based on their genotype, highlighted by shapes drawn around BL/10 samples in blue and mdx samples in red. Samples from mdx cardiomyocytes clustered closely at the 0h time-point, but showed increased variability from each other further along the serum starvation time-course. BL/10 cardiomyocyte samples showed close clustering after the initial 24h response to serum starvation and later showed similarities on the first principal component, but a greater distance along the second principal component.

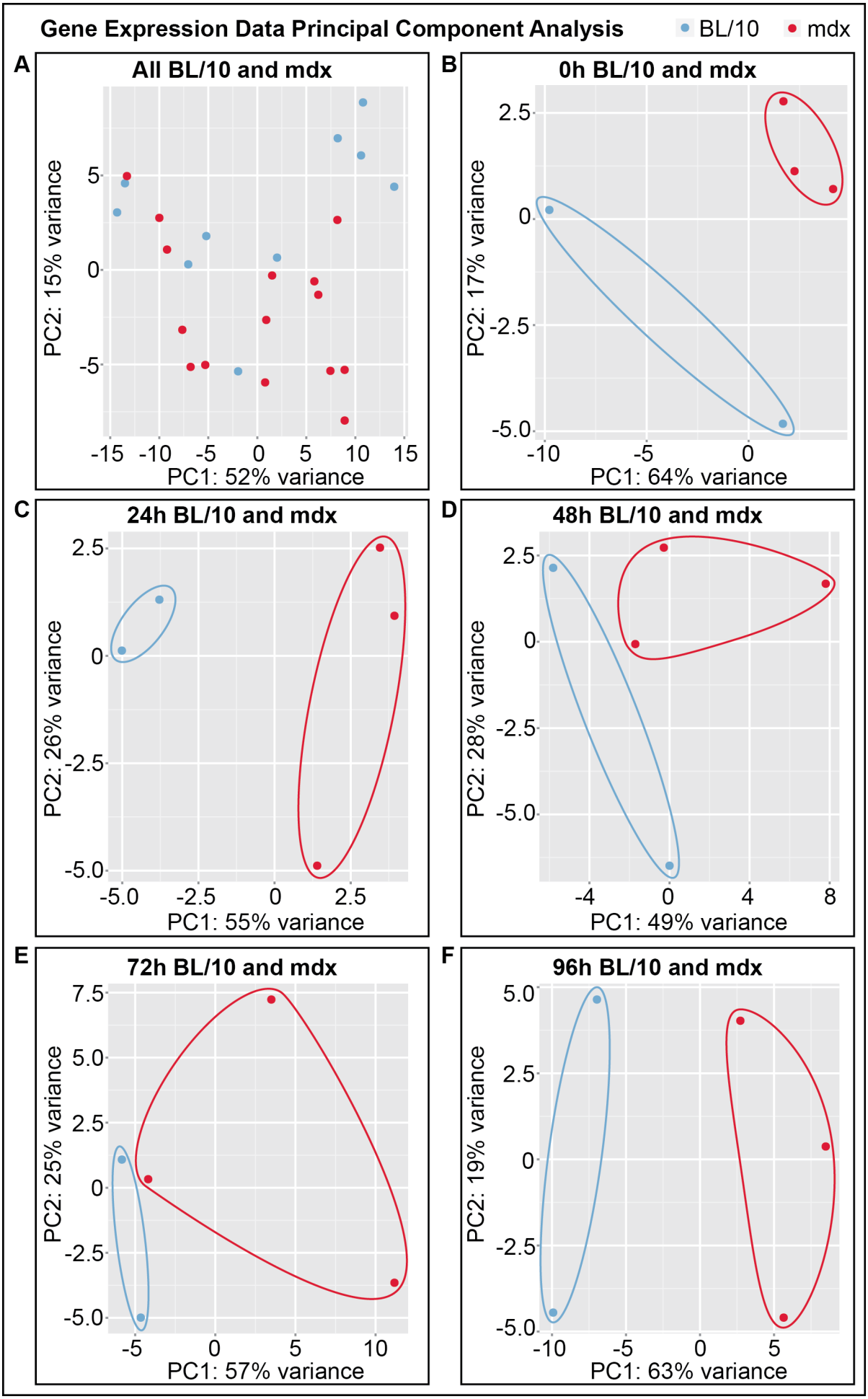
Gene Expression Data Principal Component Analysis
BL/10
mdx
A
All BL/10 and mdx
PC2: 15% variance
PC1: 52% variance
B
0h BL/10 and mdx
PC2: 17% variance
PC1: 64% variance
C
24h BL/10 and mdx
PC2: 26% variance
PC1: 55% variance
D
48h BL/10 and mdx
PC2: 28% variance
PC1: 49% variance
E
72h BL/10 and mdx
PC2: 25% variance
PC1: 57% variance
F
96h BL/10 and mdx
PC2: 19% variance
PC1: 63% variance

A heatmap was drawn to compare and contrast gene expression between samples. The heatmap in figure 4.7 features all the samples and their distances between one another based on gene expression patterns. This form of data representation helped to understand why BL/10 and mdx samples did not cluster together in the PCA plot in panel A of figure 4.6. All the BL/10 and mdx samples at the start of serum starvation (0h) clustered together, implying that they showed a greater overall similarity in gene expression to one another rather than the samples at different time-points of serum starvation drawn from the same genotype. This trend of sample clustering remained the same at the 24h and 48h time-points of serum starvation; there was greater similarity between the samples at the same time-points across genotypes than across time points of the same genotype. All samples at these two time-points clustered together to form one branch, with the exception of one BL/10 48h sample. In contrast, a clear divide between BL/10 and mdx samples emerged by the 72h and 96h serum starvation time-points, where sample gene expression diverged from the earlier pattern to form branches based on the genotype of sample origin. BL/10 72h and 96h samples formed one group, whilst mdx 72h and 96h samples were part of a separate branch. As a clear outlier, the BL/10 48h sample that did not cluster with the other 24h and 48h samples clustered with the same group as 72h and 96h mdx samples.

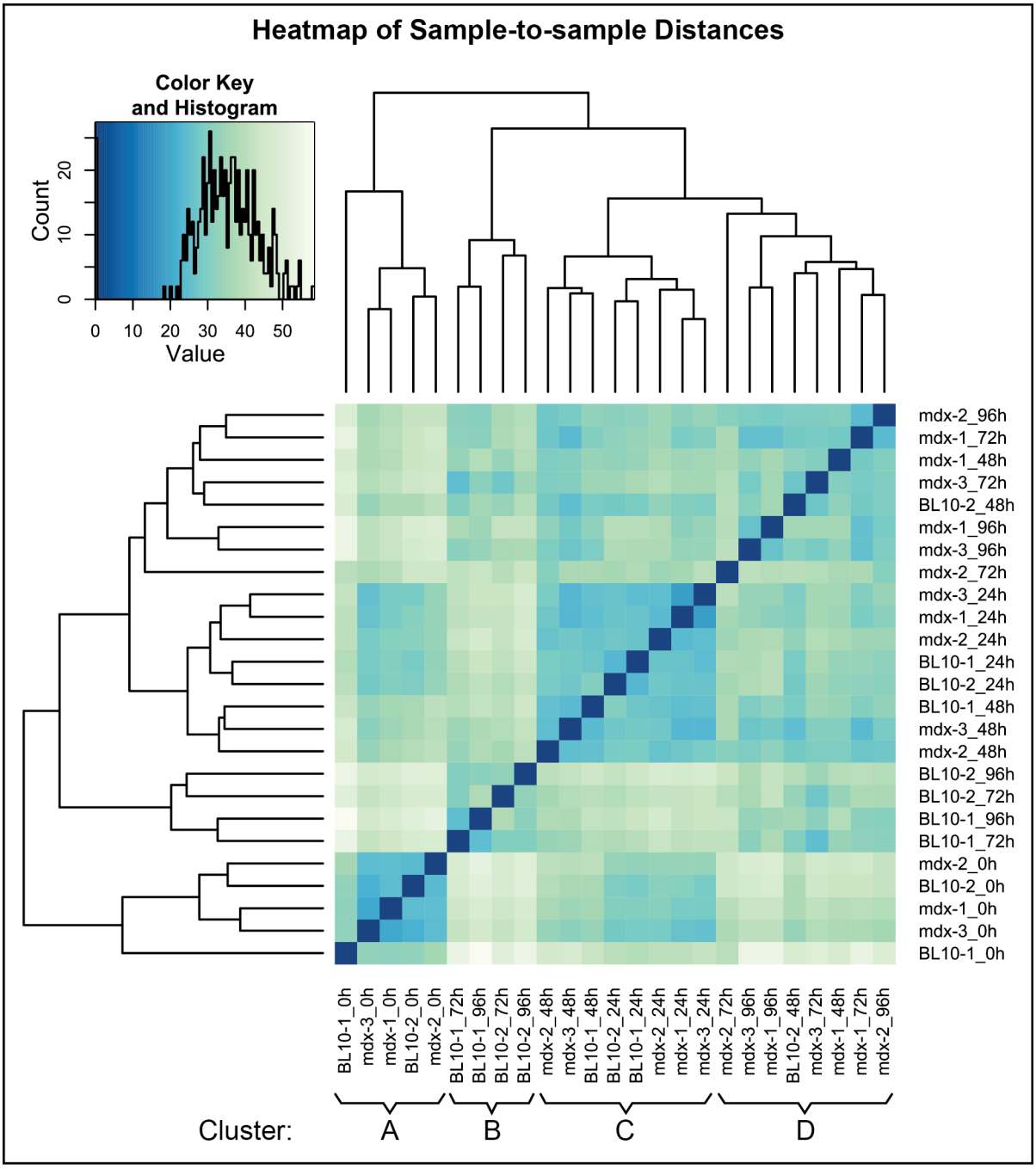

Figure 4.7. BL/10 and mdx cardiomyocyte gene expression sample-to-sample distances. Samples that were not serum starved formed cluster A. Samples in the first half of the serum starvation time-course (24h and 48h) also grouped together into cluster C, with the exception of one BL/10 48h sample, which fell into cluster D. Samples in the second half of the serum starvation time-course grouped together based on their genotype: BL/10 72h and 96h samples formed cluster B, mdx 72h and 96h samples formed cluster D.

MA-plots to visualise the spread of Log_2FC reads of all individual genes in a comparison were drawn using DeSeq2. These plots are based on the Bland-Altman plot and the name – MA-plot – is derived from the way it originally represented microarray (MA) data in the form of log ratios (M, here Log_2FC) against the mean of normalised counts (A). The plot allows visual representation of the fold changes for all genes as well as distinguishing the differentially expressed genes that were significant based on meeting the set FDR adjusted p-value cut-off (figure 4.8).

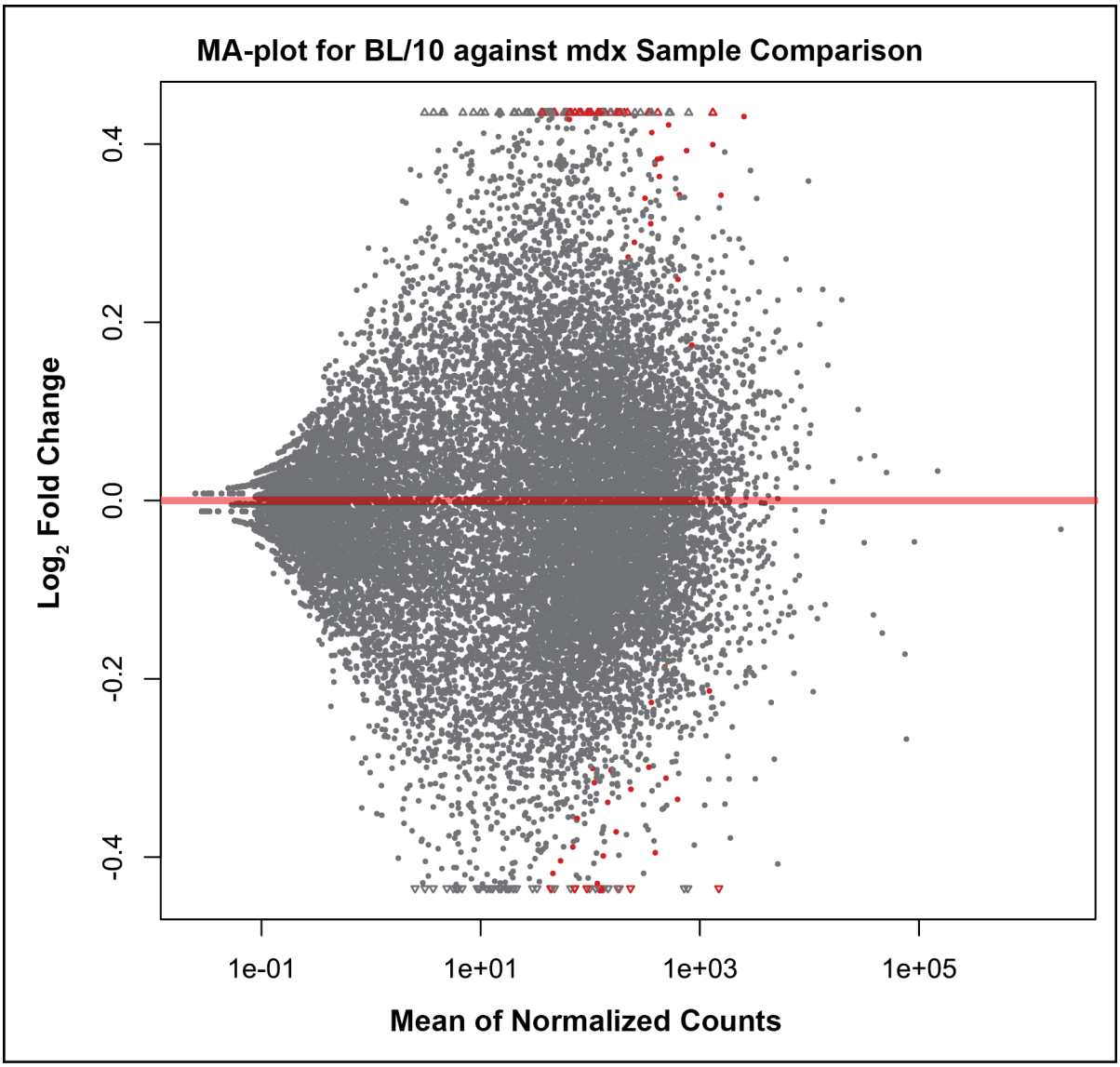

Figure 4.8. Gene expression MA-plot of BL/10 against mdx sample comparison. Each point on the graph is a gene, either up- or downregulated on a Log_2FC scale. The x-axis represents the mean count of a given gene, normalised to values across all the samples in the comparison. Significant differentially expressed genes are shown in red (adjusted p-value<0.1).

4.4.2 Clustering Genes Based on Trends in Expression Data

A second heatmap was drawn from each pair of samples, where rLog transformation data was used to contrast expression levels of genes that were differentially expressed in a given comparison. As an example, depicted in figure 4.9, when comparing all BL/10 samples against mdx samples the differentially expressed genes formed four visually distinct clusters. The first cluster had one gene, *Erdr1*, which showed a much higher expression level in BL/10 cardiomyocytes in comparison to mdx samples. The second cluster of ten genes included those, which showed a similar pattern of higher expression in BL/10 samples. The *Dmd* gene was one of these ten genes. The third cluster again only had one gene, 3110056K07Rik, which was expressed at a higher level in mdx samples. The fourth cluster was comprised of those genes which did not show a distinct pattern of expression differences between samples, although most appeared to have higher expression in mdx samples in comparison to BL/10 cardiomyocytes.

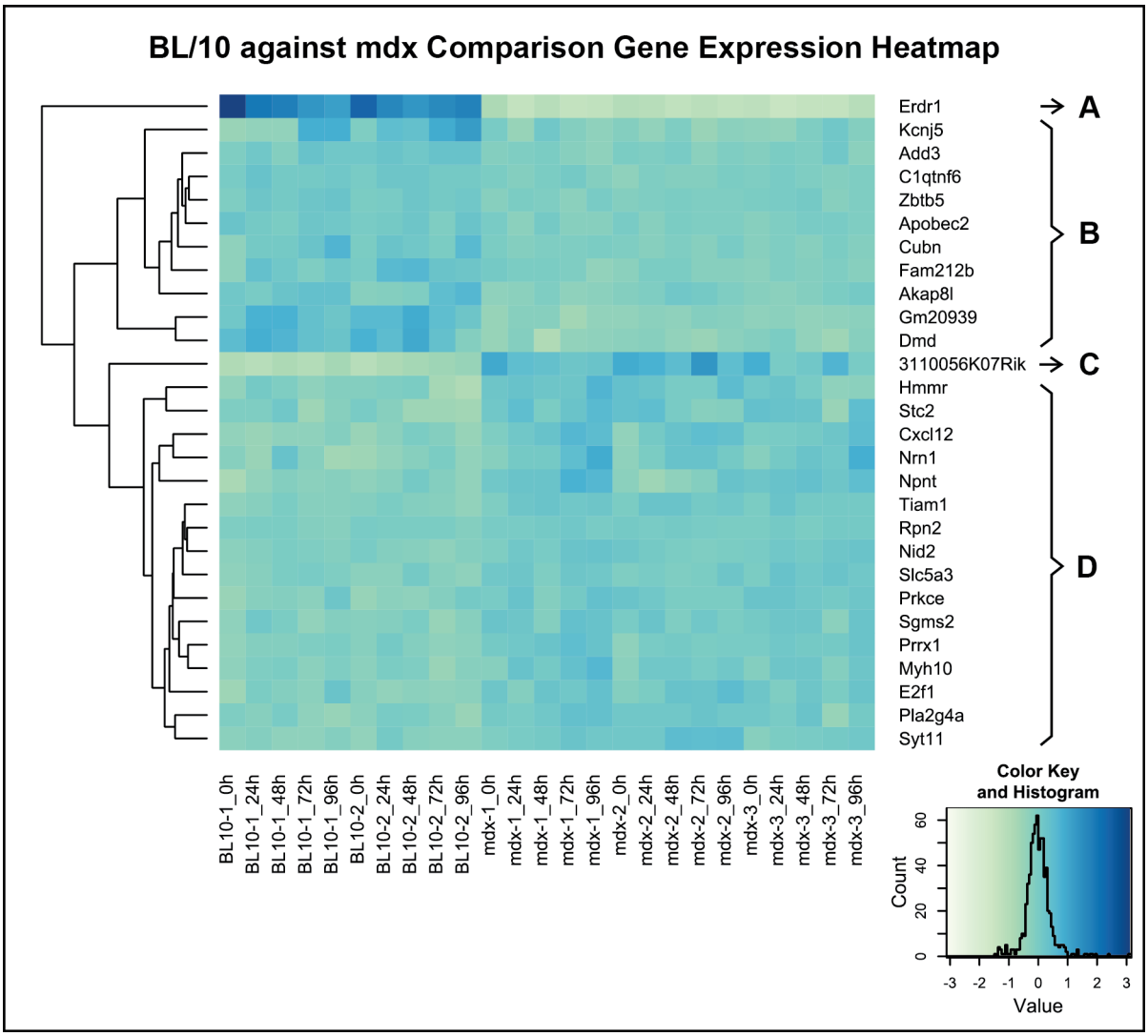

Figure 4.9 Heatmap of differentially expressed genes between BL/10 and mdx cardiomyocytes. All BL/10 cardiomyocyte samples were compared with all mdx samples. DeSeq2 identified genes that were differentially expressed and plotted their relative expression data into the heatmap. Gene-to-gene distance analysis revealed four clusters with distinct expression patterns (A-D).

In order to improve the understanding of gene expression patterns between samples, a self-organising tree algorithm (SOTA) analysis (Herrero et al., 2001) was performed to statistically cluster together genes with similar expression patterns. Figure 4.10 represents the four clusters of gene expression patterns that emerged when performing SOTA analysis on the 340 genes with a significantly altered expression pattern in the two-dimensional differential expression analysis between BL/10 and mdx cardiomyocytes across the duration of serum starvation.

The first cluster consisted of a group of 137 genes which showed an average higher expression in BL/10 samples in comparison to mdx samples. The second cluster had 123 genes and showed a reduction in gene expression levels along the time-course of serum starvation in BL/10 cardiomyocytes, whilst two of the three mdx biological replicates showed more or less stable expression levels for these genes as opposed to one replicate where a reduction of average expression levels was seen by the 72h and 96h time-points. The third cluster consisted of 25 genes with an increasing expression pattern across the serum starvation time-course in both BL/10 and mdx samples and a stronger upregulation in one mdx sample in comparison to BL/10 and the other two mdx samples. The fourth cluster comprised of 55 genes with a lower relative expression level in BL/10 samples in comparison to mdx samples serum starved for 24h or longer.

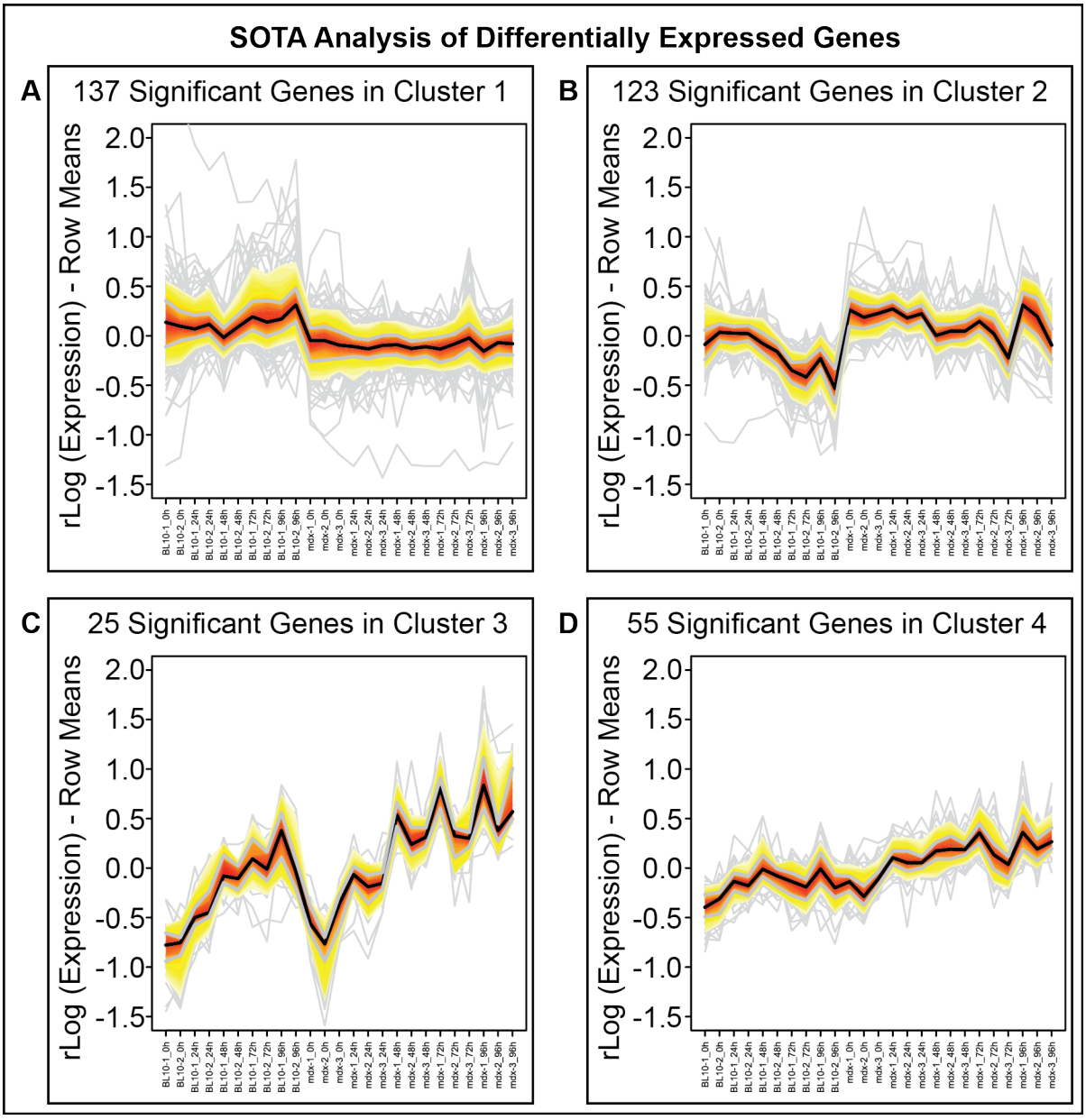
SOTA Analysis of Differentially Expressed Genes
A
137 Significant Genes in Cluster 1
B
123 Significant Genes in Cluster 2
C
25 Significant Genes in Cluster 3
D
55 Significant Genes in Cluster 4
rLog (Expression) - Row Means
2.0
1.5
1.0
0.5
0.0
-0.5
-1.0
-1.5
BL10-1_0h
BL10-2_0h
BL10-1_24h
BL10-2_24h
BL10-1_48h
BL10-2_48h
BL10-1_72h
BL10-2_72h
BL10-1_96h
BL10-2_96h
mdx-1_0h
mdx-2_0h
mdx-3_0h
mdx-1_24h
mdx-2_24h
mdx-3_24h
mdx-1_48h
mdx-2_48h
mdx-3_48h
mdx-1_72h
mdx-2_72h
mdx-3_72h
mdx-1_96h
mdx-2_96h
mdx-3_96h

Figure 4.10. SOTA analysis gene clusters. Each cluster contained a set of significant differentially expressed genes which displayed similar expression patterns, where significant indicates that a Benjamini-Hochberg corrected p-value<0.05 was recorded for each of the clustered genes. Cluster 1 showed a higher average expression level in BL/10 cardiomyocytes compared to mdx samples. Cluster 2 showed a diminishing level of expression along the serum starvation time-course in both BL/10 and one of the mdx samples, as opposed to a stably higher expression level in the other two mdx samples. Cluster 3 showed escalating gene expression levels for both BL/10 and mdx samples, with one mdx sample showing a higher increase in expression levels across the serum starvation time-course than other samples. Genes in cluster 4 showed a lower average expression level in all BL/10 and mdx 0h samples, with higher expression levels in serum starved mdx samples (24h-96h). Samples were arranged along the x-axis of the graphs, with ascending serum starvation time from 0h to 96h, first in BL/10 samples, followed by mdx samples. Each grey line represents the expression pattern for one gene. The black line links the relative mean rLog gene expression values of all the genes in each sample, compared to the average of all samples and genes in the cluster. The red area represents +/- 1 standard deviation (SD) from the mean and the yellow area combined with the red area represents +/- 2 SDs from the mean.

4.4.3 Filtering Differentially Expressed Gene Lists and Building Expression Databases

All lists of genes were filtered based on their false discovery rate (FDR), in order to improve data quality and confidence for further analyses. The FDR cut-off was originally set to adjusted p-value<0.05. It was now lowered to 1% (Benjamini-Hochberg corrected p-value <0.01) to further correct for multiple testing. A differential expression fold change cut-off was subsequently introduced to eliminate any statistically significant differentially expressed genes that had a small change in expression level. The Log_2FC cut-off was set to +/-0.6, which equals to a nominal +/-1.5-fold change (FC). Table 4.2 summarises the changes in the numbers of differentially expressed genes after introducing each of the cut-offs for DeSeq2 results.

Log_2FC cut-off		None	None	+/-0.6
adjusted p-value		0.05	0.01	0.01
Condition 1	Condition 2	Differentially Expressed Genes		
All BL/10	All mdx	28	8	5
Type	Time	340	109	12
BL/10 0h	mdx 0h	10	7	7
BL/10 24h	mdx 24h	166	85	62
BL/10 48h	mdx 48h	1	1	1
BL/10 72h	mdx 72h	19	12	12
BL/10 96h	mdx 96h	365	217	217
BL/10 0h	BL/10 24h	190	89	89
BL/10 0h	BL/10 48h	509	222	222
BL/10 0h	BL/10 72h	1263	749	749
BL/10 0h	BL/10 96h	1580	1041	1041
BL/10 24h	BL/10 48h	100	48	47
BL/10 24h	BL/10 72h	813	547	533
BL/10 24h	BL/10 96h	1120	760	750
BL/10 48h	BL/10 72h	261	129	129
BL/10 48h	BL/10 96h	525	355	355
BL/10 72h	BL/10 96h	45	22	22
mdx 0h	mdx 24h	1094	605	327
mdx 0h	mdx 48h	1065	986	842
mdx 0h	mdx 72h	1255	714	704
mdx 0h	mdx 96h	2495	1690	1413
mdx 24h	mdx 48h	253	117	99
mdx 24h	mdx 72h	470	264	260
mdx 24h	mdx 96h	1065	640	502
mdx 48h	mdx 72h	2	1	1
mdx 48h	mdx 96h	112	44	42
mdx 72h	mdx 96h	0	0	0
Total unique		4209	2807	2507

Table 4.2. Filtering lists of significant differentially expressed genes. Here significant indicates a Benjamini-Hochberg adjusted p-value<0.05 or <0.01 recorded for each gene, depending on the level indicated in the second row of the table. Differential gene expression comparisons were performed in DeSeq2. A multi-factor analysis, taking the time-course into consideration, was performed between BL/10 and mdx samples was performed in addition to conducting an overall comparison of averaged BL/10 gene expression against mdx samples. Lists of genes were filtered further to include only those with adjusted p-values below 0.01 and subsequently also filtered for a fold change cut-off at Log_2FC +/-0.6, which equates to nominal FC +/-1.5.

Altering the FDR reduced the number of significant genes in all but two of the sample comparisons: BL/10 48h v mdx 48h comparison only identified one gene with a low adjusted p-value, the mdx 72h v mdx 96h comparison did not return differentially expressed genes even at the <0.05 p-adjusted level. Introducing the +/-0.6 Log_2FC cut-off eliminated almost 90% of the remaining genes in the multi-factor (type versus time) comparison and whilst there were many significant genes with low expression differentials in the intra-mdx time-point comparisons, the numbers of genes in intra-BL/10 time-point sample comparisons remained unchanged. This was probably down to the fact that each time-point only had two samples and therefore the FC levels needed to be higher to meet the stringent FDR criterion.

These 27 modified lists of differentially expressed genes were combined into two databases in Microsoft Excel to improve ease of access to the relevant data. These databases combined the FC information as well as flagging which comparisons included the specific gene's expression change as significant (figure 4.11). These databases complemented each other and were used simultaneously when investigating the expression patterns of genes on an individual basis. Data from the database with FC information was also subsequently used to derive gene ontology diagrams. Appendix 1 includes differential expression data for all the genes discussed in this thesis, but not the complete databases.

Gene Expression Databases

A

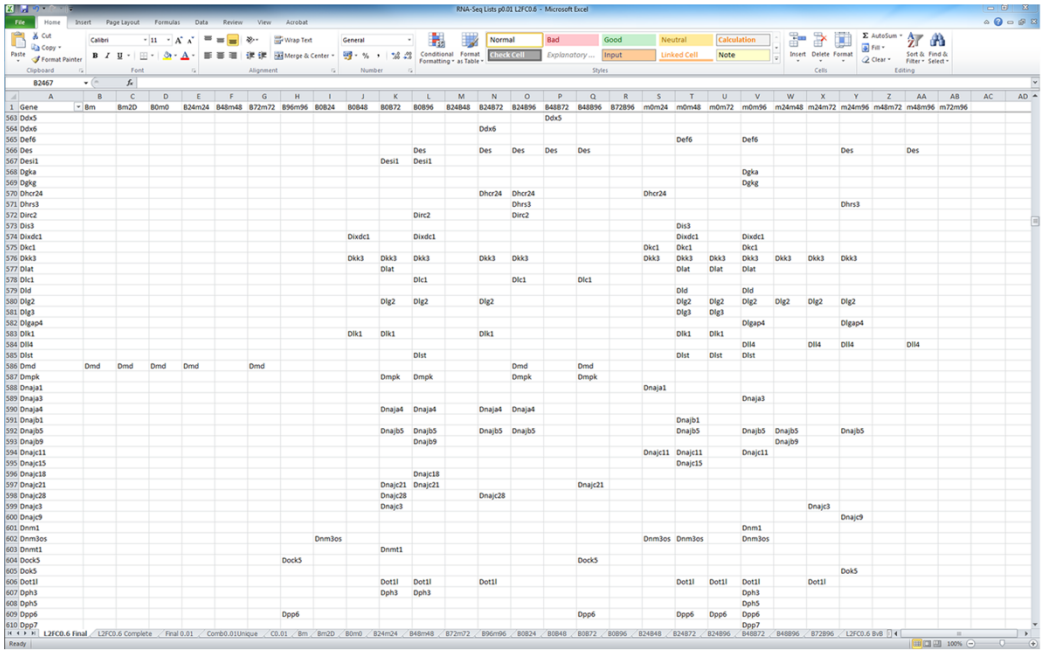

B

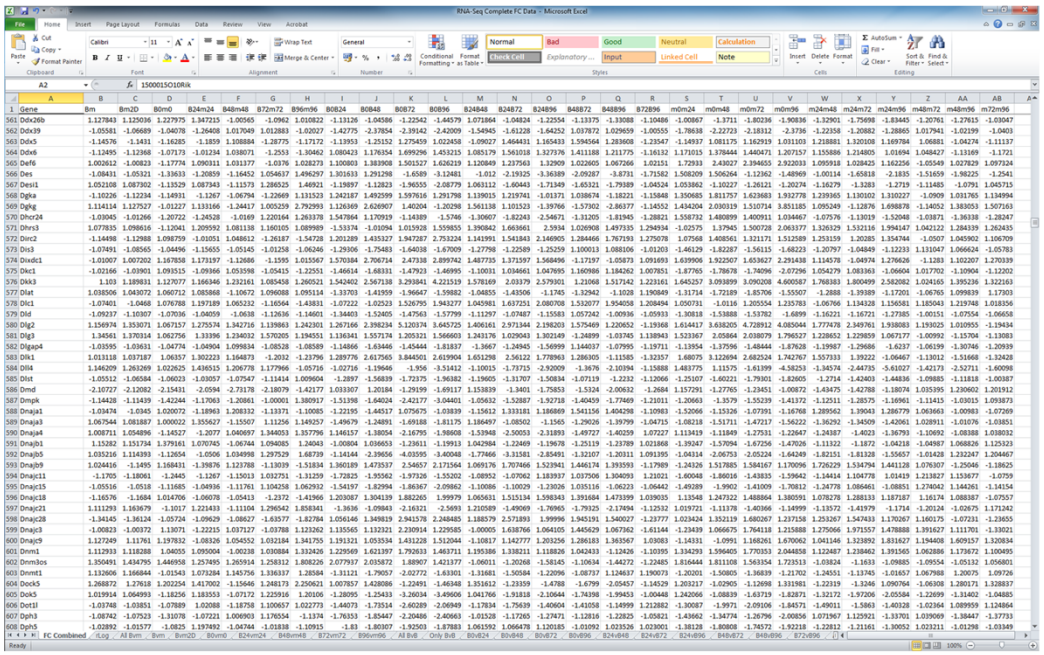

Figure 4.11. Snapshots of gene expression databases. Database A gave information about which comparisons flagged a gene as significant (adjusted p-value<0.01) and Log_2FC above or below +/-0.6. Each column represented a comparison and each row represented a gene. When a gene was differentially expressed according to the stated criteria in each comparison then its name was present in the relevant column. When the expression levels were not significantly altered in a given comparison then the cell was left blank. Database B combined all FC data for each gene in each of the DeSeq2 comparisons, flagged in any of the comparisons as having a significantly altered expression pattern. These databases were used in tandem when investigating gene expression patterns.

4.4.4 Secondary Analysis of Gene Expression Data

Further lists of genes were derived from the 27 comparisons shown in table 4.2. Venn diagrams in figure 4.12 show the rationale in creating these additional lists of genes with the example of showing relationships between significantly regulated genes from intra-BL/10 inter-time, intra-mdx inter-time and inter-type (BL/10 against mdx) comparisons. Furthermore, diagram B in figure 4.12 illustrates the categorising of genes from the mdx 0h against mdx 96h and BL/10 0h against BL/10 96h comparisons. New lists of genes were created based on these comparisons containing groups of genes unique to control cardiomyocytes, dystrophic phenotype or both. Such comparisons improved the workflow for showing distinct enrichment terms and pathways only involved in dystrophic pathology.

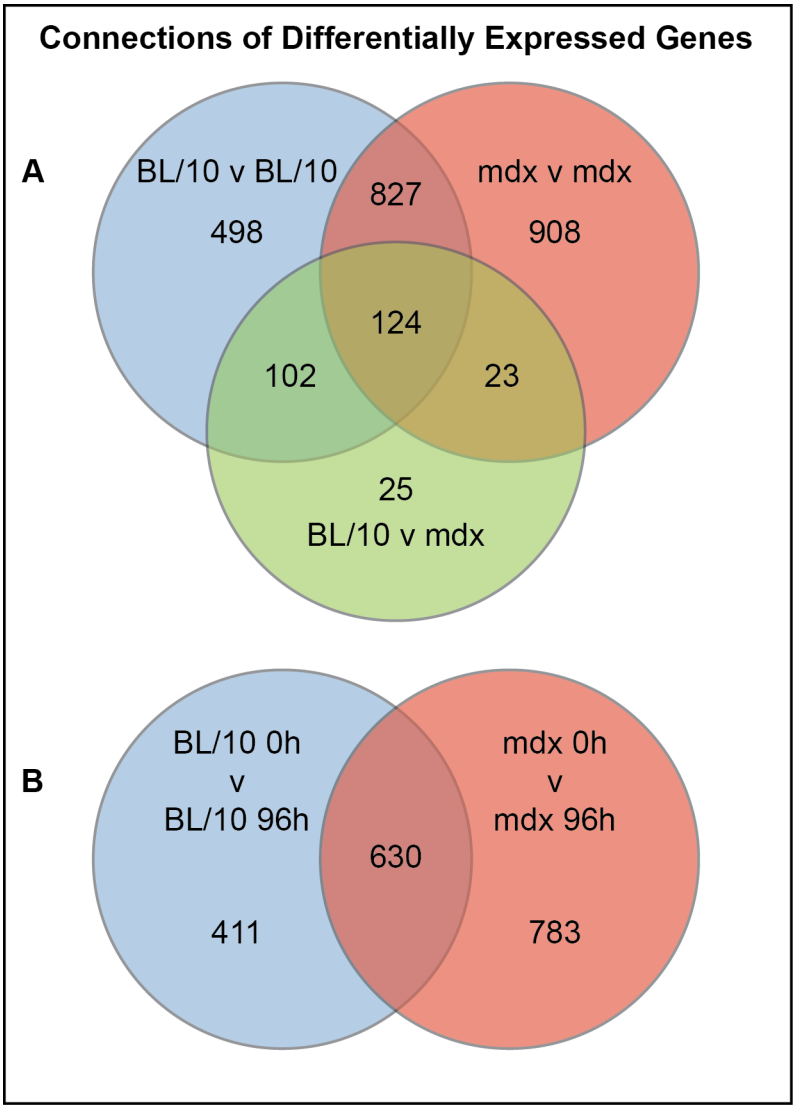

Figure 4.12. Venn diagrams of differentially expressed genes. Diagram A gives an outline of the genes from all comparisons of BL/10 serum starvation time-points relative to each other (in blue), all mdx serum starvation time-point comparisons (in red) and those comparisons between BL/10 and mdx samples at specific time-points, including the overarching comparison of all BL/10 samples against mdx samples in both the type-only and two-dimensional basis (in green). Diagram B illustrates how the two comparisons of the 0h time-point against the 96h time-point of serum starvation in BL/10 (in blue) and mdx samples (in red) give further information when genes are sub-categorised to those unique to either the BL/10 or mdx comparisons or overlapping in both comparisons.

4.5 Gene Ontology Analysis with DAVID

Gene ontology (GO) is routinely used for identifying gene enrichment for terms, processes or pathways. Lists of differentially expressed genes derived from the analyses above were used for GO analyses. A term enrichment analysis was conducted with the complete list of differentially expressed genes from all comparisons using the Database for Annotation, Visualization and Integrated Discovery (DAVID) (Huang et al., 2009), an online-access free software package. Annotation clusters with the highest enrichment scores (ES) were related to translation, sarcomere structure, mitochondria, extracellular matrix and the cytoskeleton. With an ES score of 8.19 hypertrophic cardiomyopathy and dilated cardiomyopathy cluster together, with Benjamini-Hochberg corrected p-values of $7.1x10^{-10}$ and $3.5x10^{-9}$, respectively. Hypertrophic cardiomyopathy disease process schematics were drawn in DAVID, based on Kyoto Encyclopedia of Genes and Genomes (KEGG) (Ogata et al., 1999) pathway information, to visualise the involved genes and processes in cardiac myocytes (figure 4.13).

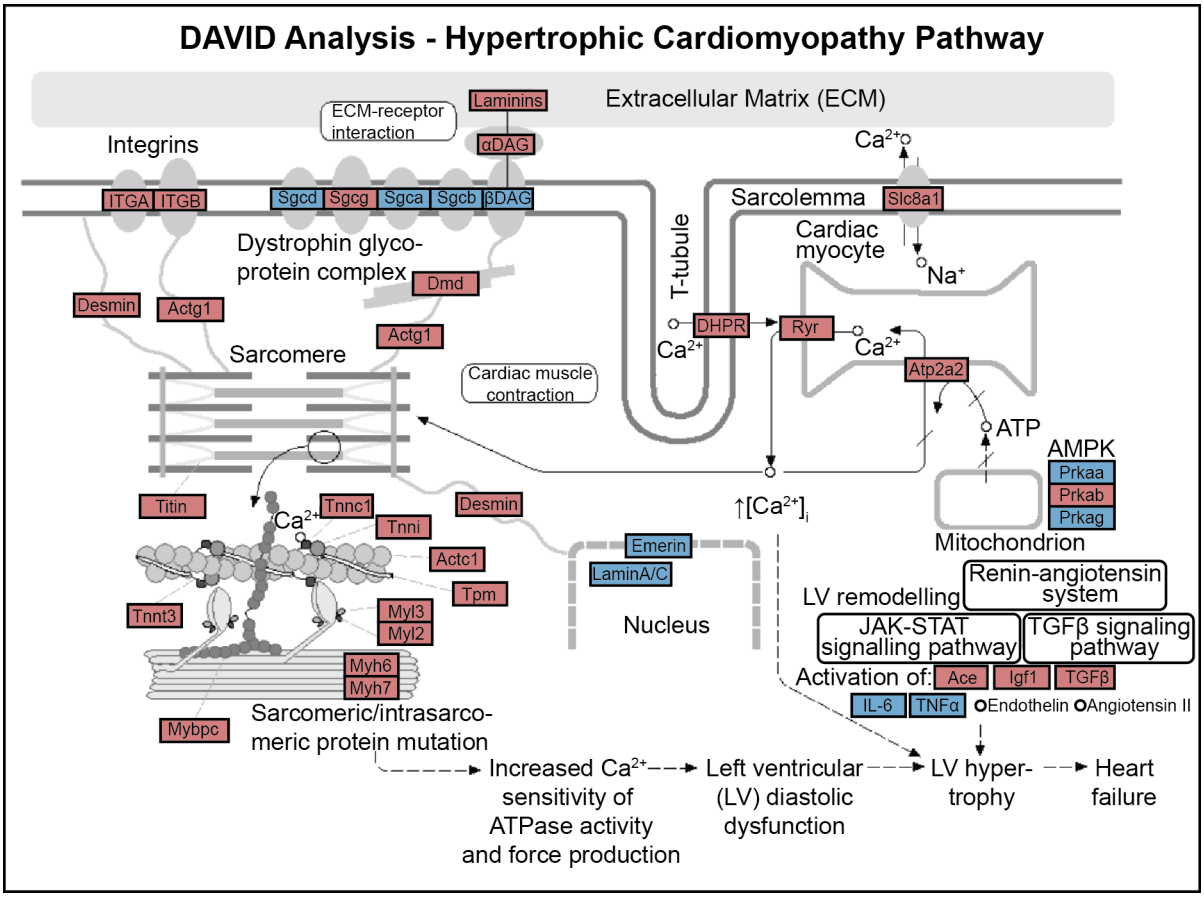

Figure 4.13. Gene ontology analysis with DAVID. This schematic shows hypertrophic cardiomyopathy pathways and processes in cardiomyocytes. Genes and groups of genes are highlighted in boxes, with those differentially expressed in the analyses above on a red background. The diagram illustrates how aberrant Ca^{2+} handling and sarcomeric abnormalities lead to a hypertrophic response in the heart. Adapted from the Kanehisa Laboratories' KEGG image (05410 5/29/12) returned as part of DAVID GO analysis results.

4.6 Gene Ontology Analysis with Genomatix

Genomatix software was used to create an in-depth understanding of gene interactions and associations. The software package allowed investigating individual gene lists as well as combined lists and drawing interaction maps based on genes identified in literature searches (Frisch et al., 2009).

4.6.1 Tissue, Disease, Biological Processes and Molecular Function Analyses

Ontology level confirmation of anticipated characteristics of the dataset was performed when investigating enrichment of significantly altered genes, summarised in table 4.3. Genomatix gave two types of enrichment lists for tissues, based on Genomatix literature mining algorithms and those of the UniGene transcriptome database. The former resulted in skeletal muscle, heart and myocardium coming out as top three enriched tissue types, whilst the latter gave the cardiovascular system, heart and lung in descending order of significance as the top three tissues. The heart showed the highest nominal number of genes and the myocardium the highest proportional representation from Genomatix literature mining. UniGene enrichment resulted in lung tissue showing the highest nominal number of associated genes whilst heart tissue had the highest proportional representation.

Enrichment for diseases based on Medical Subject Headings (MeSH) and Genomatix literature mining returned heart disease, cardiomegaly (twice), cardiovascular disease and animal diseases as the top five disease groups for the former and hypoxia, cardiomegaly, adverse event associated with the vascular system, cardiomyopathies and hypertrophy for the latter. Cardiomegaly and cardiomyopathies were represented by the highest proportion of potential genes in the MeSH and the Genomatix libraries, respectively.

Ontology analysis for biological processes identified translational termination, translational elongation, single-organism metabolic process, cellular component organisation or biogenesis and extracellular matrix organisation as the top five terms. Protein binding, structural constituent of ribosome, structural molecule activity, binding and cytoskeletal protein binding were the five highest enriched GO terms for molecular functions.

Tissues (Genomatix Lit. Mining)	p-value	Genes	Represented
Muscle, skeletal	7.35E-40	255 of 988	25.81%
Heart	8.46E-37	281 of 1170	24.02%
Myocardium	8.78E-37	164 of 520	31.54%
Tissues (UniGene)	p-value	Genes	Represented
Cardiovascular system	3.49E-144	1569 of 9886	15.87%
Heart	3.13E-137	1502 of 9319	16.12%
Lung	1.14E-132	1732 of 11956	14.48%
Diseases (Genomatix Lit. Mining)	p-value	Genes	Represented
Hypoxia	4.78E-30	213 of 848	25.12%
Cardiomegaly	2.17E-23	116 of 386	30.05%
Adverse event associated with the vascular system	6.38E-21	154 of 625	24.64%
Cardiomyopathies	1.54E-18	89 of 293	30.38%
Hypertrophy	1.31E-16	124 of 509	24.36%
Diseases (MeSH)	p-value	Genes	Represented
Heart Disease	1.34E-64	943 of 5693	16.56%
Cardiomegaly	4.13E-64	483 of 2170	22.26%
Cardiomegaly	6.24E-64	424 of 1784	23.77%
Cardiovascular Disease	3.68E-63	1217 of 8196	14.85%
Animal Diseases	1.11E-62	1210 of 8142	14.86%
Biological Processes (GO)	p-value	Genes	Represented
Translational termination	8.19E-30	57 of 91	62.64%
Translational elongation	2.92E-28	61 of 108	56.48%
Single-organism metabolic process	1.50E-27	572 of 3160	18.10%
Cellular Component Organization or Biogenesis	4.31E-27	756 of 4518	16.73%
Extracellular Matrix Organization	4.77E-26	110 of 315	34.92%
Molecular Functions (GO)	p-value	Genes	Represented
Protein Binding	3.11E-28	1109 of 7521	14.75%
Structural Constituent of Ribosome	4.99E-27	72 of 155	46.45%
Structural Molecule Activity	1.24E-22	161 of 627	25.68%
Binding	2.17E-15	1541 of 11958	12.89%
Cytoskeletal Protein Binding	1.01E-14	150 of 681	22.03%

Table 4.3. GO analysis of tissues, diseases, biological processes and molecular functions. Genomatix software was used to analyse the complete list of differentially expressed genes. The resulting top three tissues based on literature mining and the top five diseases, biological processes and molecular functions are summarised above based on their p-values and gene representation.

4.6.2 Cell Signalling and Interaction Pathways

Results from signalling pathway analysis corresponded to the gene association analyses on tissue types, diseases and biological processes. Several pathways associated with the vascular system were identified when analysing the complete list of genes, for example angiogenesis and hypoxia-related pathways were highly represented. Pathways conventionally regarded to be involved in hypertrophy and dystrophic cardiomyopathy, such as matrix metalloproteinase (MMP) and transforming growth factor beta (TGFβ) signalling (Nadarajah et al., 2011), were also represented in the list of most significantly represented pathways, summarised in table 4.4. The three pathways with the highest significance values in the combined gene list were angiogenesis, vascular endothelial growth factor and hypoxia-inducible factor 1 alpha (HIF-1α) signalling.

Pathway	p-value	Genes	Representation
Angiogenesis	4.91E-16	84 of 251	33.47%
Vascular Endothelial Growth Factor	8.99E-12	66 of 207	31.88%
Hypoxia Inducible Factor 1, Alpha	5.00E-09	53 of 173	30.64%
Integrin Linked Kinase	7.02E-08	32 of 88	36.36%
Thrombospondin 1	1.25E-07	24 of 57	42.11%
Rho Ras Homolog	2.87E-07	67 of 266	25.19%
Focal Adhesion Kinase	4.48E-07	56 of 121	46.28%
Matrix Metalloproteinase	1.21E-06	62 of 249	24.90%
TGF Beta	2.10E-06	126 of 623	20.22%
Mothers Against DPP Homolog	6.12E-05	77 of 367	20.98%
Endothelin	1.01E-04	28 of 99	28.28%
Protein Kinase	1.01E-04	30 of 109	27.52%
Platelet Derived Growth Factor	1.18E-04	36 of 141	25.53%
Nitric Oxide	1.37E-04	39 of 158	24.68%
Cellular Growth	1.44E-04	67 of 317	21.14%
Redox	2.29E-04	50 of 223	22.42%
Peroxisome Proliferative Activated Receptor Alpha	2.33E-04	31 of 119	26.05%
Low Density Lipoprotein Receptor Related Protein	2.75E-04	39 of 163	23.93%
Caveolin	3.47E-04	29 of 111	26.13%
Tek Tyrosine Kinase	4.43E-04	13 of 35	37.14%
Nitric Oxide Synthase	5.34E-04	35 of 146	23.97%
Lipid	6.22E-04	89 of 468	19.02%
Rho Associated, Coiled Coil Containing Protein Kinase	6.43E-04	32 of 131	24.43%
Natriuretic Peptide Receptor A Guanylate Cyclase	7.07E-04	10 of 24	41.67%

Table 4.4. GO pathway analysis of the combined differentially expressed genes list. Most significantly represented pathways based on gene enrichment from the combined list of genes.

In order to identify pathways specific for dystrophic cells the lists of genes derived on the basis represented in diagram A of figure 4.12 were used and analysed in Genomatix. The top three signal transduction pathways based on significance values for each list of genes were compiled into table 4.5. Angiogenesis and hypoxia-related pathways were at the top of both the resulting analyses from the BL/10 and mdx complete gene lists as well as the overlapping genes (intersection) of the two groups. However, when only genes specific for BL/10 or mdx comparisons within the same genotype samples were investigated, only vascular endothelial growth factor (VEGF) remained significant in the group of genes differentially expressed only in mdx sample comparisons.

Signal Transduction Pathways	p-value	Genes	Represented
All BL/10 v BL/10 Comparisons			
Vascular Endothelial Growth Factor	2.22E-11	59 of 218	27.06%
Hypoxia Inducible Factor 1, Alpha Subunit	2.08E-07	42 of 168	25.00%
Thrombospondin 1	9.42E-07	20 of 56	35.71%
All mdx v mdx Comparisons			
Vascular Endothelial Growth Factor	8.86E-13	67 of 218	30.73%
Hypoxia Inducible Factor 1, Alpha Subunit	7.72E-09	49 of 168	29.17%
Thrombospondin 1	1.94E-06	21 of 56	37.50%
Only BL/10 v BL/10 Comparisons			
Actin Related Protein 2	1.77E-05	7 of 22	31.82%
Integrin Linked Kinase	4.60E-05	13 of 87	14.94%
E2F Transcription Factor 1	4.11E-04	12 of 94	12.77%
Only mdx v mdx Comparisons			
Cyclin G2	5.61E-03	5 of 21	23.81%
Vascular Endothelial Growth Factor	6.41E-03	22 of 218	10.09%
Potassium Voltage Gated Channel	6.93E-03	5 of 22	22.73%
Intersect BL/10vBL/10 and mdx v mdx			
Vascular Endothelial Growth Factor	1.92E-11	45 of 218	20.64%
Hypoxia Inducible Factor 1, Alpha Subunit	1.02E-08	34 of 168	20.24%
Thrombospondin 1	7.37E-07	16 of 56	28.57%

Table 4.5. Comparative GO pathway analysis of BL/10 and mdx lists of differentially expressed genes.

Pathway interaction maps were drawn in Genomatix using gene expression data derived from DeSeq2. The FC values for each comparison were uploaded to the system and colour-coded based on expression levels. Figures 4.14 and 4.15 show differentially expressed genes involved in the angiogenesis and VEGF signalling pathways, respectively, and colour-coded with FC data from the BL/10 96h against mdx 96h comparison. Figures 4.16 and 4.17 show differentially expressed genes involved in the HIF-1α pathway with only the 26 significant genes in the BL/10 96h against mdx 96h comparison shown in the former and the whole pathway in the latter.

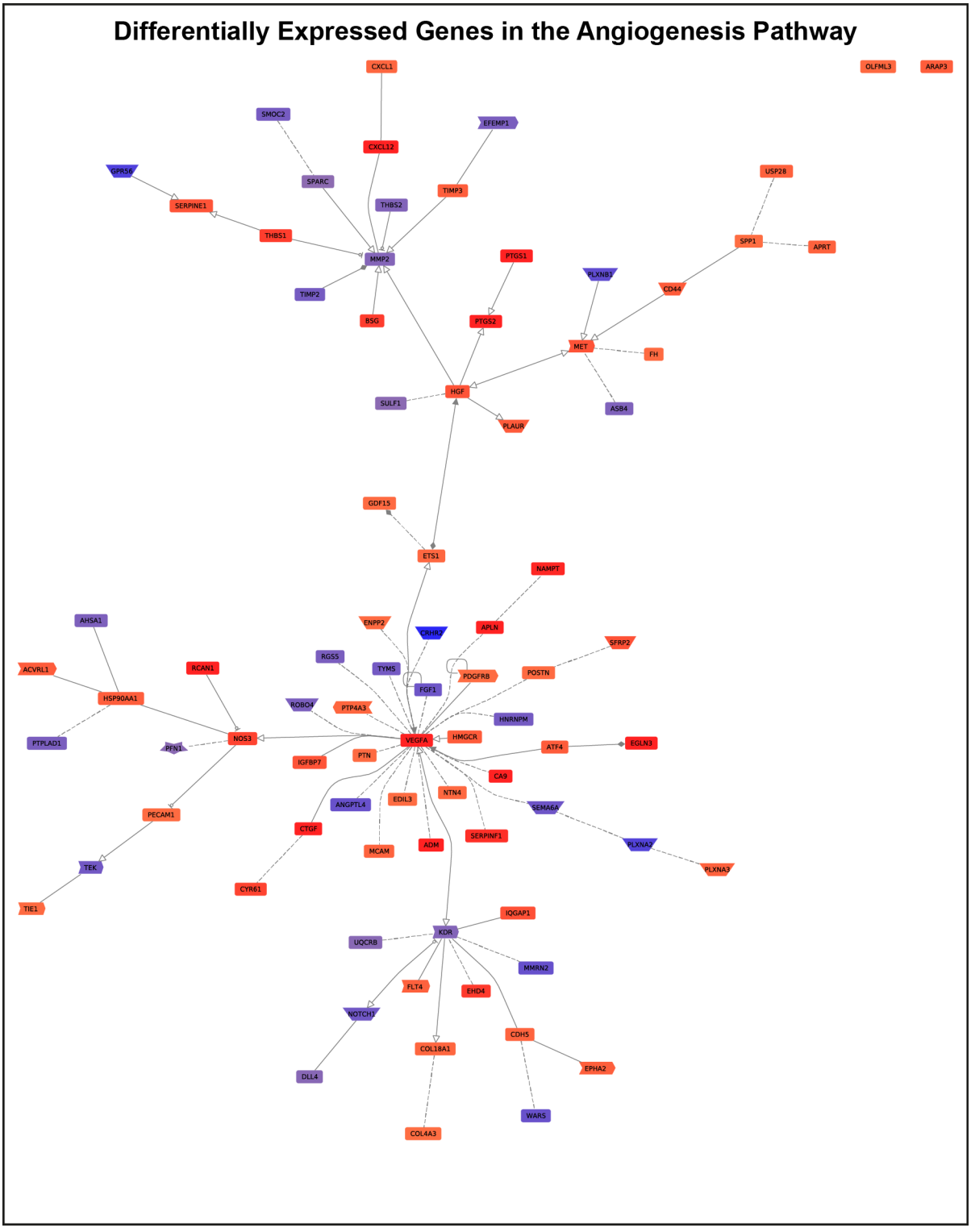

Figure 4.14. Angiogenesis signalling pathway in cardiomyocyte hypertrophy. The diagram shows interactions between the 84 differentially expressed genes from the combined gene list. Expression levels are shown for the BL/10 96h against mdx 96h comparison, represented in red where upregulated and blue where downregulated in mdx samples.

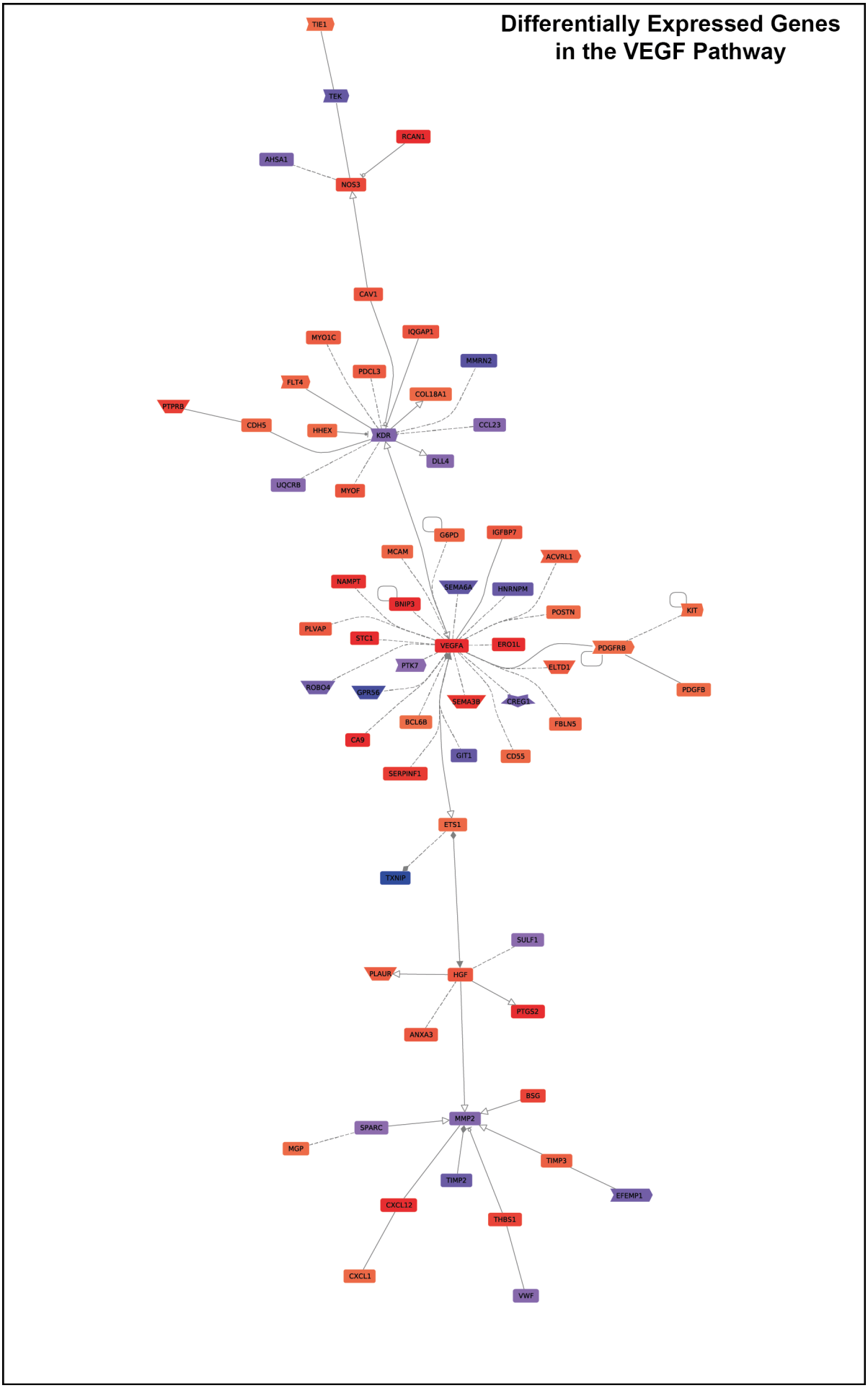
Differentially Expressed Genes
in the VEGF Pathway
TIE1
TEK
RCAN1
AHSA1
NOS3
CAV1
MYO1C
IQGAP1
MMRN2
PDCL3
FLT4
COL18A1
PTPRB
CDH5
HHEX
KDR
CCL23
DLL4
UQCRB
MYOF
G6PD
IGFBP7
MCAM
ACVRL1
NAMPT
SEMA6A
HNRNPM
BNIP3
POSTN
KIT
PLVAP
STC1
VEGFA
ERO1L
PDGFRB
PTK7
ELTD1
PDGFB
ROBO4
GPR56
SEMA3F
CREG1
BCL6B
FBLN5
CA9
GIT1
CD55
SERPINF1
ETS1
TXNIP
SULF1
PLAUR
HGF
PTGS2
ANXA3
BSG
MMP2
SPARC
MGP
TIMP3
TIMP2
EFEMP1
CXCL12
THBS1
CXCL1
VWF

Figure 4.15. VEGF signalling pathway in cardiomyocyte hypertrophy. The diagram shows interactions between the 66 differentially expressed genes from the combined gene list. Expression levels are shown for the BL/10 96h against mdx 96h comparison, represented in red where upregulated and blue where downregulated in mdx samples.

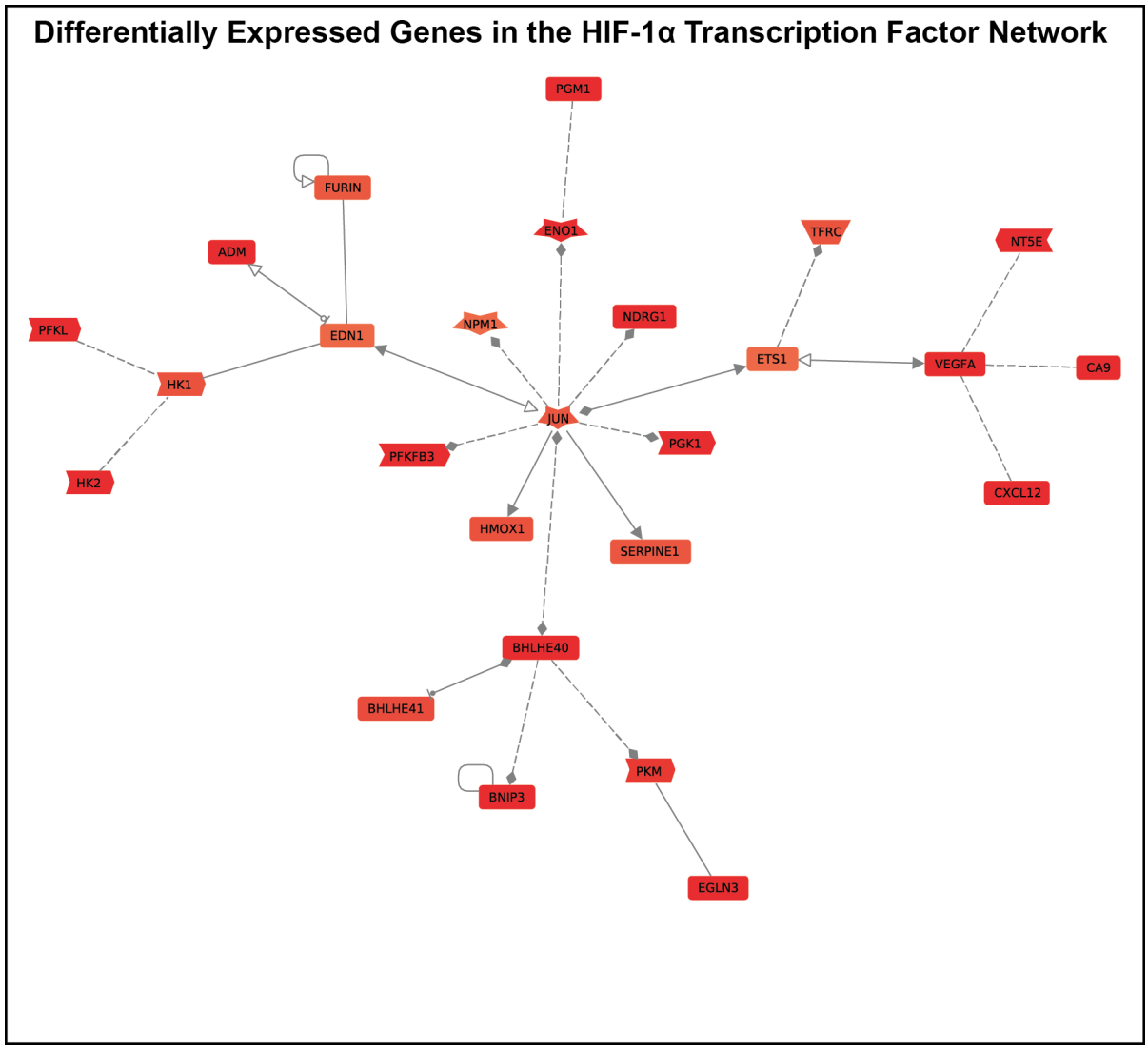

Figure 4.16. HIF-1α signalling pathway in cardiomyocyte hypertrophy. The diagram shows interactions between the 26 differentially expressed genes from the BL/10 96h against mdx 96h comparison gene list. All gene expression levels from this group were upregulated in mdx samples relative to BL/10.

Differentially Expressed Genes in the HIF-1α Canonical Pathway

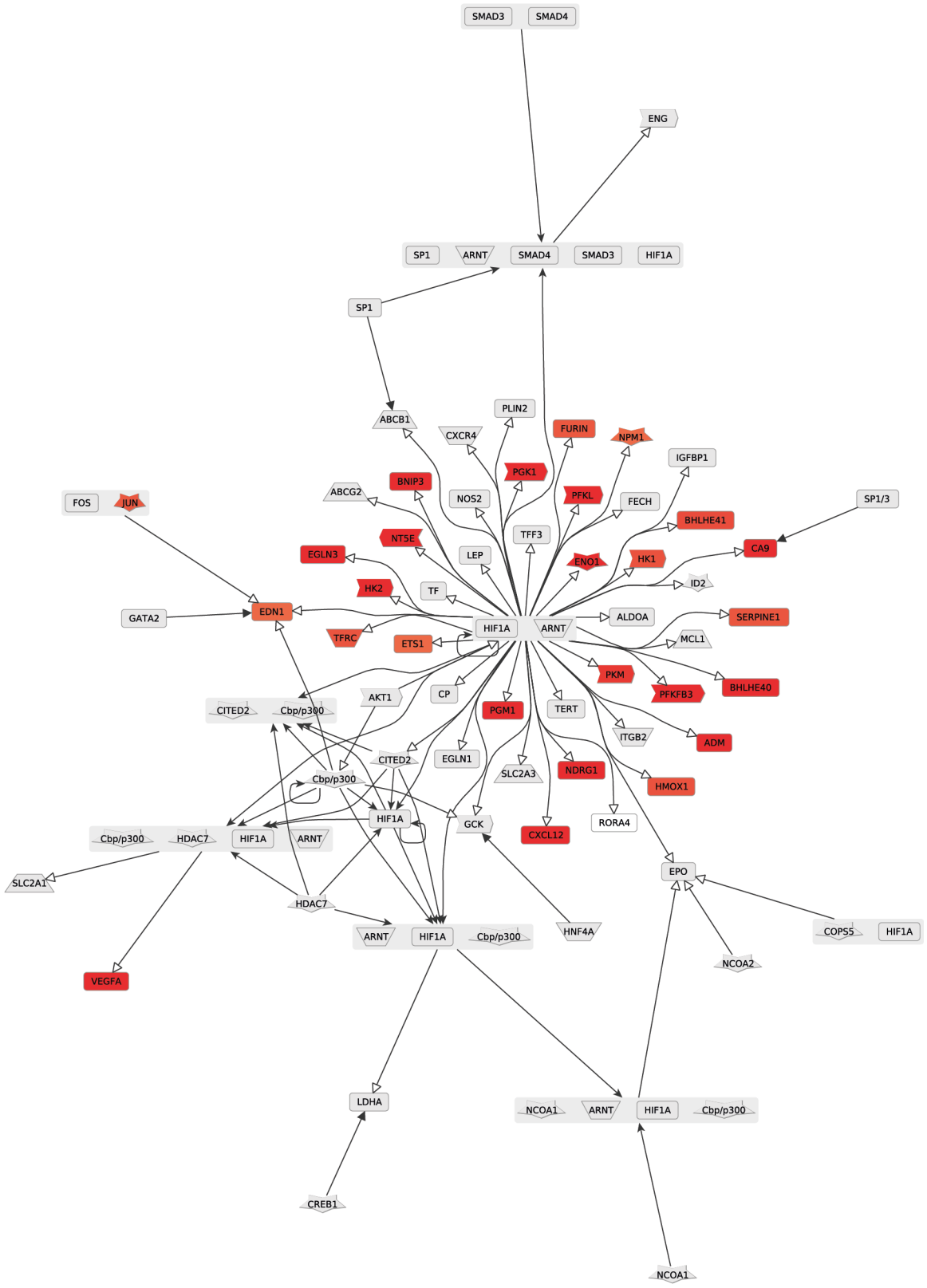

Figure 4.17. Canonical HIF-1α signalling pathway. The diagram shows interactions within the whole pathway. 26 differentially expressed genes from the BL/10 96h against mdx 96h comparison gene list. All gene expression levels from this group were upregulated in mdx samples relative to BL/10.

4.7 qRT-PCR Validation of Genes Differentially Expressed in RNA-Seq Data

A group of five genes was used for validating RNA-Seq data with quantitative real-time PCR (qRT-PCR). These genes were chosen based on their expression patterns and expected moderate to high expression levels in the target tissue. The single criterion that had to be met by all five was that they were identified in at least one of the DeSeq2 comparisons as a differentially expressed gene.

The selection of genes for validation was based on several factors. Differentially expressed gene Log_2FC values from both the BL/10 0h against BL/10 96h and mdx 0h against 96h comparisons were plotted against each other (figure 4.18). *Sod3* and *Fmod* were strongly upregulated in both BL/10 and mdx comparisons, while *Acta1* and *Angptl4* were strongly downregulated. *Nppb* was downregulated in both comparisons, but to a lesser extent in mdx serum starvation. Fibromodulin (*Fmod*) and brain natriuretic peptide (BNP, *Nppb*) were chosen as candidates for validation based on their large shift in expression across the serum starvation time-course. Phospholamban (PLN, *Pln* gene) was chosen based on previous literature showing its role in the dystrophic phenotype (Barry et al., 2008). *Pln* was also highlighted in the graph in figure 4.18 to compare its differential expression to other tested genes. Vascular endothelial growth factor A (VEGFA, *Vegfa*) was chosen based on GO results, where this gene played a central role in several signalling pathways (figures 4.14-16). Ubiquinone 1 alpha subcomplex 4-like 2 (NDUFA4L2, *Ndufa4l2*) was chosen due to its upregulation in mdx serum starvation (mdx 0h v mdx 96h) and downregulation in BL/10 serum starvation (BL/10 0h v BL/10 96h), thus giving a high overall upregulation in mdx samples when BL/10 96h and mdx 96h samples were compared against each other. In addition to four biological replicates of BL/10 and mdx samples across the serum starvation time-course (0h to 96h), expression levels of these genes in mdx and BL/10 heart tissue were also assessed. *Vegfa* was only significantly regulated in the BL/10 0h v 96h comparison and *Ndufa4l2* was significantly upregulated in the BL/10 96h v mdx 96h comparison, but not in either of the comparisons used to create figure 4.18.

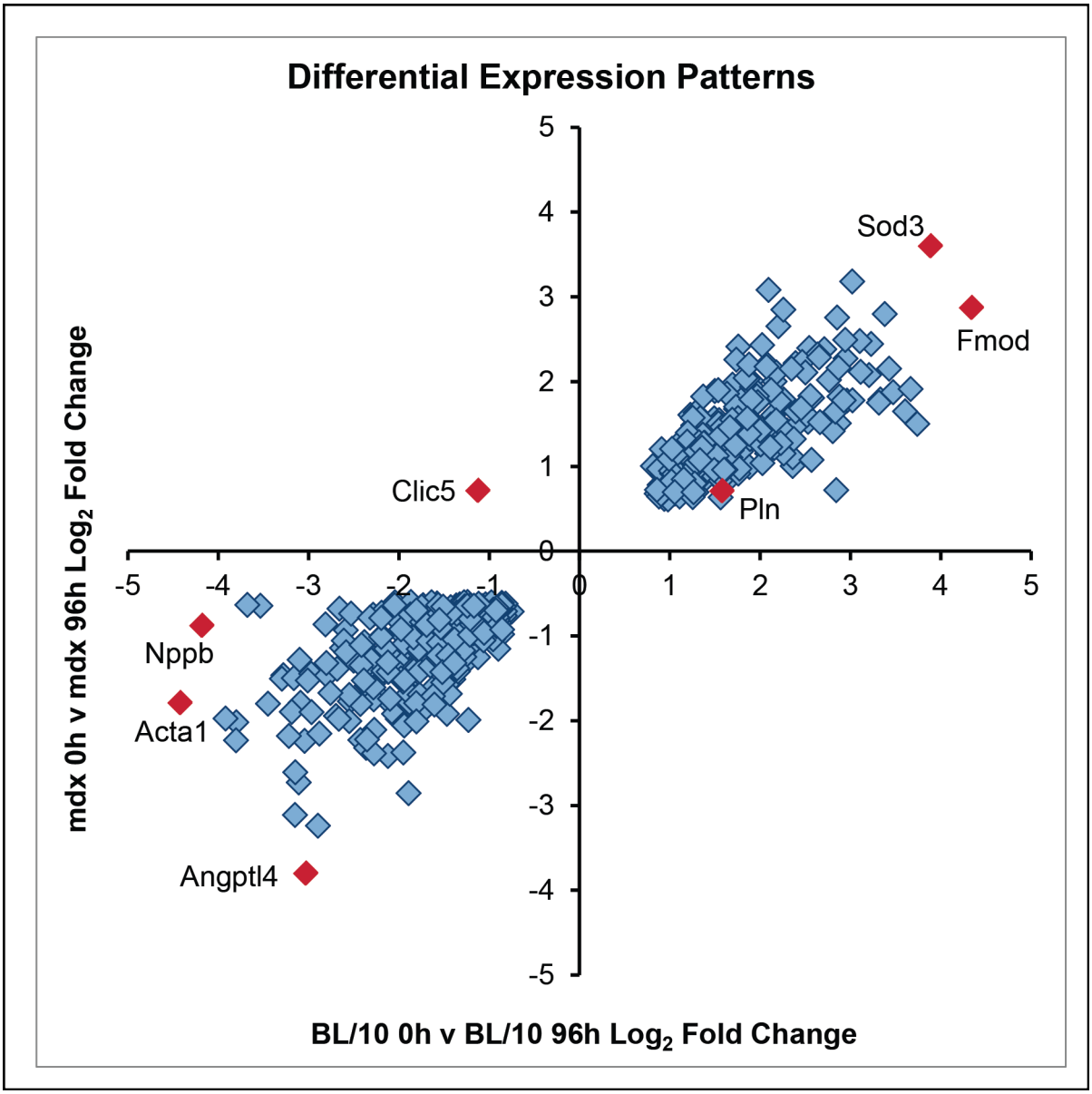

Figure 4.18. Differential Expression Patterns. The Log_2FC expression values of genes that were differentially expressed in both of the following two comparisons were plotted against each other: the BL/10 0h against 96h and mdx 0h against 96h comparisons. *Fmod*, *Nppb* and *Pln* were chosen for RNA-Seq validation with qRT-PCR and are highlighted in the diagram. Other potential candidates for further studies were also identified: *Acta1*, *Angptl4*, *Sod3* and *Clic5*.

4.7.1 Assessing Housekeeping Genes

Choosing housekeeping genes for qRT-PCR validation of RNA-Seq data was made challenging by most orthodox mouse housekeeping genes, such as *Gapdh* (glyceraldehyde 3-phosphate dehydrogenase) and *Actb* (beta-actin), having come up in differential expression comparisons as genes with significantly altered expression patterns. Two housekeeping genes – *Tpt1* and *Hsp90ab1* – were trialled. *Hsp90ab1* was used as one of twelve genes in a mouse housekeeping gene array product supplied by Qiagen (PAMM-000Z). *Tpt1* has previously been published as a relevant housekeeping gene in gene expression studies conducted on murine cardiac tissue (Pilbrow et al., 2008). Neither was included in any of the pre-filtered gene lists including all events at FDR below 0.05. *Hsp90ab1* expresses heat shock protein 90-beta and *Tpt1* encodes a translationally-controlled tumour protein.

Results in expression patterns from one qRT-PCR experiment for *Tpt1* with 30 cardiomyocyte samples were compared against two experiments for *Hsp90ab1* with ten samples in each run. One clear outlier with an RNA concentration of 0.29 ng/µl was removed from the *Tpt1* dataset. *Tpt1* showed much more reliable primer efficiency (figure 4.19) than *Hsp90ab1* (figure 4.20) when the Ct values of each sample were plotted against their base ten logarithm (Log_{10}) of RNA concentration. *Tpt1* samples gave a linear line of best fit slope value of -3.3235, which equals to 99.93% primer amplification efficiency. *Hsp90ab1* primer amplification efficiencies were 81.79% and 34.96%, determined from the slope values of -3.8524 and -7.6799 in runs A and B, respectively. There was no background amplification in the no template control samples using either of the trialled housekeeping gene primer sets. However, *Tpt1* nominal Ct values were considerably and consistently lower than *Hsp90ab1* Ct values. Therefore, based on higher amplification efficiency and lower Ct values *Tpt1* was chosen as the housekeeping gene for all qRT-PCR differential expression analyses with the $\Delta\Delta$Ct method.

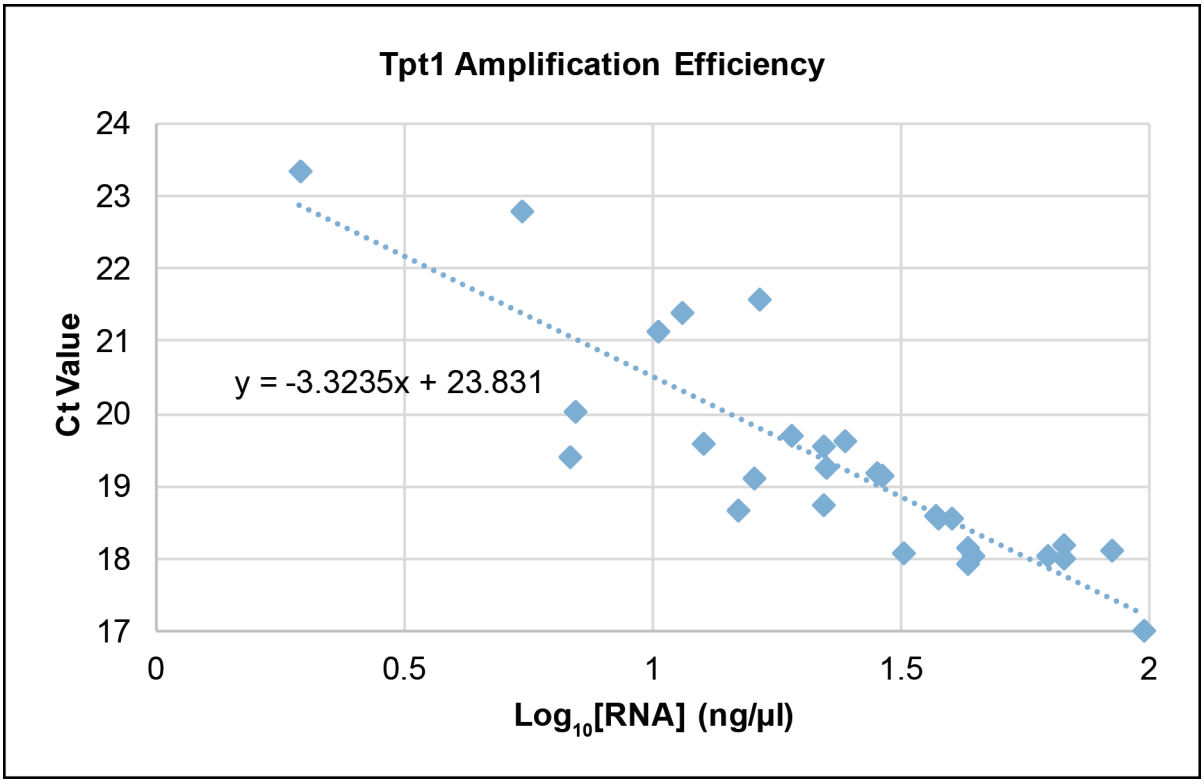

Figure 4.19. Assessing *Tpt1* as a housekeeping gene for qRT-PCR. Sample Ct values were plotted against the Log_{10} of RNA concentration and the linear line of best fit was drawn to calculate primer amplification efficiency.

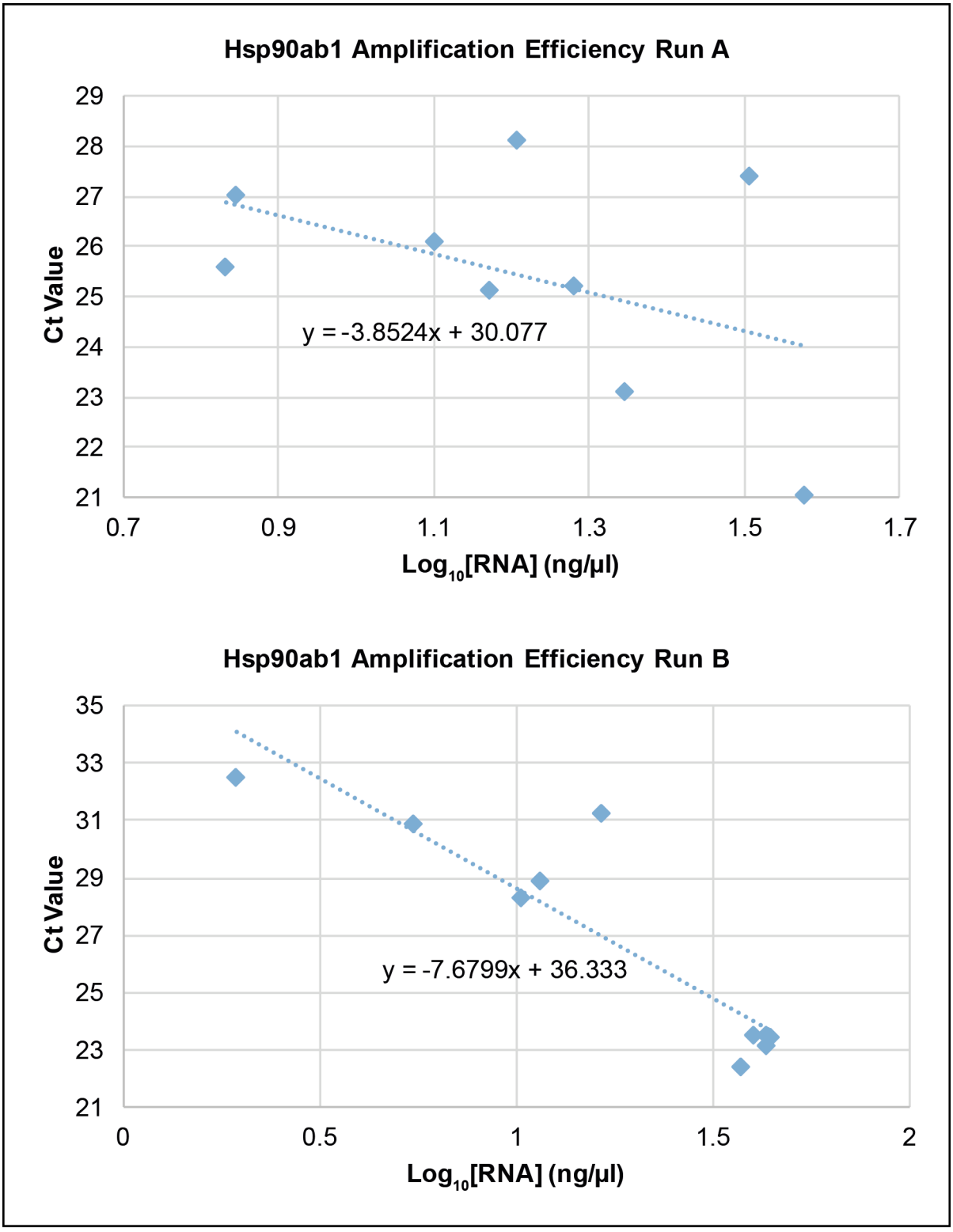

Figure 4.20. Assessing *Hsp90ab1* as a housekeeping gene for qRT-PCR. Sample Ct values were plotted against the Log_{10} of RNA concentration and the linear line of best fit was drawn for both run A and run B to calculate primer amplification efficiency.

4.7.2 Validating Expression Patterns of Differentially Expressed Genes.

BNP is upregulated in response to cardiac pathology (Zois et al., 2014). The *Nppb* mouse gene was markedly upregulated in mdx adult mouse heart tissue, compared to BL/ 10 control tissue, by 6.9-fold in nominal FC and a factor of 2.8 in Log_2FC (figure 4.21). A similar 8-fold upregulation was seen in the BL/10 96h against mdx 96h time-point comparison in RNA-Seq data. However, the opposite trend was revealed when different biological replicates were compared by qRT-PCR, where a -2.25-fold downregulation was seen. This was due to a diminished downregulatory effect in BL/10 cardiomyocytes in response to serum starvation in qRT-PCR results in contrast to RNA-Seq data. However, the same downregulation effect was seen in all but the BL/10 24h v BL/10 96h comparison, where the downregulation fold change did not cross the -0.6 Log_2FC cut-off set for RNA-Seq results (-3.66 Log_2FC seen by RNA-Seq and -0.18 by qRT-PCR analysis). RNA-Seq identified downregulation of *Nppb* in response to serum starvation. This was validated with qRT-PCR, where comparable regulation levels were seen.

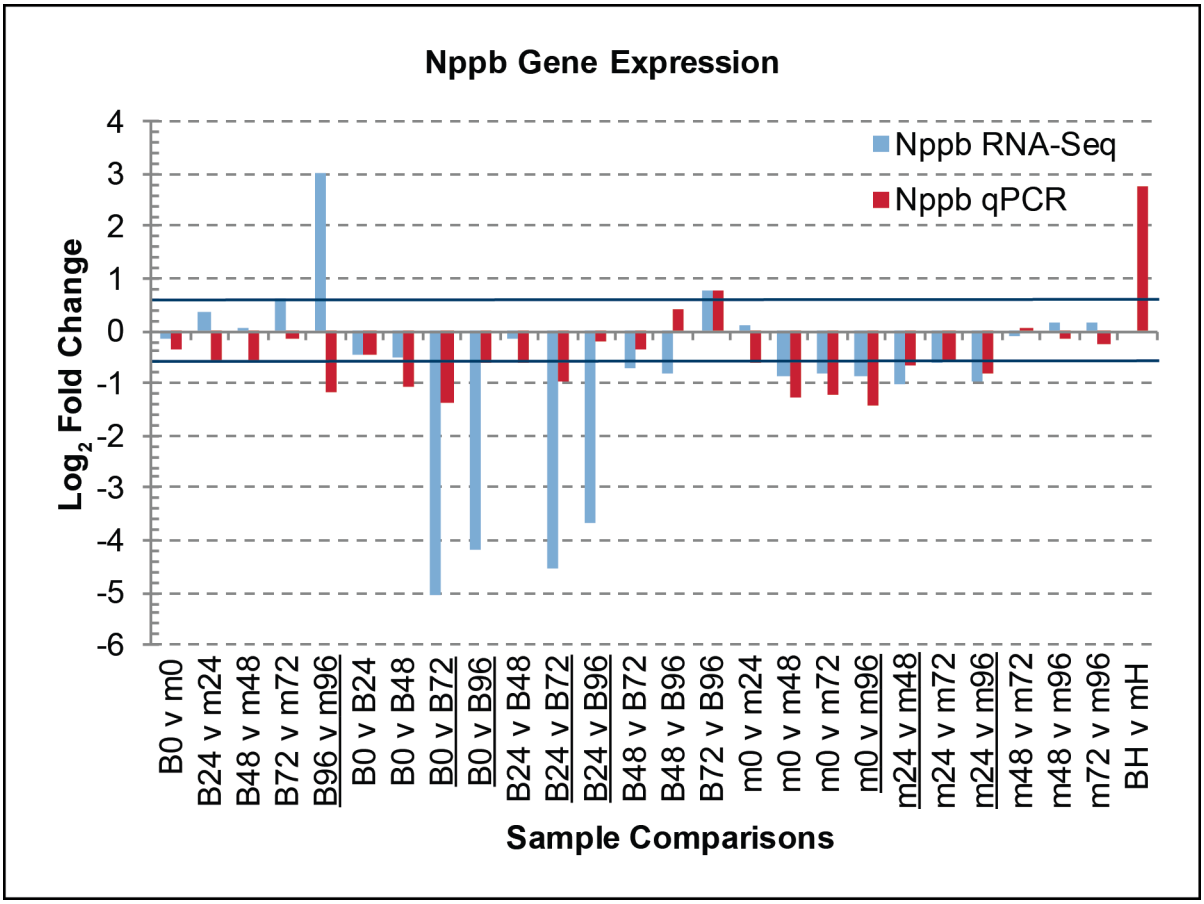

Figure 4.21. *Nppb* gene expression analyses with qRT-PCR and RNA-Seq. The Log_2FC +/-0.6 cut-off points are highlighted with blue lines across the graph. Where *Nppb* was a significant differentially expressed gene the comparison has been underlined.

PLN inhibits Ca^{2+} reuptake into the sarcoplasmic reticulum (SR) by inhibiting the cardiac SR luminal Ca^{2+}-ATPase (SERCA) and consequently exacerbating Ca^{2+}-controlled pathways of cardiac pathology (Barry et al., 2008). Figure 4.22 summarises the *Pln* expression pattern. It was upregulated in RNA-Seq expression analyses, but downregulated in qRT-PCR data in both BL/10 and mdx cardiomyocytes in response to serum starvation. When *Pln* expression was compared between BL/10 and mdx cardiomyocytes it was downregulated in mdx cardiomyocytes in RNA-Seq data, but upregulated in qRT-PCR quantification. It was also upregulated in adult mdx heart tissue in comparison to BL/10 hearts.

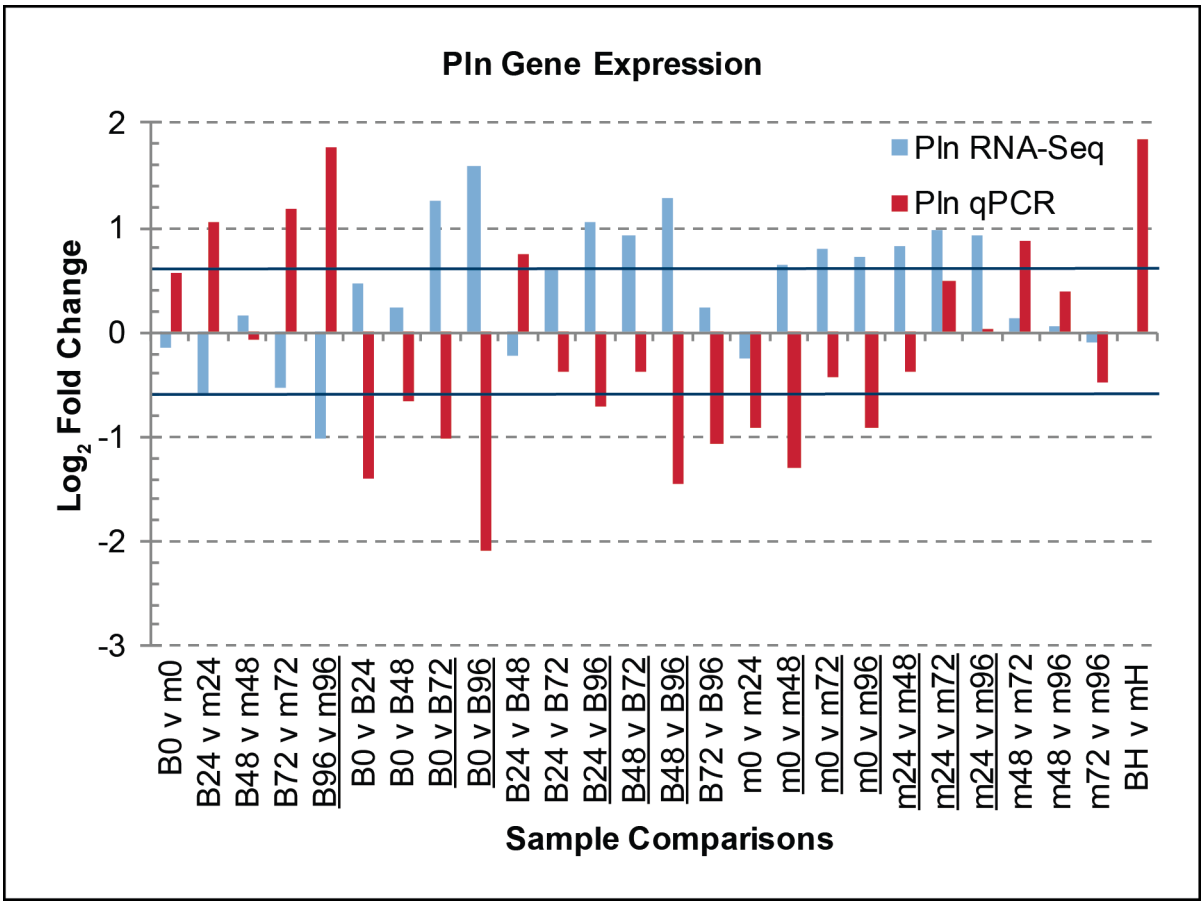

Figure 4.22. *Pln* gene expression analyses with qRT-PCR and RNA-Seq. The Log_2FC +/-0.6 cut-off points are highlighted with blue lines across the graph. Where *Pln* was a significant differentially expressed gene the comparison has been underlined.

Fibromodulin (encoded by the *Fmod* gene) is a protein that is involved in ECM assembly and composition (Kalamajski & Oldberg, 2010), the TGFβ signalling pathway and angiogenesis (Hildebrand et al., 1994; Adini et al., 2014). *Fmod* expression was significantly upregulated in BL/10 and mdx cardiomyocytes by serum starvation in both RNA-Seq and qRT-PCR results (figure 4.23). Interestingly, qRT-PCR results indicated that *Fmod* was even more strongly upregulated by serum starvation than expected from RNA-Seq analysis. However, whilst the RNA-Seq data showed a slight, but non-significant upregulation of *Fmod* in mdx samples when BL/10 samples were compared against mdx samples at individual time-points of serum starvation, the opposite effect was identified in qRT-PCR results. In four comparisons (BL/10 0h v mdx 0h, BL/10 24h v mdx 24h, BL/10 48h v mdx 48h and BL/10 96h v mdx 96h) the average Log_2FC even exceeded the -0.6 cut-off used to filter RNA-Seq gene lists. *Fmod* was also 1.8-fold downregulated in mdx adult heart in comparison to BL/10 adult heart tissue.

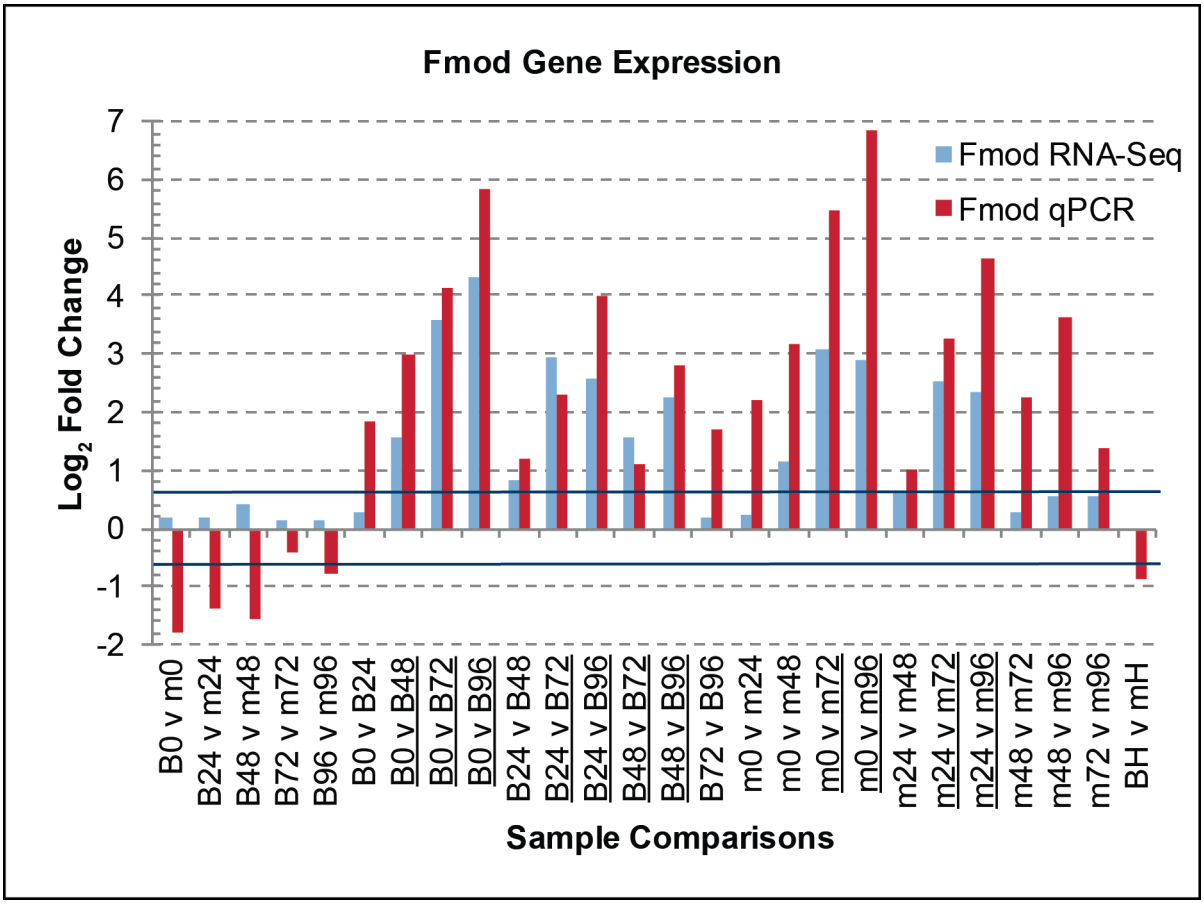

Figure 4.23. *Fmod* gene expression analyses with qRT-PCR and RNA-Seq. The Log_2FC +/-0.6 cut-off points are highlighted with blue lines across the graph. Where *Fmod* was a significant differentially expressed gene the comparison has been underlined.

VEGFA signalling is involved in several cellular responses, such as vasodilation, angiogenesis, cell survival and recruitment of vascular progenitor cells (Taimeh et al., 2013). Gene expression of *Vegfa* in mice was significantly upregulated in mdx cardiomyocytes in comparison to BL/10 cardiomyocytes at the 24h and 96h serum starvation time-points (figure 4.24), by 1.8 and 2.6 nominal FC, respectively. However, these trends were not confirmed by qRT-PCR. Instead, at the 96h time-point a 2.1-fold downregulation was observed. A similar contradictory data point was the BL/10 0h against BL/10 96h comparison, where an opposite to expected gene expression profile was also observed. None of the other significant differential expression comparisons showed anomalous results by qRT-PCR. The mdx 48h v mdx 72h and mdx 48h v mdx 96h comparisons also crossed the differential expression cut-off whilst the corresponding RNA-Seq data points did not. There was only a slight reduction in *Vegfa* expression in mdx adult heart tissue in comparison to BL/10 heart tissue.

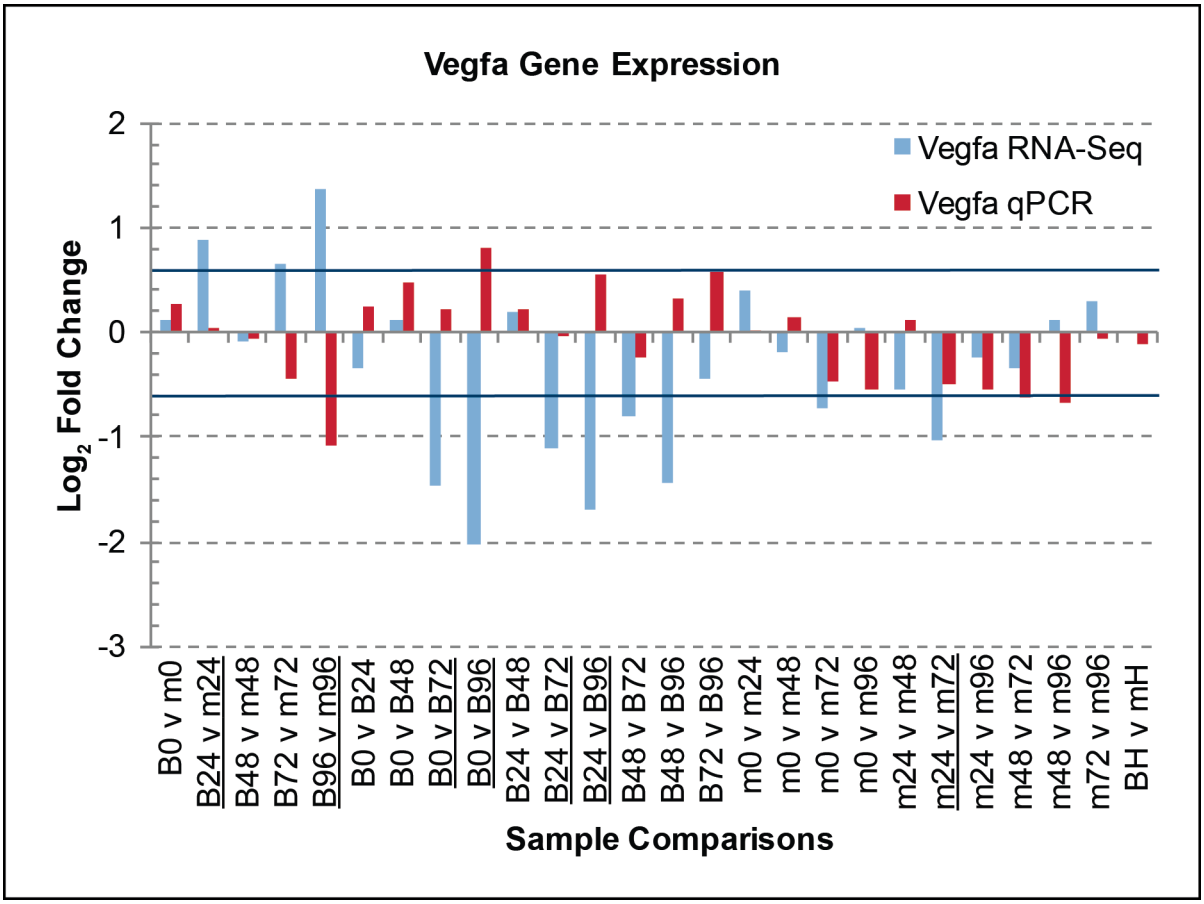

Figure 4.24. *Vegfa* gene expression analyses with qRT-PCR and RNA-Seq. The Log_2FC +/-0.6 cut-off points are highlighted with blue lines across the graph. Where *Vegfa* was a significant differentially expressed gene the comparison has been underlined.

Ndufa4l2 encodes a mitochondrial protein involved in hypoxia, regulated by HIF-1α (Tello et al., 2011). This gene was significantly upregulated by serum starvation in mdx cardiomyocytes, whilst being downregulated by serum starvation in BL/10 samples. As a result, RNA-Seq data showed a significant increase in *Ndufa4l2* expression in mdx cardiomyocytes at the 96h serum starvation time-point in contrast to BL/10 96h samples. These results, however, did not entirely replicate in qRT-PCR validation. Based on qRT-PCR results *Ndufa4l2* was upregulated by serum starvation in both BL/10 and mdx samples, therefore diminishing the differential expression between the two seen in RNA-Seq results. However, comparisons of mdx 0h samples against subsequent serum starvation time-points closely replicated RNA-Seq results, as seen in figure 4.25. *Ndufa4l2* expression was near equal in adult mdx and BL/10 heart tissue.

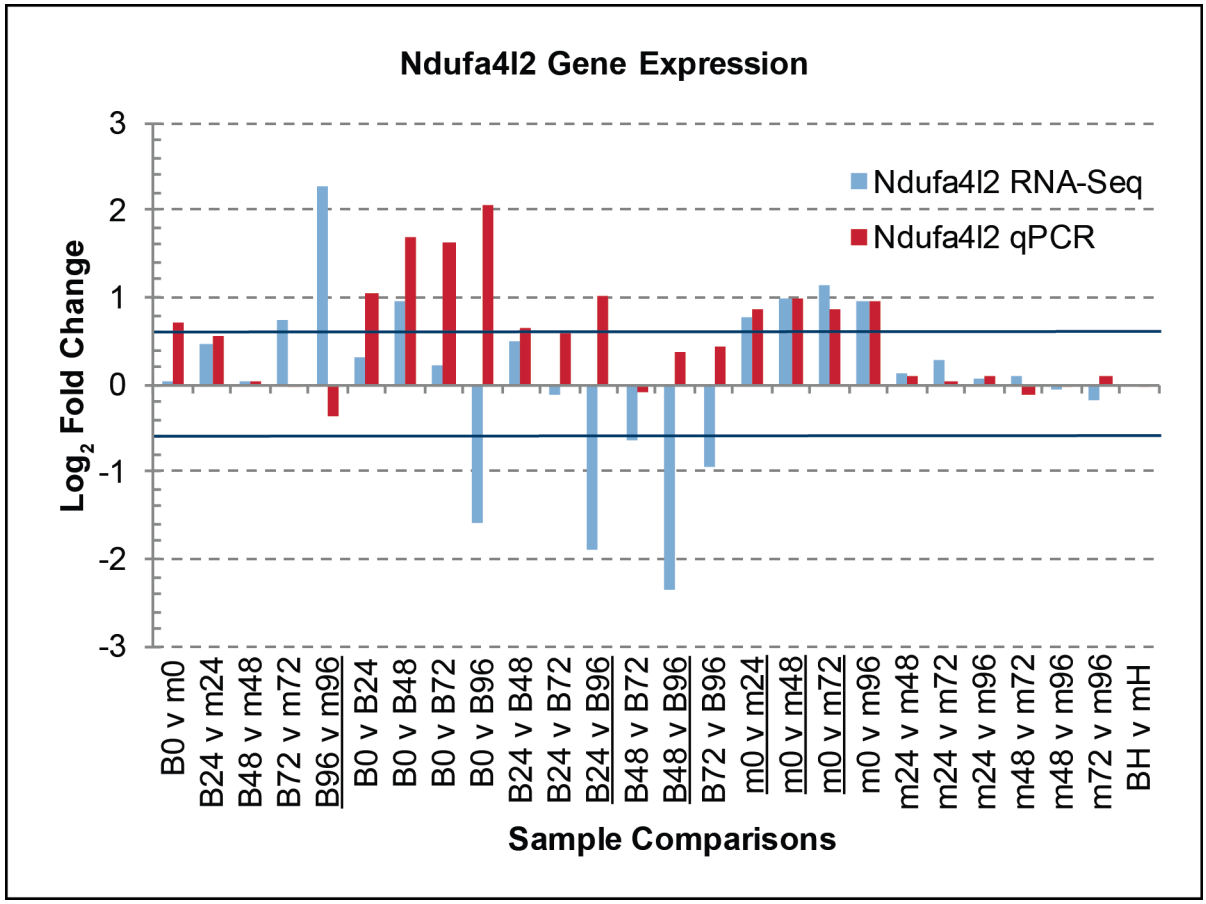

Figure 4.25. *Ndufa4l2* gene expression analyses with qRT-PCR and RNA-Seq. The Log_2FC +/-0.6 cut-off points are highlighted with blue lines across the graph. Where *Ndufa4l2* was a significant differentially expressed gene the comparison has been underlined.

Gene expression values in Log_2FC from RNA-Seq and corresponding qRT-PCR validation datasets were summarised and are shown in table 4.6. Significant results from RNA-Seq analysis were highlighted for direct comparison in qRT-PCR results.

Log_2FC	Fmod		Ndufa4l2		Nppb		Pln		Vegfa	
Comparison	R-S	qP	R-S	qP	R-S	qP	R-S	qP	R-S	qP
B0 v m0	0.18	-1.77	0.01	0.72	-0.15	-0.35	-0.14	0.58	0.12	0.27
B24 v m24	0.19	-1.40	0.46	0.56	0.38	-0.53	-0.59	1.05	0.87	0.04
B48 v m48	0.44	-1.58	0.00	0.01	0.03	-0.57	0.16	-0.06	-0.08	-0.06
B72 v m72	0.13	-0.43	0.73	-0.02	0.61	-0.16	-0.54	1.18	0.65	-0.43
B96 v m96	0.15	-0.77	2.28	-0.37	3.00	-1.17	-1.01	1.77	1.36	-1.07
B0 v B24	0.29	1.83	0.32	1.03	-0.46	-0.44	0.47	-1.40	-0.34	0.25
B0 v B48	1.56	3.01	0.95	1.69	-0.49	-1.06	0.23	-0.66	0.12	0.48
B0 v B72	3.61	4.12	0.23	1.62	-5.07	-1.39	1.26	-1.03	-1.46	0.23
B0 v B96	4.34	5.83	-1.59	2.06	-4.18	-0.62	1.58	-2.10	-2.03	0.80
B24 v B48	0.81	1.18	0.50	0.66	-0.14	-0.61	-0.22	0.74	0.21	0.23
B24 v B72	2.95	2.30	-0.12	0.58	-4.51	-0.95	0.60	-0.37	-1.11	-0.02
B24 v B96	2.60	4.00	-1.88	1.03	-3.66	-0.18	1.04	-0.70	-1.69	0.55
B48 v B72	1.56	1.12	-0.63	-0.08	-0.71	-0.34	0.94	-0.37	-0.80	-0.25
B48 v B96	2.26	2.82	-2.34	0.37	-0.81	0.44	1.27	-1.44	-1.43	0.32
B72 v B96	0.21	1.71	-0.93	0.44	0.77	0.77	0.23	-1.07	-0.44	0.57
m0 v m24	0.24	2.20	0.77	0.87	0.11	-0.63	-0.25	-0.92	0.40	0.02
m0 v m48	1.15	3.19	0.99	0.98	-0.88	-1.29	0.65	-1.29	-0.20	0.14
m0 v m72	3.09	5.46	1.12	0.88	-0.79	-1.21	0.80	-0.42	-0.73	-0.48
m0 v m96	2.88	6.83	0.94	0.96	-0.87	-1.44	0.72	-0.91	0.05	-0.54
m24 v m48	0.66	1.00	0.13	0.11	-1.03	-0.65	0.81	-0.37	-0.53	0.13
m24 v m72	2.54	3.26	0.27	0.01	-0.62	-0.58	0.97	0.50	-1.02	-0.49
m24 v m96	2.34	4.63	0.05	0.09	-0.99	-0.81	0.92	0.01	-0.24	-0.56
m48 v m72	0.29	2.26	0.11	-0.11	-0.09	0.08	0.13	0.87	-0.35	-0.62
m48 v m96	0.56	3.63	-0.07	-0.02	0.16	-0.16	0.05	0.38	0.11	-0.68
m72 v m96	0.55	1.37	-0.17	0.09	0.16	-0.24	-0.09	-0.48	0.31	-0.06
BH v mH		-0.88		-0.04		2.79		1.83		-0.12

Table 4.6. Summary of RNA-Seq validation data from qRT-PCR. All data points that were significant and above or below the +/-0.6 Log_2FC cut-off are highlighted in red.

4.8 Discussion

Triplicates of BL/10 and mdx samples at each time-point of serum starvation were obtained, but only duplicates of BL/10 samples sequenced due low RNA quality in some samples of one biological replicate. Sample quality control was also performed at the sequence level with FastQC and ensuring the Dmd gene mutation was present in mdx samples.

Gene expression heatmaps showing expression pattern distances in figure 4.9 featured the *Dmd* gene as one of the differentially expressed genes when comparing BL/10 cardiomyocytes against mdx cardiomyocytes at all time-points. *Dmd* clustered with other genes showing higher expression in BL/10 than mdx samples, which follows previously published data on the lower expression level of the gene in the mdx mouse (Chamberlain et al., 1991).

Gene lists were filtered by increasing the confidence interval to 99% (adjusted p-value<0.01) and introducing a fold-change cut-off at +/-0.6 Log_2FC. The results showed a noteworthy tendency in the number of genes differentially expressed in comparisons between serum starvation time-points within each genotype. BL/10 cardiomyocyte time-point comparisons showed a lower number of genes than mdx cardiomyocytes in the earlier time-point comparisons: BL/10 0h v 24h resulted in 89 genes, whereas mdx 0h v 24h resulted in 327 statistically significant differentially expressed genes. The opposite was witnessed later in the time-course. For instance, in the BL/10 48h v 96h comparison 355 genes were differentially expressed, while only 42 were identified from the mdx 48h v 96h comparison. The fact that the mdx 72h v 96h comparison did not return any statistically significant differentially expressed genes crossing the Log_2FC cut-off suggests that the process of hypertrophy as modelled here is complete on the gene expression level by the 72h time-point, whereas the adaptation continues in BL/10 cardiomyocytes. This could be interpreted as the process being faster in the mdx model, compared to BL/10 cardiomyocytes. However, it may also be that BL/10 cardiomyocytes adapt better to serum starvation, in a less rushed way and without the need to regulate as many genes initially to counteract the environmental cues in a hypertrophic fashion. It may only be in the later comparisons where BL/10 cardiomyocytes need to regulate more genes to avoid becoming hypertrophic.

4.8.1 Genes with the Highest Expression Response to Serum Starvation

Expression patterns of genes identified in both BL/10 and mdx 0h against 96h serum starvation comparisons revealed a set of genes that had distinct regulation patterns (figure 4.18). *Clic5* was one of the highlighted genes in the differential expression comparison graph. It was the only gene that was significantly upregulated in the mdx comparison (mdx 0h v mdx 96h by 1.6-fold) and downregulated in the BL/10 comparison (BL/10 0h v BL/10 96h by -2.2-fold). The opposing directions of regulation in the mouse models resulted in a 3.3-fold upregulation in the BL/10 96h v mdx 96h comparison. *Clic5* was originally omitted from the qRT-PCR validation panel of genes due to its lower nominal change within BL/10 and mdx comparisons, but based on validation results it would have been useful to see whether the differential expression between mdx and BL/10 samples would have replicated. The overall trend of expression based on RNA-Seq results showed initial upregulation as a result of serum starvation in both BL/10 and mdx samples within the 24-48h, followed by a sharp downregulation in BL/10 as opposed to comparatively stable expression levels in mdx throughout the remaining time-course. This expression pattern indicates that mdx cardiomyocytes keep the signalling pathways and transcription factors required for *Clic5* expression activated, while BL/10 cardiomyocytes must have inhibited the upstream signals driving the gene's expression. *Clic5* encodes for the chloride intracellular protein 5, which phosphorylates ezrin, in turn responsible for actin polymerisation in kidney tissue podocytes, colocalising with conjugated phalloidin in ICC fluorescence imaging (Al-Momany et al., 2014). Its role in cardiac muscle has not been characterised, but it has been reported to increase C2C12 cell myogenesis when overexpressed, hindering cell proliferation and accelerating differentiation (Li et al., 2010).

Serum starvation of BL/10 and mdx cardiomyocytes substantially downregulated *Angptl4* expression in cells from both mouse strains. Angiopoietin-like 4 (ANGPTL4) has protective properties against myocardial infarct size and ischaemic stroke damage by inhibiting Src-mediated VEGF signal transduction (Galaup et al., 2012) (Bouleti et al., 2013). ANGPTL4 expression is activated by peroxisome proliferator-activated receptor delta (PPARδ) and a PPARδ agonist has been shown to alleviate heart hypertrophy through *Angptl4* expression-mediated mechanisms (Kojonazarov et al., 2013). The PPARδ gene *Ppard* was not differentially expressed in the RNA-Seq dataset. ANGPTL4 enhances wound healing by increasing inducible nitric oxide

synthase (iNOS) expression via the Integrin/JAK/STAT3 pathway (Chong et al., 2014). It has been postulated that iNOS overexpression and the concomitant increase in nitric oxide (NO) exacerbates dystrophic cardiomyopathy by activating ryanodine receptors (RyR) and consequently releasing SR-stored Ca^{2+} to the intracellular space (Finsterer & Cripe, 2014). However, the iNOS gene *Nos2* was not differentially expressed in the RNA-Seq dataset. These results show that although *Angptl4* is a candidate for further studies into hypertrophy in dystrophic cardiomyocytes, its function needs to be assessed by identifying protein activation levels in the relevant pathways rather than on gene expression alone, before it could be hypothesised to be a target for therapeutic testing.

Superoxide dismutase 3 (SOD3) is an extracellular SOD, expressed by the *Sod3* gene, which was substantially upregulated in response to serum starvation in both BL/10 and mdx cardiomyocytes: in BL/10 0h v 96h by 14.7-fold and in mdx 0h v mdx 96h by 12-fold. SOD3 knockout mice develop cardiac hypertrophy and fibrosis in response to transverse aortic constriction, with a significant increase in MMP2 and MMP9 levels (Lu et al., 2008). While *Mmp9* levels were not significantly affected in the RNA-Seq dataset, *Mmp2* levels were elevated close to 3-fold by 96h of cardiomyocyte serum starvation in both BL/10 and mdx samples. SOD3 is located in the extracellular matrix (ECM), where it clears superoxides by converting them into hydrogen peroxide (Gongora & Harrison, 2008). Elevated levels of *Sod3* expression may be indicative of increased superoxide presence in the culture model, but can also be indicative of effective management of stretch-induced reactive oxygen species (ROS) levels, including superoxides. In this model SOD3 may compensate for mislocalised nNOS function tackling ROS.

Skeletal α-actin (*Acta1* gene, also highlighted in figure 4.18) expression in embryonic hearts is gradually replaced by cardiac α-actin (*Actc1* gene) expression during development and the latter structural protein is predominant in adult hearts (Cox & Marsh, 2014). A return to *Acta1* expression in adult cardiomyocytes is a hallmark of foetal gene program (FGP) activation. The emergence of FGP markers in adult cardiac tissue is indicative of heart dysfunction (Taegtmeyer et al., 2010). In this model of cardiomyocyte hypertrophy both *Acta1* and *Actc1* were downregulated by -1.8-fold in the mdx 0h v 96h comparison, and in the BL/10 0h v 96h cardiomyocyte comparison by -3.3-fold and -4.4-fold, respectively.

4.8.2 The Foetal Gene Program

In addition to the shift from *Actc1* to *Acta1*, there are other indicators of FGP onset. Regulation and effect of natriuretic peptide expression is discussed in sub-section 4.8.3. Another transcriptional shift in cardiac hypertrophy is the reduction in myosin heavy chain alpha (MHCα, *Myh6* gene) and increase in myosin heavy chain beta (MHCβ, *Myh7* gene) (Rajabi et al., 2007). This trend was confirmed by RNA-Seq in serum starved BL/10 and mdx cardiomyocytes, where *Myh6* was significantly downregulated in both cell types. Although *Myh7* was significantly upregulated in the BL/10 0h v BL/10 48h and BL/10 0h v BL/10 72h comparisons by 2.5-fold and 2-fold, respectively, there was a clear reversal of the trend and non-significant downregulation in the final 48h of serum starvation. This was not the case in mdx cardiomyocytes where a 2-fold upregulation between the 0h and 96h serum starved samples ended up being non-significant and the general trend was gradual upregulation during the time-course. Consequently, the BL/10 96h v mdx 96h comparison also resulted in a significant 1.8-fold upregulation of *Myh7* in mdx cardiomyocytes.

Other FGP factors that follow similar downregulation patterns in both BL/10 and mdx cardiomyocytes in the RNA-Seq dataset include carnitine palmitoyltransferase I (*Cpt1b*), pyruvate dehydrogenase kinase isoform 4 (*Pdk4*), muscle creatine kinase (*Ckm*) and muscle glycogen synthase (*Gys1*) (Rajabi et al., 2007).

Cytoplasmic nuclear factor of activated T-cells 4 (NFATc4, previously named NFAT3) has been shown to induce cardiac hypertrophy when phosphorylated by calcineurin (Molkentin et al., 1998). The *Nfatc4* gene was upregulated in both BL/10 and mdx cardiomyocytes, but only significantly in mdx 0h v mdx 48h and mdx 0h v mdx 96h comparisons, by 2-fold and 2.3-fold, respectively. Calcineurin was not differentially expressed in the RNA-Seq dataset. However, in order to confirm NFATc4 involvement in the hypertrophic onset in mdx cardiomyocytes, studies would be required to look into its activation levels and compared between both BL/10 and mdx cardiomyocytes, particularly as NFATc4 might not be as powerful at driving a calcineurin-activated hypertrophic response in comparison to NFATc1, NFATc2 and NFATc3 (Wilkins et al., 2002; Enwere et al., 2014). None of the other NFAT genes were differentially expressed in this model of mdx cardiomyocyte hypertrophy.

It has been shown that inhibition of nuclear factor kappa B (NFκB), also a FGP marker (Oka et al., 2007), has cardioprotective effects on the dystrophin and utrophin double knockout (dko) mouse model (Delfín et al., 2012). Although the NFκB genes *Nfkb1* and *Nfkb2* were not differentially expressed in the cardiomyocyte transcriptome, the inhibitor of kappa B alpha (IκBα) gene *Nfkbia* was downregulated around 2-fold in both BL/10 and mdx cardiomyocytes in response to serum starvation. This could mean that NFκB is more likely to be constitutively active due to reduced IκBα levels (Haskill et al., 1991) and could lead to higher activation of gene expression for mediators of hypertrophy.

Cardiac-specific upregulation of serum response factor (SRF) results in cardiomyopathy (Zhang et al., 2001). *Srf* is another developmental gene, which is included on the FGP transcription factor panel (Oka et al., 2007). However, in the cardiomyocyte serum starvation model the *Srf* gene was downregulated in both BL/10 and mdx cardiomyocytes. It is important to also mention that in addition to the discussed FGP transcription factors, some others were not differentially expressed in the RNA-Seq results, such as *Gata4*, the homeobox protein Nkx-2.5 gene *Nkx2-5* and the four myocyte enhancer factor-2 (MEF2) genes (*Mef2a*, *Mef2b*, *Mef2c* and *Mef2d*) (Oka et al., 2007).

The fact that many FGP transcription factor markers were unaltered in the cardiomyocytes indicates that the FGP initiation seen in the model primarily affects the structural proteins (actins, MHCs). It may also suggest that transcription factor modulation is not required for the type of hypertrophy seen in mdx cardiomyocytes.

4.8.3 The Effect of Natriuretic Peptides

Atrial natriuretic peptide (ANP) and BNP, also known as B-type natriuretic peptide and ventricular natriuretic peptide, are secreted in the myocardium in response to stress signals and they also form part of the FGP response mechanism to cardiac pathology (Taegtmeyer et al., 2010). The C-type natriuretic peptide was not expressed in embryonic cardiomyocytes.

Expression of the ANP gene, *Nppa*, was significantly elevated in mdx cardiomyocytes in response to serum starvation: in mdx 0h v mdx 48h by 2-fold, in mdx 0h v mdx 72h by 1.7-fold and in mdx 0h v mdx 96h by 1.8-fold. Expression of the BNP gene, *Nppb*, was significantly downregulated in both BL/10 and mdx cardiomyocytes in response to serum starvation: BL/10 0h v BL/10 96h by 18-fold and mdx 0h v mdx 96h by 1.8-fold. This resulted in a strong 8-fold upregulation in the BL/10 96h v mdx 96h comparison of *Nppb* expression. Conversely, *Nppb* levels in qRT-PCR validation experiments between BL/10 and mdx serum starved cardiomyocytes (figure 4.21) did not replicate the upregulation trend seen in RNA-Seq data. A 2.3-fold reduction in mdx 96h serum starved samples was seen in comparison to BL/10 96h samples. However, all other statistically significant reductions in intra-BL/10 and intra-mdx samples were replicated based on the -0.6 Log_2FC cut-off, apart from the BL/10 24h v BL/10 96h comparison, where a near 13-fold reduction seen in RNA-Seq data was not replicated by a 1.1-fold downregulation.

Both ANP and BNP mediate their effect via natriuretic peptide receptors (NPR), mostly through NPRA, but also at a lower affinity via NPRB and NPRC (Zois et al., 2014). The NPRA gene *Npr1* was not differentially expressed in any of the RNA-Seq comparisons, while the NPRB gene *Npr2* was significantly elevated in mdx samples in response to serum starvation, by 2.2-fold in the mdx 0h v mdx 96h comparison. The NPRC gene *Npr3* was significantly upregulated by 2-fold in BL/10 cardiomyocytes between the 24h and 48h time-points of serum starvation. It was subsequently downregulated by -2.1-fold between 48h and 72h, and by -2.7-fold between 48h and 96h. *Npr3* was not differentially expressed along the serum starvation time-course in mdx cardiomyocytes, but it was upregulated by 1.8-fold in the BL/10 against mdx comparison at the 24h serum starvation time-point. These differences make NPRC a candidate target for further investigations in the mdx cardiomyocyte hypertrophic response.

It became evident from raw HTSeq transcript number counts that the *Npr1* gene was not expressed in BL/10 or mdx embryonic cardiomyocytes. NPRA and NPRB are both linked to guanylyl cyclases (GC) that produce cyclic guanosine monophosphate (cGMP), which in turn activates the cGMP-activated protein kinase G (PKG) and consequently has an effect on Ca^{2+} transporters and inhibits PLN (Zois et al., 2014). NPRC has multiple functions. It was initially thought to only have a clearance function by internalising secreted natriuretic peptides and directing them for intracellular storage and degradation (Koller & Goeddel, 1992), but was then linked to adenylyl cyclase (AC) inhibition in vascular smooth muscle, where it also activated phospholipase C (PLC) and inositol triphosphate (IP_3) signalling, leading to increased intracellular Ca^{2+} concentration ($[Ca^{2+}]_i$) via IP_3 receptor (IP_3R) activation and consequent SR-stored Ca^{2+} release (Mouawad et al., 2004). All three IP_3R genes – *Itpr1*, *Itpr2* and *Itpr3* – were expressed in both BL/10 and mdx cardiomyocytes, but no differential expression was observed. PLC can activate canonical transient receptor potential (TRPC) channels (Rowell et al., 2010), shown to be involved in mdx skeletal muscle pathology (Vandebrouck et al., 2002). While TRPC-knockout mice developed muscular dystrophy, their hearts were unaffected (Millay et al., 2009). Out of all the seven TRPC genes only *Trpc6* was expressed and *Trpc4* at very low levels. Neither was differentially expressed. TRPCs may therefore not be involved in the hypertrophic response seen in embryo-derived mdx cardiomyocytes. The combination of higher levels of BNP and NPRC could, however, lead to Ca^{2+}-augmented pathology in mdx cardiomyocytes via IP_3 activation.

Furthermore, based on RNA-Seq data, expression of the ANP and BNP convertase furin (Ichiki et al., 2013) was significantly downregulated in BL/10 cardiomyocytes, particularly in the BL/10 24h v BL/10 96h comparison where its transcript levels are reduced by 2.8-fold. In comparison, *Furin* remains relatively stably expressed throughout serum starvation in mdx samples. Corin is another natriuretic peptide convertase (Yan et al., 2000) with the same function as furin, but *Corin* was not differentially expressed and was present at much lower levels than *Furin* in both BL/10 and mdx cardiomyocytes. It has previously been shown that in a dog model of heart failure corin expression is downregulated and furin levels are elevated (Ichiki et al., 2013). Although not upregulated in the RNA-Seq dataset, the differential trend in

regulation between mdx and BL/10 cardiomyocytes could mean that natriuretic peptide effects are elevated in mdx cardiomyocytes.

Results from *Nppb* differential gene expression validation with qRT-PCR illustrated how different techniques replicated datasets to a limited degree, particularly in terms of the two axes of comparison – mouse line and serum starvation. Here the data suggested that although overall trends in *Nppb* reduction were valid in both BL/10 and mdx samples across serum starvation, the opposite effect was seen when the mouse models were compared against each other. Based on the protein modification requirements for both ANP and BNP and the reduction in furin expression in BL/10 samples, it would be pivotal to quantify natriuretic peptides on the protein level with Western blotting. Both peptides also have a short half-life (Mezo et al., 2012; Semenov et al., 2011). Although transcripts are upregulated the translated proteins may not reach a functional form before being degraded. The mechanisms of natriuretic peptide involvement in mdx cardiomyocyte pathology are summarised in figure 4.26. The higher level of *Nppa* and *Npr2* in mdx cardiomyocytes in response to serum starvation, as well as elevated *Nppb* and *Npr3* in comparison to BL/10 cardiomyocytes taken together suggests that natriuretic peptides play an active role in mdx cardiomyocyte hypertrophy in this model.

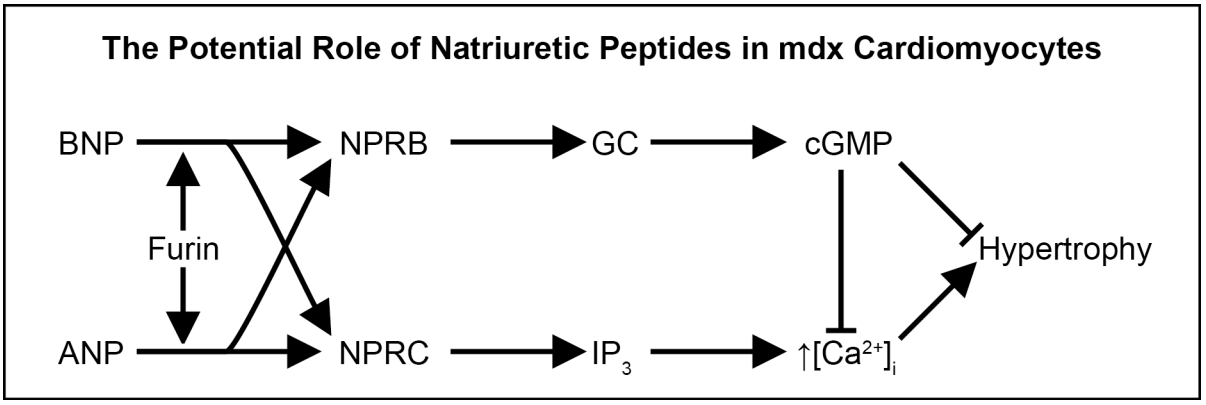

Figure 4.26. Natriuretic peptides in serum starved cardiomyocytes. Atrial natriuretic peptide (ANP) and brain natriuretic peptide (BNP) are cleaved into their active forms by furin. These active peptides interact with the two natriuretic peptide receptors A and B (NPRA, NPRB). NPRB is a guanylyl cyclase (GC) coupled receptor and has a cardioprotective effect by reducing the intracellular calcium ion concentration ($[Ca^{2+}]_i$). On the contrary, NPRC increases $[Ca^{2+}]_i$ via inositol triphosphate (IP_3) activation and can thus cause cardiac hypertrophy.

4.8.4 Phospholamban and Calcium Ion-handling

There are several regulators of Ca^{2+}-handling in cardiac myocytes, summarised in figure 4.27. In general, high $[Ca^{2+}]_i$ can lead to hypertrophy and apoptosis of cardiomyocytes through calmodulin and calcineurin activation (Frey et al., 2004; Barry et al., 2008). In the previous sub-section it was already discussed that TRPCs are probably not involved in the mdx cardiomyocyte hypertrophic response. Another group of TRP channels is the vanilloid transient receptor potential (TRPV) channels, of which TRPV1 causes muscle hypertrophy through nNOS activation (Ito et al., 2013), but the only TRPV gene that was expressed in cardiomyocytes was *Trpv2* and there were no significant changes in its expression levels. The importance of nNOS relocalisation to the SR has been recently reported by many research groups investigating engineered dystrophin constructs for gene therapy (Lai et al., 2013). It is significant to note that the dystrophin-associated nNOS gene *Nos1* was not expressed in BL/10 or mdx cardiomyocyte samples. This means the cardiomyocyte model cannot be used to test recruitment of nNOS as part of the DGC to the sarcolemma of mdx cardiomyocytes.

In addition to NPRs, NO also activates PKG (Zois et al., 2014), which affects three Ca^{2+} channels. PKG inhibits L-type calcium channels (Ca_V1, also known as dihydropyridine receptors), which transport extracellular Ca^{2+} into cardiomyocytes (Sodi et al., 2008). The two Ca_V1s expressed in BL/10 and mdx cardiomyocytes were $Ca_V1.2$ (*Cacna1c*) and $Ca_V1.3$ (*Cacna1d*). *Cacna1c* was not differentially expressed, but *Cacna1d* was significantly upregulated in BL/10 from 0h to 96h serum starvation by 6.3-fold. The second PKG effect is inhibition of the sodium-hydrogen exchanger (NHE) (Pérez et al., 2007), which consequently allows the sodium-calcium exchanger (NCX) to lower $[Ca^{2+}]_i$ (Bkaily et al., 2015). The NCX gene *Slc8a1* was downregulated in both BL/10 and mdx cardiomyocytes: -2.1-fold in BL/10 0h v BL/10 72h, -2.2-fold in BL/10 0h v BL/10 96h, -1.7-fold in mdx 0h v mdx 72h. The NHE gene *Slc9a1* was not differentially expressed in the cardiomyocyte gene expression analyses. The third function of PKG is deactivation of PLN by phosphorylating it and allowing SERCA to reduce $[Ca^{2+}]_i$ by transporting Ca^{2+} into the SR (Zois et al., 2014).

The SERCA gene *Atp2a2* was significantly downregulated in BL/10 cardiomyocytes in response to serum starvation within the first 48h: BL/10 0h v BL/10 24h by -1.7-fold and BL/10 0h v BL/10 48h by -1.8-fold. This trend was subsequently reversed and

the gene was significantly upregulated: by 1.7-fold in both BL/10 24h v BL/10 96h and BL/10 48h v BL/10 96h. However, in mdx cardiomyocytes *Atp2a2* remained downregulated: by -1.5-fold in the first 24h of serum starvation and by -1.7 in the mdx 0h v mdx 72h comparison. The SR has a much higher Ca^{2+} concentration than the sarcoplasm so to aid SERCA's function calpastatin (*Cast*), calsequestrin (*Casq1* and *Casq2*) and sarcalumenin (*Srl*) help sequester Ca^{2+} ions in the SR (Mosqueira et al., 2013). While *Cast* was not differentially expressed in response to serum starvation, both *Casq1* and *Srl* were downregulated: in BL/10 0h v BL/10 96h by -3.8 and -3.2-fold, in mdx 0h v mdx 96h by -2.4 and -2.1-fold, respectively. Reduced Ca^{2+} sequestration may make SERCA less efficient at reducing $[Ca^{2+}]_i$, but it was unexpected that calsequestrin and sarcalumenin were downregulated by a stronger factor in BL/10 cardiomyocytes.

PLN is also phosphorylated by protein kinase A (PKA), downstream of beta-adrenergic receptor (βAR) activation (MacLennan & Kranias, 2003; Haghighi et al., 2014). *Pln* was chosen as one of the genes used for RNA-Seq data validation. Unexpectedly, all of the comparisons were *Pln* was significantly downregulated based on RNA-Seq data showed upregulation in qRT-PCR data and, vice versa, where *Pln* was upregulated in RNA-Seq data, it was downregulated in qRT-PCR analysis (figure 4.22).

RyRs release SR-stored Ca^{2+} and can be activated by higher $[Ca^{2+}]_i$ as well as NO (discussed in sub-section 4.8.2) and RyR2 is upregulated in adult mdx hearts (Williams & Allen, 2007). There are three RyRs, encoded by the *Ryr1*, *Ryr2* and *Ryr3* genes. *Ryr1* was not expressed in BL/10 or mdx cardiomyocytes and the cardiac receptor gene *Ryr2* was predominant, but not differentially expressed. *Ryr3* is the brain RyR gene and the least studied, but both RyR2 and RyR3 are more easily activated by $[Ca^{2+}]_i$ (Lanner et al., 2010). *Ryr3* expression was downregulated in two of the mdx cardiomyocyte comparisons: by -2-fold in both mdx 24h v mdx 48h and mdx 24h v mdx 72h.

Store-operated calcium entry (SOCE) is mediated by the SR-bound stromal interaction molecule (STIM) responding to lowered SR Ca^{2+} levels by coupling with the sarcolemma-bound calcium release-activated calcium channel (ORAI) protein causing it to form a pore for Ca^{2+} influx from the extracellular space (Collins et al.,

2013). SOCE is enhanced in mdx skeletal muscle (Onopiuk et al., 2015), but its role in mdx cardiac tissue has not been assessed. The STIM and ORAI genes – *Stim1*, *Stim2*, *Orai1* and *Orai2* – were all expressed in both BL/10 and mdx cardiomyocytes, but there were no significant differences between any of the comparison groups.

In addition to NCX, plasma membrane Ca^{2+}-transporting ATPases (PMCA) are the second major group of sarcolemmal channels lowering $[Ca^{2+}]_i$ by pumping Ca^{2+} into the extracellular space against a high concentration gradient with ATP-supplied energy (MacLennan & Kranias, 2003). There are four PMCE genes: *Atp2b1*, *Atp2b2*, *Atp2b3* and *Atp2b4*. Out of these *Atp2b1* was the highest expressed, *Atp2b2* and *Atp2b3* were not expressed at all and only *Atp2b4* was differentially expressed, in the mdx 0h v mdx 24h comparison it was upregulated by 1.6-fold. A partner of STIM1 (POST) protein has been identified (Krapivinsky et al., 2011) as an inhibitor of PMCA in mdx skeletal muscle (Cully et al., 2012), but the POST gene *Slc35g1* was not differentially expressed in the RNA-Seq dataset.

Many Ca^{2+} channel genes remain unregulated or follow a similar trend of gene expression changes in both BL/10 and mdx serum starved cardiomyocytes. However, an initial downregulation of the SERCA gene *Atp2a2* in BL/10 cardiomyocytes was followed by a significant upregulation in these cells. On the contrary, in mdx cardiomyocytes *Atp2a2* was downregulated initially in the same way, but not subsequently upregulated. The failure of mdx cardiomyocytes to counteract an initial downregulation of SERCA may affect their ability to handle elevated $[Ca^{2+}]_i$ and therefore lead to onset of the hypertrophic effect.

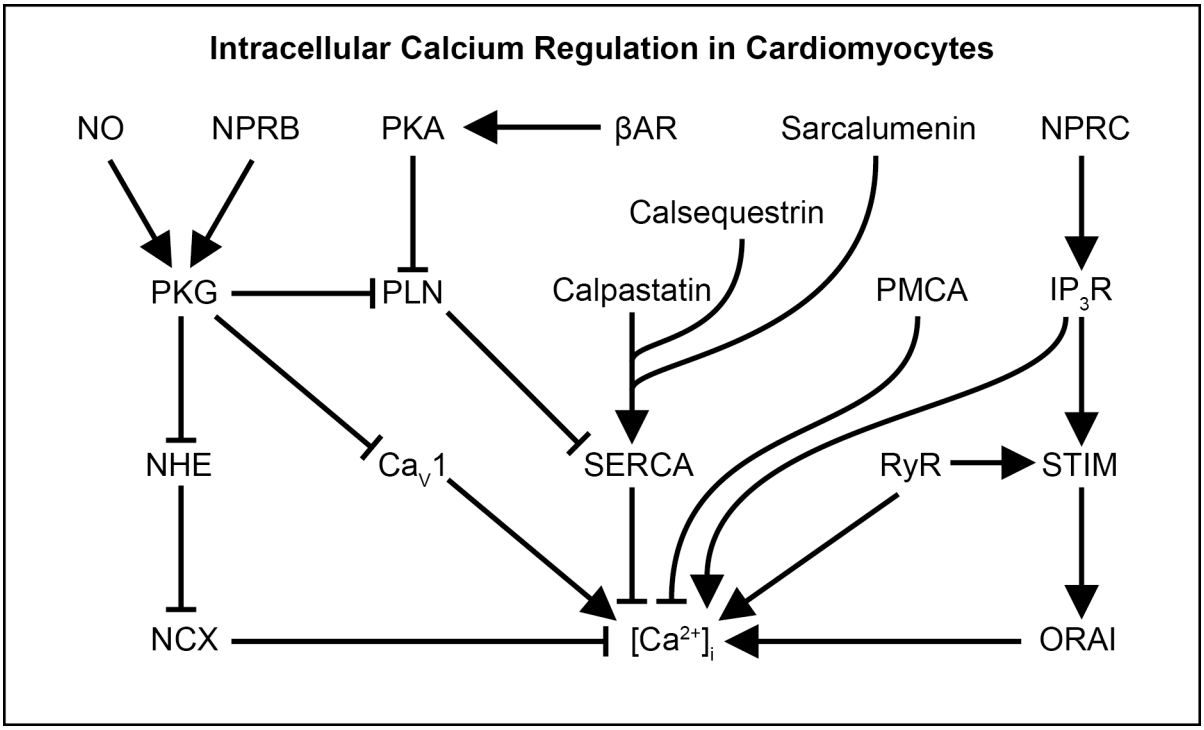

Figure 4.27 Phospholamban and calcium-handling in cardiomyocytes. Nitric oxide (NO) and natriuretic peptide receptor B (NPRB) lead to protein kinase G (PKG) activation. PKG inhibits the Na^+/H^+ exchanger (NHE) reducing intracellular Na^+ and therefore improving the Na^+/Ca^{2+} exchanger's (NCX) function to eject Ca^{2+} from the sarcoplasm to the extracellular space. PKG also inhibits L-type Ca^{2+} channels (Ca_V1), which bring in Ca^{2+} from the extracellular space. Phospholamban (PLN) is inhibited by phosphorylation by PKG and protein kinase A (PKA), which is activated by beta-adrenergic receptor (βAR) stimulation. In its phosphorylated state PLN is detached from the sarcoplasmic reticulum luminal Ca^{2+}-ATPase (SERCA), allowing the latter to store intracellular Ca^{2+} in the sarcoplasmic reticulum (SR). Calpastatin, calsequestrin and sarcalumenin sequester SR-stored Ca^{2+}, improving SERCA's function of pumping Ca^{2+} into the SR against a concentration gradient. Natriuretic peptide receptor C (NPRC) triggers IP_3 release and the SR-located IP_3 receptor (IP_3R) activation, resulting in Ca^{2+} release from the SR to the sarcoplasm. IP_3R-mediated reduction of SR Ca^{2+} activates the SR-bound stromal interaction molecule (STIM), which then opens the Ca^{2+} release-activated Ca^{2+} channel (ORAI), causing a Ca^{2+} influx to the sarcoplasm. RyR are another type of SR-stored Ca^{2+} release channel, therefore also stimulating STIM1. Plasma membrane Ca^{2+}-transporting ATPases (PMCA) reduce $[Ca^{2+}]_i$ by using energy from ATP to pump Ca^{2+} into the extracellular space.

4.8.5 SLRPs and MMPs in mdx Cardiomyocytes

Fibromodulin is a class II small leucine-rich proteoglycan (SLRP), which aids collagen fibril arrangement in the ECM and has been shown to be upregulated in fibrosis (Kalamajski & Oldberg, 2010). The protein is encoded by the *Fmod* gene, which showed one of the strongest differential upregulation values across the serum starvation time-course in both BL/10 and mdx cardiomyocytes in RNA-Seq results. These data were replicated with qRT-PCR. *Fmod* expression has been shown to be upregulated by TGFβ2 (Westergren-Thorsson et al., 1993). The TGFβ2 gene *Tgfb2* was significantly down-regulated in BL/10 cardiomyocytes in many of the time-point comparisons along the serum starvation time-course in RNA-Seq data. In contrast, it was not significantly dysregulated in mdx cardiomyocytes following serum starvation. *Tgfb2* was 1.7-fold upregulated in mdx cardiomyocytes in the BL/10 96h v mdx 96h comparison. This could also be the reason why upregulation of *Fmod* was more pronounced across the serum starvation time-course in both qRT-PCR data, but does not explain why the opposite (greater upregulation in BL/10 by serum starvation) was seen in RNA-Seq data (figure 4.23). *Fmod* expression comparison between BL/10 and mdx adult heart tissue followed the downregulation trend in qRT-PCR results from BL/10 v mdx comparisons.

Fibromodulin sequesters TGFβ1 in the ECM and consequently reduces its bioavailability (Hildebrand et al., 1994). Macrophages express MMP8, which is a collagenase and also cleaves fibromodulin, modulating its ability to sequester TGFβ1 in the ECM and consequently increasing TGFβ1 bioavailability (Wen et al., 2015). However, MMP8 also cleaves full-length decorin into an active shorter form of the protein that then actively reduces TGFβ1 bioavailability in breast cancer (Soria-Valles et al., 2014). *Mmp8* levels were significantly reduced in three RNA-Seq data comparisons: -3.4-fold in BL/10 24h v BL/10 96h, -3.7-fold in mdx 0h v mdx 96h and -2.1-fold in mdx 24h v mdx 96h. Further investigations are required to identify which of these two proposed MMP8-altered TGFβ1 signalling patterns is more prevalent in cardiomyocytes. However, the downregulation of *Mmp8* could be a cofactor in increased tissue fibrosis in response to hypertrophic remodelling of the heart due to its function as a collagenase.

MMP9 (a gelatinase) has been reported as a biomarker gradually elevated in DMD disease progression (Nadarajah et al., 2011). It can directly lead to increased TGFβ1 levels in mdx mouse skeletal muscle and knocking down MMP9 helps the dystrophic phenotype seen in muscle tissue (Li et al., 2009), but there are no data on its effect in the dystrophic heart. MMP9 has also been reported to have an analogous fibromodulin cleaving function as MMP8, although MMP13 is most efficient at cleaving fibromodulin (Heathfield et al., 2004). Neither *Mmp9* nor *Mmp13* was differentially expressed in the RNA-Seq dataset. Lumican, which is also a SLRP like fibromodulin, has been shown to reduce MMP9 levels in endothelial cells (Brézillon et al., 2013). Interestingly, lumican was also recently identified as a serum biomarker significantly reduced in mdx mice when compared to BL/10 control mice (Hathout et al., 2014). Furthermore, lumican knockout mice have been shown to develop cardiac hypertrophy (Dupuis et al., 2015). Cardiomyocyte RNA-Seq analysis revealed that the lumican gene (*Lum*) was in fact upregulated in both BL/10 and mdx cardiomyocytes across the serum starvation time-course and not differentially expressed when BL/10 and mdx samples were compared against each other.

Fibromodulin, decorin and biglycan have all been shown to bind TGFβ isoforms (Hildebrand et al., 1994). Decorin (expressed by the *Dcn* gene) has already been shown to be involved in muscle hypertrophy (Kanzleiter et al., 2014) and was also significantly upregulated in mdx, but not BL/10 cardiomyocytes in an immediate response to serum starvation within the first 24-48h: 1.6-fold in mdx 0h v mdx 24h, 2.5-fold in mdx 0h v mdx 48h, 2.3-fold in mdx 0h v mdx 72h and 2.6-fold in mdx 0h v mdx 96h.

Biglycan (expressed by the *Bgn* gene) binds to α-dystroglycan and has been shown to be upregulated in mdx skeletal muscle (Bowe et al., 2000). In cardiomyocyte RNA-Seq data *Bgn* was upregulated by serum starvation in both BL/10 and mdx cardiomyocytes and not differentially expressed when BL/10 and mdx cardiomyocytes were compared against each other. The reason for contradicting results may be down to differences between skeletal and cardiac muscle, or simply due to the fact that Bowe et al. only noted biglycan reduction in immunohistochemistry images and did not show protein level quantification with Western blots. The antibody signal pattern in their published images showed a shift from an exclusively sarcolemmal signal in control wild type muscle to both

sarcolemmal and punctate sarcoplasmic signal in mdx muscle fibres. These results may have been a consequence of the mislocalisation of DGC complex members, including α-dystroglycan, in mdx muscle and biglycan binding to the cytosol-retained dystroglycan protein.

Tissue inhibitors of metallopreoteinases (TIMP) have been shown to be reduced in mdx mouse pathology (Delfín et al., 2012). TIMP2 knockout mouse hearts become hypertrophic and TIMP3 knockout mice exhibit increased tissue fibrosis in the heart (Fan et al., 2014). *Timp2* and *Timp3* were both upregulated in BL/10 and mdx cardiomyocytes in response to serum starvation, possibly indicating their role in counteracting the trends in their environment, but there was no differential expression of either gene between the BL/10 and mdx samples. Considering the complications with developing pharmacological intervention on the MMP level, it may be beneficial to also evaluate TIMP regulation in dystrophic pathology (Delfín et al., 2012; Spinale & Villarreal, 2014).

Fibromodulin-associated pathways discussed in this sub-section have been summarised in figure 4.28. It will be essential to investigate the interaction of fibromodulin and other SLRPs with TGFβ1 and tissue fibrosis in the cardiac setting before drawing conclusions on the role SLRPs play in the hypertrophic response in mdx cardiomyocytes. If these are validated it would indicate that treatment with MMP inhibitors would be a potential therapeutic option in DMD cardiac disease.

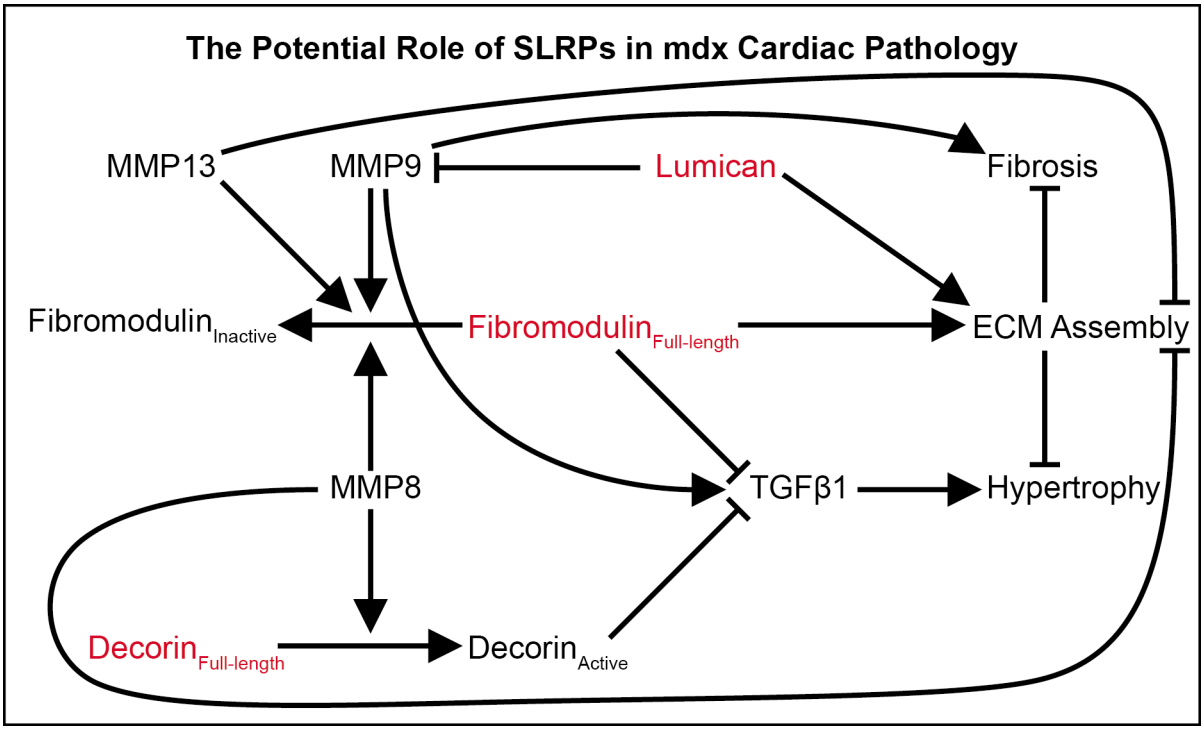

Figure 4.28. SLRPs and mdx cardiomyocyte hypertrophy. Small leucine-rich proteoglycans (SLRP) fibromodulin and decorin inhibit transforming growth factor beta (TGFβ) mediated hypertrophy. Fibromodulin and lumican hinder tissue fibrosis by facilitating extracellular matrix (ECM) assembly. Matrix metalloproteinases (MMP) modulate SLRPs and negatively affect ECM assembly. All three SLRPs, in red, were upregulated in mdx cardiomyocytes undergoing a serum starvation-induced hypertrophic response.

4.8.6 Angiogenesis and VEGF Signalling

The Genomatix GO pathway analysis results for angiogenesis (figure 4.14) and VEGF (figure 4.15) pathways resulted in overlapping central genes with several similar interactions. The key genes from both pathways were *Vegfa*, *Kdr*, *Hgf*, *Nos3* and *Mmp2*. It is important to consider the heterogeneous origin of cells in the cardiomyocyte hypertrophy model and that many angiogenesis pathway regulators may be affected in the cardiomyocytes themselves, but a feedback loop via any endothelial or myofibroblast cells cannot be ruled out in this discussion.

Vegfa expressing the VEGFA protein, which has been shown to be important in angiogenesis in dystrophic hearts (Shimizu-Motohashi & Asakura, 2014). *Vegfa* delivery with recombinant adeno-associated viruses (AAV) reduces skeletal muscle pathology in mdx mice through improved angiogenesis (Messina et al., 2007). *Vegfa* expression was downregulated in both BL/10 and mdx cardiomyocytes, near equally at the only time-point comparison that was significant in both BL/10 and mdx serum starved cardiomyocytes: BL/10 24h v BL/10 72h by -2.1-fold and mdx 24h v mdx 72h by -2-fold. Consistent with previously published data, suggesting a delayed and fluctuating VEGFA expression pattern in hypoxia-conditioned mdx cardiomyocytes as opposed to control cardiomyocytes and mdx endothelial cells (Nowak et al., 2011), gene expression was significantly higher in mdx cardiomyocytes at the 24h and 96h serum starvation time-points: BL/10 24h v mdx 24h by 1.8-fold and BL/10 96h v mdx 96h by 2.6-fold. These RNA-Seq expression data were not replicated in qRT-PCR analysis experiments, where the average trend of *Vegfa* expression was also fluctuating in BL/10 cardiomyocyte samples but in the upregulation direction. It is therefore complicated to draw conclusions from the transcriptional regulation data.

VEGFA exerts its function by activating VEGF receptor 2 (VEGFR2, also known as Flk-1 and encoded by the *Kdr* gene) (Ennen et al., 2013). It also binds at a higher affinity to VEGFR1 (also known as Flt1 and expressed by the *Flt1* gene), which has a soluble isoform, acting as a decoy receptor and inhibiting the VEGFA response by sequestering it (Taimeh et al., 2013). However, expression of the *Kdr* gene was significantly downregulated in both mdx and BL/10 cardiomyocytes in response to serum starvation: BL/10 0h v BL/10 96h by -7.4-fold and mdx 0h v mdx 96h by -9.4-fold. The *Flt1* gene was not differentially expressed.

VEGFR2 activates the phosphatidylinositide 3-kinase (PI3K) and protein kinase B (Akt) signalling pathway is also able to trigger the PI3K/Akt/mTOR (mammalian target of rapamycin) pathway (Kim et al., 2013). Both of these pathways induce angiogenesis in endothelial cells, but mTOR has been shown to promote hypertrophy in a range of tissues, including the heart (Neishabouri et al., 2015). A recent publication showed that downregulation of the *Pik3ip1* gene, which expresses an inhibitor of the PI3K/Akt/mTOR pathway, induced cardiac hypertrophy (Song et al., 2015). *Pik3ip1* was upregulated by 10.8-fold in the BL/10 0h v BL/10 96h comparison and only 4.4-fold in the mdx 0h v mdx 96h comparison in RNA-Seq data. This reduced effect seen in mdx cardiomyocytes could potentially be one of the reasons for the increased hypertrophic response. *Pik3ip1* and its protein product should therefore be further investigated as a potential target for inhibiting dystrophic hypertrophy.

The hepatocyte growth factor (HGF) gene *Hgf* was significantly upregulated only in the mdx 0h v mdx 96h comparison, by 2.5-fold. It was also upregulated in BL/10 cardiomyocytes but this increase in gene expression did not reach statistical significance. However, the HGF receptor gene *Met* was significantly downregulated in response to serum starvation, by -1.7-fold in the mdx 0h v mdx 96h comparison. The roles of HGF and its receptor in the heart are still in the process of being established. Constitutive activation of the receptor has been shown to cause hypertrophy in cardiomyocytes (Leo et al., 2011). Downregulation of *Met* could therefore be a protective mechanism that mdx cardiomyocytes undergo in response to other signals or even a negative feedback loop in response to the upregulation of *Hgf*.

Nos3 expresses endothelial nitric oxide synthase (eNOS), which was the only abundantly and differentially expressed NOS in BL/10 and mdx cardiomyocytes. The gene was downregulated by -6.4-fold in the BL/10 0h v BL/10 96h comparison and -2.6-fold in the mdx 0h v mdx 96h comparison, although, the difference between expression in BL/10 and mdx cardiomyocytes at the 96h time-point was non-significant. VEGFA can initiate vasorelaxation by activating NO production by eNOS via the PI3K/Akt pathway (Taimeh et al., 2013). It was mentioned in sub-section 4.8.4 that the nNOS gene *Nos1* was not expressed in BL/10 or mdx cardiomyocytes. The combined effect of nNOS absence and *Kdr* downregulation-caused blunting of

VEGFA signalling resulting in reduced activation of eNOS on a non-vascularised cell culture system, such as the cardiomyocyte serum starvation model, remains to be elucidated. Perhaps upregulation of *Angptl4* (discussed in sub-section 4.8.1) may counteract the severe NO-deficiency in the cardiomyocyte model by increasing iNOS-produced NO, but considering the low expression level of *Nos2* it may not suffice for a cardioprotective effect. There is mounting evidence that cGMP-specific phosphodiesterase type 5 (PDE5) inhibitors can attenuate dystrophin deficiency-related skeletal and cardiac muscle pathology (Khairallah et al., 2008; Kobayashi et al., 2008; Martin et al., 2012; Nelson et al., 2014). Considering the aberrant NO production identified in these results, and despite sildenafil (a PDE5 inhibitor) not having shown desirable effects in a recently aborted clinical trial (Leung et al., 2014), it will be useful to identify whether other PDE5 inhibitors are capable of reducing mdx cardiomyocyte hypertrophy in this model. Furthermore, the *Pde5a* gene was upregulated in both BL/10 and mdx cardiomyocytes in response to serum starvation, but only significantly in the mdx 0h v mdx 96h comparison, by 1.9-fold. This suggests that PDE5 may play a role in mdx cardiomyocyte hypertrophy and gives further confirmation of the model's potential for testing inhibitors of the protein.

VEGFA can induce *Mmp2* expression via VEGFR2 (Wagner et al., 2003). The nearly equally 3-fold elevated expression pattern of *Mmp2* in both BL/10 and mdx cardiomyocytes in response to serum starvation was discussed in sub-section 4.8.1. MMP2 is also capable of increasing TGFβ bioavailability via cleaving fibromodulin, but the counteractive function of decorin (also upregulated) may balance this effect (discussed in sub-section 4.8.5) (Wen et al., 2015).

It is possible that VEGFA triggers a hypertrophic response in serum starved cardiomyocytes through angiogenesis-related signalling. It must also be considered whether these candidate pathways, responsible for differences between BL/10 and mdx cardiomyocytes, act in an autocrine fashion (expressed and affecting the same cell) or in concert with other cells in culture. Based on observations reported in this sub-section PI3K and mTOR pathway activation and PDE5 inhibitors will be the primary targets for further investigations.

4.8.7 Hypoxia Signalling Pathways

The HIF-1α hypoxia signalling pathway was identified in GO analysis of BL/10 and mdx cardiomyocyte RNA-Seq data (shown in figures 4.16 and 4.17). HIF-1α is the oxygen-regulated subunit of the HIF-1 heterodimer, formed with HIF-1β, which is constitutively expressed (Wang et al., 1995). HIF-1 induces gene expression by binding to hypoxia response elements of genes, regulating over a thousand genes in humans (Semenza, 2014). The *Hif1a* gene, which expresses the HIF-1α subunit in mice, was significantly upregulated in BL/10 cardiomyocytes in response to serum starvation, by 2.3-fold in the BL/10 0h v BL/10 96h comparison, 2.4-fold in BL/10 24h v BL/10 96h and 2.1-fold in BL/10 48h v BL/10 96h. It was also significantly upregulated in the mdx 24h v mdx 96h comparison, by 1.8-fold.

In the Genomatix GO analysis pathway maps in figures 4.16 and 4.17 all of the differentially expressed HIF-1α related genes were red and therefore upregulated in the BL/10 96h v mdx 96h serum starvation time-point comparison. This was striking considering the slightly lower upregulation of HIF-1α in mdx cardiomyocytes and a non-significant -1.4-fold downregulation in the BL/10 and mdx cardiomyocyte comparison at 96h of serum starvation. Furthermore, investigating expression patterns of HIF-1 target genes *Bhlhe40*, *Eno1*, *Hk1* and *Hk2* revealed a trend where most genes were down-regulated in BL/10 cardiomyocytes compared to mdx cells.

It was recently discovered that hypoxic cardiomyocytes are capable of going through cell cycling and thus contribute towards regeneration in adult mouse hearts (Kimura et al., 2015). The publication listed several cell cycle genes that were upregulated in hypoxic cardiomyocytes, out of which none were differentially expressed in the RNA-Seq dataset, apart from *Ccnb1*, which was conversely downregulated in both BL/10 and mdx cardiomyocytes in response to serum starvation. Furthermore, prolyl hydroxylase 3 (*Egln3* gene), which inhibits HIF-1α (Henze et al., 2014), was drastically downregulated in the BL/10 0h v BL/10 96h comparison, by almost 10-fold, whilst in mdx cardiomyocytes its expression remained stable. This should be indicative of stronger negative regulation of HIF-1 functionality in mdx cardiomyocytes and makes it even more striking that many HIF-1 target genes are downregulated to a greater extent in BL/10 cardiomyocytes. It may be that whilst on the transcriptome level there is not as great an increase in *Hif1a* expression, increased $[Ca^{2+}]_i$ is improving *Hif1a* translation and despite lower mRNA there is

more HIF-1α protein expressed and therefore the balance of HIF-1 effect is shifted towards upregulation in mdx cardiomyocytes as compared to BL/10 cells (Hui et al., 2006).

HIF-1 regulates many mitochondrial genes in response to hypoxic conditions (Hwang et al., 2015). It positively regulates *Bnip3*, encoding Bcl-2/adenovirus E1B 19kDa-interacting protein 3, which activates apoptosis and mitochondrial autophagy while impairing mitochondrial respiration (Rikka et al., 2011). The *Bnip3* gene was markedly downregulated in BL/10 cardiomyocytes in response to serum starvation (BL/10 0h v BL/10 96h by -4.7-fold), but not differentially expressed in mdx cardiomyocytes. This could mean that BL/10 cardiomyocytes adapt to survive in the serum starvation condition, whereas mdx cardiomyocytes are less able to inhibit apoptotic signals.

The mitochondrial HIF-1 target gene *Ndufa4l2* expresses a protein shown to inhibit complex I activity and consequently reduce ROS in hypoxic conditions (Tello et al., 2011). The gene was also upregulated in skeletal muscle of mdx mice treaded with tadalafil, a PDE5 inhibitor (De Arcangelis et al., 2015). *Ndufa4l2* was initially upregulated by 48h of serum starvation and subsequently downregulated by 96h in BL/10 cardiomyocytes (but only significantly in the 24h v 96h and 48h v 96h comparisons), as opposed to being significantly upregulated in the first 24h, followed by stable expression in mdx cardiomyocytes, resulting in significant upregulation in the 0h v 24h, 0h v 48h, 0h v 72h comparisons (figure 4.25). The mdx cardiomyocyte expression pattern was very closely replicated with qRT-PCR experiments, which did not show the same expression patterns seen in BL/10 cardiomyocytes analysed with RNA-Seq. Consequently, the significant upregulation of *Ndufa4l2* witnessed in the BL/10 96h v mdx 96h comparison was diminished to a slight downregulation, which did not cross the FC cut-off limit in qRT-PCR data. Although the differences in BL/10 cardiomyocyte *Ndufa4l2* expression were unexpected, the close replication of mdx cardiomyocyte gene expression response to serum starvation was a positive result and it would be interesting to see whether PDE5 inhibitor treatment in this mdx model of hypertrophy would also upregulate *Ndufa4l2* expression in cardiomyocytes.

Results on hypoxia signalling indicate that mdx cardiomyocytes exhibit higher HIF-1 function and a consequent deficiency in the coping-mechanism to tackle the effect of

serum starvation in comparison to BL/10 cells, based on stronger downregulation of HIF-1 target genes, the HIF-1 inhibitor *Egln3* and apoptosis-inducing *Bnip3* in BL/10 cardiomyocytes. Upregulation of *Ndufa4l2* by higher HIF-1 activity in mdx cardiomyocytes may also suggest an alternative mechanism for tackling oxidative stress and reduce ROS in tandem with upregulated SOD3 (sub-section 4.8.1) to compensate for compromised NOS activity (sub-section 4.8.6).

4.8.8 Summary

In addition to the many pathways and genes already discussed, there were many differentially expressed genes that there is little known about. For example, *Erdr1* was significantly downregulated in BL/10 cardiomyocytes in response to serum starvation, but not expressed at all in mdx cells. The gene expresses an erythroid differentiation regulator, which is upregulated in adult mdx mouse heart tissue compared to BL/6 hearts (Spurney et al., 2008) and induces apoptosis in keratinocytes (Kim et al., 2011), which makes it an interesting target for further investigations.

Near negligible expression of *Erdr1* in mdx cardiomyocytes and a relatively low level of nominal transcript level in BL/10 cardiomyocytes, based on HT-Seq data, were reasons for omitting the gene from qPCR validation. In fact, out of all the genes in figure 4.9, only *Erdr1, Dmd, Cxcl12, Gm20939 and 3110056K07Rik* remained as significant differentially expressed genes once the adjusted p-value cut-off was lowered to 0.01 and a fold change cut-off introduced at Log_2FC=+/-0.6. Out of these *Gm20939* is a predicted gene only identified in mouse genome and the function of the Riken gene has not been determined yet. The disease-causing *Dmd* gene was omitted from qPCR validation because it was not seen as valuable for confirming potential members of pathways affecting the hypertrophic response. *Cxcl12* had the highest fold change in the BL/10 96h v mdx 96h comparison, where it was only upregulated 2-fold and therefore genes with higher maximum fold changes identified from other comparisons were chosen. Furthermore, *Clic5* was identified as the only gene significantly regulated in opposite directions when comparing control cell serum starvation to dystrophic cardiomyocyte hypertrophic response: downregulated in BL/10 0h v 96h by -2.2-fold and upregulated in mdx 0h v 96h by 1.6-fold (figure 4.18 and appendix 1). Whilst it was not one of the highest regulated genes in the BL/10

96h v mdx 96h comparison it remains one of the strongest candidates for further RNA-Seq data validation with qPCR.

In a similar way to *Erdr1*, there is a lot of cross-talk between the various signalling pathways already discussed in this chapter. For instance, mTOR can also be activated by Ca^{2+}-mediated signals and therefore it may be high $[Ca^{2+}]_i$ rather than VEGFA driving the mTOR hypertrophic pathway (Zhang et al., 2012).

A significant limitation to the Illumina HiSeq platform for RNA-Seq studies is the lack of micro-RNA (miRNA) expression data due to the sequencing technique the machine employs. Several roles of miRNAs in DMD pathology (Jeanson-Leh et al., 2014) and cardiovascular diseases (Pan et al., 2010) have emerged, but their roles in mdx cardiomyocyte serum starvation-induced hypertrophy could not be assessed. Many FGP markers had the same trends in both BL/10 and mdx cardiomyocytes in response to serum starvation. This is indicative of a hypertrophic response emerging in both mouse models. However, BL/10 cardiomyocytes seem to adapt better to serum starvation and arrest their size increase. Markers of cardiac hypertrophy, both confirmed and novel, that were differentially expressed in the RNA-Seq dataset need validation on protein level to confirm functional compromise in mdx cardiomyocytes. The blunted levels of differential expression seen when qRT-PCR data were compared to RNA-Seq data *Nppb* expression validation and the augmented effect witnessed in *Fmod* validation, coupled with irregular discrepancies in confirming low level regulation trends in *Vegfa* and *Pln* showed that low levels of differential expression were challenging to validate with qRT-PCR, despite very close replication of mdx cardiomyocyte *Ndufa4l2* expression seen in both RNA-Seq and qRT-PCR analyses.

These differences between the two techniques may have been caused by the omission of one set of BL/10 biological replicate samples from sequencing. Whilst the RNA-Seq method has more methodological steps open to variability factors in comparison to performing gene-by-gene analyses with qRT-PCR, DeSeq2 normalises gene expression to the geometric mean of counts across the samples for every given gene separately and then divides the nominal count by the geometric mean (Love et al., 2014). This eliminates potential sample-to-sample composition variability, dependence on primer efficiency and normalisation to house-keeping

genes, providing more reliable differential expression data. Having a third biological replicate of BL/10 cardiomyocytes for RNA-Seq analysis could have improved the power of this study, but in this case it was also important to investigate two factors: the differences between BL/10 and mdx cardiomyocytes, as well as the effect serum starvation had on the cells. Whilst there were less differentially expressed genes identified from genotype comparisons at certain time-points, data obtained from serum starvation time-point comparisons also gave information about genotype differences, independent of direct comparisons between BL/10 and mdx cardiomyocyte samples. Considering the number of comparisons performed with each dataset, the number of quality control steps and increasing cut-offs on both the FDR and FC level, the filtered results provided a powerful tool for investigating genes and pathways involved in mdx cardiomyocyte hypertrophy.

Chapter 5. Influencing the mdx Cardiomyocyte Hypertrophic Response with DMD Therapies

5.1 Introduction and Aims

Several therapies for Duchenne muscular dystrophy (DMD) have now reached clinical trial stage. Ataluren, a small molecule drug designed to promote stop codon read-through, has recently been conditionally approved for use as a prescription medicine for patient with nonsense mutation DMD (Haas et al., 2015). This drug, however, only provides hope for a fraction of the DMD patient cohort with nonsense mutations, whereas the majority of patients have large deletions (Bladen et al., 2015). Several adeno-associated virus (AAV) vector therapies for either restoring the reading frame or reintroducing dystrophin gene expression are also moving closer to approval (Okada & Takeda, 2013). The European Medicine Agency's approval of an AAV drug designed for lipoprotein lipase replacement (Ylä-Herttuala, 2012) also paved the way for AAV therapies in DMD. Until there is a universal cure available it is pivotal to provide the best patient care possible to manage DMD disease progression. A range of pharmacological compounds are currently prescribed to dystrophinopathy patients to manage their skeletal muscle and cardiac symptoms. These include corticosteroids, angiotensin converting enzyme (ACE) inhibitors and beta-adrenergic receptor (βAR) blockers (Bushby et al., 2010a).

This chapter aims to test a range of pharmacological compounds already prescribed to DMD patients for managing the progression of their disease, as well as novel treatment compounds and rescue therapies, to assess their ability to reduce mdx cardiomyocyte hypertrophy as a model for how these compounds affect, or could influence, the progression of cardiac symptoms in DMD.

5.2 Overview of the Experimental Setup

Cardiomyocytes were isolated from BL/10 and mdx E17.5 mouse hearts and cultured for 48h (figure 5.1). Treatment with therapeutic compounds or viral transductions were performed at the 24h time-point. At the subsequent 48h and 72h serum starvation time-points cells were fed with fresh medium and treatment compounds were replenished in samples undergoing therapeutic testing. Samples at specific time-points of serum starvation were fixed for ICC or collected for protein extraction.

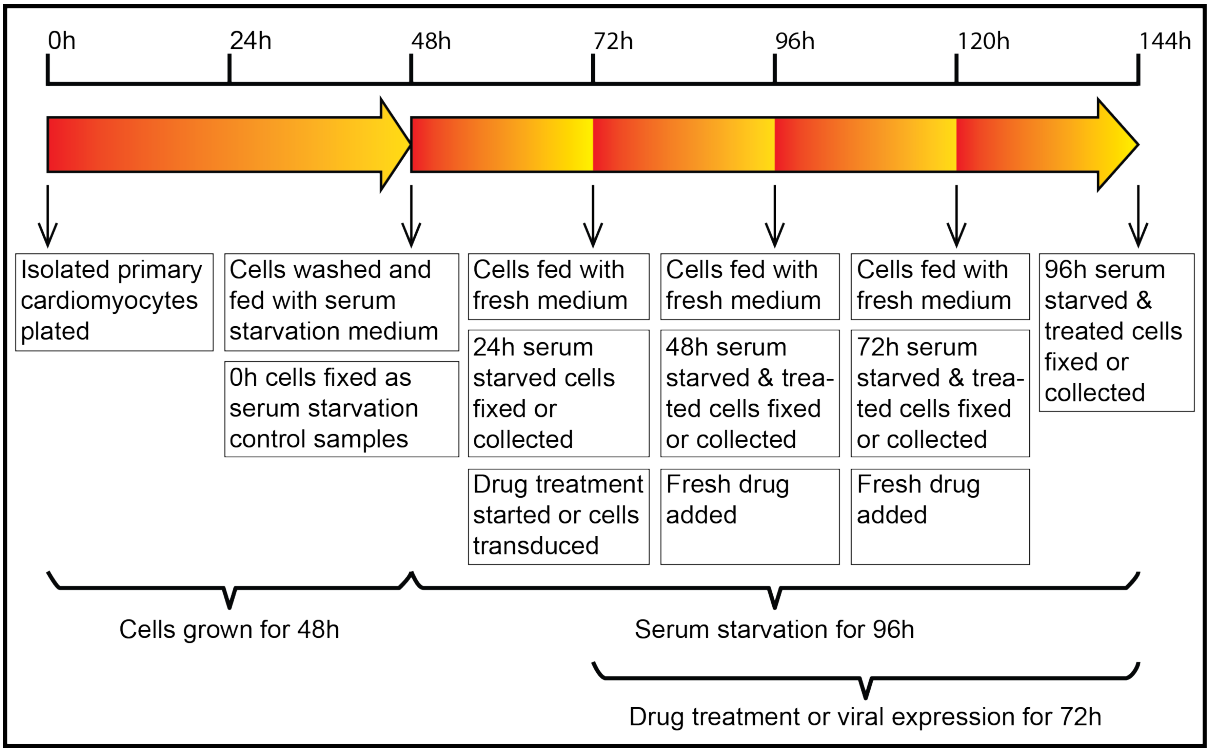

Figure 5.1. Experimental time-course of primary cardiomyocyte treatment. Cells were cultured in cardiomyocyte growth medium for 48h, followed by serum starvation for 96h, feeding with fresh medium every 24h. Viral transductions were performed at the 24h serum starvation time-point. Samples used for trialling therapeutic compounds were drug treated at the 24h serum starvation time-point and fresh compounds were added every subsequent 24h.

5.3 Corticosteroid Treatment

Prescribing corticosteroids to DMD patients is now included in care guides for disease management (Kinnett et al., 2015). Prednisolone is a corticosteroid that delays loss of ambulation in DMD patients (Takeuchi et al., 2013). Dexamethasone and prednisolone were tested for their efficacy at reducing mdx cardiomyocyte hypertrophy. Cardiomyocytes were serum starved for 96h with serum-free cardiomyocyte growth medium (SFCGM) or serum starvation cardiomyocyte medium (SSCGM), supplemented with 1% foetal bovine serum (FBS). Corticosteroid treatment was commenced at 24h serum starvation time-point.

5.3.1 Prednisolone Treatment

Prednisolone was most effective at inhibiting mdx cardiomyocyte hypertrophy when used at 100ng/ml (average area 2631μm^2). However, the observed 13% reduction in area, in comparison to untreated 96h serum starved cells (average area 3026μm^2), was not significant when compared using a one-tailed Student's t-test at equal variance based on Levene's test (figure 5.2). Cells were serum starved with SFCGM. ICC and image analysis were performed by MRes student Elizabeth Roberts. Skedasticity and t-test results from data comparisons are shown in table 5.1.

Comparison	Levene's Test p-value	Variance	t-test p-value
96h v 24h	1.51319E-05	Unequal	<u>2.3479E-18</u>
96h v 10µg/ml	0.78086589	Equal	0.2261
96h v 1µg/ml	0.481370467	Equal	0.3518
96h v 100ng/ml	0.559064721	Equal	0.0709
96h v 10ng/ml	0.034323749	Unequal	0.1864
96h v 1ng/ml	0.691998928	Equal	0.3742
96h v 100pg/ml	0.234368987	Equal	0.2803

Table 5.1. Prednisolone treatment statistical analyses results. The first column represents Levene's test and Student's t-test comparisons. 24h and 96h represent the time of non-treated control serum starvation duration. Concentrations represent prednisolone-treated 96h serum starved samples. Significant t-test p-value<0.05 is underlined.

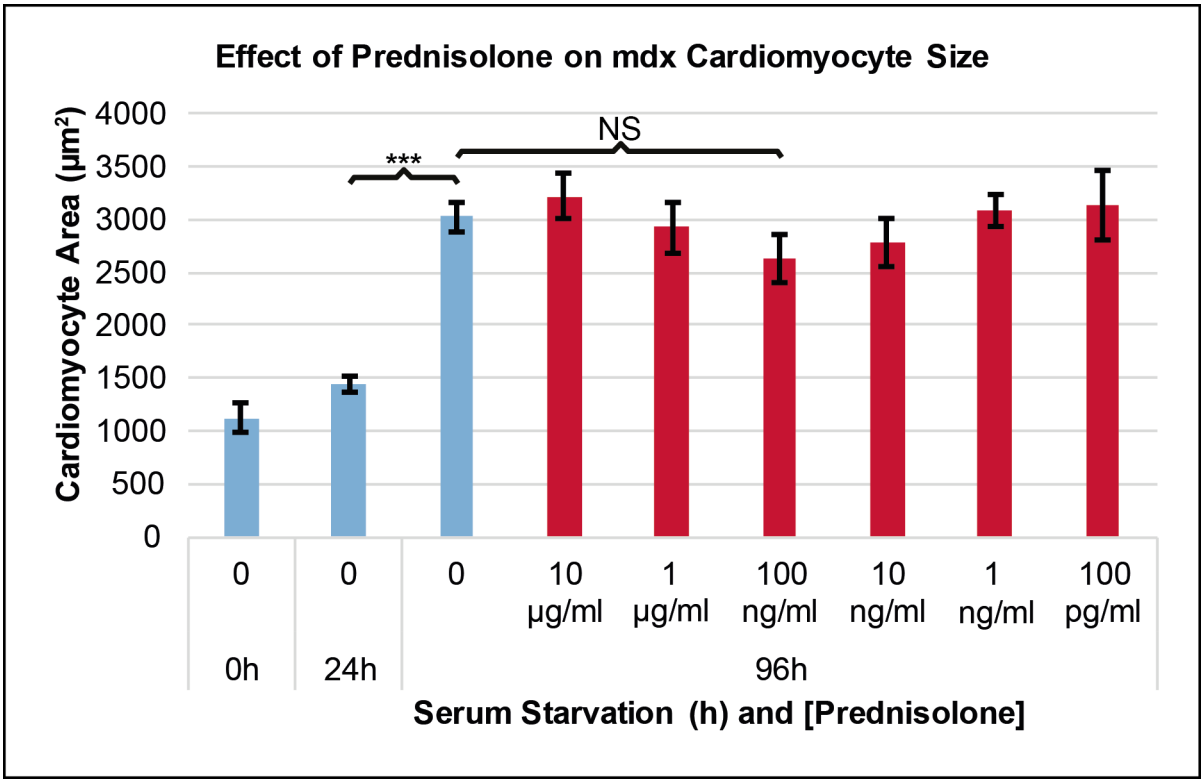

Figure 5.2. The effect of prednisolone on mdx cardiomyocyte hypertrophy. Serum starved cardiomyocytes were treated with a range of prednisolone concentrations from the 24h serum starvation time-point (red columns). Non-treated control cardiomyocytes (blue columns) serum starved for 96h were significantly larger than cells serum starved for 24h (*** corresponds to p-value<0.001). The average area measurements of cardiomyocytes treated with 1µg/ml, 100ng/ml and 10ng/ml prednisolone in SFCGM were smaller than the non-treated sample, but none of these reductions in area were statistically significant (NS stands for non-significant), based on one-tailed Student's t-test analysis. Error bars represent standard error of the mean.

5.3.2 Dexamethasone Treatment

Dexamethasone is a more potent agonist of glucocorticoid receptors (GCR) and has a longer half-life than prednisolone (Longui, 2007). It has also been shown that dexamethasone has a beneficial effect on maintaining beating functions in embryoid bodies (Dehghani et al., 2013). Serum starvation cardiomyocyte growth medium (SSCGM) was used to initiate a hypertrophic response in mdx cardiomyocytes, followed by dexamethasone treatment 24h later. Cardiomyocyte area was measured from images of cells positive for α-actinin immunostaining. A trial experiment was conducted where four 96h serum starved samples were analysed, one non-treated control and three different concentrations of dexamethasone treatment: at 20μg/ml, 2μg/ml and 200ng/ml. One-tailed Student's t-test analyses of compared samples showed that treating cardiomyocytes with all three concentrations of dexamethasone resulted in significantly reduced cardiomyocyte area (figure 5.3 and table 5.2).

Comparison	Levene's Test p-value	Variance	t-test p-value
96h v 20μg/ml	0.05927345	Equal	0.000382483
96h v 2μg/ml	0.000705371	Unequal	2.77107E-07
96h v 200ng/ml	0.005331064	Unequal	4.69495E-09

Table 5.2. Dexamethasone treatment statistical analyses results. The first column represents Levene's and Student's t-test comparisons. All samples were serum starved for 96h. In the column, 96h represents the non-treated control sample and the concentrations represent samples treated with dexamethasone. Significant t-test p-values<0.05 are underlined.

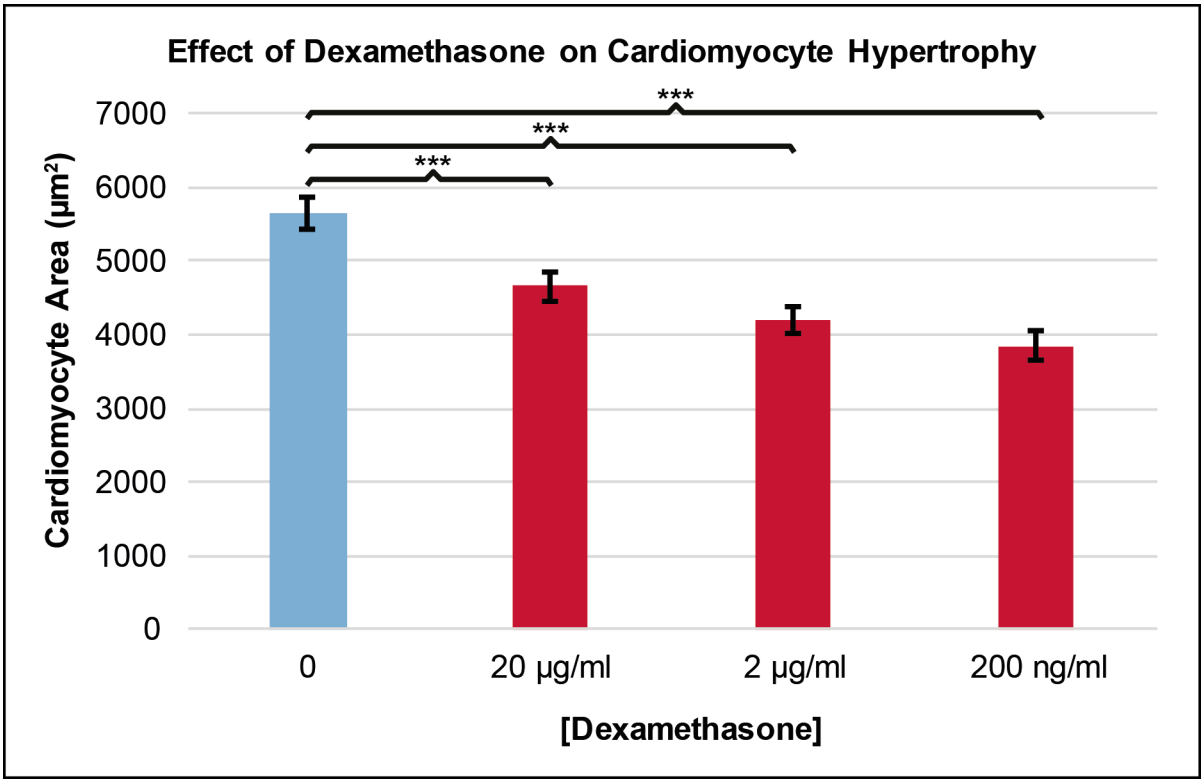

Figure 5.3. Small-scale study of dexamethasone effect on mdx cardiomyocyte hypertrophy. Serum starved cardiomyocytes were treated with three concentrations of dexamethasone from the 24h serum starvation time-point (red columns). Non-treated control cardiomyocytes serum starved for 96h (blue column) were significantly larger than cells treated with dexamethasone (*** corresponds to p-value<0.001), assessed by one-tailed Student's t-test. Error bars represent standard error of the mean.

Dexamethasone powder was dissolved in ethanol and the 20μg/ml treatment solution had a 2% (V/V) ethanol concentration. Two studies were subsequently performed where a separate corresponding ethanol concentration vehicle-treated control sample was also included in parallel with each dexamethasone-treated sample (figure 5.4). Although the results showed that dexamethasone-treated cardiomyocytes were on average smaller than 96h serum starved non-treated cells, the vehicle-only treated cardiomyocytes were also smaller, and at 200ng/ml dexamethasone / 0.02% ethanol in the first study (figure 5.4.A) vehicle-treated cells were even smaller than the non-treated 24h serum starvation control sample.

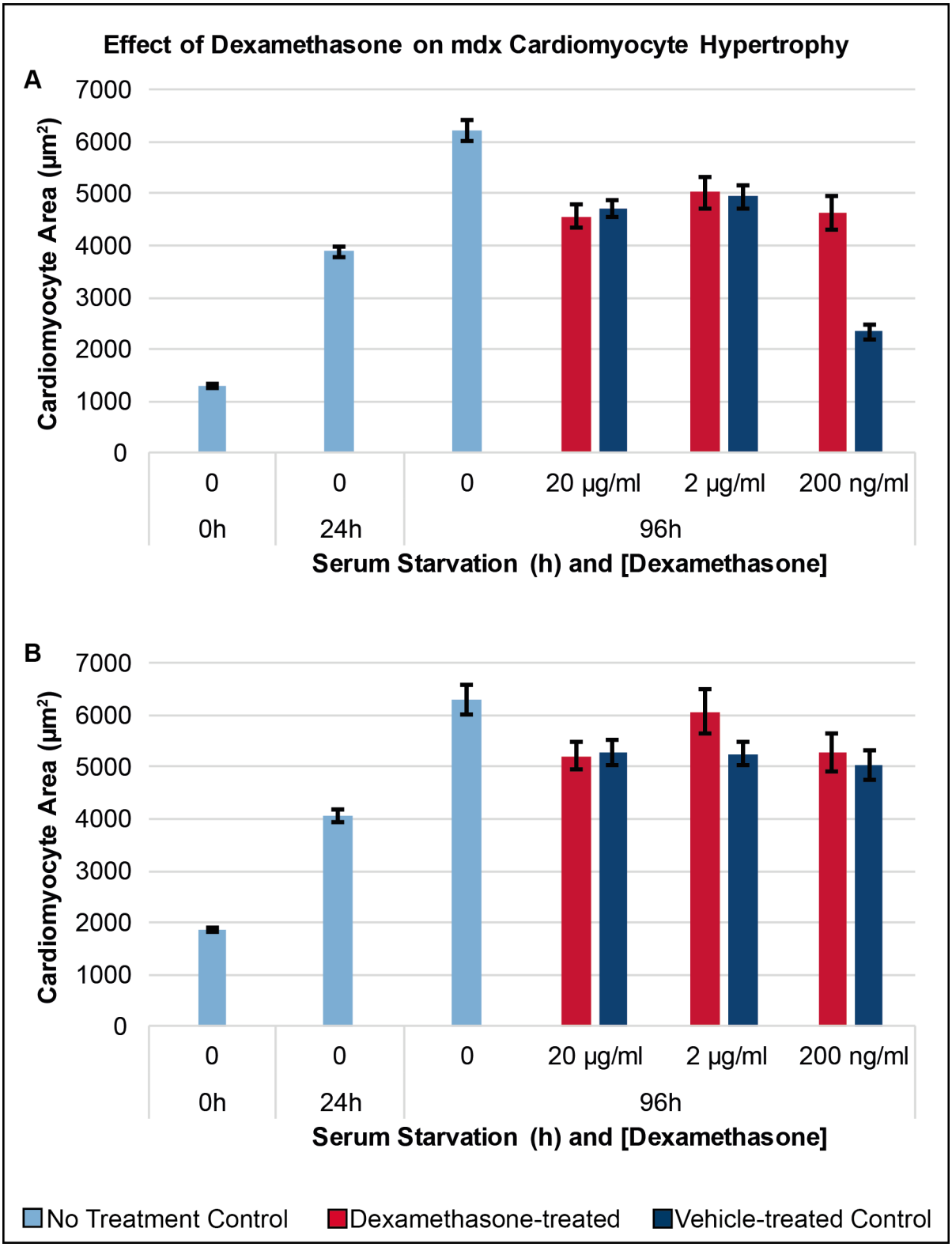

Figure 5.4. Controlled studies of dexamethasone effect on mdx cardiomyocyte hypertrophy. Serum starved cardiomyocytes were treated with three concentrations of dexamethasone (red columns) and the corresponding ethanol vehicle (dark blue columns) from the 24h serum starvation time-point. Non-treated control cardiomyocytes (light blue columns) serum starved for 96h were on average larger than cells treated with dexamethasone or ethanol. Error bars represent SEM.

5.4 Angiotensin Converting Enzyme Inhibitor Treatment

ACE inhibitors are considered a first-line therapy to tackle DMD cardiac pathology (Bushby et al., 2010a). The effect of captopril – an ACE inhibitor drug – on mdx cardiomyocyte hypertrophy was assessed. Adding 1g of captopril to 10ml of SFCGM caused a drop in the stock solution pH, observed from the change in SFCGM colouration. In order to compensate for this change the solution was supplemented with 450μl of 1M sodium hydroxide (NaOH), restoring the normal pH level of SFCGM (figure 5.5).

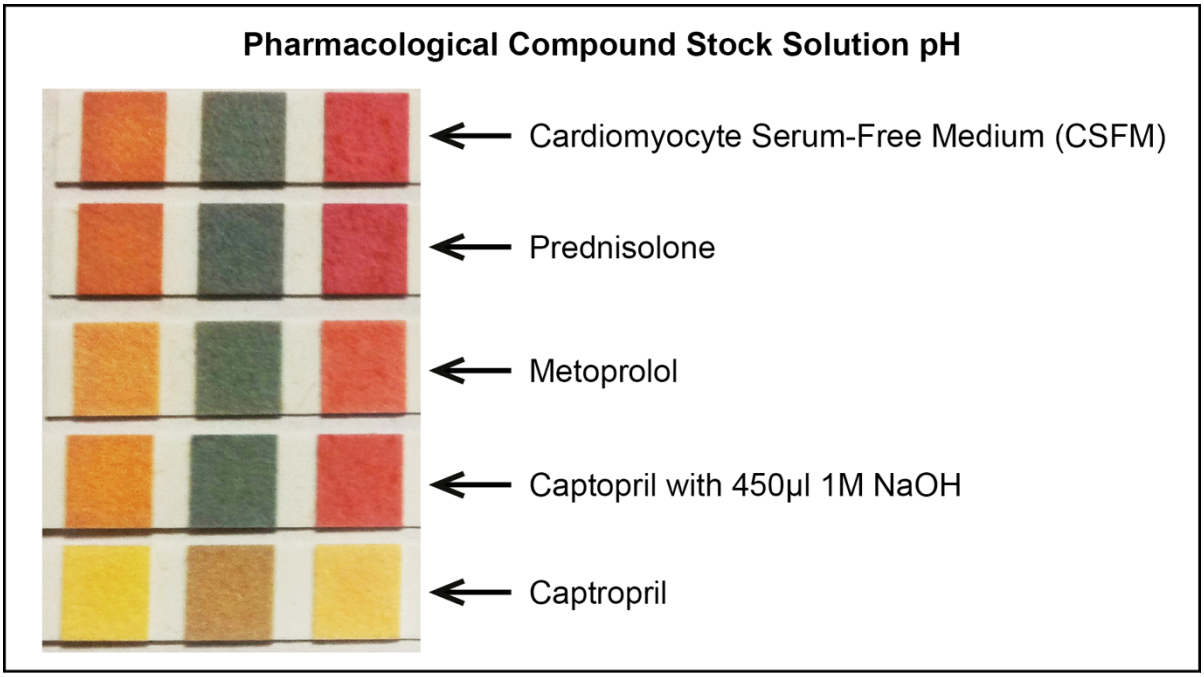

Figure 5.5. Pharmacological Compound stock solution pH. Adding captopril to serum-free cardiomyocyte growth medium (SFCGM) changed the solution's pH. The stock solution pH was adjusted with 450μl of 1M sodium hydroxide (NaOH) to bring it back to the physiological level of SFCGM.

Cardiomyocytes isolated from mdx E17.5 hearts were serum starved and treated with 100μg/ml, 10μg/ml, 1μg/ml, 100ng/ml or 10ng/ml captopril. MRes student Elizabeth Roberts quantified the area of non-treated cells at 0h, 24h and 96h of serum starvation, along with captopril-treated cells at each of the concentrations. On average, 100μg/ml, 1μg/ml and 100ng/ml captopril treated cells were considerably smaller than the 96h non-treated control sample (figure 5.6), but only the 100μg/ml caused a significant reduction in cardiomyocyte area, determined by a one-tail Student's t-test (p-value<0.05). This reduction resulted in the treated cardiomyocyte average area being non-significantly different from the 24h serum starved non-treated control cells, assessed by the same method, taking into account heteroskedasticity between the samples, assessed by Levene's test (table 5.3). Although there was no significant difference between the 24h control cardiomyocytes and 1μg/ml captopril treated cells, the difference between 96h control cells and 1 μg/ml treated cells was also non-significant.

Comparison	Levene's Test p-value	Variance	t-test p-value
96h v 24h	0.030863692	Unequal	<u>0.0130</u>
96h v 100μg/ml	0.097869639	Equal	<u>0.0420</u>
24h v 100μg/ml	0.326658334	Unequal	0.3554
96h v 10μg/ml	0.260166933	Equal	0.3907
24h v 10μg/ml	0.001030229	Equal	<u>0.0130</u>
96h v 1μg/ml	0.147505382	Equal	0.0524
24h v 1μg/ml	0.246194231	Equal	0.2986
96h v 100ng/ml	0.60258218	Equal	0.1181
96h v 10ng/ml	0.449104105	Equal	0.4121

Table 5.3. Captopril treatment statistical analyses results. The first column represents Levene's and Student's t-test comparisons. 24h and 96h represent the non-treated control samples and the concentrations represent 96h serum starved samples treated with captopril. Significant t-test p-values<0.05 are underlined.

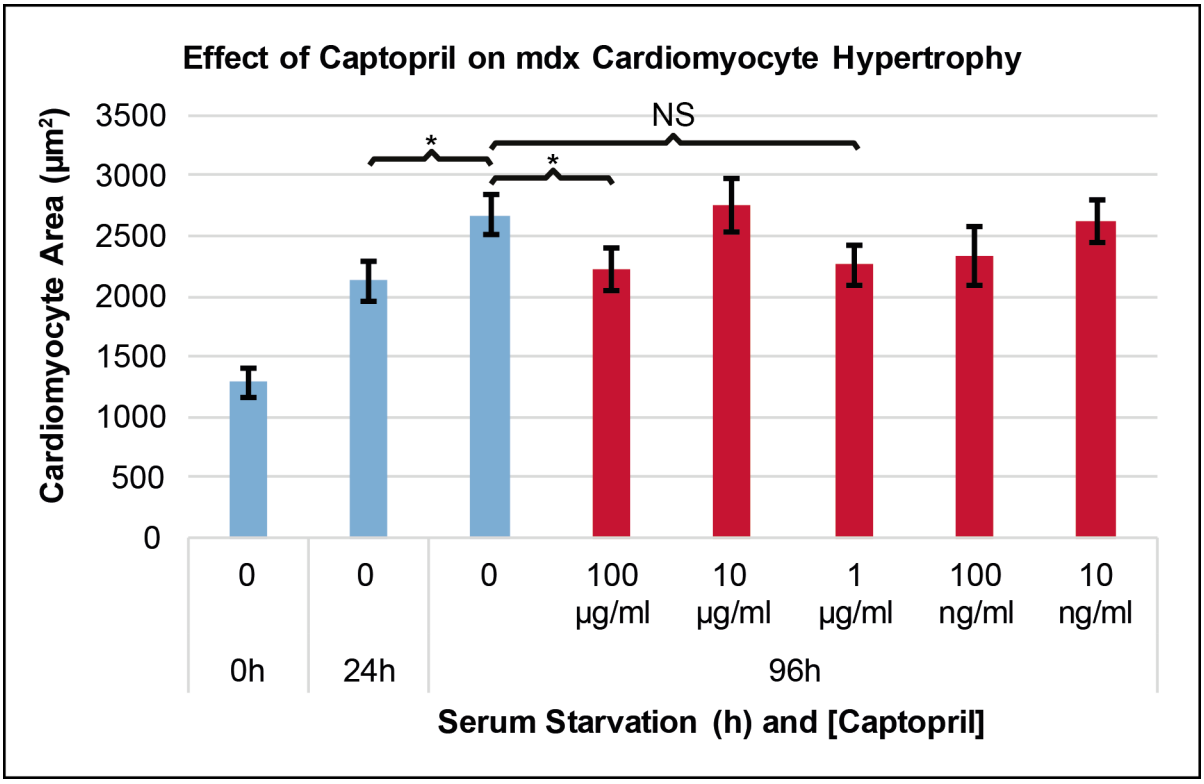

Figure 5.6. The effect of Captopril on mdx cardiomyocyte hypertrophy. Serum starved cardiomyocytes were treated with a range of captopril concentrations from the 24h serum starvation time-point (red columns). Non-treated control cardiomyocytes (blue columns) serum starved for 96h were significantly larger than cells serum starved for 24h and cells treated with 100µg/ml captopril (* corresponds to p-value<0.05). The average area measurements of cardiomyocytes treated with 1µg/ml, 100ng/ml and 10ng/ml captopril in SFCGM were also smaller than the non-treated sample, but none of these reductions in area were statistically significant (NS stands for non-significant), based on one-tailed Student's t-test analysis. Error bars represent standard error of the mean.

5.5 Beta-adrenergic Receptor Blocker Treatment

The combination treatment of cardiomyopathy with ACE inhibitors and βAR blockers has shown improved left ventricular function in DMD patients (Jefferies et al., 2005). The effect of metoprolol, a β_1AR blocker, on mdx cardiomyocyte hypertrophy was assessed. MRes student Elizabeth Roberts serum starved cardiomyocytes with SFCGM for 24h, followed by metoprolol treatment at five concentrations in one magnitude steps from 50μg/ml to 5ng/ml. All of metoprolol treated cardiomyocytes were on average larger than non-treated 96h serum starved control cells. In fact, based on one-tailed Student's t-test analyses the 500ng/ml, 50ng/ml and 5ng/ml metoprolol treatments caused a significant increase in average cardiomyocyte area in comparison to 96h serum starved non-treated control cells (table 5.4).

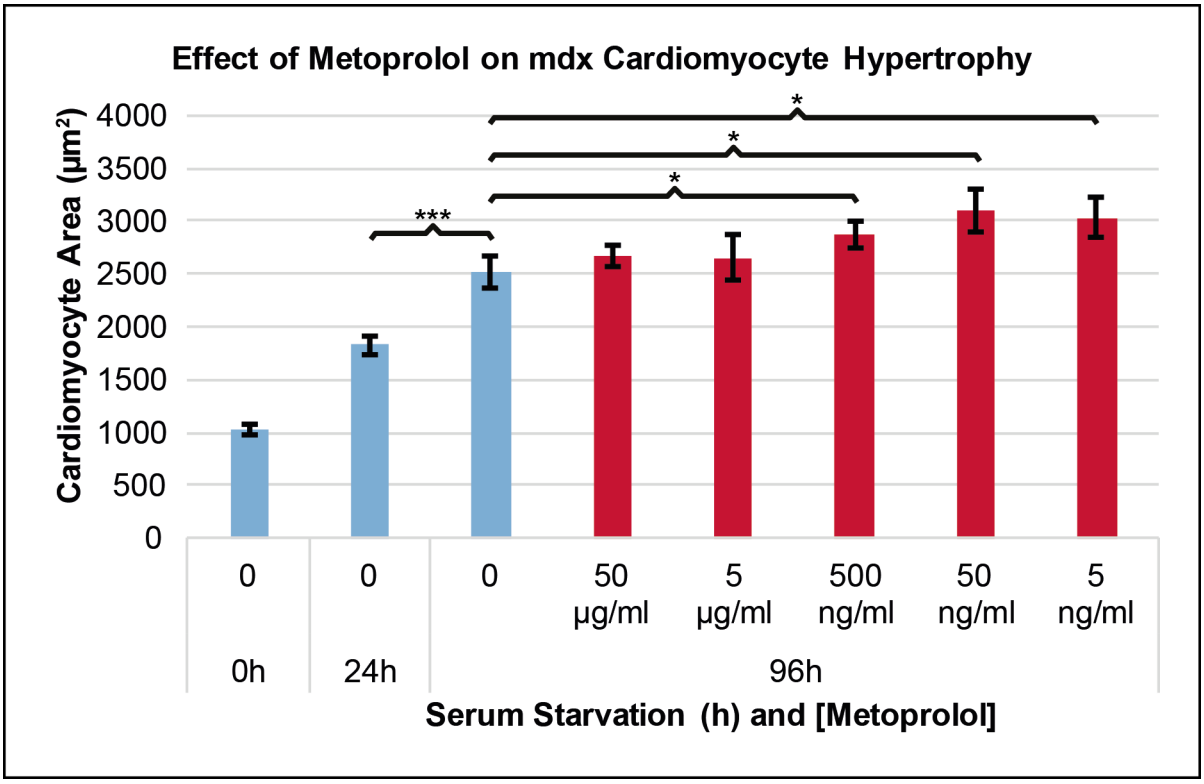

Figure 5.7. The effect of metoprolol on mdx cardiomyocyte hypertrophy. Serum starved cardiomyocytes were treated with a range of metoprolol concentrations (red columns) from the 24h serum starvation time-point. Non-treated control cardiomyocytes (blue columns) serum starved for 96h were significantly larger than cells serum starved for 24h (*** corresponds to p-value<0.001). The average area measurements of cardiomyocytes treated with 500ng/ml, 50ng/ml and 5ng/ml metoprolol in SFCGM were significantly larger than the non-treated 96h serum starved control sample (* corresponds to p-value<0.05), based on one-tailed Student's t-test analysis. Error bars represent standard error of the mean.

Comparison	Levene's Test p-value	Variance	t-test p-value
96h v 24h	0.001130576	Unequal	4.44297E-05
96h v 50µg/ml	0.864760912	Equal	0.2148
96h v 5µg/ml	0.353772268	Equal	0.2408
96h v 500ng/ml	0.183411251	Equal	0.0287
96h v 50ng/ml	0.656947668	Equal	0.0187
96h v 5ng/ml	0.918614095	Equal	0.0189

Table 5.4. Metoprolol treatment statistical analyses results. The first column represents Levene's and Student's t-test comparisons. 24h and 96h represent the non-treated control samples and the concentrations represent 96h serum starved samples treated with metoprolol. Significant t-test p-values<0.05 are underlined.

Angiotensin (Ang) signalling is mediated by the mitogen-activated protein kinase (MAPK) and extracellular signal-regulated kinase (ERK) mediated pathways (Schlüter & Wenzel, 2008). The protein level of β_1AR and activation of ERK pathway in BL/10 and mdx cardiomyocytes undergoing serum starvation were assessed by Western blotting with antibodies targeting β_1AR and phosphorylated ERK1/2, respectively (figure 5.8). Protein expression patterns were similar along the serum starvation course in both types of cardiomyocytes, assessed by quantifying protein band intensities and adjusting to skeletal myosin heavy chain (MYH6) band intensities with ImageJ software. Phosphorylated ERK1/2 levels were lower in mdx cardiomyocytes in comparison to BL/10 cells at the start of serum starvation (0h). By 48h of serum starvation the protein level of activated ERKs in mdx cardiomyocytes was higher and although at 72h the levels were relatively equal, by 96h there was again more phosphorylated ERK 1/2 in mdx cells. β_1AR expression was near two-fold higher in BL/10 cardiomyocytes at the start of serum starvation in comparison to serum starved BL/10 cells and all mdx samples. In mdx cardiomyocytes an initial reduction in β_1AR protein level in response to serum starvation by the 24h time-point was reversed and expression levels similar to the 0h sample were evident in the remaining serum starvation time course. Pearson's chi-squared test was used to identify whether there was a significant difference in ERK phosphorylation or β_1AR expression between all BL/10 and mdx samples or only serum starved (24h, 48h, 72, 96h) BL/10 and mdx cardiomyocyte samples. In both comparisons for both proteins of interest the observed expression levels in mdx cardiomyocytes were significantly different (p-value<0.001) than BL/10 cells (table 5.5).

Comparison	Protein	$\Sigma (O-E)^2/E$	DoF	X^2 p<0.001	H_0
All BL/10 v mdx	β_1AR	9634	4	18.47	Reject
All BL/10 v mdx	p-ERK	5632	4	18.47	Reject
SS BL/10 v mdx	β_1AR	1029	3	16.27	Reject
SS BL/10 v mdx	p-ERK	2379	3	16.27	Reject

Table 5.5. Protein expression and activation statistical analyses. Sample relative protein levels were determined and compared. BL/10 cardiomyocytes were the expected (E) and mdx cells the observed (O) datasets. Chi squared (X^2) values for p-value<0.001 based on degrees of freedom (DoF) were used to either accept or reject the null hypothesis (H_0) of observed values not differing from expected values.

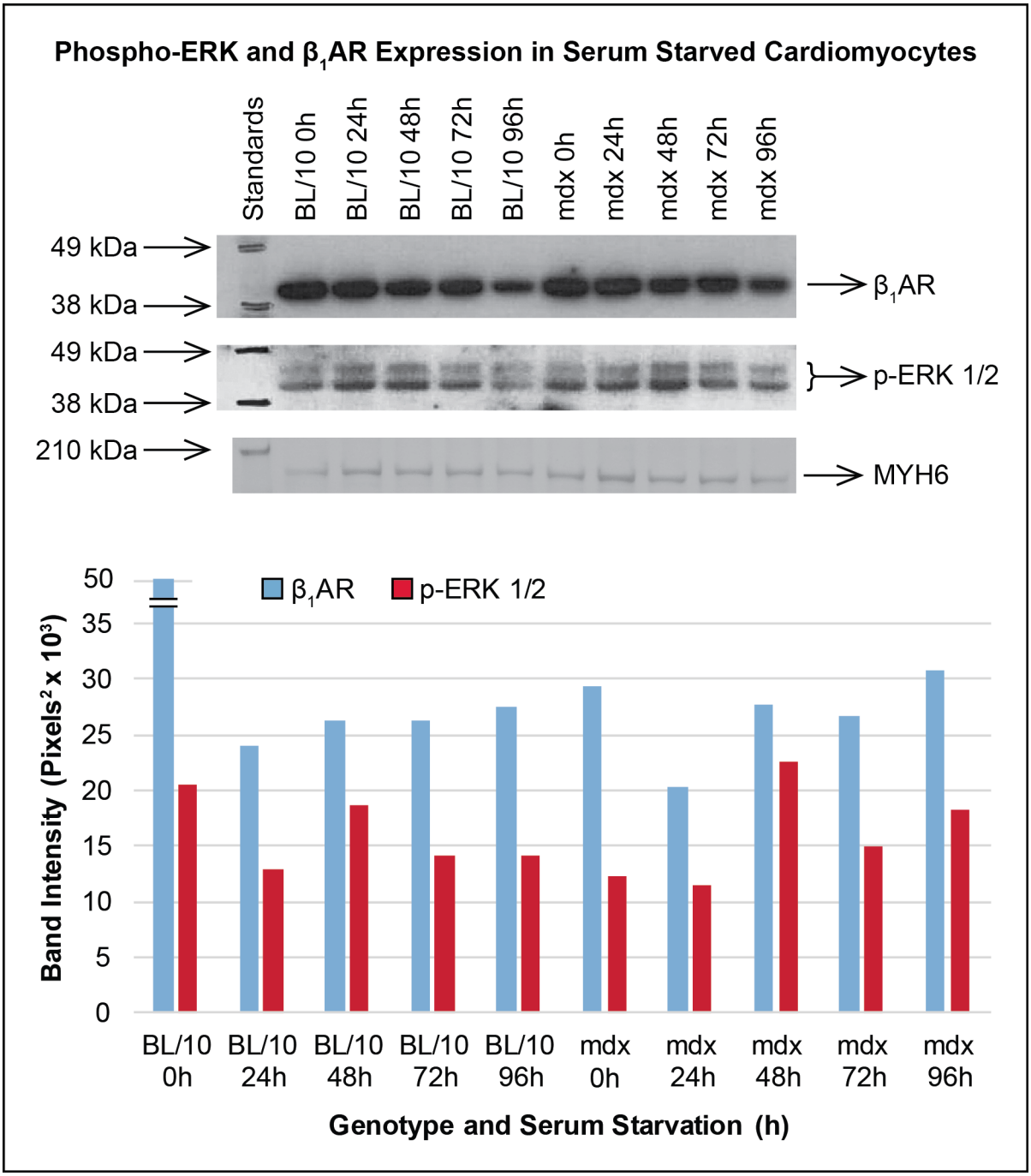

Figure 5.8. ERK activation and β_1AR expression in mdx cardiomyocytes. Protein samples from BL/10 and mdx cardiomyocytes along the serum starvation time-course were analysed by Western blotting, with antibodies targeting beta-1 adrenergic receptor (β_1AR) and phosphorylated extracellular signal-regulated kinase (p-ERK1/2). Protein expression levels were normalised to skeletal myosin heavy chain (MYH6).

5.6 Sodium-hydrogen Exchanger Inhibitor Treatment

The role of sodium-hydrogen exchanger (NHE) in cardiomyocyte hypertrophy was discussed in sub-section 4.8.4. It has been hypothesised that inhibiting the NHE channel may reduce cardiomyocyte hypertrophy by reducing the sodium gradient in cardiomyocytes and thus aiding the sodium-calcium exchanger (NCX) to clear intracellular Ca^{2+} ions from the sarcoplasm (Bkaily et al., 2015). KR-33028 is a potent compound used to inhibit NHE activity (Jung et al., 2006).

The effect of KR-33028 treatment on mdx cardiomyocyte hypertrophy was assessed at five drug concentrations ranging from 100μM to 10nM in one order of magnitude increments. The compound was dissolved in polyethylene glycol (PEG) and vehicle-only control samples treated with corresponding PEG concentrations were therefore also conducted for each compound concentration used. Cardiomyocytes treated with 100μM of KR-33028 in SSCGM were significantly smaller than non-treated control cardiomyocytes by the 96h serum starvation time-point (figure 5.9).

Although the 0.85% PEG (V/V) vehicle-treated cardiomyocytes, corresponding to the PEG content in 100μM KR-33028, also showed a significant reduction in mdx cardiomyocyte hypertrophy, there was a significant difference between the average area measurements of 100μM KR-33028 and 0.85% PEG treated samples. There was no significant difference between the no treatment control 96h serum starved sample and the 0.085% as well as 0.0085% PEG treated samples, but 0.00085% and 0.000085% PEG treatment resulted in significant cardiomyocyte area reduction. A significant reduction in average cardiomyocyte area was also recorded in 10nM KR-33028-treated cells (table 5.6).

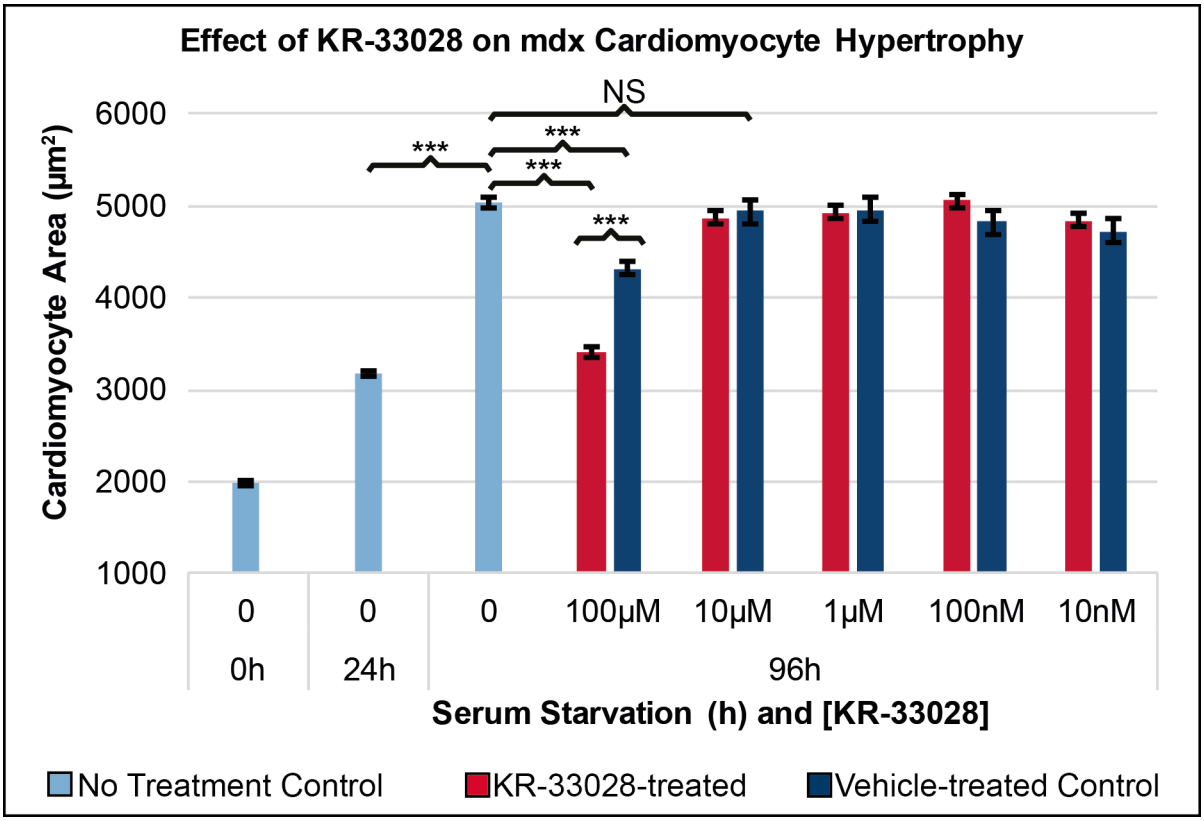

Figure 5.9. The effect of KR-33028 on mdx cardiomyocyte hypertrophy. Serum starved cardiomyocytes were treated with a range of KR-33028 (red columns) and corresponding PEG vehicle concentrations (dark blue columns) from the 24h serum starvation time-point. Non-treated control cardiomyocytes (light blue columns) serum starved for 96h were significantly larger than cells serum starved for 24h, as well as 100µM KR-33028 and 0.85% PEG-treated cells (*** corresponds to p-value<0.001). The average area of cardiomyocytes treated with 100µM KR-33028 was also significantly lower than 0.85% PEG-treated cells. One-tailed Student's t-test and Levene's test were used for statistical analyses. Error bars represent standard error of the mean.

Comparison	Levene's Test p-value	Variance	t-test p-value
24h v96h	6.98923E-88	Unequal	2.3479E-18
24h v 100μM	1.08952E-20	Unequal	0.0003
96h v 100μM	2.26175E-25	Unequal	1.3092E-84
100μM v .85%	1.3551E-11	Unequal	5.37354E-22
24h v .85%	8.10486E-53	Unequal	7.61135E-40
96h v .85%	0.008976764	Unequal	3.64483E-14
96h v 10μM	0.545493143	Equal	0.0228
96h v .085%	0.030950756	Unequal	0.2448
96h v 1μM	0.628426431	Equal	0.1024
96h v .0085%	0.424205853	Equal	0.2734
96h v 100nM	0.078347397	Equal	0.4513
96h v 0.00085%	0.41591503	Equal	0.0481
96h v 10nM	0.589148296	Equal	0.0138
96h v 0.000085%	0.901567295	Equal	0.0102

Table 5.6. KR-33028 and PEG vehicle treatment statistical analyses. The first column represents Levene's and Student's t-test comparisons. 24h and 96h represent the non-treated control samples and the concentrations represent 96h serum starved samples treated with KR-33028 in molar units and PEG in percentage values (V/V). Significant t-test p-values<0.05 are underlined.

5.7 Purinergic Receptor Inhibitor Treatment

Purinergic receptor P2X ligand-gated ion channel 7 (P2RX7) has emerged as a novel target for ameliorating the DMD phenotype (Sinadinos et al., 2015). P2RX7 is an ATP-activated ion channel, which opens a pore on the sarcolemma upon exposure to extracellular ATP, allowing Ca^{2+} and small molecule influx to the sarcoplasm, consequently increasing $[Ca^{2+}]_i$ and triggering autophagic and apoptotic cascades (Young et al., 2015). A potent P2RX7 inhibitor compound A804598 (Donnelly-Roberts et al., 2009) was used to treat mdx cardiomyocytes undergoing serum starvation-induced hypertrophy. A804598 was dissolved in dimethyl sulfoxide (DMSO) and diluted in SFCGM or SSCGM. The compound was used to treat cardiomyocytes at seven concentrations ranging from 1μM to 1pM at one order of magnitude increments. DMSO treatment was also conducted to account for vehicle effect on cardiomyocyte hypertrophy.

Two experiments were conducted where A804598 was dissolved in SFCGM and the highest concentration of the drug used for treatment was 1μM, containing 0.01% (V/V) DMSO (figure 5.10). BSc student Sophie Wright assessed mdx cardiomyocyte hypertrophy in these two experiments by measuring the volume of immunostained cells positive for α-actinin signal. In both biological replicates 1nM and 100pM A804598 treatment significantly reduced mdx cardiomyocyte hypertrophy. In the first replicate (figure 5.10 A) 10nM A804598 did not cause a significant reduction in cardiomyocyte area, whereas in the second replicate (figure 5.10 B) a significant reduction was observed in the treated sample. Furthermore, in the first biological replicate A804598 treated cardiomyocytes were only significantly smaller than the corresponding DMSO vehicle-only treated samples at the 0.00001% and 1nM concentrations, respectively. In the second biological replicate all three of the lowest A804598 concentration treated samples were also significantly smaller on average than the corresponding DMSO-treated vehicle control cells (table 5.7).

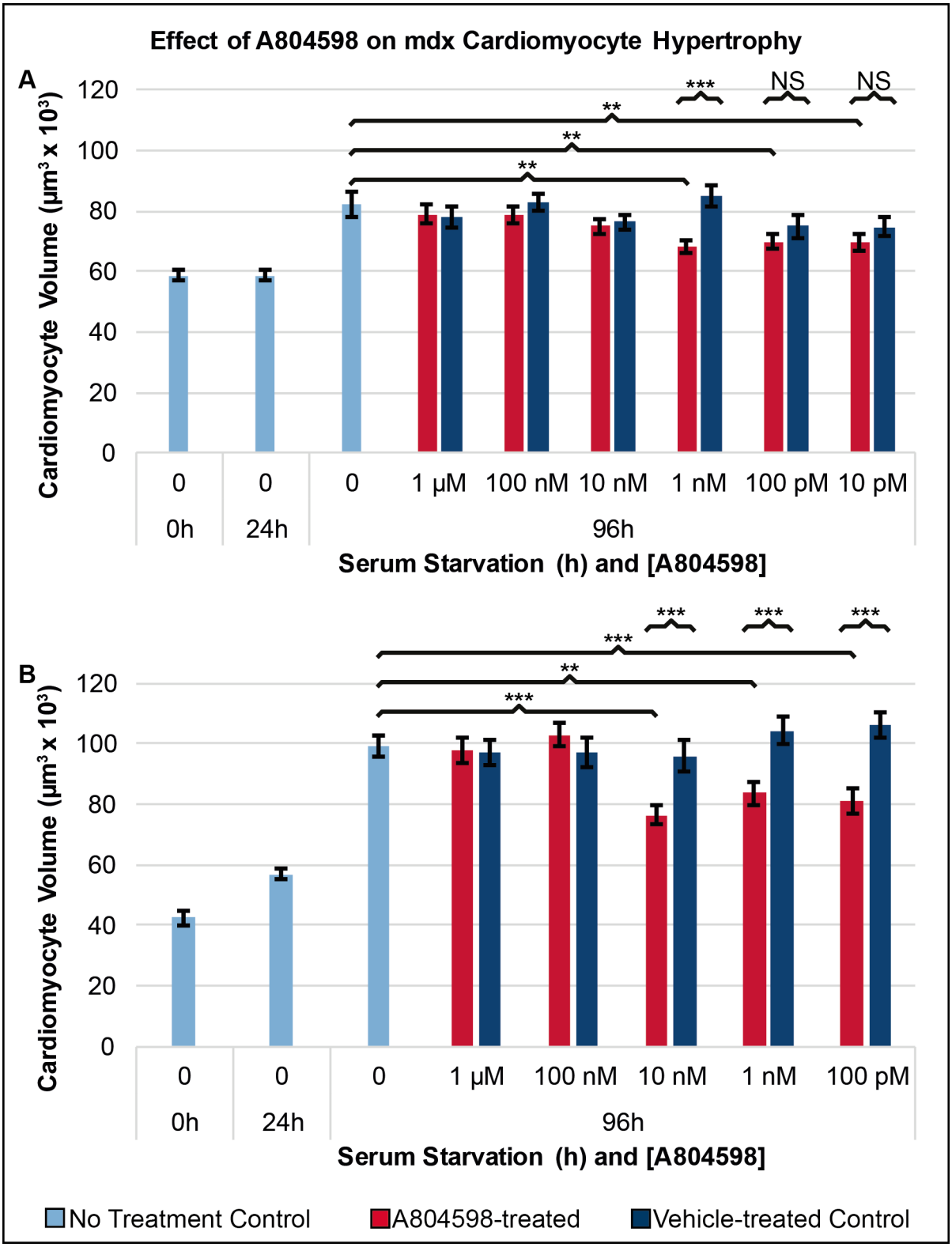
Effect of A804598 on mdx Cardiomyocyte Hypertrophy
A
Cardiomyocyte Volume (µm³ x 10³)
120
100
80
60
40
20
0
**
**
**
***
NS
NS
0
0
0
1 µM
100 nM
10 nM
1 nM
100 pM
10 pM
0h
24h
96h
Serum Starvation (h) and [A804598]
B
Cardiomyocyte Volume (µm³ x 10³)
***
**
***
***
***
***
0
0
0
1 µM
100 nM
10 nM
1 nM
100 pM
0h
24h
96h
Serum Starvation (h) and [A804598]
No Treatment Control
A804598-treated
Vehicle-treated Control

Figure 5.10. A804598 effect on mdx cardiomyocyte hypertrophy induced by SFCGM. Two biological replicate experiments were conducted. Volume measurements of six different concentrations of A804598 (red columns) treated and DMSO vehicle treated (dark blue columns) cardiomyocytes in the first replicate (A) and five concentrations in the second replicate (B) were compared to non-treated cardiomyocytes (light blue). In both samples 1nM and 100pM treated cells were significantly smaller than the 96h serum starved non-treated control cardiomyocytes (** corresponds to p-value<0.01 and *** corresponds to p-value<0.001). In the second replicate three of the drug treated samples (10nM, 1nM and 100pM) were significantly smaller than the corresponding DMSO vehicle treated controls (0.0001%, 0.00001% 0.000001%), whilst only the 1nM A804598 and 0.00001% DMSO treatment comparison showed a significant reduction in the drug treated cells (NS stands for non-significant). One-tailed Student's t-test and Levene's test were used for statistical analyses. Error bars represent standard error of the mean.

Comparison A	Levene's Test p-value	Variance	t-test p-value
24h v 96h	1.38596E-08	Unequal	8.03675E-08
96h v 1μM	0.477255677	Equal	0.2825
96h v .01%	0.137505372	Equal	0.2145
1μM v .01%	0.354265771	Equal	0.4102
96h v 100nM	0.480822159	Equal	0.2217
96h v .001%	0.593109685	Equal	0.4264
100nM v .001%	0.809172041	Equal	0.1263
96h v 10nM	0.228692712	Equal	0.0572
96h v .0001%	0.001512264	Unequal	0.1058
10nM v .0001%	0.00794106	Unequal	0.3447
96h v 1nM	0.004194548	Unequal	0.0011
96h v .00001%	0.822602694	Equal	0.3007
1nM v .00001%	0.00262294	Unequal	2.7136E-05
96h v 100pM	0.003522354	Unequal	0.0044
96h v .000001%	0.342066521	Equal	0.1070
100pM v .000001%	0.087855495	Equal	0.1149
96h v 10pM	0.025658596	Unequal	0.0050
96h v .0000001%	0.014567125	Unequal	0.0821
10pM v .0000001%	0.421222705	Equal	0.1175
Comparison B	Levene's Test p-value	Variance	t-test p-value
24h v 96h	4.39809E-13	Unequal	1.71964E-22
96h v 1μM	0.01403757	Unequal	0.3828
96h v .01%	0.263353414	Equal	0.3415
1μM v .01%	0.00109465	Unequal	0.4593
96h v 100nM	0.898080185	Equal	0.2446
96h v .001%	0.206009378	Equal	0.3600
100nM v .001%	0.3241352	Equal	0.1714
96h v 10nM	0.006808231	Unequal	1.00698E-06
96h v .0001%	0.024604463	Unequal	0.3052
10nM v .0001%	1.07016E-05	Unequal	0.0005
96h v 1nM	0.074301449	Equal	0.0021
96h v .00001%	0.025351859	Unequal	0.1895
1nM v .00001%	0.51914125	Equal	0.0004
96h v 100pM	0.443073794	Equal	0.0005
96h v .000001%	0.564385123	Equal	0.1018
100pM v .000001%	0.215287585	Equal	1.13739E-05

Table 5.7. A804598 and DMSO vehicle treatment statistical analyses. The first column represents Levene's and Student's t-test comparisons. 24h and 96h represent the non-treated control samples and the concentrations represent 96h serum starved samples treated with A804598 in molar units and DMSO in percentage values (V/V). Significant t-test p-values<0.05 are underlined.

A third biological replicate of A804598 treatment was conducted where SSCGM was used to serum starve mdx cardiomyocytes. The drug was less soluble in SSCGM and required a stronger vehicle concentration in the medium (10% DMSO for 1μM A804598). The high vehicle concentration was toxic to the cells and cardiomyocytes surviving the 10% DMSO (V/V) treatment were very small in their average area, almost comparable to 0h serum starved control samples (figure 5.11). 10nM and 1nM A804598 treated cells were significantly smaller than non-treated 96h serum starved control cells, but the 0.01% DMSO vehicle treated cardiomyocytes were also smaller and unexpectedly the 0.001% DMSO treated cardiomyocytes were significantly larger than 96h non-treated control cells (table 5.8).

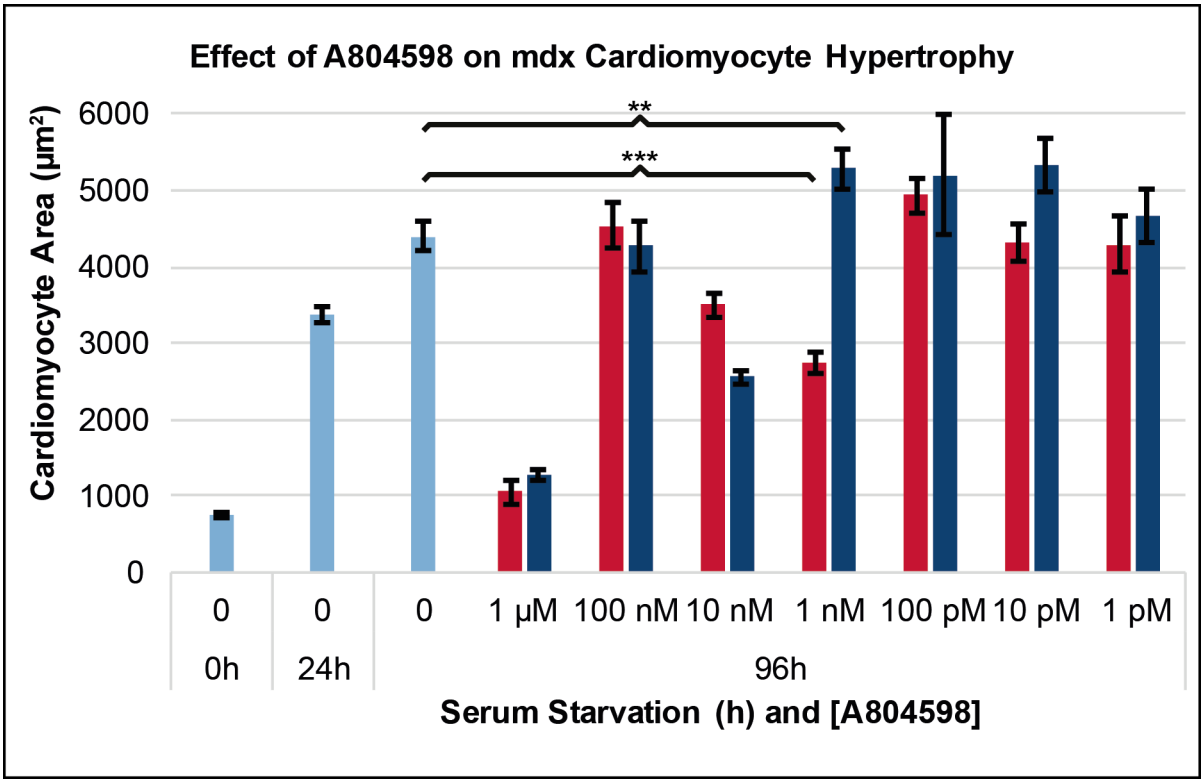

Figure 5.11. A804598 effect on mdx cardiomyocyte hypertrophy induced by SSCGM. Average area measurements of non-treated 0h, 24h and 96h serum starved control cardiomyocytes (light blue columns) were compared to A804598 (red columns) and DMSO vehicle (dark blue columns) treated cells. 1nM A804598 treated cardiomyocytes were significantly smaller (*** corresponds to p-value<0.001) and 0.001% DMSO vehicle treated cells significantly larger (** corresponds to p-value<0.01) than 96h non-treated control cardiomyocytes. One-tailed Student's t-test and Levene's test were used for statistical analyses. Error bars represent standard error of the mean.

Comparison	Levene's Test p-value	Variance	t-test p-value
24h v96h	3.71683E-09	Unequal	3.82646E-06
96h v 100nM	0.947835254	Unequal	0.3612
96h v 1% DMSO	0.421799589	Equal	0.3866
96h v 10nM	0.045706928	Unequal	0.0002
96h v 1nM	1.11473E-07	Unequal	2.35631E-11
24h v 1nM	0.267579681	Equal	0.0004
96h v 0.01% DMSO	0.361897323	Equal	0.0032
96h v 100pM	0.402365579	Equal	0.0528

Table 5.8. A804598 and DMSO vehicle treatment statistical analyses. The first column represents Levene's and Student's t-test comparisons. 24h and 96h represent the non-treated control samples and the concentrations represent 96h serum starved samples treated with A804598 in molar units and DMSO in percentage values (V/V). Significant t-test p-values<0.05 are underlined.

5.8 Transducing mdx Cardiomyocytes with eGFP and µDys

Becker muscular dystrophy (BMD) is a milder form of dystrophinopathy, mostly caused by large open reading frame deletions in the rod domain of the *DMD* gene (Ferreiro et al., 2009). BMD mutations have been used prototypically to derive smaller functional versions of dystrophin deliverable as gene therapy using viral vectors with restricted genetic packaging capacity (Fabb et al., 2002). The m2 micro-dystrophin (µDys) construct, characterised in Newcastle (Jørgensen et al., 2009), was packaged into adeno-associated viruses (AAV) by Oliver Müller's research group in Heidelberg and used to attenuate the dystrophic phenotype in mdx mouse hearts (Schinkel et al., 2012). These constructs were optimised from a cytomegalovirus (CMV) promoter to an improved CMV promoter with a myosin light chain (MLC) enhancer region MLC0.26 combination, packaged into AAV6 and AAV9 in Heidelberg and shipped to Newcastle for testing their efficacy in transducing mdx cardiomyocytes.

AAV6-CMV-eGFP and AAV6-CMV-MLC0.26-eGFP both successfully transduced mdx cardiomyocytes at multiplicity of infection (MOI) 100,000vg/cell (vg is a unit for the number of viral genomes) and expressed eGFP 72h post-transduction (panels A and B in figure 5.12, respectively). It was also possible to perform ICC for α-actinin expression on PFA-fixed cardiomyocytes serum starved for 96h and transduced at

the 24h serum starvation time-point with AAV6-CMV-MLC0.26-eGFP and AAV6-CMV-MLC0.26-μDys (panels D and E in figure 5.12, respectively) to investigate cardiomyocyte specificity of construct expression due to the MLC0.26 enhancer region incorporation. Expression of eGFP was exclusively found in α-actinin-positive cardiomyocytes. Expression of μDys could not be detected using mouse monoclonal dystrophin antibody MANDRA1 or with the rabbit polyclonal dystrophin antibody ab15277. The latter antibody yielded punctate fluorophore signal in cells negative for α-actinin expression, also seen in α-actinin-negative cells in a control sample where the secondary fluorophore-conjugate antibody was added without the ab15277 antibody to mdx cells not transduced with μDys (figure 5.12 panels E and F, respectively).

Figure 5.12. Transduction of mdx cardiomyocytes with eGFP and μDys-containing AAV6 vectors. (A) AAV6-CMV-eGFP and (B) AAV6-CMV-MLC0.26-eGFP transduction resulted in eGFP signal in mdx cells isolated from E17.5 mouse embryo hearts 72h post-transduction, while (C) in non-transduced control cells no eGFP signal was detected. (D) ICC for α-actinin (in red) was performed to identify cardiomyocyte-specific expression of CMV-MLC0.26-driven expression of eGFP 72h post-transduction in cells serum starved for 96h. (E) AAV6-CMV-MLC0.26-μDys was used to transduce cells serum starved for 24h and ICC dual-stained at the 96h serum starvation time-point for α-actinin (red) and dystrophin (green). Punctate signal for dystrophin signal was seen in α-actinin-negative cells. (F) A similar punctate pattern of fluorophore signal was observed in non-transduced control primary mdx cells negative for α-actinin staining, also serum starved for 96h. Scale bars represent 200μm.

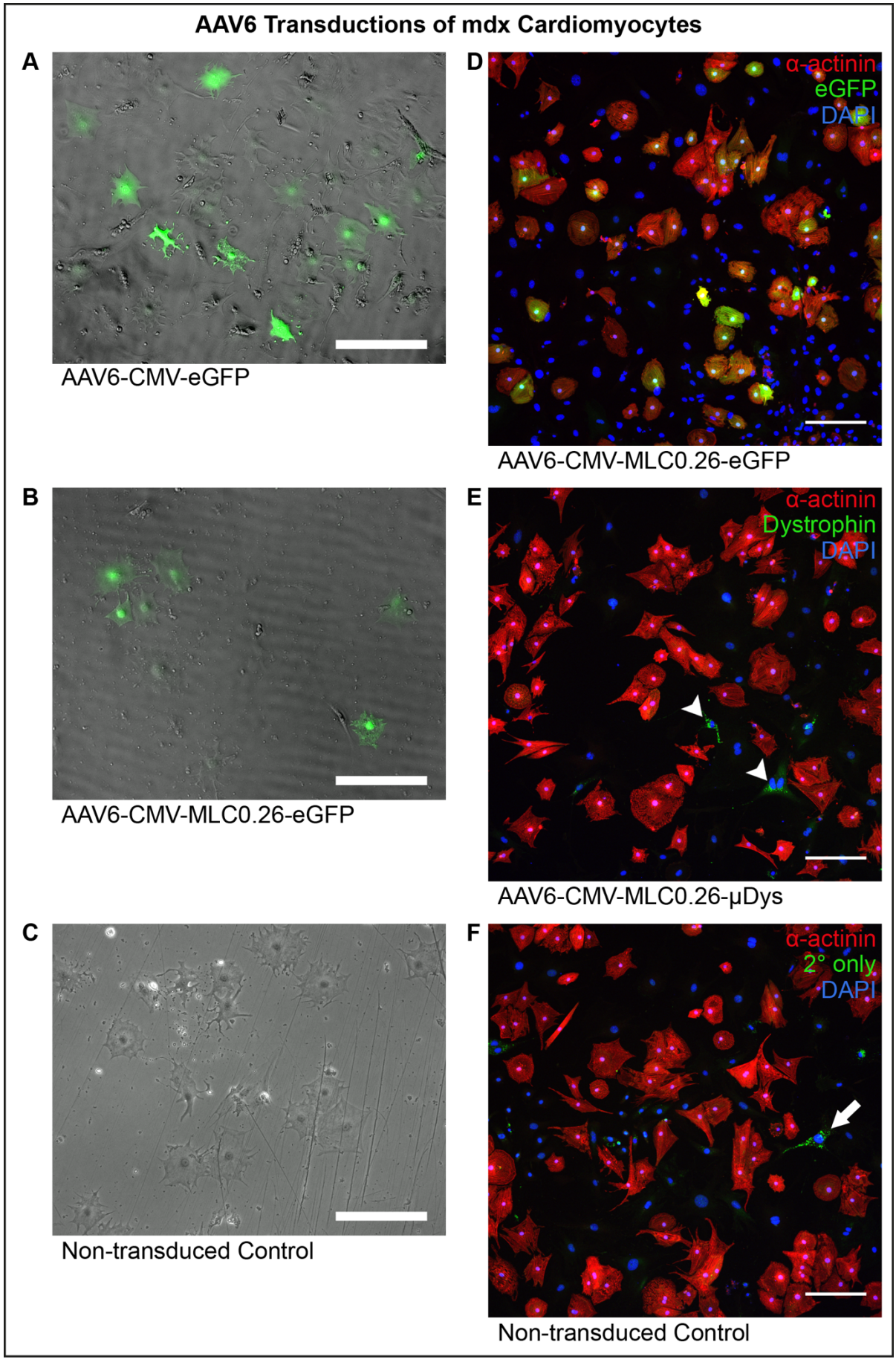
AAV6 Transductions of mdx Cardiomyocytes
A
AAV6-CMV-eGFP
B
AAV6-CMV-MLC0.26-eGFP
C
Non-transduced Control
D
α-actinin
eGFP
DAPI
AAV6-CMV-MLC0.26-eGFP
E
α-actinin
Dystrophin
DAPI
AAV6-CMV-MLC0.26-μDys
F
α-actinin
2° only
DAPI
Non-transduced Control

The effect of eGFP and μDys transduction with AAV6 on mdx cardiomyocyte hypertrophy was determined by transducing 24h serum starved cells with AAV6-CMV-MLC0.26-eGFP or AAV6-CMV-MLC0.26-μDys and quantifying cell area 72h later (figure 5.13). There was no significant difference between μDys transduced cardiomyocytes and non-transduced control cells serum starved with SSCGM for 96h. Cardiomyocytes transduced with eGFP were used as a control to detect whether AAV6 transduction affected the mdx hypertrophic response. Area measurements were recorded separately for eGFP positive (n=1069) and negative (n=131) cells in the sample, then also combined. There was no statistical reduction or increase in mdx cardiomyocyte average area by AAV6 transduction with eGFP when the overall cardiomyocyte population and only eGFP positive cells were compared to 96h serum starved non-transduced control cells (table 5.9). Transduction efficiency with AAV6-CMV-MLC0.26-eGFP at 100,000vg/ml was 89%, determined by the proportion of cardiomyocytes positive for eGFP signal in the population used for area measurements (1,069 of 1,200).

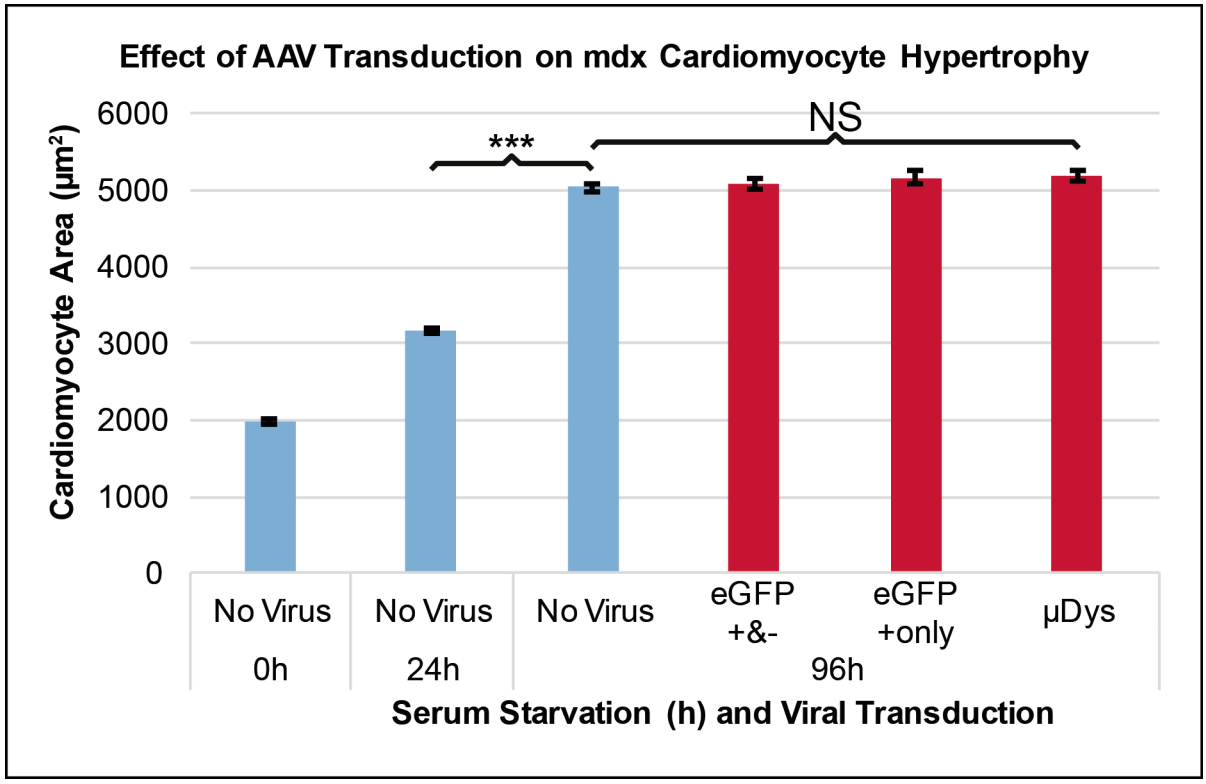

Figure 5.13. Effect of AAV6 Transduction on mdx cardiomyocyte hypertrophy. Average area measurements of non-treated 0h, 24h and 96h serum starved control cardiomyocytes (blue columns) were compared to cells transduced with AAV6 vectors containing either an eGFP or a µDys construct (red columns). 24h serum starved cardiomyocytes were significantly smaller than 96h serum starved non-treated cells (*** corresponds to p-value<0.001). Transduced cardiomyocytes were not significantly (NS) larger or smaller than non-transduced control cells serum starved for 96h. One-tailed Student's t-test and Levene's test were used for statistical analyses. Error bars represent standard error of the mean.

Comparison	Levene's Test p-value	Variance	t-test p-value
24h v96h	6.98923E-88	Unequal	1.9981E-143
96h v eGFP+&-	0.093644555	Equal	0.3085
96h v eGFP+	0.036544958	Unequal	0.1133
96h v μDys	0.525337377	Equal	0.0559
eGFP+ v μDys	0.163529799	Equal	0.4261
eGFP+&- v μDys	0.318357788	Equal	0.1783
eGFP+&- v eGFP+	0.697673949	Equal	0.2535

Table 5.9. AAV6 μDys and eGFP cardiomyocyte transduction statistical analyses. The first column represents Levene's and Student's t-test comparisons. 24h and 96h represent the non-transduced control samples and μDys represents AAV6-CMV-MLC0.26-μDys transduced cardiomyocytes. Cells transduced with AAV6-CMV-MLC0.26-eGFP were analysed as either all cardiomyocytes positive and negative for eGFP signal combined (eGFP+&-) or only the eGFP positive cells on their own as a dataset (eGFP+). Significant t-test p-value<0.05 is underlined.

It was not possible to detect μDys expression with ICC in mdx cardiomyocytes transduced with AAV6 vectors and these transduced cells displayed a hypertrophic response comparable to non-transduced serum starved cardiomyocytes. It was subsequently investigated with Western blotting whether μDys was expressed in AAV6 transduced cells. Cardiomyocytes from mdx mouse embryos were serum starved with SSCGM and transduced with AAV6-CMV-MLC0.26-μDys virus at 100,00vg/ml. Cells were collected for protein extraction at the 0h, 24h, 72h and 96h non-transduced, as well as μDys-transduced 72h and 96h serum starvation time-points. The same rabbit polyclonal antibody ab15277, which was used to detect μDys by ICC was also used for immunoblotting. A band was detected in the anticipated 125kDa region for m2 μDys (Jørgensen et al., 2009) in the transduced samples at both 72h and 96h of serum starvation (figure 5.14), which correspond to 48h and 72h of transcript expression, respectively.

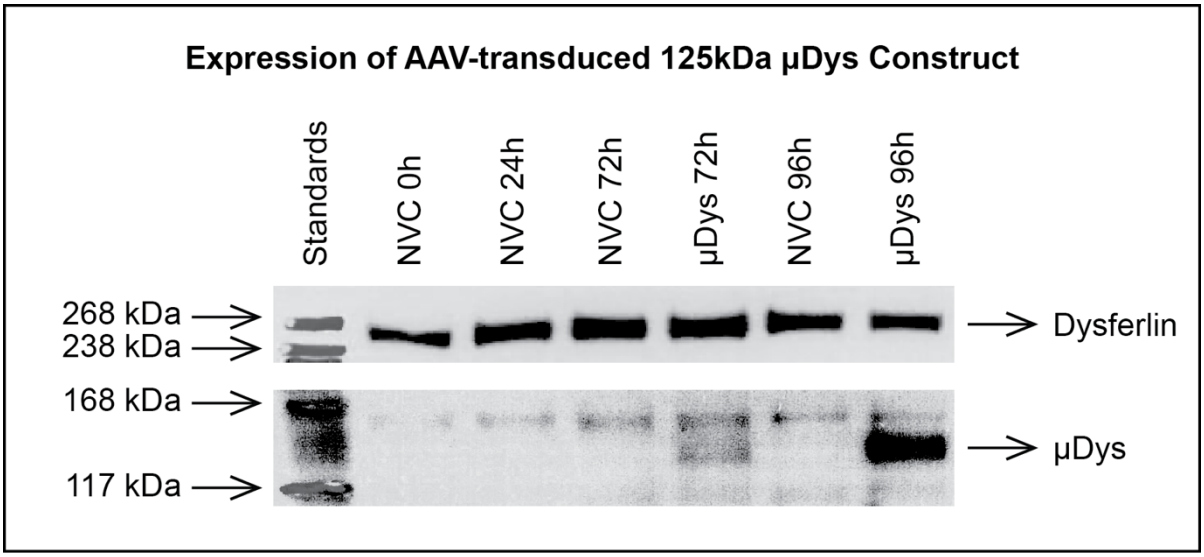

Figure 5.14. AAV6-transduced mdx cardiomyocytes express μDys protein. A band in the anticipated 125kDa range was detected in both 72h and 96h μDys-transduced samples. This band was absent in the non-transduced no virus control (NVC) samples at all time-points of serum starvation included in this experiment. Dysferlin expression was used as the loading control.

Two further experiments were conducted where both AAV6-CMV-MLC0.26-μDys and AAV9-CMV-MLC0.26-μDys were used in separate samples to assess their effect on mdx cardiomyocyte hypertrophy. Primary cells from mdx E17.5 hearts were serum starved with SSCGM and transduced with μDys AAV6 and AAV9 vectors. ICC for α-actinin expression was performed to measure the area of cardiomyocytes. MRes student Stephanie Carr performed the image analysis of μDys-transduced samples. Both AAV6 and AA9 μDys transduced cardiomyocytes were on average significantly smaller than 96h serum starved non-transduced control cardiomyocytes in both biological replicates (figure 5.15). On average AAV9 transduced cardiomyocytes in replicate A were smaller than AAV6 transduced cells, but this was not a statistically significant reduction in size, whilst AAV6 transduced cells in replicate B were significantly smaller than AAV9 transduced cardiomyocytes. Both AAV6 and AAV9 transduced cardiomyocytes in replicate B were still significantly larger than 24h serum starved non-transduced control cells. However, in replicate A the AAV9 transduced cardiomyocytes were not statistically larger than the control cells fixed at the start of transduction (table 5.10).

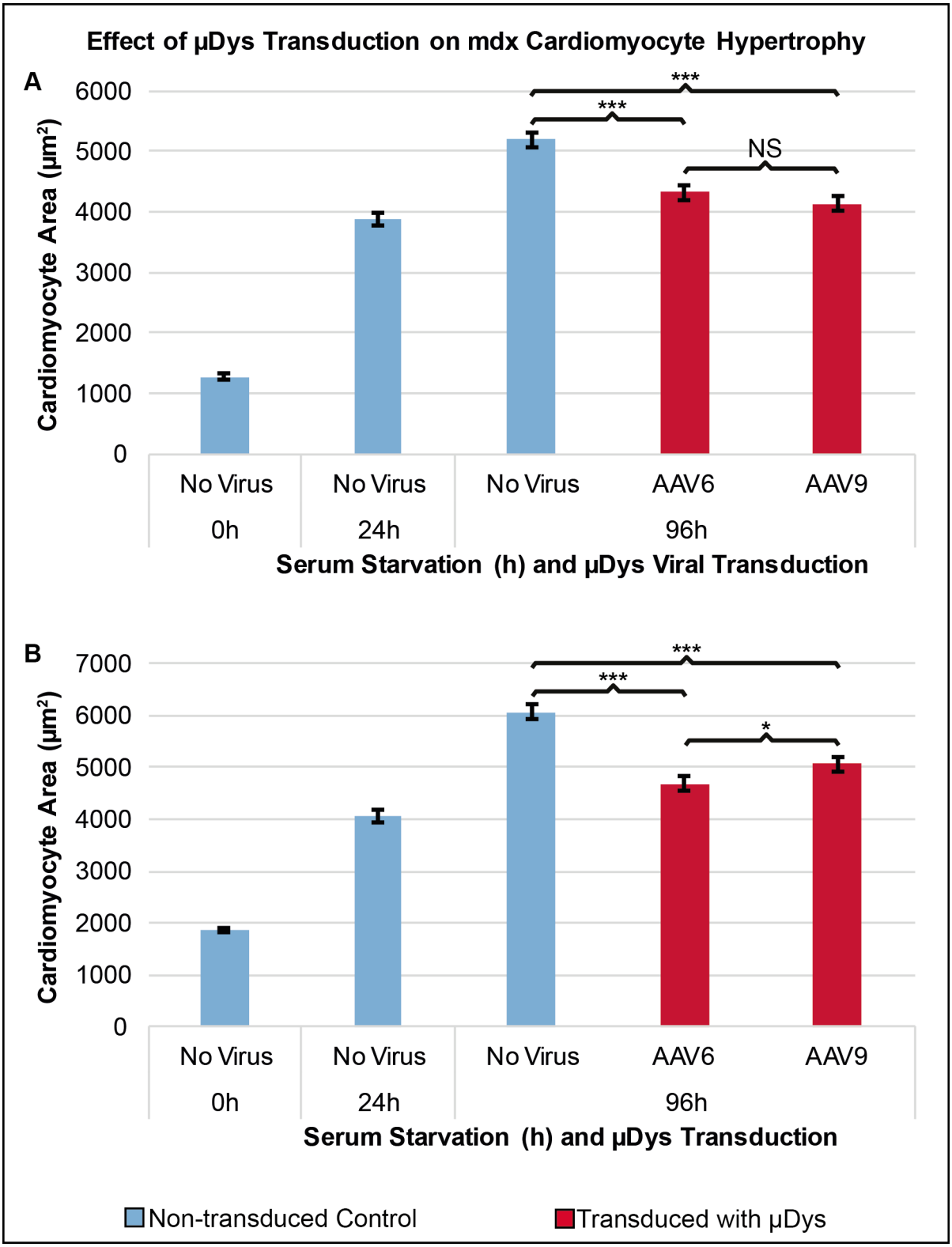
Effect of µDys Transduction on mdx Cardiomyocyte Hypertrophy
A
Cardiomyocyte Area (µm²)
6000
5000
4000
3000
2000
1000
0
***
***
NS
No Virus
0h
No Virus
24h
No Virus
AAV6
AAV9
96h
Serum Starvation (h) and µDys Viral Transduction
B
Cardiomyocyte Area (µm²)
7000
6000
5000
4000
3000
2000
1000
0
***
***
*
No Virus
0h
No Virus
24h
No Virus
AAV6
AAV9
96h
Serum Starvation (h) and µDys Transduction
Non-transduced Control
Transduced with µDys

Figure 5.15. AAV6 and AAV9 μDys transduction reduced mdx cardiomyocyte hypertrophy. Average area measurements of non-treated 0h, 24h and 96h serum starved control cardiomyocytes (blue columns) were compared to cells transduced with AAV6 or AAV9 for μDys delivery (red columns). (A) In the first biological replicate μDys delivered by both AAV serotypes significantly attenuated the serum-induced hypertrophic response in comparison to 96h serum starved non-transduced control cells (*** corresponds to p-value<0.001). AAV9 transduced cardiomyocytes were smaller than AAV6 transduced cells on average, but this difference was non-significant (NS). (B) In the second biological replicate both AAV6 and AAV9-delivered μDys significantly diminished the serum starvation effect on mdx cardiomyocyte area. One-tailed Student's t-test and Levene's test were used for statistical analyses. Error bars represent standard error of the mean.

Comparison A	Levene's Test p-value	Variance	t-test p-value
24h v 96h	6.00257E-14	Unequal	1.5606E-17
24h v AAV6	2.99671E-05	Unequal	0.0019
24h v AAV9	0.001861874	Unequal	0.0573
96h v AAV6	0.001634265	Unequal	1.31011E-07
96h v AAV9	0.000112922	Unequal	5.99851E-10
AAV6 v AAV9	0.385821353	Equal	0.1350
Comparison B	Levene's Test p-value	Variance	t-test p-value
24h v 96h	4.75866E-11	Unequal	3.07159E-26
24h v AAV6	1.25517E-09	Unequal	0.0008
24h v AAV9	9.3752E-10	Unequal	1.44938E-07
96h v AAV6	0.149120859	Equal	1.05186E-10
96h v AAV9	0.895266543	Equal	4.53942E-07
AAV6 v AAV9	0.217540267	Equal	0.0458

Table 5.10. Statistical analyses of AAV6 and AAV9 μDys transduced mdx cardiomyocytes. The first column represents Levene's and Student's t-test comparisons. 24h and 96h represent the non-transduced control samples, AAV6 represents AAV6-CMV-MLC0.26-μDys transduced cardiomyocytes and AAV9 represents AAV9-CMV-MLC0.26-μDys transduced cardiomyocytes. Significant t-test p-values<0.05 are underlined.

5.9 Discussion

Cardiomyocyte size data comparison assessed in chapter 3 (figure 3.14) showed a strong correlation between mdx cardiomyocyte area and volume measurements. Therefore, all but two mdx cardiomyocyte treatment experiments were evaluated by area quantification. Area measurements performed with SSCGM also showed a greater difference between the 24h and 96h serum starvation time-points in comparison to SFCGM-induced hypertrophic response experiments. Therefore, the sensitivity of this model to detect therapeutic rescue of mdx cardiomyocyte hypertrophy was also improved.

The effect of the seven therapies tested for their efficacy in reducing mdx cardiomyocyte hypertrophy is summarised in table 5.11. Out of the three groups of compounds currently prescribed to DMD patients to manage their cardiac pathology corticosteroids prednisolone and dexamethasone showed no direct effect on mdx cardiomyocyte hypertrophy, the β_1AR antagonist metoprolol caused a significant escalation of serum starvation-induced hypertrophy and captopril significantly reduced mdx cardiomyocyte size. NHE inhibitor KR-33028 and P2RX7 inhibitor A804598 showed promising results of their ability to tackle the hypertrophic response and in preliminary studies discussed in sections 5.6 and 5.7, respectively, illustrated that there is potential in further exploration of their efficacy as DMD therapeutic compounds. AAV delivery of μDys significantly reduced mdx cardiomyocyte hypertrophy and therefore shows this model of hypertrophy can be used as an outcome measure in pre-clinical trials of DMD rescue therapies.

Therapy	Type of Compound/Delivery	Effect on hypertrophy
Prednisolone	Corticosteroid	0
Dexamethasone	Corticosteroid	0
Metoprolol	β_1-adrenergic receptor antagonist	↑
Captopril	Angiotensin-converting enzyme inhibitor	↓
KR-33028	Sodium-hydrogen antiporter inhibitor	↓
A804598	P2X7 receptor antagonist	↓
μDys	AAV6 and AAV9 transduction	↓

Table 5.11. Summary of pharmacological compound and rescue therapy trials. Metoprolol significantly increased, corticosteroids had no significant effect and four of the seven trialled therapies significantly reduced cardiomyocyte hypertrophy.

5.9.1 Systemic and Cellular Effect

Although there are many retrospective studies now published on both the beneficial effects and negative side-effects of steroid treatment on DMD patients (Ricotti et al., 2013; Kim et al., 2015), the specific mechanisms delaying the age at which patients become non-ambulant are not well characterised. Furthermore, corticosteroid treatment has been shown not to have a significant effect on delaying the cardiac pathology in DMD when administered independently from cardioprotective medication (Barp et al., 2015). The GCR gene *Nr3c1* was not differentially expressed in the RNA-Seq dataset. While this indicates that receptor gene expression does not affect drug treatment efficacy, it does not account for receptor protein level differences, the baseline presence of competitor compounds for the active site, or receptor nuclear translocation efficiency. Results from prednisolone and dexamethasone treatment of mdx cardiomyocytes undergoing a hypertrophic response to serum starvation suggest that these corticosteroids do not have a direct effect on cardiomyocytes, but may be able to deliver their protective effect via other types of cells, both in skeletal muscle and cardiac tissue, where they have been shown to slow disease progression by anti-inflammatory impact (Falzarano et al., 2015) and a novel glucocorticoid-like compound VBP15 improves membrane strength (Heier et al., 2013). However, the latter effect has not been reported in treatment with other corticosteroids and most anti-inflammatory drugs alone do not rescue DMD pathology, therefore corticosteroids must also protect dystrophic muscle via some other mechanism (Rosenberg et al., 2015).

There are also stark geographical corticosteroid-of-choice differences in clinical care offered to DMD patients. In Germany, Italy and the US deflazacort is most frequently prescribed to patients at all ambulatory stages, while in the UK prednisolone is by far the most prevalent administered corticosteroid (Landfeldt et al., 2015). Dexamethasone was not featured in this publication. Its higher potency for GCR activation and longer *in vivo* half-life (Longui, 2007) may also exacerbate side-effects caused by steroid use in young males, which are now targeted with testosterone treatment trials, but there is still no consensus on whether testosterone treatment is beneficial to DMD patients (Wood et al., 2015). New steroid compounds, such as VBP15, with improved efficacy on GCR translocalisation to the nucleus and subsequent NFκB signal transduction inhibition similar to dexamethasone effectiveness, but with reduced affinity for hormonal signal transduction and

consequent undesirable side-effects are now under investigation and may provide improved DMD disease management alternatives (Reeves et al., 2013; Heier et al., 2013). The mdx cardiomyocyte hypertrophy model could be used to compare treatment with novel steroid-like compounds to currently prescribed corticosteroids, identifying whether they exhibit a direct effect on cardiomyocytes in addition to a system effect.

βAR blockers, such as metoprolol, are prescribed for managing cardiac complications of DMD pathology (Bushby et al., 2010b). Based on RNA-Seq data of mdx and BL/10 cardiomyocytes only the β_1AR gene *Adrb1* was expressed at above negligible levels, but was not identified as a differentially expressed gene in any of the serum starvation or genotype comparisons. In the mdx cardiomyocyte treatment study metoprolol augmented the hypertrophic response to serum starvation. Other studies have shown that stimulation of βARs causes cell apoptosis (Dalal et al., 2012) (Wang et al., 2015) and inhibition of these receptors can have a cardioprotective effect via mitigated apoptotic signalling (Zhao et al., 2014). While the drug may have a protective effect systemically and when administered long-term, it may be that the short-term effect within this model was in fact to inhibit cardiomyocyte apoptosis and allow cells that had outgrown their natural size limitations to keep expanding rather than going through programmed cell death.

Hypertrophy-stimulating tendencies in this metoprolol treatment experiment also supported results from a study where metoprolol and propranolol (a non-selective βAR inhibitor) treatment switched on the foetal gene program in rat ventricular cardiomyocytes (Patrizio et al., 2007). It may be that without the native tissue environment βAR antagonists have a damaging effect on mdx cardiomyocytes. A similar β_1AR protein expression pattern in both BL/10 and mdx serum starved cardiomyocytes, identified by Western blotting (figure 5.8), also supports the hypothesis that βAR signalling was not responsible for the differences identified in cardiomyocyte size between the control and dystrophinopathy mouse models.

ACE inhibitors are commonly prescribed as a combination therapy with βAR to DMD patients (Ogata et al., 2009). However, early combinational βAR and ACE inhibitor treatment *in vivo* has not shown the same beneficial effects in mdx mice (Blain et al., 2015). Cardiac improvement in mdx mice has been shown in a study using losartan, an ACE inhibitor (Spurney et al., 2011). Captopril treatment also showed significant reduction in mdx cardiomyocyte hypertrophy (figure 5.6), but only at the highest dose. The effect of ACE inhibitors is also most likely systemic, as it has been suggested to be mediated through vasorelaxation (Ennen et al., 2013) rather than a direct effect on cardiomyocytes. In RNA-Seq results discussed in the previous chapter, the Ang gene *Agt* expression was significantly upregulated in mdx cardiomyocytes (by 2.8-fold from 0h to 96h of serum starvation). Granted, the nominal transcript levels identified from HT-Seq data did show relatively low expression throughout the serum starvation time-course in both BL/10 and mdx samples, which could mean that the autocrine effect is not large enough to have significant effect on the hypertrophic response. Furthermore, the ACE gene *Ace* was upregulated in both BL/10 and mdx cardiomyocytes in response to serum starvation, which could enhance the autocrine effect of Ang expression from mdx cardiomyocytes. However, the AngII receptor genes *Agtr1b* and *Agtr2* were not expressed at all in most mdx cardiomyocyte samples and *Agtr1a* was expressed at a very low level, based on HTSeq gene count data from RNA-Seq experiments. These results make it difficult to believe that the significant reducing effect of captopril reported in section 5.4 would replicate in future experiments. Expression patterns of *Agt* and *Ace* in E17.5-derived cardiomyocytes may explain why captopril showed a cardiomyocyte cell-level effect in the hypertrophy drug treatment trial experiment, but low receptor gene expression suggests the drug effect may have been artefactual.

P2RX7 and angiotensin receptor type 1 (AT_1R) can both activate ERK and cause a downstream hypertrophic response (Young et al., 2015; Schlüter & Wenzel, 2008). Data in figure 5.8 suggest that there is more phosphorylated ERK in mdx cardiomyocytes from the 48h serum starvation time-point onwards, but these findings also need comparison of p-ERK1/2 to the overall protein level of ERK1/2 to assess activation level more adequately rather than just overall protein content or normalising to a reference protein band. A drawback of Western blotting in this model is also that the total protein content can be affected by levels of the protein of interest in the whole heterogeneous primary cell population, whereas size measurements

were only done on α-actinin positive cells and therefore a homogeneous cardiomyocyte population. However, taking the protein levels at face value, these results on ERK phosphorylation may support the reason why both captopril and A804598 had an attenuating effect on mdx cardiomyocyte hypertrophy. Data on ERK activation alone does not give a conclusive account on the specific downstream signalling pathway that was inhibited by these compounds until drug treated cardiomyocyte protein lysates are compared against non-treated control cells with the appropriate non-activated protein control.

Previously published findings of elevated P2RX7 expression in mdx skeletal muscle (Young et al., 2012) were not confirmed in RNA-Seq analyses of serum starved BL/10 and mdx cardiomyocytes, where the *P2rx7* gene was not differentially expressed. In addition to skeletal and cardiac muscle, P2RX7s are also located on macrophages and mdx/P2RX7 double knockout mice have reduced inflammatory infiltration in skeletal muscle (Sinadinos et al., 2015). Taking into account that the presence of macrophages in the primary mdx cardiomyocyte population in this model is improbable, it is more plausible that the A804598 drug effect on P2RX7 may have been mediated by improved Ca^{2+} homeostasis. In dystrophic skeletal muscle and heart tissue tears in the sarcolemma can cause increased external adenosine triphosphate (ATP), which is able to activate P2RX7 pore formation, resulting in Ca_{2+} influx to myocytes and consequent hypertrophic signalling pathway activation (Yeung et al., 2006). Lack of dystrophin also results in mislocalised dystrophin glycoprotein complex (DGC) members (Matsumura et al., 1992). It has been suggested that dystrophic muscle also has impaired extracellular ATP clearance capacity due to mislocalised DGC member α-sarcoglycan, which is a transmembrane protein with an ectopic ATP hydrolase activity (Berry et al., 2000). Therefore, it is possible that P2RX7 inhibition with A804598 contributed towards improved Ca^{2+} handling in mdx cardiomyocytes, resulting in a diminished hypertrophic response. It will be important to address the discrepancies witnessed in the third biological replicate of A804598 treatment, where SSCGM-treated mdx cardiomyocytes did not respond to the therapeutic compound in the same way as SFCGM-treated cells in the previous two replicates. This may have been caused by a difference in vehicle concentration required to solubilise A804598. Further repeats of therapeutic treatment will be required before concluding that the drug had a hypertrophy-reducing effect on mdx cardiomyocytes.

The role of NHE in DMD cardiac pathology was discussed in detail in the previous chapter (sub-section 4.8.4). NHE inhibitor KR-33028 was expected to have an $[Ca^{2+}]_i$-reducing effect on mdx cardiomyocytes and previous work done on a hamster model of muscular dystrophy supports this hypothesis (Bkaily et al., 2015). The results from a single biological replicate experiment conducted on serum starved mdx cardiomyocytes (figure 5.9) revealed that KR-33028 treatment had a significant effect on the hypertrophic response. However, the corresponding PEG vehicle-only treated sample also showed a significant effect on cardiomyocyte area. It may be necessary to explore alternative vehicles for preparation of the treatment compound stock solution in order to fully explore the potential of the drug in an *in vitro* setting.

5.9.2 AAV μDys Rescue Therapy

It is difficult to package the whole dystrophin gene into viral vectors due to its large size. A wide range of smaller constructs with deletions in the internal rod domain, cysteine-rich domain carboxy- or amino-terminus of the protein have been designed and based on their size named either mini-dystrophins (mDys) or μDys (Scott et al., 2002). It is possible to package μDys constructs into AAV vectors and these have been used in several studies to restore dystrophin expression in animal model and more recently in human clinical trials (Fabb et al., 2002; Yue et al., 2015; Mendell et al., 2010). Engineering viral capsids and testing different AAV serotypes has improved tissue tropism of the proposed therapies (Nance & Duan, 2015).

The skeletal muscle and heart-targeting tissue tropism characteristics of AAV6 and AAV9 have been previously documented (Hastie & Samulski, 2015). In this study a μDys construct, expressed under a muscle-specific CMV promoter with a MLC0.26 enhancer region, was packaged into AAV6 and AAV9 vectors, which were subsequently used to transduce mdx cardiomyocytes undergoing a hypertrophic response to serum starvation. This AAV9 was used in preclinical *in vivo* mdx mouse studies, where it produced long-term μDys expression and arrested disease progression in cardiac tissue (Schinkel et al., 2012). Delivery of μDys with both AAV6 and AAV9 vectors significantly reduced mdx cardiomyocyte hypertrophy (figure 5.15) and expression of the μDys protein product was detected by Western blotting (figure 5.14).

Viral transduction was optimised using eGFP reporter gene delivery with an AAV6 vector, which yielded an 89% transduction efficiency when 100,000 viral genomes per cell were used to deliver the construct of interest to cardiomyocytes. This did not, however, mean that the same transduction efficiency was reached when delivering μDys with the same serotype of AAV, nor was efficiency of eGFP delivery quantified for AAV9 transduction. Identifying an antibody that binds to μDys in ICC experiments will be important to quantify differences between μDys positive and negative cells in the same transduced sample. Alternatively, having eGFP cloned into the same construct as μDys would be an option, but an already challenged capacity of AAV vectors may mean that any further increase in the construct DNA size would result in no successful packaging at all.

5.9.3 Summary

Results reported in this chapter illustrated that serum starvation-induced hypertrophy in mdx cardiomyocytes can be reduced with a range of pharmacological compounds. The significant reduction in hypertrophy in response to μDys delivery with AAV6 and AAV9 demonstrated that this model can be used as an *in vitro* platform for testing rescue therapies.

Chapter 6. General Discussion and Future Directions

6.1 Establishing the Cardiomyocyte Hypertrophy Model

Duchenne Muscular Dystrophy is a severe debilitating childhood-onset disease. Although several therapies are in pre-clinical and early clinical trials, with one approved rescue therapy now conditionally available as a prescription drug for patients with specific mutations (Haas et al., 2015), there is still an urgent need for an effective and more universal therapy for all DMD patients. One hurdle for developing DMD therapies is that the disease affects both skeletal and cardiac muscle, which have subtle differences when it comes to delivering therapies to these tissues. Successful delivery to the whole musculature, including the heart is a challenging task.

This thesis established a dystrophic cardiomyocyte hypertrophy model with potential use as an outcome measure in pre-clinical trials of therapeutic compounds for DMD. Cardiomyocytes isolated from embryos of the DMD mouse model (mdx) became hypertrophic in response to serum starvation. Control BL/10 mouse embryos were also serum starved, but did not show the equivalent size increase. The technique was used to identify potential pathways responsible for the hypertrophy seen in mdx cardiomyocytes by RNA-Seq analysis. Current drug therapies for managing the dystrophic phenotype of DMD patients, along with novel treatment compounds and viral vector-delivered gene therapy were trialled for their efficacy in reducing serum-induced hypertrophy in mdx cardiomyocytes. Results showed that the hypertrophic response can be reversed and therefore indicate the potential for using this model in a pre-clinical setting for discovering and improving potential treatments for DMD.

6.2 Limitations of the Cardiomyocyte Hypertrophy Model and Potential Improvements

The mdx mouse is a widely used model in DMD research and whilst it does not reflect the wide variety of mutations seen in the patient population (Bladen et al., 2015), it is still an irreplaceable tool for conducting research into therapies. For instance, even with the one mutation, mdx mice are useful for testing efficacy of exon skipping compounds with different chemical backbones and conjugates (Gebski et al., 2003; Lu et al., 2003). The dystrophin and utrophin double knockout mouse model (dko) exhibits earlier onset of dystrophic pathology, comparable to the human disease, but does not reflect the genotype of DMD (Deconinck et al., 1997). It would be an option to investigate whether the hypertrophic response is more pronounced in dko mice, further improving the sensitivity of assaying cell size.

Therapeutic testing was standardised to only measuring the effect of treatments at the 96h serum starvation end-point. There may be variability in compound effect time and function in terms of their ability to either arrest the hypertrophic response from the time of reaching peak effect or reverse the size increase process to reduction back to baseline. This effect could be monitored by extending the observed time-course and analysing intermediate time-points once an optimal concentration of the therapeutic compound of interest has been determined. Furthermore, the long-term effect of compounds remains unknown in the current setting. It has been shown that long-term steroid treatment causes fibrosis and cardiomyopathy in mdx mouse hearts (Bauer et al., 2009; Sali et al., 2012). The short investigated time-frame when testing steroid treatment on mdx cardiomyocytes does not reveal these effects, nor does it mimic the compounds' systemic contributions *in vivo*.

The presence of other cell types in addition to cardiomyocytes may have been responsible for the effect of systemic-effect therapeutic compounds on mdx cell samples. Contaminating cell number variability between batches could also affect results obtained when testing such compounds. However, removing the contaminating population through cell sorting could also limit the model's applications for therapeutic testing. In addition to the temporal and systemic effect limitations of the model, biological variability between batches of cardiomyocytes as a result of pooling hearts of embryos may also affect data replication, as observed when establishing the model and also when testing some of the therapeutic compounds.

AAV therapy follow-up is important also to investigate safety of the drug in terms of the insertion site, expression length and immunogenicity (Mendell et al., 2012; Nance & Duan, 2015). Clinical relevance of the hypertrophy model is compromised due to the viral delivery mechanism being simplified in culture, as opposed to living organisms where cardiomyocytes are less accessible. When moving from *in vitro* studies onwards it will still be necessary to conduct pre-clinical *in vivo* animal model testing.

Combination therapies are now starting to emerge in DMD research. Recently it was shown that ibuprofen as an anti-inflammatory drug administered with nitric oxide donor isosorbide dinitrate can markedly improve dystrophic pathology of mdx hearts (Sciorati et al., 2013). Using the mdx cardiomyocyte hypertrophy model in a high-throughput screening method could accelerate the process of identifying potential composite effects ahead of *in vivo* studies. For this to be achieved a streamlined and robust method for scaling up the cardiomyocyte extraction technique would be required, preferably with minimised variability arising from biological replicates.
To ensure direct effect of therapeutic compounds only on cardiomyocytes, it would be important to purify the primary cell population by FACS. However, cardiomyocytes from mdx mice may be dependent on and also susceptible to hypertrophic factors derived from fibroblasts and other cell types in the heterogeneous primary cell culture population (Kamo et al., 2015). Therefore, the model may in fact be more valuable for investigating mechanisms of dystrophy and testing therapies in the low presence of other cells of cardiac origin as it provides a cell population enriched for cardiomyocytes, but not entirely depleted cells potentially acting as contributors to therapeutic effect. For these reasons further purification of the primary cell population may lead to undesirable outcomes in the future functions this *in vitro* model of hypertrophy may have.

Despite the benefits of mixed cardiac cell type presence, it may be necessary to validate some key signalling gene and protein expression patterns in a purified cardiomyocyte population and to attempt replicating mdx cardiomyocyte hypertrophy in a homogeneous population before optimising this model in DMD patient cardiomyocytes derived from induced pluripotent stem cells (iPSC). The serum starvation-induced hypertrophic response may not replicate in iPSC-derived cardiomyocytes because of the epigenetic origin of reprogrammed cells as well as

variance in mechanical and current conductance properties (Lee et al., 2014; Dixit & Katare, 2015).

Interestingly, it was recently reported that the Diablo-Xiap-Caspase 3 axis of mitochondrial-mediated apoptosis signalling cascade genes were upregulated in DMD patient iPSC-derived cardiomyocytes in comparison to healthy patient iPSC-derived cells (Lin et al., 2015). While none of these specific genes were differentially expressed in the cardiomyocyte hypertrophy model RNA-Seq data, other trends of gene expression followed similar patterns in response to serum starvation. The authors stated that the purity of cardiomyocytes in their transcriptome studies was 75%, which suggests that their dataset should bear similarities to the data discussed in chapter 4 of this thesis, in terms of gene regulation. However, the non-cardiomyocytes in the iPSC population may not share the same origins or functions as the ones in primary mdx cardiomyocyte culture. Despite these complications that will need to be addressed, DMD iPSC-derived cardiomyocytes can also improve testing therapies *in vitro* by providing cells with a range of patient mutations. For instance, exon skipping compounds could be tested in cells that have the exact reading frame disruptions these drugs were designed to rescue. As further standardised reprogramming techniques into various types of heart cells become available (Xin et al., 2013), options for investigating pathways involved in DMD disease mechanisms and treatment methods on specific cardiac cell types in a dystrophic setting may provide novel treatment targets and methods.

6.3 RNA-Seq Data Interpretation and Validation

Based on the discrepancies recorded in the RNA-Seq dataset validation experiments with qRT-PCR, it will be useful to mine the transcriptome data for identifying most relevant housekeeping genes within this model, analysing the dataset in a way to find genes with the lowest fluctuation in expression level across all the compared time-points and genotype (Zeng et al., 2015). This may improve normalisation of gene expression to the most relevant housekeeping genes and therefore provide a more accurate gene-by-gene validation with the ΔΔCt method.

The sequencing platform used to obtain RNA-Seq data did not allow identifying differential expression of miRNA. It is possible to perform this investigation with miRNA microarrays (Yang et al., 2015). However, RNA-Seq was chosen for cardiomyocyte transcriptome studies because it has superior sensitivity for both differential gene expression and alternative splicing detection (Li et al., 2015; Zhao et al., 2014). As a future analysis option the mixture of isoforms (MISO) (Katz et al., 2010) or hierarchical indexing for spliced alignment of transcripts (HISAT) (Kim et al., 2015) analysis packages can provide more robust data on potential alternative splicing events from RNA-Seq data to assess genotype and serum starvation effects in the cardiomyocyte hypertrophy model.

Gene expression analysis with DeSeq2 identified differential expression of several foetal gene program (FGP) markers (sub-section 4.8.2). The observed trends showed that the embryonic origin of analysed cardiomyocytes did not mask the FGP expression trends identified in adult hypertrophic hearts. Despite *Nfatc4* being the only differentially expressed FGP transcription factor, these results provide evidence for the strength of the mdx cardiomyocyte serum starvation technique for modelling dystrophic hypertrophy in the heart.

Several genes discussed in this thesis express proteins that need to be further processed in order to perform their function in the cardiac environment. Recent developments in proteomics have provided information about transcriptome-to-proteome correlation in a range of tissues, allowing translation of gene regulation data to corresponding effect on protein expression (Nesvizhskii, 2014; Wilhelm et al., 2014). Furthermore, it is now also possible to identify protein activation and degradation profiles in given samples by phosphoproteomics (Humphrey et al., 2015)

and ubiquitination proteomics (Beaudette et al., 2015). Much like MISO and HISAT have added new functionality to transcriptome sequencing, these innovative proteomics techniques may provide invaluable insight to the hypertrophic pathways altered in mdx cardiomyocytes.

6.4 Future Directions

In the short run, it will be important to provide further evidence that in addition to introducing μDys with AAV vectors, a second rescue therapy already proven to be efficacious in pre-clinical DMD studies can also reduce serum starvation-induced mdx cardiomyocyte hypertrophy in this model. For instance, either the 2OMePS or PMO antisense oligonucleotides could be trialled for their impact on cardiomyocyte size.

Developments in computing power along with the arrival of next generation sequencing and new proteomics technologies have paved the way for developing new methods for analysing disease mechanisms in previously unimaginable high-throughput capacity. Performing alternative splicing and protein activation analyses on serum starved cardiomyocyte transcriptome and proteome data, respectively, may elucidate novel therapeutic targets for DMD therapy in the medium-term.

In order to develop this model into a drug screening tool, it will be important to streamline the mouse breeding and cardiomyocyte isolation processes to provide faster data replication. Alternatively, to reduce biological replicate variability arising from differences in mouse litters, a standardised protocol for iPSC-derived cardiomyocyte production could provide a multi-faceted approach with improved cell availability and several human mutation models for identifying treatments with higher efficacy for patients with specific *DMD* gene mutations.

Promising results presented in this thesis on inhibiting hypertrophy in mdx cardiomyocytes with P2RX7 and NHE antagonist compounds have provided evidence for justification of further studies into these potential therapeutic compounds. In the long run, it is therefore envisioned that this cardiomyocyte hypertrophy model may provide stepping stones for a range of therapies to be taken into further pre-clinical and clinical trials to ultimately provide a cure for DMD.

Appendix 1. Differential Gene Expression Data

DeSeq2 was used to determine differentially expressed genes from RNA-Seq data. The results are presented in fold change (FC) and base 2 logarithm fold change (Log_2FC), summarised in a table format. Expression comparisons were performed between BL/10 (B) and mdx (m) samples across the serum starvation time-course (0, 24, 48, 72, 96h) and a multi-factor analysis of genotype differences across the serum starvation time-points (Bm2D). Significant differentially expressed genes (Benjamini-Hochberg adjusted p-value<0.01, Log_2FC +/-0.6) are highlighted on a red background.

Gene/FC	Bm	Bm2D	B0m0	B24m24	B48m48	B72m72	B96m96	B0B24	B0B48	B0B72	B0B96	B24B48	B24B72	B24B96
Ace														
Log_2 FC	0.186	0.372	0.259	0.887	0.085	0.277	0.413	0.792	2.300	2.173	2.147	1.201	1.163	1.120
FC	1.138	1.294	1.196	1.849	1.060	1.211	1.332	1.732	4.924	4.511	4.429	2.299	2.240	2.174
Acta1														
Log_2 FC	-0.065	-0.090	-0.351	0.150	-0.699	-0.209	0.820	0.052	0.175	-2.043	-4.424	0.113	-2.088	-3.517
FC	-1.046	-1.064	-1.276	1.109	-1.623	-1.156	1.766	1.036	1.129	-4.120	-21.466	1.081	-4.252	-11.449
Actc1														
Log_2 FC	-0.046	0.023	-0.220	-0.055	-0.391	0.338	0.648	-0.179	-0.306	-1.514	-1.726	-0.115	-1.327	-1.549
FC	-1.033	1.016	-1.165	-1.039	-1.311	1.264	1.567	-1.132	-1.236	-2.856	-3.309	-1.083	-2.510	-2.927
Agt														
Log_2 FC	0.267	0.376	0.077	-0.083	0.384	0.159	0.717	0.159	0.630	1.148	0.616	0.194	0.654	0.222
FC	1.204	1.298	1.054	-1.059	1.305	1.117	1.644	1.116	1.548	2.217	1.533	1.144	1.574	1.166
Angptl4														
Log_2 FC	-0.008	-0.083	0.022	0.111	0.105	-0.242	-0.412	-2.902	-3.650	-1.810	-3.032	-0.455	0.375	-0.008
FC	-1.005	-1.059	1.016	1.080	1.075	-1.183	-1.331	-7.472	-12.552	-3.505	-8.181	-1.371	1.297	-1.006
Atp2a2														
Log_2 FC	-0.153	-0.182	-0.063	0.148	-0.213	-0.389	-0.301	-0.794	-0.848	-0.444	-0.094	-0.039	0.383	0.737
FC	-1.112	-1.135	-1.045	1.108	-1.159	-1.309	-1.232	-1.734	-1.800	-1.361	-1.068	-1.027	1.304	1.667
Atp2b4														
Log_2 FC	0.255	0.280	0.110	0.096	0.169	0.278	0.658	0.556	0.501	0.179	-0.118	-0.099	-0.468	-0.788
FC	1.193	1.214	1.079	1.069	1.124	1.213	1.578	1.470	1.415	1.132	-1.085	-1.071	-1.383	-1.726
Bgn														
Log_2 FC	0.237	0.337	0.144	0.349	0.413	0.269	0.371	0.744	1.360	1.654	1.684	0.591	0.874	0.891
FC	1.178	1.263	1.105	1.274	1.332	1.205	1.294	1.675	2.567	3.148	3.213	1.506	1.833	1.854
Bhlhe40														
Log_2 FC	0.223	0.301	-0.031	0.378	-0.007	0.601	1.238	-0.154	-0.119	-1.476	-1.674	-0.019	-1.328	-1.536
FC	1.167	1.232	-1.022	1.299	-1.005	1.517	2.358	-1.113	-1.086	-2.781	-3.190	-1.013	-2.511	-2.900
Bnip3														
Log_2 FC	0.169	0.233	0.026	0.202	-0.261	0.250	2.270	0.289	0.664	-0.274	-2.241	0.357	-0.591	-2.564
FC	1.124	1.175	1.018	1.150	-1.198	1.189	4.823	1.222	1.584	-1.209	-4.727	1.281	-1.506	-5.914

Gene/FC	B48B72	B48B96	B72B96	m0m24	m0m48	m0m72	m0m96	m24m48	m24m72	m24m96	m48m72	m48m96	m72m96
Ace													
Log $_2$ FC	-0.243	-0.329	-0.054	1.345	1.430	1.333	1.604	0.425	0.399	0.439	-0.019	-0.024	0.003
FC	-1.184	-1.256	-1.038	2.540	2.694	2.519	3.040	1.343	1.318	1.356	-1.013	-1.017	1.002
Acta1													
Log $_2$ FC	-2.060	-4.394	-1.616	0.611	-0.298	-1.863	-1.783	-0.924	-2.399	-1.719	-1.144	-0.796	-0.232
FC	-4.169	-21.020	-3.065	1.527	-1.230	-3.639	-3.442	-1.897	-5.276	-3.292	-2.210	-1.736	-1.174
Actc1													
Log $_2$ FC	-1.139	-1.379	-0.192	0.008	-0.536	-0.850	-0.822	-0.520	-0.830	-0.822	-0.248	-0.237	0.050
FC	-2.202	-2.601	-1.143	1.006	-1.450	-1.803	-1.768	-1.434	-1.778	-1.768	-1.187	-1.178	1.035
Agt													
Log $_2$ FC	0.212	-0.178	-0.187	-0.115	1.481	1.270	1.474	1.150	1.161	1.271	-0.093	-0.085	0.030
FC	1.158	-1.132	-1.139	-1.083	2.792	2.411	2.777	2.219	2.236	2.414	-1.067	-1.061	1.021
Angptl4													
Log $_2$ FC	0.800	0.550	-0.198	-2.853	-3.691	-2.900	-3.794	-0.528	-0.102	-0.629	0.304	-0.031	-0.347
FC	1.741	1.464	-1.147	-7.224	-12.916	-7.463	-13.874	-1.442	-1.073	-1.546	1.234	-1.021	-1.272
Atp2a2													
Log $_2$ FC	0.417	0.772	0.304	-0.606	-1.038	-0.793	-0.332	-0.427	-0.204	0.245	0.185	0.607	0.376
FC	1.335	1.707	1.235	-1.522	-2.054	-1.733	-1.259	-1.344	-1.152	1.185	1.137	1.523	1.298
Atp2b4													
Log $_2$ FC	-0.318	-0.634	-0.216	0.630	0.654	0.389	0.462	-0.016	-0.256	-0.213	-0.182	-0.167	0.041
FC	-1.247	-1.552	-1.161	1.548	1.573	1.310	1.377	-1.011	-1.194	-1.159	-1.134	-1.123	1.029
Bgn													
Log $_2$ FC	0.244	0.263	0.021	0.574	1.292	1.524	1.525	0.695	0.726	0.855	0.028	0.101	0.066
FC	1.184	1.200	1.014	1.489	2.449	2.876	2.877	1.619	1.653	1.809	1.020	1.073	1.047
Bhlhe40													
Log $_2$ FC	-0.520	-0.751	-0.160	0.284	-0.203	-0.614	-0.374	-0.449	-0.812	-0.658	-0.279	-0.133	0.207
FC	-1.434	-1.684	-1.117	1.217	-1.151	-1.531	-1.296	-1.365	-1.756	-1.578	-1.213	-1.097	1.155
Bnip3													
Log $_2$ FC	-0.927	-2.868	-1.710	0.514	0.356	-0.002	0.206	-0.148	-0.504	-0.295	-0.277	-0.120	0.164
FC	-1.902	-7.303	-3.271	1.428	1.280	-1.001	1.153	-1.108	-1.418	-1.227	-1.212	-1.087	1.120

Gene/FC	Bm	Bm2D	B0m0	B24m24	B48m48	B72m72	B96m96	B0B24	B0B48	B0B72	B0B96	B24B48	B24B72	B24B96
Cacna1d														
Log $_2$ FC	-0.366	-0.401	0.083	-0.071	-0.058	-0.473	-1.086	0.271	0.507	1.504	2.675	0.063	0.777	1.763
FC	-1.289	-1.321	1.060	-1.051	-1.041	-1.388	-2.123	1.206	1.421	2.836	6.385	1.044	1.713	3.395
Casq1														
Log $_2$ FC	-0.066	-0.039	-0.158	-0.134	-0.082	-0.193	0.456	-0.044	-0.171	-0.810	-1.923	-0.116	-0.762	-1.542
FC	-1.046	-1.027	-1.116	-1.097	-1.058	-1.143	1.371	-1.031	-1.126	-1.753	-3.792	-1.084	-1.696	-2.913
Ccnb1														
Log $_2$ FC	0.419	0.545	0.442	0.069	0.514	0.616	0.843	0.227	-0.531	-1.051	-1.099	-0.640	-1.242	-1.298
FC	1.337	1.459	1.358	1.049	1.428	1.533	1.794	1.171	-1.445	-2.072	-2.143	-1.559	-2.366	-2.459
Ckm														
Log $_2$ FC	-0.239	-0.382	-0.543	-0.193	-0.414	-0.379	-0.250	-0.501	-0.901	-1.703	-1.925	-0.380	-1.180	-1.403
FC	-1.180	-1.303	-1.457	-1.143	-1.332	-1.300	-1.189	-1.416	-1.867	-3.257	-3.796	-1.302	-2.266	-2.645
Clic5														
Log $_2$ FC	0.193	0.224	-0.009	0.560	-0.223	0.353	1.736	0.295	1.035	-0.273	-1.126	0.686	-0.589	-1.451
FC	1.143	1.168	-1.006	1.475	-1.167	1.277	3.331	1.227	2.049	-1.208	-2.183	1.609	-1.504	-2.733
Cpt1b														
Log $_2$ FC	-0.199	-0.239	-0.541	0.206	-0.299	-0.020	-0.232	-1.485	-1.835	-1.871	-1.739	-0.193	-0.192	-0.040
FC	-1.148	-1.180	-1.455	1.153	-1.230	-1.014	-1.175	-2.799	-3.568	-3.658	-3.338	-1.143	-1.143	-1.028
Dcn														
Log $_2$ FC	0.118	0.117	-0.049	-0.028	0.293	0.255	0.078	0.519	0.777	0.790	0.875	0.223	0.197	0.441
FC	1.085	1.084	-1.035	-1.020	1.225	1.193	1.055	1.433	1.714	1.729	1.834	1.167	1.146	1.358
Dmd														
Log $_2$ FC	-1.075	-1.085	-1.107	-1.042	-1.450	-1.125	-0.508	0.047	0.265	-0.370	-0.758	0.206	-0.422	-0.814
FC	-2.107	-2.121	-2.154	-2.059	-2.732	-2.181	-1.422	1.033	1.202	-1.292	-1.691	1.154	-1.340	-1.759
Egln3														
Log $_2$ FC	0.293	0.342	0.016	1.070	-0.095	1.251	1.472	-0.563	0.298	-2.110	-3.299	0.345	-0.965	-2.640
FC	1.225	1.267	1.011	2.099	-1.068	2.380	2.775	-1.477	1.230	-4.317	-9.845	1.270	-1.953	-6.232
Eno1														
Log $_2$ FC	0.256	0.345	-0.183	0.469	-0.011	0.839	1.182	-0.754	-0.479	-1.354	-2.041	0.297	-0.521	-1.201
FC	1.194	1.270	-1.135	1.385	-1.008	1.789	2.269	-1.686	-1.394	-2.556	-4.116	1.228	-1.435	-2.299

Gene/FC	B48B72	B48B96	B72B96	m0m24	m0m48	m0m72	m0m96	m24m48	m24m72	m24m96	m48m72	m48m96	m72m96
Cacna1d													
Log $_2$ FC	0.487	1.362	0.418	0.026	0.183	0.426	0.772	0.096	0.320	0.560	0.084	0.248	0.155
FC	1.402	2.570	1.336	1.018	1.135	1.343	1.707	1.069	1.248	1.474	1.060	1.187	1.113
Casq1													
Log $_2$ FC	-0.606	-1.687	-0.939	0.004	-0.060	-0.807	-1.249	-0.073	-0.791	-1.198	-0.629	-1.017	-0.346
FC	-1.522	-3.219	-1.917	1.003	-1.043	-1.750	-2.376	-1.052	-1.731	-2.295	-1.546	-2.024	-1.271
Ccnb1													
Log $_2$ FC	-0.392	-0.466	-0.033	-0.190	-0.377	-0.773	-0.626	-0.167	-0.536	-0.395	-0.287	-0.194	0.105
FC	-1.312	-1.381	-1.023	-1.141	-1.298	-1.709	-1.543	-1.123	-1.450	-1.315	-1.220	-1.144	1.076
Ckm													
Log $_2$ FC	-0.717	-0.947	-0.176	-0.074	-0.817	-1.473	-1.352	-0.675	-1.352	-1.325	-0.455	-0.327	-0.049
FC	-1.644	-1.928	-1.129	-1.052	-1.762	-2.776	-2.552	-1.596	-2.552	-2.505	-1.370	-1.255	-1.035
Clic5													
Log $_2$ FC	-1.294	-2.179	-0.773	0.941	0.333	0.192	0.720	-0.282	-0.658	-0.224	-0.078	0.130	0.373
FC	-2.452	-4.529	-1.709	1.919	1.260	1.142	1.647	-1.216	-1.578	-1.168	-1.056	1.094	1.295
Cpt1b													
Log $_2$ FC	0.050	0.210	0.104	-0.673	-1.762	-1.237	-1.335	-0.843	-0.466	-0.537	0.345	0.336	-0.050
FC	1.035	1.157	1.075	-1.594	-3.392	-2.357	-2.522	-1.793	-1.381	-1.451	1.270	1.262	-1.035
Dcn													
Log $_2$ FC	-0.036	0.307	0.285	0.672	1.344	1.204	1.385	0.587	0.486	0.636	-0.106	0.003	0.121
FC	-1.026	1.237	1.219	1.593	2.538	2.304	2.612	1.502	1.400	1.554	-1.076	1.002	1.088
Dmd													
Log $_2$ FC	-0.616	-1.005	-0.343	0.211	-0.353	-0.304	-0.013	-0.521	-0.514	-0.240	0.050	0.299	0.265
FC	-1.532	-2.006	-1.268	1.157	-1.278	-1.235	-1.009	-1.435	-1.428	-1.181	1.035	1.231	1.202
Egln3													
Log $_2$ FC	-0.961	-3.316	-0.718	0.576	-0.006	-0.554	0.281	-0.364	-1.094	-0.104	-0.368	0.120	0.326
FC	-1.946	-9.962	-1.645	1.490	-1.004	-1.468	1.215	-1.287	-2.135	-1.075	-1.290	1.087	1.254
Eno1													
Log $_2$ FC	-0.815	-1.502	-0.567	-0.078	-0.267	-0.042	-0.603	-0.176	0.024	-0.510	0.147	-0.242	-0.387
FC	-1.760	-2.832	-1.481	-1.056	-1.203	-1.029	-1.518	-1.130	1.017	-1.424	1.107	-1.183	-1.308

Gene/FC	Bm	Bm2D	B0m0	B24m24	B48m48	B72m72	B96m96	B0B24	B0B48	B0B72	B0B96	B24B48	B24B72	B24B96
Erdr1														
Log $_2$ FC	-3.349	-4.492	-3.847	-3.542	-2.710	-3.747	-4.200	-1.065	-1.299	-1.580	-1.556	-0.176	-0.396	-0.377
FC	-10.189	-22.505	-14.386	-11.645	-6.545	-13.422	-18.376	-2.092	-2.461	-2.990	-2.940	-1.129	-1.316	-1.299
Fmod														
Log $_2$ FC	0.059	0.255	0.179	0.190	0.435	0.128	0.146	0.287	1.563	3.606	4.339	0.811	2.947	2.596
FC	1.042	1.194	1.132	1.141	1.352	1.093	1.106	1.220	2.956	12.180	20.241	1.755	7.714	6.048
Furin														
Log $_2$ FC	0.010	0.059	-0.258	-0.419	0.076	0.543	0.409	0.518	-0.121	-0.676	-0.894	-0.616	-1.227	-1.463
FC	1.007	1.041	-1.196	-1.337	1.054	1.457	1.327	1.432	-1.087	-1.597	-1.858	-1.532	-2.340	-2.757
Gys1														
Log $_2$ FC	0.142	0.210	-0.106	0.417	-0.288	0.261	1.735	-0.082	0.112	-0.850	-2.285	0.090	-0.753	-2.180
FC	1.103	1.157	-1.076	1.335	-1.221	1.198	3.328	-1.059	1.081	-1.803	-4.874	1.064	-1.685	-4.531
Hgf														
Log $_2$ FC	0.044	0.052	-0.099	0.128	-0.161	0.044	0.439	0.235	0.963	1.078	0.376	0.403	0.599	-0.018
FC	1.031	1.037	-1.071	1.093	-1.118	1.031	1.356	1.177	1.950	2.111	1.297	1.322	1.514	-1.012
Hif1a														
Log $_2$ FC	-0.067	-0.029	0.245	-0.089	0.094	0.098	-0.500	-0.092	0.074	0.205	1.172	0.161	0.299	1.263
FC	-1.048	-1.021	1.185	-1.064	1.068	1.070	-1.414	-1.066	1.052	1.153	2.253	1.118	1.230	2.400
Hk1														
Log $_2$ FC	0.047	0.085	-0.302	0.298	-0.267	0.381	0.501	-0.599	-0.519	-1.225	-1.182	0.071	-0.586	-0.552
FC	1.033	1.061	-1.232	1.230	-1.204	1.302	1.415	-1.515	-1.433	-2.337	-2.270	1.050	-1.501	-1.466
Hk2														
Log $_2$ FC	0.139	0.296	-0.116	0.299	-0.233	1.155	1.764	-0.370	-0.443	-2.610	-2.657	-0.062	-2.214	-2.273
FC	1.101	1.227	-1.084	1.230	-1.175	2.227	3.396	-1.293	-1.359	-6.104	-6.307	-1.044	-4.639	-4.833
Kdr														
Log $_2$ FC	0.028	0.077	-0.031	0.178	0.031	0.294	-0.123	-0.069	-0.777	-2.284	-2.895	-0.512	-2.002	-2.629
FC	1.019	1.055	-1.021	1.131	1.022	1.226	-1.089	-1.049	-1.713	-4.871	-7.438	-1.426	-4.006	-6.184
Lum														
Log $_2$ FC	0.254	0.540	0.544	0.362	0.711	0.375	0.386	1.009	1.876	2.652	2.556	0.666	1.423	0.962
FC	1.193	1.454	1.458	1.285	1.637	1.297	1.307	2.012	3.671	6.283	5.880	1.587	2.682	1.948

Gene/FC	B48B72	B48B96	B72B96	m0m24	m0m48	m0m72	m0m96	m24m48	m24m72	m24m96	m48m72	m48m96	m72m96
Erdr1													
Log $_2$ FC	-0.150	-0.143	0.014	-0.183	-0.322	-0.288	-0.300	NA	0.081	0.087	0.030	0.042	0.006
FC	-1.110	-1.104	1.010	-1.135	-1.250	-1.221	-1.231	NA	1.058	1.062	1.021	1.030	1.004
Fmod													
Log $_2$ FC	1.565	2.259	0.208	0.242	1.148	3.093	2.878	0.661	2.542	2.337	0.293	0.556	0.548
FC	2.958	4.787	1.155	1.182	2.217	8.535	7.349	1.581	5.824	5.054	1.225	1.470	1.462
Furin													
Log $_2$ FC	-0.521	-0.758	-0.192	0.380	0.286	0.312	-0.151	-0.103	-0.052	-0.511	0.038	-0.354	-0.325
FC	-1.435	-1.691	-1.143	1.302	1.219	1.242	-1.111	-1.074	-1.037	-1.425	1.026	-1.278	-1.253
Gys1													
Log $_2$ FC	-0.847	-2.216	-1.229	0.504	-0.168	-0.419	-0.282	-0.606	-0.913	-0.761	-0.178	-0.084	0.110
FC	-1.799	-4.646	-2.343	1.418	-1.123	-1.337	-1.216	-1.522	-1.882	-1.695	-1.132	-1.060	1.079
Hgf													
Log $_2$ FC	-0.034	-0.636	-0.321	0.674	1.078	1.535	1.348	0.142	0.489	0.256	0.195	0.052	-0.175
FC	-1.024	-1.554	-1.249	1.596	2.111	2.897	2.546	1.104	1.404	1.194	1.144	1.036	-1.129
Hif1a													
Log $_2$ FC	0.128	1.061	0.806	-0.446	-0.056	0.065	0.383	0.375	0.505	0.812	0.113	0.402	0.279
FC	1.093	2.087	1.748	-1.362	-1.039	1.046	1.304	1.297	1.420	1.756	1.081	1.321	1.213
Hk1													
Log $_2$ FC	-0.605	-0.594	0.039	0.028	-0.553	-0.421	-0.292	-0.550	-0.433	-0.313	0.105	0.215	0.101
FC	-1.521	-1.509	1.028	1.019	-1.467	-1.339	-1.224	-1.464	-1.350	-1.242	1.075	1.160	1.072
Hk2													
Log $_2$ FC	-1.997	-2.133	0.010	0.064	-0.617	-0.909	-0.678	-0.604	-0.899	-0.731	-0.186	-0.015	0.212
FC	-3.990	-4.386	1.007	1.046	-1.533	-1.878	-1.600	-1.520	-1.865	-1.660	-1.138	-1.010	1.159
Kdr													
Log $_2$ FC	-1.190	-1.782	-0.197	0.104	-0.756	-1.925	-3.238	-0.753	-1.899	-3.008	-0.710	-1.562	-0.716
FC	-2.281	-3.438	-1.147	1.074	-1.688	-3.796	-9.434	-1.685	-3.730	-8.045	-1.636	-2.952	-1.642
Lum													
Log $_2$ FC	0.629	0.572	-0.012	0.411	1.425	2.029	1.829	1.162	1.365	1.515	0.046	0.183	0.142
FC	1.547	1.487	-1.009	1.329	2.685	4.081	3.552	2.237	2.575	2.858	1.032	1.135	1.103

Gene/FC	Bm	Bm2D	B0m0	B24m24	B48m48	B72m72	B96m96	B0B24	B0B48	B0B72	B0B96	B24B48	B24B72	B24B96
Mmp2														
Log $_2$ FC	0.052	0.078	-0.058	0.253	0.215	0.088	-0.117	0.380	0.849	1.017	1.542	0.435	0.608	1.119
FC	1.037	1.055	-1.041	1.191	1.161	1.063	-1.084	1.301	1.801	2.023	2.911	1.352	1.524	2.171
Mmp8														
Log $_2$ FC	0.044	0.060	0.273	-0.183	0.036	-0.037	0.188	0.195	-0.429	-0.773	-1.689	-0.434	-0.915	-1.777
FC	1.031	1.042	1.209	-1.135	1.025	-1.026	1.139	1.144	-1.347	-1.709	-3.224	-1.351	-1.886	-3.428
Myh6														
Log $_2$ FC	-0.172	-0.209	-0.342	-0.006	-0.179	-0.117	-0.312	-0.286	-0.603	-0.994	-0.887	-0.297	-0.695	-0.598
FC	-1.127	-1.156	-1.267	-1.004	-1.132	-1.084	-1.241	-1.220	-1.518	-1.992	-1.849	-1.229	-1.619	-1.514
Myh7														
Log $_2$ FC	0.021	0.040	0.029	0.093	-0.338	-0.199	0.878	0.395	1.302	0.978	0.250	0.517	0.551	-0.152
FC	1.015	1.028	1.021	1.067	-1.264	-1.148	1.837	1.315	2.466	1.970	1.189	1.431	1.465	-1.111
Ndufa4l2														
Log $_2$ FC	0.383	0.397	0.008	0.457	0.001	0.728	2.276	0.317	0.954	0.232	-1.587	0.503	-0.124	-1.882
FC	1.304	1.316	1.006	1.373	1.001	1.657	4.844	1.246	1.937	1.175	-3.004	1.417	-1.090	-3.687
Nfatc4														
Log $_2$ FC	0.419	0.524	0.384	0.173	0.178	0.566	0.775	0.985	1.321	1.264	1.187	0.127	-0.076	-0.185
FC	1.337	1.438	1.305	1.128	1.132	1.480	1.711	1.980	2.499	2.402	2.277	1.092	-1.054	-1.137
Nfkbia														
Log $_2$ FC	0.081	0.138	-0.074	-0.153	0.121	0.638	0.161	-0.047	-0.702	-1.276	-1.170	-0.534	-1.164	-1.090
FC	1.058	1.100	-1.052	-1.112	1.088	1.556	1.118	-1.033	-1.627	-2.422	-2.250	-1.448	-2.241	-2.129
Nos3														
Log $_2$ FC	0.200	0.390	-0.106	0.297	0.239	0.498	0.648	-0.225	-0.515	-1.118	-2.682	-0.176	-0.733	-2.023
FC	1.148	1.310	-1.076	1.228	1.181	1.413	1.567	-1.169	-1.429	-2.171	-6.419	-1.130	-1.662	-4.066
Nppa														
Log $_2$ FC	0.033	0.013	-0.217	-0.056	0.123	-0.038	0.271	0.240	0.565	0.522	0.268	0.318	0.269	0.005
FC	1.023	1.009	-1.163	-1.039	1.089	-1.027	1.207	1.181	1.480	1.436	1.204	1.246	1.205	1.003
Nppb														
Log $_2$ FC	0.122	0.238	-0.153	0.383	0.032	0.609	2.999	-0.459	-0.489	-5.068	-4.182	-0.136	-4.511	-3.661
FC	1.088	1.180	-1.112	1.304	1.023	1.525	7.994	-1.375	-1.404	-33.552	-18.153	-1.099	-22.797	-12.652

Gene/FC	B48B72	B48B96	B72B96	m0m24	m0m48	m0m72	m0m96	m24m48	m24m72	m24m96	m48m72	m48m96	m72m96
Mmp2													
Log $_2$ FC	0.140	0.637	0.426	0.734	1.224	1.180	1.506	0.436	0.415	0.706	-0.013	0.241	0.239
FC	1.102	1.555	1.343	1.663	2.336	2.265	2.841	1.353	1.334	1.631	-1.009	1.182	1.180
Mmp8													
Log $_2$ FC	-0.199	-0.847	-0.268	-0.421	-0.777	-1.237	-1.895	-0.222	-0.607	-1.080	-0.177	-0.475	-0.206
FC	-1.148	-1.798	-1.204	-1.339	-1.714	-2.357	-3.719	-1.166	-1.523	-2.114	-1.130	-1.390	-1.154
Myh6													
Log $_2$ FC	-0.348	-0.258	0.096	0.077	-0.446	-0.743	-0.845	-0.508	-0.813	-0.918	-0.246	-0.352	-0.082
FC	-1.273	-1.195	1.069	1.055	-1.362	-1.674	-1.797	-1.422	-1.757	-1.890	-1.186	-1.276	-1.058
Myh7													
Log $_2$ FC	-0.389	-0.771	-0.608	0.325	0.671	0.714	0.996	0.220	0.179	0.563	-0.118	0.204	0.361
FC	-1.309	-1.706	-1.524	1.252	1.592	1.640	1.995	1.165	1.132	1.478	-1.086	1.152	1.284
Ndufa4l2													
Log $_2$ FC	-0.633	-2.345	-0.929	0.775	0.986	1.123	0.943	0.133	0.269	0.053	0.112	-0.070	-0.174
FC	-1.551	-5.079	-1.904	1.711	1.981	2.179	1.922	1.096	1.205	1.037	1.081	-1.050	-1.128
Nfatc4													
Log $_2$ FC	-0.211	-0.337	-0.061	0.618	1.009	1.172	1.227	0.234	0.411	0.415	0.133	0.140	-0.025
FC	-1.157	-1.263	-1.043	1.535	2.012	2.253	2.341	1.176	1.329	1.333	1.096	1.102	-1.018
Nfkbia													
Log $_2$ FC	-0.435	-0.373	0.069	-0.129	-0.431	-0.306	-0.901	-0.259	-0.162	-0.698	0.087	-0.349	-0.404
FC	-1.352	-1.295	1.049	-1.093	-1.348	-1.236	-1.868	-1.196	-1.119	-1.623	1.062	-1.274	-1.323
Nos3													
Log $_2$ FC	-0.386	-1.410	-0.365	0.298	0.057	-0.230	-1.388	-0.240	-0.538	-1.505	-0.181	-0.918	-0.703
FC	-1.307	-2.657	-1.288	1.230	1.040	-1.173	-2.617	-1.181	-1.452	-2.838	-1.134	-1.889	-1.628
Nppa													
Log $_2$ FC	-0.050	-0.312	-0.228	0.449	1.005	0.738	0.811	0.517	0.277	0.335	-0.208	-0.179	0.049
FC	-1.035	-1.241	-1.171	1.365	2.007	1.668	1.755	1.431	1.212	1.262	-1.155	-1.132	1.035
Nppb													
Log $_2$ FC	-0.706	-0.811	0.768	0.112	-0.878	-0.791	-0.872	-1.035	-0.620	-0.987	-0.087	0.156	0.155
FC	-1.631	-1.754	1.702	1.081	-1.837	-1.730	-1.830	-2.049	-1.537	-1.982	-1.062	1.114	1.114

Gene/FC	Bm	Bm2D	B0m0	B24m24	B48m48	B72m72	B96m96	B0B24	B0B48	B0B72	B0B96	B24B48	B24B72	B24B96
Npr2														
Log $_2$ FC	0.076	0.064	-0.033	-0.041	-0.033	0.082	0.354	0.518	0.720	0.624	0.660	0.141	0.032	0.051
FC	1.054	1.045	-1.023	-1.029	-1.023	1.059	1.278	1.432	1.647	1.541	1.581	1.102	1.022	1.036
Npr3														
Log $_2$ FC	0.249	0.207	-0.064	0.813	-0.415	0.142	0.528	-0.543	0.593	-0.634	-0.911	1.015	-0.033	-0.296
FC	1.188	1.155	-1.045	1.757	-1.333	1.104	1.442	-1.457	1.508	-1.552	-1.880	2.021	-1.023	-1.228
Pdk4														
Log $_2$ FC	-0.115	-0.259	0.029	0.111	-0.118	-0.585	-0.671	-2.008	-1.546	-0.723	-1.229	0.366	1.409	0.928
FC	-1.083	-1.196	1.021	1.080	-1.085	-1.501	-1.592	-4.022	-2.919	-1.651	-2.344	1.289	2.655	1.902
Pik3ip1														
Log $_2$ FC	0.404	0.392	0.136	0.564	0.040	0.398	1.175	0.030	0.141	-0.499	-0.693	0.067	-0.579	-0.773
FC	-1.086	-1.131	1.126	-1.141	1.177	-1.445	-1.463	2.874	4.262	9.574	10.781	1.147	2.047	2.171
Pln														
Log $_2$ FC	-0.408	-0.454	-0.141	-0.593	0.161	-0.542	-1.010	0.468	0.233	1.257	1.576	-0.217	0.601	1.045
FC	-1.327	-1.370	-1.103	-1.508	1.118	-1.456	-2.014	1.383	1.176	2.389	2.981	-1.162	1.516	2.063
Ryr3														
Log $_2$ FC	-0.199	-0.228	-0.017	-0.004	-0.914	-0.212	0.398	0.325	0.534	-0.506	-0.727	0.158	-0.836	-1.085
FC	-1.148	-1.172	-1.012	-1.003	-1.884	-1.158	1.318	1.253	1.448	-1.420	-1.655	1.115	-1.785	-2.122
Slc2a1														
Log $_2$ FC	0.270	0.405	0.198	0.586	-0.116	0.990	2.065	-0.227	-0.026	-1.974	-2.373	0.189	-1.719	-2.126
FC	1.206	1.324	1.147	1.501	-1.084	1.987	4.185	-1.171	-1.018	-3.930	-5.179	1.140	-3.293	-4.366
Slc8a1														
Log $_2$ FC	0.057	0.094	-0.007	0.028	-0.257	0.240	0.591	-0.144	-0.364	-1.057	-1.128	-0.208	-0.907	-0.989
FC	1.040	1.068	-1.005	1.020	-1.195	1.181	1.506	-1.105	-1.287	-2.081	-2.186	-1.155	-1.875	-1.985
Sod3														
Log $_2$ FC	0.023	0.152	0.006	0.069	0.149	0.152	-0.042	0.308	1.125	2.521	3.884	0.300	1.387	2.624
FC	1.016	1.111	1.004	1.049	1.108	1.111	-1.029	1.238	2.181	5.742	14.766	1.231	2.615	6.166
Srf														
Log $_2$ FC	-0.122	-0.115	-0.191	-0.273	0.045	0.143	-0.260	-0.305	-1.027	-1.141	-0.822	-0.631	-0.788	-0.491
FC	-1.088	-1.083	-1.142	-1.208	1.032	1.104	-1.197	-1.235	-2.038	-2.206	-1.768	-1.549	-1.726	-1.405

Gene/FC	B48B72	B48B96	B72B96	m0m24	m0m48	m0m72	m0m96	m24m48	m24m72	m24m96	m48m72	m48m96	m72m96
Npr2													
Log $_2$ FC	-0.118	-0.110	0.015	0.555	0.797	0.788	1.118	0.163	0.167	0.455	0.001	0.258	0.238
FC	-1.085	-1.079	1.010	1.470	1.738	1.726	2.171	1.120	1.123	1.371	1.001	1.196	1.179
Npr3													
Log $_2$ FC	-1.098	-1.415	-0.157	0.504	0.076	-0.032	0.579	-0.361	-0.269	0.156	-0.028	0.200	0.169
FC	-2.141	-2.666	-1.115	1.418	1.054	-1.023	1.493	-1.285	-1.205	1.114	-1.020	1.149	1.124
Pdk4													
Log $_2$ FC	0.840	0.425	-0.411	-2.034	-1.873	-1.409	-1.993	0.181	0.423	0.071	0.204	-0.098	-0.277
FC	1.791	1.342	-1.330	-4.095	-3.662	-2.655	-3.979	1.133	1.341	1.050	1.152	-1.070	-1.211
Pik3ip1													
Log $_2$ FC	-0.353	-0.555	-0.125	0.367	0.169	-0.389	0.180	-0.193	-0.697	-0.191	-0.378	0.011	0.406
FC	1.644	1.755	1.026	1.993	4.332	3.752	4.444	1.689	1.513	1.670	-1.107	-1.061	1.061
Pln													
Log $_2$ FC	0.936	1.272	0.229	-0.250	0.651	0.800	0.716	0.812	0.973	0.915	0.132	0.047	-0.094
FC	1.913	2.415	1.172	-1.189	1.570	1.741	1.643	1.755	1.963	1.886	1.096	1.033	-1.068
Ryr3													
Log $_2$ FC	-0.900	-1.198	-0.114	0.363	-0.880	-0.758	-0.204	-1.019	-1.047	-0.538	0.091	0.453	0.359
FC	-1.866	-2.295	-1.082	1.286	-1.840	-1.691	-1.152	-2.026	-2.066	-1.452	1.065	1.369	1.283
Slc2a1													
Log $_2$ FC	-1.806	-2.256	-0.315	0.180	-0.442	-0.848	-0.414	-0.445	-0.943	-0.585	-0.201	0.104	0.349
FC	-3.496	-4.775	-1.244	1.133	-1.359	-1.800	-1.332	-1.361	-1.923	-1.500	-1.150	1.075	1.274
Slc8a1													
Log $_2$ FC	-0.649	-0.741	-0.061	-0.096	-0.646	-0.754	-0.502	-0.528	-0.659	-0.411	-0.077	0.140	0.233
FC	-1.568	-1.671	-1.043	-1.069	-1.564	-1.687	-1.416	-1.442	-1.579	-1.329	-1.055	1.102	1.175
Sod3													
Log $_2$ FC	0.616	1.634	0.579	0.485	1.751	2.655	3.605	0.644	1.489	2.191	0.443	1.049	0.484
FC	1.532	3.105	1.494	1.399	3.366	6.297	12.167	1.563	2.807	4.566	1.359	2.070	1.398
Srf													
Log $_2$ FC	-0.044	0.261	0.249	-0.399	-0.748	-0.680	-0.882	-0.324	-0.277	-0.459	0.039	-0.068	-0.099
FC	-1.031	1.198	1.189	-1.318	-1.679	-1.602	-1.844	-1.251	-1.212	-1.374	1.027	-1.048	-1.071

Gene/FC	Bm	Bm2D	B0m0	B24m24	B48m48	B72m72	B96m96	B0B24	B0B48	B0B72	B0B96	B24B48	B24B72	B24B96
Srl														
Log $_2$ FC	-0.071	-0.055	-0.146	-0.057	-0.276	-0.089	0.424	-0.239	-0.467	-1.105	-1.672	-0.211	-0.851	-1.432
FC	-1.050	-1.039	-1.106	-1.040	-1.211	-1.064	1.341	-1.180	-1.382	-2.152	-3.188	-1.157	-1.804	-2.698
Tgfb2														
Log $_2$ FC	0.238	0.305	0.061	-0.087	0.028	0.925	0.764	-0.027	-0.097	-1.378	-0.912	-0.062	-1.345	-0.890
FC	1.180	1.236	1.043	-1.063	1.019	1.898	1.698	-1.019	-1.070	-2.598	-1.882	-1.044	-2.540	-1.853
Timp2														
Log $_2$ FC	-0.011	0.035	0.187	0.020	0.155	0.066	-0.277	0.472	0.747	1.132	1.883	0.259	0.633	1.372
FC	-1.008	1.024	1.138	1.014	1.113	1.047	-1.212	1.387	1.679	2.192	3.689	1.196	1.551	2.588
Timp3														
Log $_2$ FC	0.187	0.303	0.185	-0.033	0.525	0.506	0.270	0.646	0.986	1.497	2.072	0.309	0.800	1.362
FC	1.138	1.234	1.136	-1.023	1.439	1.420	1.206	1.565	1.981	2.822	4.206	1.239	1.742	2.571
Vegfa														
Log $_2$ FC	0.301	0.366	0.123	0.873	-0.082	0.647	1.364	-0.337	0.118	-1.456	-2.027	0.206	-1.110	-1.691
FC	1.232	1.289	1.089	1.831	-1.059	1.566	2.573	-1.263	1.085	-2.743	-4.074	1.153	-2.158	-3.229

Gene/FC	B48B72	B48B96	B72B96	m0m24	m0m48	m0m72	m0m96	m24m48	m24m72	m24m96	m48m72	m48m96	m72m96
Srl													
Log $_2$ FC	-0.588	-1.167	-0.484	-0.140	-0.641	-1.037	-1.060	-0.475	-0.879	-0.894	-0.299	-0.335	-0.014
FC	-1.503	-2.245	-1.399	-1.102	-1.560	-2.053	-2.085	-1.390	-1.839	-1.858	-1.231	-1.261	-1.010
Tgfb2													
Log $_2$ FC	-1.201	-0.788	0.389	-0.174	-0.101	-0.211	-0.180	0.056	-0.052	-0.015	-0.078	-0.066	0.036
FC	-2.300	-1.727	1.309	-1.128	-1.072	-1.158	-1.133	1.039	-1.037	-1.011	-1.055	-1.047	1.025
Timp2													
Log $_2$ FC	0.347	1.069	0.653	0.245	0.768	0.981	1.380	0.394	0.613	0.982	0.174	0.512	0.296
FC	1.272	2.098	1.573	1.185	1.702	1.973	2.604	1.314	1.530	1.975	1.128	1.426	1.228
Timp3													
Log $_2$ FC	0.455	1.006	0.478	0.448	1.453	1.822	2.176	0.959	1.293	1.690	0.343	0.660	0.158
FC	1.371	2.008	1.393	1.364	2.738	3.536	4.519	1.945	2.450	3.227	1.268	1.580	1.116
Vegfa													
Log $_2$ FC	-0.799	-1.432	-0.444	0.404	-0.199	-0.726	0.050	-0.534	-1.020	-0.239	-0.346	0.112	0.306
FC	-1.740	-2.699	-1.360	1.324	-1.148	-1.654	1.035	-1.448	-2.028	-1.180	-1.271	1.081	1.236

References

Aartsma-Rus, A. & van Ommen, G.-J.B. (2009) Less is more: therapeutic exon skipping for Duchenne muscular dystrophy. *Lancet neurology*. 8 (10), 873–875.

Adini, I., Ghosh, K., Adini, A., Chi, Z.-L., Yoshimura, T., Benny, O., Connor, K.M., Rogers, M.S., Bazinet, L., Birsner, A.E., Bielenberg, D.R. & D'Amato, R.J. (2014) Melanocyte-secreted fibromodulin promotes an angiogenic microenvironment. *Journal of Clinical Investigation*. 124 (1), 425–436.

Al-Momany, A., Li, L., Alexander, R.T. & Ballermann, B.J. (2014) Clustered PI(4,5)P_2 accumulation and ezrin phosphorylation in response to CLIC5A. *Journal of Cell Science*. 127 (24), 5164–5178.

Alderton, J.M. & Steinhardt, R.A. (2000) Calcium influx through calcium leak channels is responsible for the elevated levels of calcium-dependent proteolysis in dystrophic myotubes. *The Journal of biological chemistry*. 275 (13), 9452–9460.

Alman, B.A., Raza, S.N. & Biggar, W.D. (2004) Steroid treatment and the development of scoliosis in males with duchenne muscular dystrophy. *The Journal of bone and joint surgery. American volume*. 86-A (3), 519–524.

Amthor, H., Christ, B., Weil, M. & Patel, K. (1998) The importance of timing differentiation during limb muscle development. *Current biology : CB*. 8 (11), 642–652.

Anders, S., Pyl, P.T. & Huber, W. (2015) HTSeq--a Python framework to work with high-throughput sequencing data. *Bioinformatics (Oxford, England)*. 31 (2), 166–169.

Andrews, S. (2010) *FastQC: A quality control tool for high throughput sequence data.* [online]. Available from: http://www.bioinformatics.babraham.ac.uk/projects/fastqc/ (Accessed 15 October 2015).

Asakura, A., Seale, P., Girgis-Gabardo, A. & Rudnicki, M.A. (2002) Myogenic specification of side population cells in skeletal muscle. *The Journal of Cell Biology*. 159 (1), 123–134.

Bailey, P., Holowacz, T. & Lassar, A.B. (2001) The origin of skeletal muscle stem cells in the embryo and the adult. *Current opinion in cell biology*. 13 (6), 679–689.

Baldelli, S., Lettieri Barbato, D., Tatulli, G., Aquilano, K. & Ciriolo, M.R. (2014) The role of nNOS and PGC-1α in skeletal muscle cells. *Journal of Cell Science*. 127 (Pt 22), 4813–4820.

Barp, A., Bello, L., Politano, L., Melacini, P., Calore, C., Polo, A., Vianello, S., Sorarù, G., Semplicini, C., Pantic, B., Taglia, A., Picillo, E., Magri, F., Gorni, K., Messina, S., Vita, G.L., Vita, G., Comi, G.P., Ermani, M., et al. (2015) Genetic Modifiers of Duchenne Muscular Dystrophy and Dilated Cardiomyopathy. Ashok Kumar (ed.). *PLoS ONE*. 10 (10), e0141240.

Barry, S.P., Davidson, S.M. & Townsend, P.A. (2008) Molecular regulation of cardiac hypertrophy. *The international journal of biochemistry & cell biology*. 40 (10), 2023–2039.

Barth, K., Pfleger, C., Linge, A., Sim, J.A., Surprenant, A., Steinbronn, N., Strasser, R.H. & Kasper, M. (2010) Increased P2X7R expression in atrial cardiomyocytes of caveolin-1 deficient mice. *Histochemistry and cell biology*. 134 (1), 31–38.

Bassett, D. & Currie, P.D. (2004) '*Identification of a zebrafish model of muscular dystrophy.*', in [Online]. August 2004 Blackwell Science Pty. pp. 537–540.

Bauer, R., Straub, V., Blain, A., Bushby, K. & MacGowan, G.A. (2009) Contrasting effects of steroids and angiotensin-converting-enzyme inhibitors in a mouse model of dystrophin-deficient cardiomyopathy. *European journal of heart failure*. 11 (5), 463–471.

Beaudette, P., Popp, O. & Dittmar, G. (2015) Proteomic techniques to probe the ubiquitin landscape. *Proteomics*. n/a–n/a.

Beenakker, E.A.C., Maurits, N.M., Fock, J.M., Brouwer, O.F. & van der Hoeven, J.H. (2005) Functional ability and muscle force in healthy children and ambulant Duchenne muscular dystrophy patients. *European journal of paediatric neurology : EJPN : official journal of the European Paediatric Neurology Society*. 9 (6), 387–393.

Benjamini, Y. & Hochberg, Y. (1995) Controlling the false discovery rate: a practical and powerful approach to multiple testing. *Journal of the Royal Statistical Society Series B ….*

Berry, D.A., Balcar, V.J., Barden, J.A., Keogh, A. & Remedios, dos, C.G. (2000) Determination of P2X1alpha-sarcoglycan (adhalin) expression levels in failing human dilated cardiomyopathic left ventricles. *Electrophoresis*. 21 (17), 3857–3862.

Betts, C., Saleh, A.F., Arzumanov, A.A., Hammond, S.M., Godfrey, C., Coursindel, T., Gait, M.J. & Wood, M.J. (2012) Pip6-PMO, A New Generation of Peptide-oligonucleotide Conjugates With Improved Cardiac Exon Skipping Activity for DMD Treatment. *Molecular therapy. Nucleic acids*. 1 (8), e38.

Betts, C.A., Saleh, A.F., Carr, C.A., Hammond, S.M., Coenen-Stass, A.M.L., Godfrey, C., McClorey, G., Varela, M.A., Roberts, T.C., Clarke, K., Gait, M.J. & Wood, M.J.A. (2015) Prevention of exercised induced cardiomyopathy following Pip-PMO treatment in dystrophic mdx mice. *Scientific reports*. 58986.

Betts, C.A., Saleh, A.F., Carr, C.A., Muses, S., Wells, K.E., Hammond, S.M., Godfrey, C., McClorey, G., Woffindale, C., Clarke, K., Wells, D.J., Gait, M.J. & Wood, M.J.A. (2015) Implications for Cardiac Function Following Rescue of the Dystrophic Diaphragm in a Mouse Model of Duchenne Muscular Dystrophy. *Scientific reports*. 511632.

Bhatnagar, S. & Kumar, A. (2012) The TWEAK-Fn14 system: breaking the silence of cytokine-induced skeletal muscle wasting. *Current molecular medicine*. 12 (1), 3–13.

Bianchi, M.L., Biggar, D., Bushby, K., Rogol, A.D., Rutter, M.M. & Tseng, B. (2011) '*Endocrine aspects of Duchenne muscular dystrophy.*', in [Online]. April 2011 pp. 298–303.

Birnkrant, D.J., Ashwath, M.L., Noritz, G.H., Merrill, M.C., Shah, T.A., Crowe, C.A. & Bahler, R.C. (2010) Cardiac and pulmonary function variability in Duchenne/Becker muscular dystrophy: an initial report. *Journal of child neurology*. 25 (9), 1110–1115.

Bishu, K., Hamdani, N., Mohammed, S.F., Kruger, M., Ohtani, T., Ogut, O., Brozovich, F.V., Burnett, J.C., Linke, W.A. & Redfield, M.M. (2011) Sildenafil and B-type natriuretic peptide acutely phosphorylate titin and improve diastolic distensibility in vivo. *Circulation*. 124 (25), 2882–2891.

Bismuth, K. & Relaix, F. (2010) Genetic regulation of skeletal muscle development. *Experimental Cell Research*. 316 (18), 3081–3086.

Bkaily, G., Chahine, M., Al-Khoury, J., Avedanian, L., Beier, N., Scholz, W. & Jacques, D. (2015) Na(+)-H(+) exchanger inhibitor prevents early death in hereditary cardiomyopathy. *Canadian journal of physiology and pharmacology*. 1–12.

Bladen, C.L., Salgado, D., Monges, S., Foncuberta, M.E., Kekou, K., Kosma, K., Dawkins, H., Lamont, L., Roy, A.J., Chamova, T., Guergueltcheva, V., Chan, S., Korngut, L., Campbell, C., Dai, Y., Wang, J., Barišić, N., Brabec, P., Lahdetie, J., et al. (2015) The TREAT-NMD DMD Global database: Analysis of More Than 7000 Duchenne Muscular Dystrophy Mutations. *Human mutation*.

Blain, A., Greally, E., Laval, S.H., Blamire, A.M., MacGowan, G.A. & Straub, V.W. (2015) Absence of Cardiac Benefit with Early Combination ACE Inhibitor and Beta Blocker Treatment in mdx Mice. *Journal of cardiovascular translational research*.

Blanco-Bose, W.E., Yao, C.C., Kramer, R.H. & Blau, H.M. (2001) Purification of mouse primary myoblasts based on alpha 7 integrin expression. *Experimental Cell Research*. 265 (2), 212–220.

Bodensteiner, J.B. & Engel, A.G. (1978) Intracellular calcium accumulation in Duchenne dystrophy and other myopathies: a study of 567,000 muscle fibers in 114 biopsies. *Neurology*. 28 (5), 439–446.

Booz, G.W. (2005) Putting the brakes on cardiac hypertrophy: exploiting the NO-cGMP counter-regulatory system. *Hypertension*. 45 (3), 341–346.

Bouleti, C., Mathivet, T., Coqueran, B., Serfaty, J.-M., Lesage, M., Berland, E., Ardidie-Robouant, C., Kauffenstein, G., Henrion, D., Lapergue, B., Mazighi, M., Duyckaerts, C., Thurston, G., Valenzuela, D.M., Murphy, A.J., Yancopoulos, G.D., Monnot, C., Margaill, I. & Germain, S. (2013) Protective effects of angiopoietin-like 4 on cerebrovascular and functional damages in ischaemic stroke. *European heart journal*. 34 (47), 3657–3668.

Bowe, M.A., Mendis, D.B. & Fallon, J.R. (2000) The small leucine-rich repeat proteoglycan biglycan binds to alpha-dystroglycan and is upregulated in dystrophic muscle. *The Journal of Cell Biology*. 148 (4), 801–810.

Brézillon, S., Pietraszek, K., Maquart, F.-X. & Wegrowski, Y. (2013) Lumican effects in the control of tumour progression and their links with metalloproteinases and integrins. *The FEBS journal*. 280 (10), 2369–2381.

Buckingham, M., Meilhac, S. & Zaffran, S. (2005) Building the mammalian heart from two sources of myocardial cells. *Nature Publishing Group*. 6 (11), 826–835.

Bulfield, G., Siller, W.G., Wight, P.A. & Moore, K.J. (1984) X chromosome-linked muscular dystrophy (mdx) in the mouse. *Proceedings of the National Academy of Sciences of the United States of America*. 81 (4), 1189–1192.

Bushby, K M, Thambyayah, M. & Gardner-Medwin, D. (1991) Prevalence and incidence of Becker muscular dystrophy. *The Lancet*. 337 (8748), 1022–1024.

Bushby, Kate, Lochmüller, H., Lynn, S. & Straub, V. (2009) Interventions for muscular dystrophy: molecular medicines entering the clinic. *Lancet*. 374 (9704), 1849–1856.

Bushby, Katharine, Finkel, R., Birnkrant, D.J., Case, L.E., Clemens, P.R., Cripe, L., Kaul, A., Kinnett, K., Mcdonald, C., Pandya, S., Poysky, J., Shapiro, F., Tomezsko, J., Constantin, C.DMD Care Considerations Working Group (2010a) Diagnosis and management of Duchenne muscular dystrophy, part 1: diagnosis, and pharmacological and psychosocial management. Lancet neurology 9 (1) 77–93.

Bushby, Katharine, Finkel, R., Birnkrant, D.J., Case, L.E., Clemens, P.R., Cripe, L., Kaul, A., Kinnett, K., Mcdonald, C., Pandya, S., Poysky, J., Shapiro, F., Tomezsko, J., Constantin, C.DMD Care Considerations Working Group (2010b) Diagnosis and management of Duchenne muscular dystrophy, part 2: implementation of multidisciplinary care. *Lancet neurology*. 9 (2), 177–189.

Bushby, Katharine, Finkel, R., Wong, B., Barohn, R., Campbell, C., Comi, G.P., Connolly, A.M., Day, J.W., Flanigan, K.M., Goemans, N., Jones, K.J., Mercuri, E., Quinlivan, R., Renfroe, J.B., Russman, B., Ryan, M.M., Tulinius, M., Voit, T., Moore, S.A., et al. (2014) Ataluren treatment of patients with nonsense mutation dystrophinopathy. *Muscle & Nerve*. 50 (4), 477–487.

Camargo, F.D., Green, R., Capetanaki, Y., Jackson, K.A., Goodell, M.A. & Capetenaki, Y. (2003) Single hematopoietic stem cells generate skeletal muscle through myeloid intermediates. *Nature Medicine*. 9 (12), 1520–1527.

Carvajal-Vergara, X., Sevilla, A., D'souza, S.L., Ang, Y.-S., Schaniel, C., Lee, D.-F., Yang, L., Kaplan, A.D., Adler, E.D., Rozov, R., Ge, Y., Cohen, N., Edelmann, L.J., Chang, B., Waghray, A., Su, J., Pardo, S., Lichtenbelt, K.D., Tartaglia, M., et al. (2010) Patient-specific induced pluripotent stem-cell-derived models of LEOPARD syndrome. *Nature*. 465 (7299), 808–812.

Chal, J., Oginuma, M., Tanoury, Al, Z., Gobert, B., Sumara, O., Hick, A., Bousson, F., Zidouni, Y., Mursch, C., Moncuquet, P., Tassy, O., Vincent, S., Miyanari, A., Bera, A., Garnier, J.-M., Guevara, G., Hestin, M., Kennedy, L., Hayashi, S., et al. (2015) Differentiation of pluripotent stem cells to muscle fiber to model Duchenne muscular dystrophy. *Nature Biotechnology*. 33 (9), 962–969.

Chamberlain, J.S., Farwell, N.J., Chamberlain, J.R., Cox, G.A. & Caskey, C.T. (1991) PCR analysis of dystrophin gene mutation and expression. *Journal of Cellular Biochemistry*. 46 (3), 255–259.

Chan, E.M., Ratanasirintrawoot, S., Park, I.-H., Manos, P.D., Loh, Y.-H., Huo, H., Miller, J.D., Hartung, O., Rho, J., Ince, T.A., Daley, G.Q. & Schlaeger, T.M. (2009) Live cell imaging distinguishes bona fide human iPS cells from partially reprogrammed cells. *Nature Biotechnology*. 27 (11), 1033–1037.

Chiu, Y.-H., Hornsey, M.A., Klinge, L., Jørgensen, L.H., Laval, S.H., Charlton, R., Barresi, R., Straub, V., Lochmüller, H. & Bushby, K. (2009) Attenuated muscle regeneration is a key factor in dysferlin-deficient muscular dystrophy. *Human Molecular Genetics*. 18 (11), 1976–1989.

Chong, H.C., Chan, J.S.K., Goh, C.Q., Gounko, N.V., Luo, B., Wang, X., Foo, S., Wong, M.T.C., Choong, C., Kersten, S. & Tan, N.S. (2014) Angiopoietin-like 4 stimulates STAT3-mediated iNOS expression and enhances angiogenesis to accelerate wound healing in diabetic mice. *Molecular Therapy*. 22 (9), 1593–1604.

Chung, W. & Campanelli, J. (1999) WW and EF hand domains of dystrophin-family proteins mediate dystroglycan binding. *Molecular Cell Biology Research …*.

Cirak, S., Arechavala-Gomeza, V., Guglieri, M., Feng, L., Torelli, S., Anthony, K., Abbs, S., Garralda, M.E., Bourke, J., Wells, D.J., Dickson, G., Wood, M.J.A., Wilton, S.D., Straub, V., Kole, R., Shrewsbury, S.B., Sewry, C., Morgan, J.E., Bushby, K., et al. (2011) Exon skipping and dystrophin restoration in patients with Duchenne muscular dystrophy after systemic phosphorodiamidate morpholino oligomer treatment: an open-label, phase 2, dose-escalation study. *Lancet*. 378 (9791), 595–605.

Cohen, N. (2004) Multiple pathogenetic mechanisms in X linked dilated cardiomyopathy. *Heart*. 90 (8), 835–841.

Cohn, R.D. (2005) Dystroglycan: important player in skeletal muscle and beyond. *Neuromuscular Disorders*. 15 (3), 207–217.

Cohn, R.D., Henry, M.D., Michele, D.E., Barresi, R., Saito, F., Moore, S.A., Flanagan, J.D., Skwarchuk, M.W., Robbins, M.E., Mendell, J.R., Williamson, R.A. & Campbell, K.P. (2002) Disruption of DAG1 in differentiated skeletal muscle reveals a role for dystroglycan in muscle regeneration. *Cell*. 110 (5), 639–648.

Collins, H.E., Zhu-Mauldin, X., Marchase, R.B. & Chatham, J.C. (2013) STIM1/Orai1-mediated SOCE: current perspectives and potential roles in cardiac function and pathology. *AJP: Heart and Circulatory Physiology*. 305 (4), H446–58.

Cooper, B.J., Winand, N.J., Stedman, H., Valentine, B.A., Hoffman, E.P., Kunkel, L.M., Scott, M.O., Fischbeck, K.H., Kornegay, J.N. & Avery, R.J. (1988) The homologue of the Duchenne locus is defective in X-linked muscular dystrophy of dogs. *Nature*. 334 (6178), 154–156.

Corbel, S.Y., Lee, A., Yi, L., Duenas, J., Brazelton, T.R., Blau, H.M. & Rossi, F.M.V. (2003) Contribution of hematopoietic stem cells to skeletal muscle. *Nature Medicine*. 9 (12), 1528–1532.

Cossu, G., Previtali, S.C., Napolitano, S., Cicalese, M.P., Tedesco, F.S., Nicastro, F., Noviello, M., Roostalu, U., Natali Sora, M.G., Scarlato, M., De Pellegrin, M., Godi, C., Giuliani, S., Ciotti, F., Tonlorenzi, R., Lorenzetti, I., Rivellini, C., Benedetti, S., Gatti, R., et al. (2015) Intra-arterial transplantation of HLA-matched donor mesoangioblasts in Duchenne muscular dystrophy. *EMBO molecular medicine*. e201505636.

Cox, E.J. & Marsh, S.A. (2014) A systematic review of fetal genes as biomarkers of cardiac hypertrophy in rodent models of diabetes. *PLoS ONE*. 9 (3), e92903.

Cully, T.R., Edwards, J.N., Friedrich, O., Stephenson, D.G., Murphy, R.M. & Launikonis, B.S. (2012) Changes in plasma membrane Ca-ATPase and stromal interacting molecule 1 expression levels for Ca(2+) signaling in dystrophic mdx mouse muscle. *AJP: Cell Physiology*. 303 (5), C567–76.

Cyranoski, D. (2009) Woo Suk Hwang convicted, but not of fraud. *Nature*. 461 (7268), 1181–1181.

Dalal, S., Foster, C.R., Das, B.C., Singh, M. & Singh, K. (2012) B-adrenergic receptor stimulation induces endoplasmic reticulum stress in adult cardiac myocytes: role in apoptosis. *Molecular and cellular biochemistry*. 364 (1-2), 59–70.

De Arcangelis, V., Strimpakos, G., Gabanella, F., Corbi, N., Luvisetto, S., Magrelli, A., Onori, A., Passananti, C., Pisani, C., Rome, S., Severini, C., Naro, F., Mattei, E., Di Certo, M.G. & Monaco, L. (2015) Pathways Implicated in Tadalafil Amelioration of Duchenne Muscular Dystrophy. *Journal of cellular physiology*. 231 (1), 224–232.

Deconinck, A.E., Rafael, J.A., Skinner, J.A., Brown, S.C., Potter, A.C., Metzinger, L., Watt, D.J., Dickson, J.G., Tinsley, J.M. & Davies, K.E. (1997) Utrophin-dystrophin-deficient mice as a model for Duchenne muscular dystrophy. *Cell*. 90 (4), 717–727.

Dehghani, L., Farokhpour, M., Karbalaie, K., Nematollahi, M., Tanhaie, S., Hayati-Rodbari, N., Kiani-Esfahani, A., Hescheler, J., Nasr-Esfahani, M.H. & Baharvand, H. (2013) The influence of dexamethasone administration on the protection against doxorubicin-induced cardiotoxicity in purified embryonic stem cell-derived cardiomyocytes. *Tissue & cell*. 45 (2), 101–106.

Delfín, D.A., Zang, K.E., Schill, K.E., Patel, N.T., Janssen, P.M.L., Raman, S.V. & Rafael-Fortney, J.A. (2012) Cardiomyopathy in the dystrophin/utrophin-deficient mouse model of severe muscular dystrophy is characterized by dysregulation of matrix metalloproteinases. *Neuromuscular disorders : NMD*. 22 (11), 1006–1014.

Dellavalle, A., Sampaolesi, M., Tonlorenzi, R., Tagliafico, E., Sacchetti, B., Perani, L., Innocenzi, A., Galvez, B.G., Messina, G., Morosetti, R., Li, S., Belicchi, M., Peretti, G., Chamberlain, J.S., Wright, W.E., Torrente, Y., Ferrari, S., Bianco, P. & Cossu, G. (2007) Pericytes of human skeletal muscle are myogenic precursors distinct from satellite cells. *Nature Cell Biology*. 9 (3), 255–267.

Dick, E., Kalra, S., Anderson, D., George, V., Ritso, M., Laval, S.H., Barresi, R., Aartsma-Rus, A., Lochmüller, H. & Denning, C. (2013) Exon skipping and gene transfer restore dystrophin expression in human induced pluripotent stem cells-cardiomyocytes harboring DMD mutations. *Stem cells and development*. 22 (20), 2714–2724.

Dick, E., Matsa, E., Young, L.E., Darling, D. & Denning, C. (2011) Faster generation of hiPSCs by coupling high-titer lentivirus and column-based positive selection. *Nature Protocols*. 6 (6), 701–714.

Dixit, P. & Katare, R. (2015) Challenges in identifying the best source of stem cells for cardiac regeneration therapy. *Stem cell research & therapy*. 6 (1), 26.

Donnelly-Roberts, D.L., Namovic, M.T., Surber, B., Vaidyanathan, S.X., Perez-Medrano, A., Wang, Y., Carroll, W.A. & Jarvis, M.F. (2009) [3H]A-804598 ([3H]2-cyano-1-[(1S)-1-phenylethyl]-3-quinolin-5-ylguanidine) is a novel, potent, and selective antagonist radioligand for P2X7 receptors. *Neuropharmacology*. 56 (1), 223–229.

Duan, D. (2006) Challenges and opportunities in dystrophin-deficient cardiomyopathy gene therapy. *Human Molecular Genetics*. 15 Spec No 2R253–61.

Duan, D. (2011) Duchenne muscular dystrophy gene therapy: Lost in translation? *Research and reports in biology*. 2011 (2), 31–42.

Dumont, N.A., Wang, Y.X. & Rudnicki, M.A. (2015) Intrinsic and extrinsic mechanisms regulating satellite cell function. *Development*. 142 (9), 1572–1581.

Dunant, P., Larochelle, N., Thirion, C., Stucka, R., Ursu, D., Petrof, B.J., Wolf, E. & Lochmüller, H. (2003) Expression of dystrophin driven by the 1.35-kb MCK promoter ameliorates muscular dystrophy in fast, but not in slow muscles of transgenic mdx mice. *Molecular Therapy*. 8 (1), 80–89.

Dupuis, L.E., Berger, M.G., Feldman, S., Doucette, L., Fowlkes, V., Chakravarti, S., Thibaudeau, S., Alcala, N.E., Bradshaw, A.D. & Kern, C.B. (2015) Lumican deficiency results in cardiomyocyte hypertrophy with altered collagen assembly. *Journal of Molecular and Cellular Cardiology*. 8470–80.

Ennen, J.P., Verma, M. & Asakura, A. (2013) Vascular-targeted therapies for Duchenne muscular dystrophy. *Skeletal muscle*. 3 (1), 9.

Enwere, E.K., Lacasse, E.C., Adam, N.J. & Korneluk, R.G. (2014) Role of the TWEAK-Fn14-cIAP1-NF-κB Signaling Axis in the Regulation of Myogenesis and Muscle Homeostasis. *Frontiers in immunology*. 534.

Evans, M.D.R. & Kelley, J. (2011) US attitudes toward human embryonic stem cell research. *Nature Biotechnology*. 29 (6), 484–488.

Evans, S.M., Yelon, D., Conlon, F.L. & Kirby, M.L. (2010) Myocardial lineage development. *Circulation Research*. 107 (12), 1428–1444.

Fabb, S.A., Wells, D.J., Serpente, P. & Dickson, G. (2002) Adeno-associated virus vector gene transfer and sarcolemmal expression of a 144 kDa micro-dystrophin effectively restores the dystrophin-associated protein complex and inhibits myofibre degeneration in nude/mdx mice. *Human Molecular Genetics*. 11 (7), 733–741.

Falzarano, M.S., Scotton, C., Passarelli, C. & Ferlini, A. (2015) Duchenne Muscular Dystrophy: From Diagnosis to Therapy. *Molecules (Basel, Switzerland)*. 20 (10), 18168–18184.

Fan, C.M., Porter, J.A., Chiang, C., Chang, D.T., Beachy, P.A. & Tessier-Lavigne, M. (1995) Long-range sclerotome induction by sonic hedgehog: direct role of the amino-terminal cleavage product and modulation by the cyclic AMP signaling pathway. *Cell*. 81 (3), 457–465.

Fan, D., Takawale, A., Basu, R., Patel, V., Lee, J., Kandalam, V., Wang, X., Oudit, G.Y. & Kassiri, Z. (2014) Differential role of TIMP2 and TIMP3 in cardiac hypertrophy, fibrosis, and diastolic dysfunction. *Cardiovascular research*. 103 (2), 268–280.

Farini, A., Razini, P., Erratico, S., Torrente, Y. & Meregalli, M. (2009) Cell based therapy for Duchenne muscular dystrophy. *Journal of cellular physiology*. 221 (3), 526–534.

Ferlini, A., Neri, M. & Gualandi, F. (2013) The medical genetics of dystrophinopathies: molecular genetic diagnosis and its impact on clinical practice. *Neuromuscular disorders : NMD*. 23 (1), 4–14.

Ferreiro, V., Giliberto, F., Muñiz, G.M.N., Francipane, L., Marzese, D.M., Mampel, A., Roqué, M., Frechtel, G.D. & Szijan, I. (2009) Asymptomatic Becker muscular dystrophy in a family with a multiexon deletion. *Muscle & Nerve*. 39 (2), 239–243.

Field, L.J. (1988) Atrial natriuretic factor-SV40 T antigen transgenes produce tumors and cardiac arrhythmias in mice. *Science*. 239 (4843), 1029–1033.

Figeac, N., Daczewska, M., Marcelle, C. & Jagla, K. (2007) Muscle stem cells and model systems for their investigation. *Developmental Dynamics*. 236 (12), 3332–3342.

Finsterer, J. & Cripe, L. (2014) Treatment of dystrophin cardiomyopathies. *Nature reviews. Cardiology*. 11 (3), 168–179.

Fishman, M.C. & Chien, K.R. (1997) Fashioning the vertebrate heart: earliest embryonic decisions. *Development*. 124 (11), 2099–2117.

Frey, N., Katus, H.A., Olson, E.N. & Hill, J.A. (2004) Hypertrophy of the heart: a new therapeutic target? *Circulation*. 109 (13), 1580–1589.

Frisch, M., Klocke, B., Haltmeier, M. & Frech, K. (2009) LitInspector: literature and signal transduction pathway mining in PubMed abstracts. *Nucleic acids research*. 37 (Web Server issue), W135–40.

Fujioka, D., Kawabata, K.-I., Saito, Y., Kobayashi, T., Nakamura, T., Kodama, Y., Takano, H., Obata, J.-E., Kitta, Y., Umetani, K. & Kugiyama, K. (2006) Role of adiponectin receptors in endothelin-induced cellular hypertrophy in cultured cardiomyocytes and their expression in infarcted heart. *American journal of physiology. Heart and circulatory physiology*. 290 (6), H2409–16.

Fukada, S.-I., Higuchi, S., Segawa, M., Koda, K.-I., Yamamoto, Y., Tsujikawa, K., Kohama, Y., Uezumi, A., Imamura, M., Miyagoe-Suzuki, Y., Takeda, S. & Yamamoto, H. (2004) Purification and cell-surface marker characterization of quiescent satellite cells from murine skeletal muscle by a novel monoclonal antibody. *Experimental Cell Research*. 296 (2), 245–255.

Galaup, A., Gomez, E., Souktani, R., Durand, M., Cazes, A., Monnot, C., Teillon, J., Le Jan, S., Bouleti, C., Briois, G., Philippe, J., Pons, S., Martin, V., Assaly, R., Bonnin, P., Ratajczak, P., Janin, A., Thurston, G., Valenzuela, D.M., et al. (2012) Protection against myocardial infarction and no-reflow through preservation of vascular integrity by angiopoietin-like 4. *Circulation*. 125 (1), 140–149.

Gannier, F., White, E., Lacampagne, A., Garnier, D. & Guennec, J.Y.L. (1994) Streptomycin reverses a large stretch induced increase in [Ca2+]i in isolated guinea pig ventricular myocytes. *Cardiovascular research*. 28 (8), 1193–1198.

Garbincius, J.F. & Michele, D.E. (2015) Dystrophin-glycoprotein complex regulates muscle nitric oxide production through mechanoregulation of AMPK signaling. *Proceedings of the National Academy of Sciences*. 201512991.

Gardner, D.G., Chen, S., Glenn, D.J. & Grigsby, C.L. (2007) Molecular biology of the natriuretic peptide system: implications for physiology and hypertension. *Hypertension*. 49 (3), 419–426.

Gaspar-Pereira, S., Fullard, N., Townsend, P.A., Banks, P.S., Ellis, E.L., Fox, C., Maxwell, A.G., Murphy, L.B., Kirk, A., Bauer, R., Caamaño, J.H., Figg, N., Foo, R.S., Mann, J., Mann, D.A. & Oakley, F. (2012) The NF-κB subunit c-Rel stimulates cardiac hypertrophy and fibrosis. *The American Journal of Pathology*. 180 (3), 929–939.

Gebski, B.L., Mann, C.J., Fletcher, S. & Wilton, S.D. (2003) Morpholino antisense oligonucleotide induced dystrophin exon 23 skipping in mdx mouse muscle. *Human Molecular Genetics*. 12 (15), 1801–1811.

Gehrig, S.M., Koopman, R., Naim, T., Tjoakarfa, C. & Lynch, G.S. (2010) Making fast-twitch dystrophic muscles bigger protects them from contraction injury and attenuates the dystrophic pathology. *The American Journal of Pathology*. 176 (1), 29–33.

Goecks, J., Nekrutenko, A., Taylor, J.Galaxy Team (2010) Galaxy: a comprehensive approach for supporting accessible, reproducible, and transparent computational research in the life sciences. *Genome biology*. 11 (8), R86.

Goehringer, C., Rutschow, D., Bauer, R., Schinkel, S., Weichenhan, D., Bekeredjian, R., Straub, V., Kleinschmidt, J.A., Katus, H.A. & Müller, O.J. (2009) Prevention of cardiomyopathy in delta-sarcoglycan knockout mice after systemic transfer of targeted adeno-associated viral vectors. *Cardiovascular research*. 82 (3), 404–410.

Goemans, N.M., Tulinius, M., van den Akker, J.T., Burm, B.E., Ekhart, P.F., Heuvelmans, N., Holling, T., Janson, A.A., Platenburg, G.J., Sipkens, J.A., Sitsen, J.M.A., Aartsma-Rus, A., van Ommen, G.-J.B., Buyse, G., Darin, N., Verschuuren, J.J., Campion, G.V., de Kimpe, S.J. & van Deutekom, J.C. (2011) Systemic administration of PRO051 in Duchenne's muscular dystrophy. *The New England journal of medicine*. 364 (16), 1513–1522.

Gongora, M.C. & Harrison, D.G. (2008) Sad heart from no SOD. *Hypertension*. 51 (1), 28–30.

Goulding, M., Lumsden, A. & Paquette, A.J. (1994) Regulation of Pax-3 expression in the dermomyotome and its role in muscle development. *Development*. 120 (4), 957–971.

Goyenvalle, A., Griffith, G., Babbs, A., Andaloussi, S.E., Ezzat, K., Avril, A., Dugovic, B., Chaussenot, R., Ferry, A., Voit, T., Amthor, H., Bühr, C., Schürch, S., Wood, M.J.A., Davies, K.E., Vaillend, C., Leumann, C. & Garcia, L. (2015) Functional correction in mouse models of muscular dystrophy using exon-skipping tricyclo-DNA oligomers. *Nature Medicine*.

Gros, J., Manceau, M., Thomé, V. & Marcelle, C. (2005) A common somitic origin for embryonic muscle progenitors and satellite cells. *Nature*. 435 (7044), 954–958.

Haas, M., Vlcek, V., Balabanov, P., Salmonson, T., Bakchine, S., Markey, G., Weise, M., Schlosser-Weber, G., Brohmann, H., Yerro, C.P., Mendizabal, M.R., Stoyanova-Beninska, V. & Hillege, H.L. (2015) European Medicines Agency review of ataluren for the treatment of ambulant patients aged 5 years and older with Duchenne muscular dystrophy resulting from a nonsense mutation in the dystrophin gene. *Neuromuscular disorders : NMD*. 25 (1), 5–13.

Haghighi, K., Bidwell, P. & Kranias, E.G. (2014) Phospholamban interactome in cardiac contractility and survival: A new vision of an old friend. *Journal of Molecular and Cellular Cardiology*. 77160–167.

Hamed, S. (2006) Drug evaluation: PTC-124--a potential treatment of cystic fibrosis and Duchenne muscular dystrophy. *IDrugs: the investigational drugs journal*. 9 (11), 783–789.

Hartigan-O'Connor, D., Kirk, C.J., Crawford, R., Mulé, J.J. & Chamberlain, J.S. (2001) Immune evasion by muscle-specific gene expression in dystrophic muscle. *Molecular Therapy*. 4 (6), 525–533.

Haskill, S., Beg, A.A., Tompkins, S.M., Morris, J.S., Yurochko, A.D., Sampson-Johannes, A., Mondal, K., Ralph, P. & Baldwin, A.S. (1991) Characterization of an immediate-early gene induced in adherent monocytes that encodes I kappa B-like activity. *Cell*. 65 (7), 1281–1289.

Hastie, E. & Samulski, R.J. (2015) Adeno-associated virus at 50: a golden anniversary of discovery, research, and gene therapy success--a personal perspective. *Human Gene Therapy*. 26 (5), 257–265.

Hathout, Y., Marathi, R.L., Rayavarapu, S., Zhang, A., Brown, K.J., Seol, H., Gordish-Dressman, H., Cirak, S., Bello, L., Nagaraju, K., Partridge, T., Hoffman, E.P., Takeda, S., Mah, J.K., Henricson, E. & Mcdonald, C. (2014) Discovery of serum protein biomarkers in the mdx mouse model and cross-species comparison to Duchenne muscular dystrophy patients. *Human Molecular Genetics*. 23 (24), 6458–6469.

Hawke, T.J. & Garry, D.J. (2001) Myogenic satellite cells: physiology to molecular biology. *Journal of applied physiology (Bethesda, Md. : 1985)*. 91 (2), 534–551.

Heathfield, T.F., Onnerfjord, P., Dahlberg, L. & Heinegård, D. (2004) Cleavage of fibromodulin in cartilage explants involves removal of the N-terminal tyrosine sulfate-rich region by proteolysis at a site that is sensitive to matrix metalloproteinase-13. *The Journal of biological chemistry*. 279 (8), 6286–6295.

Heier, C.R., Damsker, J.M., Yu, Q., Dillingham, B.C., Huynh, T., van der Meulen, J.H., Sali, A., Miller, B.K., Phadke, A., Scheffer, L., Quinn, J., Tatem, K., Jordan, S., Dadgar, S., Rodriguez, O.C., Albanese, C., Calhoun, M., Gordish-Dressman, H., Jaiswal, J.K., et al. (2013) VBP15, a novel anti-inflammatory and membrane-stabilizer, improves muscular dystrophy without side effects. *EMBO molecular medicine*. 5 (10), 1569–1585.

Henze, A.-T., Garvalov, B.K., Seidel, S., Cuesta, A.M., Ritter, M., Filatova, A., Foss, F., Dopeso, H., Essmann, C.L., Maxwell, P.H., Reifenberger, G., Carmeliet, P., Acker-Palmer, A. & Acker, T. (2014) Loss of PHD3 allows tumours to overcome hypoxic growth inhibition and sustain proliferation through EGFR. *Nature communications*. 55582.

Herrero, J., Valencia, A. & Dopazo, J. (2001) A hierarchical unsupervised growing neural network for clustering gene expression patterns. *Bioinformatics (Oxford, England)*. 17 (2), 126–136.

Hildebrand, A., Romarís, M., Rasmussen, L.M., Heinegård, D., Twardzik, D.R., Border, W.A. & Ruoslahti, E. (1994) Interaction of the small interstitial proteoglycans biglycan, decorin and fibromodulin with transforming growth factor beta. *The Biochemical journal*. 302 (Pt 2)527–534.

Hockemeyer, D., Wang, H., Kiani, S., Lai, C.S., Gao, Q., Cassady, J.P., Cost, G.J., Zhang, L., Santiago, Y., Miller, J.C., Zeitler, B., Cherone, J.M., Meng, X., Hinkley, S.J., Rebar, E.J., Gregory, P.D., Urnov, F.D. & Jaenisch, R. (2011) Genetic engineering of human pluripotent cells using TALE nucleases. *Nature Biotechnology*. 29 (8), 731–734.

Huang, D.W., Sherman, B.T. & Lempicki, R.A. (2009) Systematic and integrative analysis of large gene lists using DAVID bioinformatics resources. *Nature Protocols*. 4 (1), 44–57.

Huang, P., He, Z., Ji, S., Sun, H., Xiang, D., Liu, C., Hu, Y., Wang, X. & Hui, L. (2011) Induction of functional hepatocyte-like cells from mouse fibroblasts by defined factors. *Nature*. 475 (7356), 386–389.

Hui, A.S., Bauer, A.L., Striet, J.B., Schnell, P.O. & Czyzyk-Krzeska, M.F. (2006) Calcium signaling stimulates translation of HIF-alpha during hypoxia. *The FASEB Journal*. 20 (3), 466–475.

Humphrey, S.J., Azimifar, S.B. & Mann, M. (2015) High-throughput phosphoproteomics reveals in vivo insulin signaling dynamics. *Nature Biotechnology*. 33 (9), 990–995.

Hwang, H.J., Lynn, S.G., Vengellur, A., Saini, Y., Grier, E.A., Ferguson-Miller, S.M. & LaPres, J.J. (2015) Hypoxia Inducible Factors Modulate Mitochondrial Oxygen Consumption and Transcriptional Regulation of Nuclear-Encoded Electron Transport Chain Genes. *Biochemistry*. 54 (24), 3739–3748.

Ichiki, T., Boerrigter, G., Huntley, B.K., Sangaralingham, S.J., McKie, P.M., Harty, G.J., Harders, G.E. & Burnett, J.C. (2013) Differential expression of the pro-natriuretic peptide convertases corin and furin in experimental heart failure and atrial fibrosis. *American journal of physiology. Regulatory, integrative and comparative physiology*. 304 (2), R102–9.

Ihaka, R. & Gentleman, R. (1996) R: A Language for Data Analysis and Graphics. *Journal of Computational and Graphical Statistics*. 5 (3), 299–314.

Ito, N., Ruegg, U.T., Kudo, A., Miyagoe-Suzuki, Y. & Takeda, S. (2013) Activation of calcium signaling through Trpv1 by nNOS and peroxynitrite as a key trigger of skeletal muscle hypertrophy. *Nature Medicine*. 19 (1), 101–106.

Iwata, Y., Katanosaka, Y., Arai, Y., Komamura, K., Miyatake, K. & Shigekawa, M. (2003) A novel mechanism of myocyte degeneration involving the Ca2+-permeable growth factor-regulated channel. *The Journal of Cell Biology*. 161 (5), 957–967.

Jat, P.S., Noble, M.D., Ataliotis, P., Tanaka, Y., Yannoutsos, N., Larsen, L. & Kioussis, D. (1991) Direct derivation of conditionally immortal cell lines from an H-2Kb-tsA58 transgenic mouse. *Proceedings of the National Academy of Sciences of the United States of America*. 88 (12), 5096–5100.

Jeanson-Leh, L., Lameth, J., Krimi, S., Buisset, J., Amor, F., Le Guiner, C., Barthélémy, I., Servais, L., Blot, S., Voit, T. & Israeli, D. (2014) Serum Profiling Identifies Novel Muscle miRNA and Cardiomyopathy-Related miRNA Biomarkers in Golden Retriever Muscular Dystrophy Dogs and Duchenne Muscular Dystrophy Patients. *The American Journal of Pathology*.

Jefferies, J.L., Eidem, B.W., Belmont, J.W., Craigen, W.J., Ware, S.M., Fernbach, S.D., Neish, S.R., Smith, E.O. & Towbin, J.A. (2005) Genetic predictors and remodeling of dilated cardiomyopathy in muscular dystrophy. *Circulation*. 112 (18), 2799–2804.

Jia, Q., Zhang, Q., Zhang, Z., Wang, Y., Zhang, W., Zhou, Y., Wan, Y., Cheng, T., Zhu, X., Fang, X., Yuan, W. & Jia, H. (2013) Transcriptome analysis of the zebrafish model of Diamond-Blackfan anemia from RPS19 deficiency via p53-dependent and -independent pathways. Hatem E Sabaawy (ed.). *PLoS ONE*. 8 (8), e71782.

Jia, Y., Warin, R., Yu, X., Epstein, R. & Noguchi, C.T. (2009) Erythropoietin signaling promotes transplanted progenitor cell survival. *The FASEB Journal*. 23 (9), 3089–3099.

Jiang, T., Yeung, D., Lien, C.-F. & Górecki, D.C. (2005) Localized expression of specific P2X receptors in dystrophin-deficient DMD and mdx muscle. *Neuromuscular Disorders*. 15 (3), 225–236.

Jung, Y.-S., Kim, M.-Y., Kim, M.J., Oh, K.-S., Yi, K.Y., Lee, S., Yoo, S.-E. & Lee, B.H. (2006) Pharmacological profile of KR-33028, a highly selective inhibitor of Na+/H+ exchanger. *European journal of pharmacology*. 535 (1-3), 220–227.

Jørgensen, L.H., Blain, A., Greally, E., Laval, S.H., Blamire, A.M., Davison, B.J., Brinkmeier, H., MacGowan, G.A., Schrøder, H.D., Bushby, K., Straub, V. & Lochmüller, H. (2011) Long-term blocking of calcium channels in mdx mice results in differential effects on heart and skeletal muscle. *The American Journal of Pathology*. 178 (1), 273–283.

Jørgensen, L.H., Larochelle, N., Orlopp, K., Dunant, P., Dudley, R.W.R., Stucka, R., Thirion, C., Walter, M.C., Laval, S.H. & Lochmüller, H. (2009) Efficient and fast functional screening of microdystrophin constructs in vivo and in vitro for therapy of duchenne muscular dystrophy. *Human Gene Therapy*. 20 (6), 641–650.

Kalamajski, S. & Oldberg, A. (2010) The role of small leucine-rich proteoglycans in collagen fibrillogenesis. *Matrix biology : journal of the International Society for Matrix Biology*. 29 (4), 248–253.

Kamo, T., Akazawa, H. & Komuro, I. (2015) Cardiac nonmyocytes in the hub of cardiac hypertrophy. *Circulation Research*. 117 (1), 89–98.

Kanzleiter, T., Rath, M., Görgens, S.W., Jensen, J., Tangen, D.S., Kolnes, A.J., Kolnes, K.J., Lee, S., Eckel, J., Schürmann, A. & Eckardt, K. (2014) The myokine decorin is regulated by contraction and involved in muscle hypertrophy. *Biochemical and Biophysical Research Communications*. 450 (2), 1089–1094.

Katz, Y., Wang, E.T., Airoldi, E.M. & Burge, C.B. (2010) Analysis and design of RNA sequencing experiments for identifying isoform regulation. *Nature Methods*. 7 (12), 1009–1015.

Kay, M.A. (2011) State-of-the-art gene-based therapies: the road ahead. *Nature reviews. Genetics*. 12 (5), 316–328.

Khairallah, M., Khairallah, R.J., Young, M.E., Allen, B.G., Gillis, M.A., Danialou, G., Deschepper, C.F., Petrof, B.J. & Rosiers, Des, C. (2008) Sildenafil and cardiomyocyte-specific cGMP signaling prevent cardiomyopathic changes associated with dystrophin deficiency. *Proceedings of the National Academy of Sciences*. 105 (19), 7028–7033.

Kim, D., Langmead, B. & Salzberg, S.L. (2015) HISAT: a fast spliced aligner with low memory requirements. *Nature Methods*. 12 (4), 357–360.

Kim, D., Pertea, G., Trapnell, C., Pimentel, H., Kelley, R. & Salzberg, S.L. (2013) TopHat2: accurate alignment of transcriptomes in the presence of insertions, deletions and gene fusions. *Genome biology*. 14 (4), R36.

Kim, G.D., Cheong, O.J., Bae, S.Y., Shin, J. & Lee, S.K. (2013) 6"-Debromohamacanthin A, a bis (indole) alkaloid, inhibits angiogenesis by targeting the VEGFR2-mediated PI3K/AKT/mTOR signaling pathways. *Marine drugs*. 11 (4), 1087–1103.

Kim, H.J., Song, S.B., Yang, Y., Eun, Y.S., Cho, B.K., Park, H.J. & Cho, D.H. (2011) Erythroid differentiation regulator 1 (Erdr1) is a proapototic factor in human keratinocytes. *Experimental dermatology*. 20 (11), 920–925.

Kim, S., Campbell, K.A., Fox, D.J., Matthews, D.J., Valdez, R.MD STARnet (2015) Corticosteroid Treatments in Males With Duchenne Muscular Dystrophy: Treatment Duration and Time to Loss of Ambulation. *Journal of child neurology*. 30 (10), 1275–1280.

Kimura, W., Xiao, F., Canseco, D.C., Muralidhar, S., Thet, S., Zhang, H.M., Abdulrahman, Y., Chen, R., Garcia, J.A., Shelton, J.M., Richardson, J.A., Ashour, A.M., Asaithamby, A., Liang, H., Xing, C., Lu, Z., Zhang, C.C. & Sadek, H.A. (2015) Hypoxia fate mapping identifies cycling cardiomyocytes in the adult heart. *Nature*.

Kinali, M., Arechavala-Gomeza, V., Feng, L., Cirak, S., Hunt, D., Adkin, C., Guglieri, M., Ashton, E., Abbs, S., Nihoyannopoulos, P., Garralda, M.E., Rutherford, M., Mcculley, C., Popplewell, L., Graham, I.R., Dickson, G., Wood, M.J.A., Wells, D.J., Wilton, S.D., et al. (2009) Local restoration of dystrophin expression with the morpholino oligomer AVI-4658 in Duchenne muscular dystrophy: a single-blind, placebo-controlled, dose-escalation, proof-of-concept study. *Lancet neurology*. 8 (10), 918–928.

Kinnett, K., Rodger, S., Vroom, E., Furlong, P., Aartsma-Rus, A. & Bushby, K. (2015) Imperatives for DUCHENNE MD: a Simplified Guide to Comprehensive Care for Duchenne Muscular Dystrophy. *PLoS currents*. 7.

Klymiuk, N., Blutke, A., Graf, A., Krause, S., Burkhardt, K., Wuensch, A., Krebs, S., Kessler, B., Zakhartchenko, V., Kurome, M., Kemter, E., Nagashima, H., Schoser, B., Herbach, N., Blum, H., Wanke, R., Aartsma-Rus, A., Thirion, C., Lochmüller, H., et al. (2013) Dystrophin-deficient pigs provide new insights into the hierarchy of physiological derangements of dystrophic muscle. *Human Molecular Genetics*. 22 (21), 4368–4382.

Kobayashi, Y.M., Rader, E.P., Crawford, R.W., Iyengar, N.K., Thedens, D.R., Faulkner, J.A., Parikh, S.V., Weiss, R.M., Chamberlain, J.S., Moore, S.A. & Campbell, K.P. (2008) Sarcolemma-localized nNOS is required to maintain activity after mild exercise. *Nature*. 456 (7221), 511–515.

Kojonazarov, B., Luitel, H., Sydykov, A., Dahal, B.K., Paul-Clark, M.J., Bonvini, S., Reed, A., Schermuly, R.T. & Mitchell, J.A. (2013) The peroxisome proliferator-activated receptor β/δ agonist GW0742 has direct protective effects on right heart hypertrophy. *Pulmonary circulation*. 3 (4), 926–935.

Koller, K.J. & Goeddel, D.V. (1992) Molecular biology of the natriuretic peptides and their receptors. *Circulation*. 86 (4), 1081–1088.

Konno, T., Chen, D., Wang, L., Wakimoto, H., Teekakirikul, P., Nayor, M., Kawana, M., Eminaga, S., Gorham, J.M., Pandya, K., Smithies, O., Naya, F.J., Olson, E.N., Seidman, J.G. & Seidman, C.E. (2010) Heterogeneous myocyte enhancer factor-2 (Mef2) activation in myocytes predicts focal scarring in hypertrophic cardiomyopathy. *Proceedings of the National Academy of Sciences*. 107 (42), 18097–18102.

Krapivinsky, G., Krapivinsky, L., Stotz, S.C., Manasian, Y. & Clapham, D.E. (2011) POST, partner of stromal interaction molecule 1 (STIM1), targets STIM1 to multiple transporters. *Proceedings of the National Academy of Sciences*. 108 (48), 19234–19239.

Kroll, K.W., Mokaram, N.E., Pelletier, A.R., Frankhouser, D.E., Westphal, M.S., Stump, P.A., Stump, C.L., Bundschuh, R., Blachly, J.S. & Yan, P. (2014) Quality Control for RNA-Seq (QuaCRS): An Integrated Quality Control Pipeline. *Cancer informatics*. 13 (Suppl 3), 7–14.

Kuppuswamy, D., Kerr, C., Narishige, T., Kasi, V.S., Menick, D.R. & Cooper, G. (1997) Association of tyrosine-phosphorylated c-Src with the cytoskeleton of hypertrophying myocardium. *Journal of Biological Chemistry*. 272 (7), 4500–4508.

Lai, Y., Zhao, J., Yue, Y. & Duan, D. (2013) α2 and α3 helices of dystrophin R16 and R17 frame a microdomain in the α1 helix of dystrophin R17 for neuronal NOS binding. *Proceedings of the National Academy of Sciences*. 110 (2), 525–530.

Landfeldt, E., Lindgren, P., Bell, C.F., Schmitt, C., Guglieri, M., Straub, V., Lochmüller, H. & Bushby, K. (2015) Compliance to Care Guidelines for Duchenne Muscular Dystrophy. *Journal of Neuromuscular Diseases*. 2.

Lanner, J.T., Georgiou, D.K., Joshi, A.D. & Hamilton, S.L. (2010) Ryanodine receptors: structure, expression, molecular details, and function in calcium release. *Cold Spring Harbor perspectives in biology*. 2 (11), a003996–a003996.

Lattanzi, L., Salvatori, G., Coletta, M., Sonnino, C., Cusella De Angelis, M.G., Gioglio, L., Murry, C.E., Kelly, R., Ferrari, G., Molinaro, M., Crescenzi, M., Mavilio, F. & Cossu, G. (1998) High efficiency myogenic conversion of human fibroblasts by adenoviral vector-mediated MyoD gene transfer. An alternative strategy for ex vivo gene therapy of primary myopathies. *Journal of Clinical Investigation*. 101 (10), 2119–2128.

Le Grand, F. & Rudnicki, M.A. (2007) Skeletal muscle satellite cells and adult myogenesis. *Current opinion in cell biology*. 19 (6), 628–633.

Lee, J.-H., Lee, J.B., Shapovalova, Z., Fiebig-Comyn, A., Mitchell, R.R., Laronde, S., Szabo, E., Benoit, Y.D. & Bhatia, M. (2014) Somatic transcriptome priming gates lineage-specific differentiation potential of human-induced pluripotent stem cell states. *Nature communications*. 55605.

Leo, C., Sala, V., Morello, M., Chiribiri, A., Riess, I., Mancardi, D., Schiaffino, S., Ponzetto, C. & Crepaldi, T. (2011) Activated Met signalling in the developing mouse heart leads to cardiac disease. Harald H H W Schmidt (ed.). *PLoS ONE*. 6 (2), e14675.

Lescroart, F., Chabab, S., Lin, X., Rulands, S., Paulissen, C., Rodolosse, A., Auer, H., Achouri, Y., Dubois, C., Bondue, A., Simons, B.D. & Blanpain, C. (2014) Early lineage restriction in temporally distinct populations of Mesp1 progenitors during mammalian heart development. *Nature Cell Biology*. 16 (9), 829–840.

Leung, D.G., Herzka, D.A., Thompson, W.R., He, B., Bibat, G., Tennekoon, G., Russell, S.D., Schuleri, K.H., Lardo, A.C., Kass, D.A., Thompson, R.E., Judge, D.P. & Wagner, K.R. (2014) Sildenafil does not improve cardiomyopathy in Duchenne/Becker muscular dystrophy. *Annals of Neurology*. 76 (4), 541–549.

Li, F., Yin, J., Yue, T., Liu, L. & Zhang, H. (2010) The CLIC5 (chloride intracellular channel 5) involved in C2C12 myoblasts proliferation and differentiation. *Cell biology international*. 34 (4), 379–384.

Li, H., Mittal, A., Makonchuk, D.Y., Bhatnagar, S. & Kumar, A. (2009) Matrix metalloproteinase-9 inhibition ameliorates pathogenesis and improves skeletal muscle regeneration in muscular dystrophy. *Human Molecular Genetics*. 18 (14), 2584–2598.

Li, J., Hou, R., Niu, X., Liu, R., Wang, Q., Wang, C., Li, X., Hao, Z., Yin, G. & Zhang, K. (2015) Comparison of microarray and RNA-Seq analysis of mRNA expression in dermal mesenchymal stem cells. *Biotechnology letters*. 1–9.

Lin, B., Li, Y., Han, L., Kaplan, A.D., Ao, Y., Kalra, S., Bett, G.C.L., Rasmusson, R.L., Denning, C. & Yang, L. (2015) Modeling and studying mechanism of dilated cardiomyopathy using induced pluripotent stem cells derived from Duchenne Muscular Dystrophy (DMD) patients. *Disease models & mechanisms*.

Liu, Q., Chen, Y., Auger-Messier, M. & Molkentin, J.D. (2012) Interaction between NFκB and NFAT coordinates cardiac hypertrophy and pathological remodeling. *Circulation Research*. 110 (8), 1077–1086.

Lodi, D., Iannitti, T. & Palmieri, B. (2011) Stem cells in clinical practice: applications and warnings. *Journal of experimental & clinical cancer research : CR*. 309.

Longui, C.A. (2007) Glucocorticoid therapy: minimizing side effects. *Jornal de pediatria*. 83 (5 Suppl), S163–77.

Love, M.I., Huber, W. & Anders, S. (2014) Moderated estimation of fold change and dispersion for RNA-seq data with DESeq2. *Genome biology*. 15 (12), 550.

Lu, J., McKinsey, T.A., Nicol, R.L. & Olson, E.N. (2000) Signal-dependent activation of the MEF2 transcription factor by dissociation from histone deacetylases. *Proceedings of the National Academy of Sciences of the United States of America*. 97 (8), 4070–4075.

Lu, Q.L., Mann, C.J., Lou, F., Bou-Gharios, G., Morris, G.E., Xue, S.-A., Fletcher, S., Partridge, T.A. & Wilton, S.D. (2003) Functional amounts of dystrophin produced by skipping the mutated exon in the mdx dystrophic mouse. *Nature Medicine*. 9 (8), 1009–1014.

Lu, Z., Xu, X., Hu, X., Zhu, G., Zhang, P., van Deel, E.D., French, J.P., Fassett, J.T., Oury, T.D., Bache, R.J. & Chen, Y. (2008) Extracellular superoxide dismutase deficiency exacerbates pressure overload-induced left ventricular hypertrophy and dysfunction. *Hypertension*. 51 (1), 19–25.

Lyons, G.E. (1996) Vertebrate heart development. *Current opinion in genetics & development*. 6 (4), 454–460.

MacLennan, D.H. & Kranias, E.G. (2003) Phospholamban: a crucial regulator of cardiac contractility. *Nature Reviews Molecular Cell Biology*. 4 (7), 566–577.

Maekawa, M., Yamaguchi, K., Nakamura, T., Shibukawa, R., Kodanaka, I., Ichisaka, T., Kawamura, Y., Mochizuki, H., Goshima, N. & Yamanaka, S. (2011) Direct reprogramming of somatic cells is promoted by maternal transcription factor Glis1. *Nature*. 474 (7350), 225–229.

Maillet, M., van Berlo, J.H. & Molkentin, J.D. (2013) Molecular basis of physiological heart growth: fundamental concepts and new players. *Nature Reviews Molecular Cell Biology*. 14 (1), 38–48.

Maltsev, V.A., Wobus, A.M., Rohwedel, J., Bader, M. & Hescheler, J. (1994) Cardiomyocytes differentiated in vitro from embryonic stem cells developmentally express cardiac-specific genes and ionic currents. *Circulation Research*. 75 (2), 233–244.

Maroto, M., Reshef, R., Munsterberg, A.E., Koester, S., Goulding, M. & Lassar, A.B. (1997) Ectopic Pax-3 activates MyoD and Myf-5 expression in embryonic mesoderm and neural tissue. *Cell*. 89 (1), 139–148.

Martin, E.A., Barresi, R., Byrne, B.J., Tsimerinov, E.I., Scott, B.L., Walker, A.E., Gurudevan, S.V., Anene, F., Elashoff, R.M., Thomas, G.D. & Victor, R.G. (2012) Tadalafil alleviates muscle ischemia in patients with Becker muscular dystrophy. *Science translational medicine*. 4 (162), 162ra155–162ra155.

Matsumura, K., Ervasti, J.M., Ohlendieck, K., Kahl, S.D. & Campbell, K.P. (1992) Association of dystrophin-related protein with dystrophin-associated proteins in mdx mouse muscle. *Nature*. 360 (6404), 588–591.

Mauro, A. (1961) Satellite cell of skeletal muscle fibers. *The Journal of biophysical and biochemical cytology*. 9 (2), 493–495.

Mayhew, A., Cano, S., Scott, E., Eagle, M., Bushby, K., Muntoni, F.North Star Clinical Network for Paediatric Neuromuscular Disease (2011) Moving towards meaningful measurement: Rasch analysis of the North Star Ambulatory Assessment in Duchenne muscular dystrophy. *Developmental medicine and child neurology*. 53 (6), 535–542.

Mendell, J.R., Campbell, K., Rodino-Klapac, L., Sahenk, Z., Shilling, C., Lewis, S., Bowles, D., Gray, S., Li, C., Galloway, G., Malik, V., Coley, B., Clark, K.R., Li, J., Xiao, X., Samulski, J., McPhee, S.W., Samulski, R.J. & Walker, C.M. (2010) Dystrophin immunity in Duchenne's muscular dystrophy. *The New England journal of medicine*. 363 (15), 1429–1437.

Mendell, J.R., Rodino-Klapac, L., Sahenk, Z., Malik, V., Kaspar, B.K., Walker, C.M. & Clark, K.R. (2012) Gene therapy for muscular dystrophy: lessons learned and path forward. *Neuroscience letters*. 527 (2), 90–99.

Mendell, J.R., Rodino-Klapac, L.R., Sahenk, Z., Roush, K., Bird, L., Lowes, L.P., Alfano, L., Gomez, A.M., Lewis, S., Kota, J., Malik, V., Shontz, K., Walker, C.M., Flanigan, K.M., Corridore, M., Kean, J.R., Allen, H.D., Shilling, C., Melia, K.R., et al. (2013) Eteplirsen for the treatment of Duchenne muscular dystrophy. *Annals of Neurology*. 74 (5), 637–647.

Merly, F., Lescaudron, L., Rouaud, T., Crossin, F. & Gardahaut, M.F. (1999) Macrophages enhance muscle satellite cell proliferation and delay their differentiation. *Muscle & Nerve*. 22 (6), 724–732.

Messina, S., Altavilla, D., Aguennouz, M., Seminara, P., Minutoli, L., Monici, M.C., Bitto, A., Mazzeo, A., Marini, H., Squadrito, F. & Vita, G. (2006) Lipid peroxidation inhibition blunts nuclear factor-kappaB activation, reduces skeletal muscle degeneration, and enhances muscle function in mdx mice. *AJPA*. 168 (3), 918–926.

Messina, S., Mazzeo, A., Bitto, A., Aguennouz, M., Migliorato, A., De Pasquale, M.G., Minutoli, L., Altavilla, D., Zentilin, L., Giacca, M., Squadrito, F. & Vita, G. (2007) VEGF overexpression via adeno-associated virus gene transfer promotes skeletal muscle regeneration and enhances muscle function in mdx mice. *The FASEB Journal*. 21 (13), 3737–3746.

Mezo, A.R., McDonnell, K.A., Low, S.C., Song, J., Reidy, T.J., Lu, Q., Amari, J.V., Hoehn, T., Peters, R.T., Dumont, J. & Bitonti, A.J. (2012) Atrial natriuretic peptide-Fc, ANP-Fc, fusion proteins: semisynthesis, in vitro activity and pharmacokinetics in rats. *Bioconjugate chemistry*. 23 (3), 518–526.

Michelfelder, S., Varadi, K., Raupp, C., Hunger, A., Körbelin, J., Pahrmann, C., Schrepfer, S., Müller, O.J., Kleinschmidt, J.A. & Trepel, M. (2011) Peptide ligands incorporated into the threefold spike capsid domain to re-direct gene transduction of AAV8 and AAV9 in vivo. *PLoS ONE*. 6 (8), e23101.

Millay, D.P., Goonasekera, S.A., Sargent, M.A., Maillet, M., Aronow, B.J. & Molkentin, J.D. (2009) Calcium influx is sufficient to induce muscular dystrophy through a TRPC-dependent mechanism. *Proceedings of the National Academy of Sciences*. 106 (45), 19023–19028.

Millay, D.P., O'Rourke, J.R., Sutherland, L.B., Bezprozvannaya, S., Shelton, J.M., Bassel-Duby, R. & Olson, E.N. (2013) Myomaker is a membrane activator of myoblast fusion and muscle formation. *Nature*. 499 (7458), 301–305.

Moisset, P.A., Gagnon, Y., Karpati, G. & Tremblay, J.P. (1998) Expression of human dystrophin following the transplantation of genetically modified mdx myoblasts. *Gene therapy*. 5 (10), 1340–1346.

Mokri, B. & Engel, A.G. (1975) Duchenne dystrophy: electron microscopic findings pointing to a basic or early abnormality in the plasma membrane of the muscle fiber. *Neurology*. 25 (12), 1111–1120.

Molkentin, J.D., Lu, J.R., Antos, C.L., Markham, B., Richardson, J., Robbins, J., Grant, S.R. & Olson, E.N. (1998) A calcineurin-dependent transcriptional pathway for cardiac hypertrophy. *Cell*. 93 (2), 215–228.

Montarras, D., Morgan, J., Collins, C., Relaix, F., Zaffran, S., Cumano, A., Partridge, T. & Buckingham, M. (2005) Direct isolation of satellite cells for skeletal muscle regeneration. *Science*. 309 (5743), 2064–2067.

Morgan, J.E., Beauchamp, J.R., Pagel, C.N., Peckham, M., Ataliotis, P., Jat, P.S., Noble, M.D., Farmer, K. & Partridge, T.A. (1994) Myogenic cell lines derived from transgenic mice carrying a thermolabile T antigen: a model system for the derivation of tissue-specific and mutation-specific cell lines. *Developmental biology*. 162 (2), 486–498.

Mosqueira, M., Zeiger, U., Förderer, M., Brinkmeier, H. & Fink, R.H.A. (2013) Cardiac and respiratory dysfunction in Duchenne muscular dystrophy and the role of second messengers. *Medicinal research reviews*. 33 (5), 1174–1213.

Mouawad, R., Li, Y. & Anand-Srivastava, M.B. (2004) Atrial natriuretic peptide-C receptor-induced attenuation of adenylyl cyclase signaling activates phosphatidylinositol turnover in A10 vascular smooth muscle cells. *Molecular pharmacology*. 65 (4), 917–924.

Muntoni, F. & Wood, M.J.A. (2011) Targeting RNA to treat neuromuscular disease. *Nature reviews. Drug discovery*. 10 (8), 621–637.

Muses, S., Morgan, J.E. & Wells, D.J. (2011) A new extensively characterised conditionally immortal muscle cell-line for investigating therapeutic strategies in muscular dystrophies. *PLoS ONE*. 6 (9), e24826.

Nadarajah, V.D., van Putten, M., Chaouch, A., Garrood, P., Straub, V., Lochmuller, H., Ginjaar, H.B., Aartsma-Rus, A.M., van Ommen, G.J.B., Dunnen, den, J.T. & 't Hoen, P.A.C. (2011) Serum matrix metalloproteinase-9 (MMP-9) as a biomarker for monitoring disease progression in Duchenne muscular dystrophy (DMD). *Neuromuscular disorders : NMD*. 21 (8), 569–578.

Nagata, Y., Partridge, T.A., Matsuda, R. & Zammit, P.S. (2006) Entry of muscle satellite cells into the cell cycle requires sphingolipid signaling. *The Journal of Cell Biology*. 174 (2), 245–253.

Nance, M.E. & Duan, D. (2015) Perspective on Adeno-Associated Virus (AAV) Capsid Modification for Duchenne Muscular Dystrophy Gene Therapy. *Human Gene Therapy*. hum.2015.107.

Neishabouri, S.H., Hutson, S.M. & Davoodi, J. (2015) Chronic activation of mTOR complex 1 by branched chain amino acids and organ hypertrophy. *Amino acids*. 47 (6), 1167–1182.

Nelson, M.D., Rader, F., Tang, X., Tavyev, J., Nelson, S.F., Miceli, M.C., Elashoff, R.M., Sweeney, H.L. & Victor, R.G. (2014) PDE5 inhibition alleviates functional muscle ischemia in boys with Duchenne muscular dystrophy. *Neurology*. 82 (23), 2085–2091.

Nesbeth, D., Williams, S.L., Chan, L., Brain, T., Slater, N.K.H., Farzaneh, F. & Darling, D. (2006) Metabolic biotinylation of lentiviral pseudotypes for scalable paramagnetic microparticle-dependent manipulation. *Molecular Therapy*. 13 (4), 814–822.

Nesvizhskii, A.I. (2014) Proteogenomics: concepts, applications and computational strategies. *Nature Methods*. 11 (11), 1114–1125.

Nowak, D., Kozlowska, H., Gielecki, J.S., Rowinski, J., Zurada, A., Goralczyk, K. & Bozilow, W. (2011) Cardiomyopathy in the mouse model of Duchenne muscular dystrophy caused by disordered secretion of vascular endothelial growth factor. *Medical science monitor : international medical journal of experimental and clinical research*. 17 (11), BR332–338.

Ogata, H., Goto, S., Sato, K., Fujibuchi, W., Bono, H. & Kanehisa, M. (1999) KEGG: Kyoto Encyclopedia of Genes and Genomes. *Nucleic acids research*. 27 (1), 29–34.

Ogata, H., Ishikawa, Y., Ishikawa, Y. & Minami, R. (2009) Beneficial effects of beta-blockers and angiotensin-converting enzyme inhibitors in Duchenne muscular dystrophy. *Journal of cardiology*. 53 (1), 72–78.

Oka, T., Xu, J. & Molkentin, J.D. (2007) Re-employment of developmental transcription factors in adult heart disease. *Seminars in cell & developmental biology*. 18 (1), 117–131.

Okada, T. & Takeda, S. (2013) Current Challenges and Future Directions in Recombinant AAV-Mediated Gene Therapy of Duchenne Muscular Dystrophy. *Pharmaceuticals (Basel, Switzerland)*. 6 (7), 813–836.

Ono, Y., Calhabeu, F., Morgan, J.E., Katagiri, T., Amthor, H. & Zammit, P.S. (2011) BMP signalling permits population expansion by preventing premature myogenic differentiation in muscle satellite cells. *Cell death and differentiation*. 18 (2), 222–234.

Onopiuk, M., Brutkowski, W., Young, C., Krasowska, E., Róg, J., Ritso, M., Wojciechowska, S., Arkle, S., Zabłocki, K. & Górecki, D.C. (2015) Store-operated calcium entry contributes to abnormal Ca(2+) signalling in dystrophic mdx mouse myoblasts. *Archives of biochemistry and biophysics*. 5691–9.

Ozawa, E., Hagiwara, Y. & Yoshida, M. (1999) Creatine kinase, cell membrane and Duchenne muscular dystrophy. *Molecular and cellular biochemistry*. 190 (1-2), 143–151.

Pan, Z.-W., Lu, Y.-J. & Yang, B.-F. (2010) MicroRNAs: a novel class of potential therapeutic targets for cardiovascular diseases. *Acta pharmacologica Sinica*. 31 (1), 1–9.

Pang, Z.P., Yang, N., Vierbuchen, T., Ostermeier, A., Fuentes, D.R., Yang, T.Q., Citri, A., Sebastiano, V., Marro, S., Südhof, T.C. & Wernig, M. (2011) Induction of human neuronal cells by defined transcription factors. *Nature*. 476 (7359), 220–223.

Parker, M.H., Seale, P. & Rudnicki, M.A. (2003) Looking back to the embryo: defining transcriptional networks in adult myogenesis. *Nature Publishing Group*. 4 (7), 497–507.

Parodi, E.M. & Kuhn, B. (2014) Signalling between microvascular endothelium and cardiomyocytes through neuregulin. *Cardiovascular research*. 102 (2), 194–204.

Patrizio, M., Musumeci, M., Stati, T., Fasanaro, P., Palazzesi, S., Catalano, L. & Marano, G. (2007) Propranolol causes a paradoxical enhancement of cardiomyocyte foetal gene response to hypertrophic stimuli. *British journal of pharmacology*. 152 (2), 216–222.

Penton, C.M., Thomas-Ahner, J.M., Johnson, E.K., McAllister, C. & Montanaro, F. (2013) Muscle side population cells from dystrophic or injured muscle adopt a fibro-adipogenic fate. Atsushi Asakura (ed.). *PLoS ONE*. 8 (1), e54553.

Petrof, B.J., Shrager, J.B., Stedman, H.H., Kelly, A.M. & Sweeney, H.L. (1993) Dystrophin protects the sarcolemma from stresses developed during muscle contraction. *Proceedings of the National Academy of Sciences of the United States of America*. 90 (8), 3710–3714.

Pérez, N.G., Piaggio, M.R., Ennis, I.L., Garciarena, C.D., Morales, C., Escudero, E.M., Cingolani, O.H., Chiappe de Cingolani, G., Yang, X.-P. & Cingolani, H.E. (2007) Phosphodiesterase 5A inhibition induces Na+/H+ exchanger blockade and protection against myocardial infarction. *Hypertension*. 49 (5), 1095–1103.

Pilbrow, A.P., Ellmers, L.J., Black, M.A., Moravec, C.S., Sweet, W.E., Troughton, R.W., Richards, A.M., Frampton, C.M. & Cameron, V.A. (2008) Genomic selection of reference genes for real-time PCR in human myocardium. *BMC medical genomics*. 164.

Pleasure, D. (2011) Advances in translational research in neuromuscular diseases. *Archives of neurology*. 68 (4), 429–433.

Rajabi, M., Kassiotis, C., Razeghi, P. & Taegtmeyer, H. (2007) Return to the fetal gene program protects the stressed heart: a strong hypothesis. *Heart failure reviews*. 12 (3-4), 331–343.

Ramachandran, J., Schneider, J.S., Crassous, P.A., Zheng, R., Gonzalez, J.P., Xie, L.H., Beuve, A., Fraidenraich, D. & Peluffo, R.D. (2012) Nitric oxide signalling pathway in Duchenne muscular dystrophy mice: up-regulation of L-arginine transporters. *Biochemical Journal*. 449 (1), 133–142.

Rando, T.A. (2001) The dystrophin-glycoprotein complex, cellular signaling, and the regulation of cell survival in the muscular dystrophies. *Muscle & Nerve*. 24 (12), 1575–1594.

Rao, N.A.S., McCalman, M.T., Moulos, P., Francoijs, K.-J., Chatziioannou, A., Kolisis, F.N., Alexis, M.N., Mitsiou, D.J. & Stunnenberg, H.G. (2011) Coactivation of GR and NFKB alters the repertoire of their binding sites and target genes. *Genome research*. 21 (9), 1404–1416.

Reeves, E.K.M., Hoffman, E.P., Nagaraju, K., Damsker, J.M. & McCall, J.M. (2013) VBP15: preclinical characterization of a novel anti-inflammatory delta 9,11 steroid. *Bioorganic & medicinal chemistry*. 21 (8), 2241–2249.

Ren, M.-Y. & Sui, S.-J. (2012) The role of TWEAK/Fn14 in cardiac remodeling. *Molecular biology reports*. 39 (11), 9971–9977.

Ren, R., Oakley, R.H., Cruz-Topete, D. & Cidlowski, J.A. (2012) Dual role for glucocorticoids in cardiomyocyte hypertrophy and apoptosis. *Endocrinology*. 153 (11), 5346–5360.

Reshef, R., Maroto, M. & Lassar, A.B. (1998) Regulation of dorsal somitic cell fates: BMPs and Noggin control the timing and pattern of myogenic regulator expression. *Genes & Development*. 12 (3), 290–303.

Ricotti, V., Ridout, D.A., Scott, E., Quinlivan, R., Robb, S.A., Manzur, A.Y., Muntoni, F.NorthStar Clinical Network (2013) Long-term benefits and adverse effects of intermittent versus daily glucocorticoids in boys with Duchenne muscular dystrophy. *Journal of neurology, neurosurgery, and psychiatry*. 84 (6), 698–705.

Rikka, S., Quinsay, M.N., Thomas, R.L., Kubli, D.A., Zhang, X., Murphy, A.N. & Gustafsson, Å.B. (2011) Bnip3 impairs mitochondrial bioenergetics and stimulates mitochondrial turnover. *Cell death and differentiation*. 18 (4), 721–731.

Rochais, F., Mesbah, K. & Kelly, R.G. (2009) Signaling pathways controlling second heart field development. *Circulation Research*. 104 (8), 933–942.

Roest, P.A., van der Tuijn, A.C., Ginjaar, H.B., Hoeben, R.C., Hoger-Vorst, F.B., Bakker, E., Dunnen, den, J.T. & van Ommen, G.J. (1996) Application of in vitro Myo-differentiation of non-muscle cells to enhance gene expression and facilitate analysis of muscle proteins. *Neuromuscular Disorders*. 6 (3), 195–202.

Romfh, A. & Mcnally, E.M. (2010) Cardiac assessment in duchenne and becker muscular dystrophies. *Current heart failure reports*. 7 (4), 212–218.

Rosenberg, A.S., Puig, M., Nagaraju, K., Hoffman, E.P., Villalta, S.A., Rao, V.A., Wakefield, L.M. & Woodcock, J. (2015) Immune-mediated pathology in Duchenne muscular dystrophy. *Science translational medicine*. 7 (299), 299rv4.

Rowell, J., Koitabashi, N. & Kass, D.A. (2010) TRP-ing up heart and vessels: canonical transient receptor potential channels and cardiovascular disease. *Journal of cardiovascular translational research*. 3 (5), 516–524.

Rybkin, I.I., Markham, D.W., Yan, Z., Bassel-Duby, R., Williams, R.S. & Olson, E.N. (2003) Conditional expression of SV40 T-antigen in mouse cardiomyocytes facilitates an inducible switch from proliferation to differentiation. *Journal of Biological Chemistry*. 278 (18), 15927–15934.

Saito, S., Hiroi, Y., Zou, Y., Aikawa, R., Toko, H., Shibasaki, F., Yazaki, Y., Nagai, R. & Komuro, I. (2000) beta-Adrenergic pathway induces apoptosis through calcineurin activation in cardiac myocytes. *Journal of Biological Chemistry*. 275 (44), 34528–34533.

Sali, A., Guerron, A.D., Gordish-Dressman, H., Spurney, C.F., Iantorno, M., Hoffman, E.P. & Nagaraju, K. (2012) Glucocorticoid-treated mice are an inappropriate positive control for long-term preclinical studies in the mdx mouse. Thomas H Gillingwater (ed.). *PLoS ONE*. 7 (4), e34204.

Salva, M.Z., Himeda, C.L., Tai, P.W., Nishiuchi, E., Gregorevic, P., Allen, J.M., Finn, E.E., Nguyen, Q.G., Blankinship, M.J., Meuse, L., Chamberlain, J.S. & Hauschka, S.D. (2007) Design of tissue-specific regulatory cassettes for high-level rAAV-mediated expression in skeletal and cardiac muscle. *Molecular Therapy*. 15 (2), 320–329.

Sampaolesi, M., Blot, S., D'antona, G., Granger, N., Tonlorenzi, R., Innocenzi, A., Mognol, P., Thibaud, J.-L., Galvez, B.G., Barthélémy, I., Perani, L., Mantero, S., Guttinger, M., Pansarasa, O., Rinaldi, C., Cusella De Angelis, M.G., Torrente, Y., Bordignon, C., Bottinelli, R., et al. (2006) Mesoangioblast stem cells ameliorate muscle function in dystrophic dogs. *Nature*. 444 (7119), 574–579.

Sampaolesi, M., Torrente, Y., Innocenzi, A., Tonlorenzi, R., D'antona, G., Pellegrino, M.A., Barresi, R., Bresolin, N., De Angelis, M.G.C., Campbell, K.P., Bottinelli, R. & Cossu, G. (2003) Cell therapy of alpha-sarcoglycan null dystrophic mice through intra-arterial delivery of mesoangioblasts. *Science*. 301 (5632), 487–492.

Sandonà, D. & Betto, R. (2009) Sarcoglycanopathies: molecular pathogenesis and therapeutic prospects. *Expert reviews in molecular medicine*. 11e28.

Schinkel, S., Bauer, R., Bekeredjian, R., Stucka, R., Rutschow, D., Lochmüller, H., Kleinschmidt, J.A., Katus, H.A. & Müller, O.J. (2012) Long-Term Preservation of Cardiac Structure and Function After Adeno-Associated Virus Serotype 9-Mediated Microdystrophin Gene Transfer in mdx Mice. *Human Gene Therapy*. 23 (6), 566–575.

Schlüter, K.-D. & Wenzel, S. (2008) Angiotensin II: a hormone involved in and contributing to pro-hypertrophic cardiac networks and target of anti-hypertrophic cross-talks. *Pharmacology & therapeutics*. 119 (3), 311–325.

Sciorati, C., Staszewsky, L., Zambelli, V., Russo, I., Salio, M., Novelli, D., Di Grigoli, G., Moresco, R.M., Clementi, E. & Latini, R. (2013) Ibuprofen plus isosorbide dinitrate treatment in the mdx mice ameliorates dystrophic heart structure. *Pharmacological research : the official journal of the Italian Pharmacological Society*. 7335–43.

Scott, J.M., Li, S., Harper, S.Q., Welikson, R., Bourque, D., DelloRusso, C., Hauschka, S.D. & Chamberlain, J.S. (2002) Viral vectors for gene transfer of micro-, mini-, or full-length dystrophin. *Neuromuscular Disorders*. 12 Suppl 1S23–9.

Seale, P., Sabourin, L.A., Girgis-Gabardo, A., Mansouri, A., Gruss, P. & Rudnicki, M.A. (2000) Pax7 is required for the specification of myogenic satellite cells. *Cell*. 102 (6), 777–786.

Sekiya, S. & Suzuki, A. (2011) Direct conversion of mouse fibroblasts to hepatocyte-like cells by defined factors. *Nature*. 475 (7356), 390–393.

Semenov, A.G., Seferian, K.R., Tamm, N.N., Artem'eva, M.M., Postnikov, A.B., Bereznikova, A.V., Kara, A.N., Medvedeva, N.A. & Katrukha, A.G. (2011) Human pro-B-type natriuretic peptide is processed in the circulation in a rat model. *Clinical chemistry*. 57 (6), 883–890.

Semenza, G.L. (2014) Hypoxia-inducible factor 1 and cardiovascular disease. *Annual review of physiology*. 76 (1), 39–56.

Shelton, M., Kocharyan, A., Liu, J., Skerjanc, I.S. & Stanford, W.L. (2015) Robust generation and expansion of skeletal muscle progenitors and myocytes from human pluripotent stem cells. *Methods (San Diego, Calif.)*.

Sherwood, R.I., Christensen, J.L., Conboy, I.M., Conboy, M.J., Rando, T.A., Weissman, I.L. & Wagers, A.J. (2004) Isolation of adult mouse myogenic progenitors: functional heterogeneity of cells within and engrafting skeletal muscle. *Cell*. 119 (4), 543–554.

Shimizu-Motohashi, Y. & Asakura, A. (2014) Angiogenesis as a novel therapeutic strategy for Duchenne muscular dystrophy through decreased ischemia and increased satellite cells. *Frontiers in physiology*. 550.

Sicinski, P., Geng, Y., Ryder-Cook, A.S., Barnard, E.A., Darlison, M.G. & Barnard, P.J. (1989) The molecular basis of muscular dystrophy in the mdx mouse: a point mutation. *Science*. 244 (4912), 1578–1580.

Sinadinos, A., Young, C.N.J., Al-Khalidi, R., Teti, A., Kalinski, P., Mohamad, S., Floriot, L., Henry, T., Tozzi, G., Jiang, T., Wurtz, O., Lefebvre, A., Shugay, M., Tong, J., Vaudry, D., Arkle, S., doRego, J.-C. & Górecki, D.C. (2015) P2RX7 Purinoceptor: A Therapeutic Target for Ameliorating the Symptoms of Duchenne Muscular Dystrophy. Gary Peltz (ed.). *PLoS medicine*. 12 (10), e1001888.

Sirbu, I.O., Zhao, X. & Duester, G. (2008) Retinoic acid controls heart anteroposterior patterning by down-regulating Isl1 through the Fgf8 pathway. *Developmental Dynamics*. 237 (6), 1627–1635.

Smythe, G.M. (2009) Dystrophic pathology in the intrinsic and extrinsic laryngeal muscles in the mdx mouse. *Journal of otolaryngology - head & neck surgery = Le Journal d'oto-rhino-laryngologie et de chirurgie cervico-faciale*. 38 (3), 323–336.

Sodi, R., Dubuis, E., Shenkin, A. & Hart, G. (2008) B-type natriuretic peptide (BNP) attenuates the L-type calcium current and regulates ventricular myocyte function. *Regulatory peptides*. 151 (1-3), 95–105.

Song, H.K., Kim, J., Lee, J.S., Nho, K.J., Jeong, H.C., Kim, J., Ahn, Y., Park, W.J. & Kim, D.H. (2015) Pik3ip1 modulates cardiac hypertrophy by inhibiting PI3K pathway. Luc Bertrand (ed.). *PLoS ONE*. 10 (3), e0122251.

Soria-Valles, C., Gutiérrez-Fernández, A., Guiu, M., Mari, B., Fueyo, A., Gomis, R.R. & López-Otín, C. (2014) The anti-metastatic activity of collagenase-2 in breast cancer cells is mediated by a signaling pathway involving decorin and miR-21. *Oncogene*. 33 (23), 3054–3063.

Spinale, F.G. & Villarreal, F. (2014) Targeting matrix metalloproteinases in heart disease: lessons from endogenous inhibitors. *Biochemical pharmacology*. 90 (1), 7–15.

Spurney, C.F., Knoblach, S., Pistilli, E.E., Nagaraju, K., Martin, G.R. & Hoffman, E.P. (2008) Dystrophin-deficient cardiomyopathy in mouse: expression of Nox4 and Lox are associated with fibrosis and altered functional parameters in the heart. *Neuromuscular Disorders*. 18 (5), 371–381.

Spurney, C.F., Sali, A., Guerron, A.D., Iantorno, M., Yu, Q., Gordish-Dressman, H., Rayavarapu, S., van der Meulen, J., Hoffman, E.P. & Nagaraju, K. (2011) Losartan decreases cardiac muscle fibrosis and improves cardiac function in dystrophin-deficient mdx mice. *Journal of cardiovascular pharmacology and therapeutics*. 16 (1), 87–95.

Sreejit, P., Kumar, S. & Verma, R.S. (2008) An improved protocol for primary culture of cardiomyocyte from neonatal mice. *In vitro cellular & developmental biology Animal*. 44 (3-4), 45–50.

Stone, M.R., O'Neill, A., Catino, D. & Bloch, R.J. (2005) *Specific Interaction of the Actin-binding Domain of Dystrophin with Intermediate Filaments Containing Keratin 19*.

Strober, J.B. (2006) Therapeutics in duchenne muscular dystrophy. *NeuroRx : the journal of the American Society for Experimental NeuroTherapeutics*. 3 (2), 225–234.

Sussman, M. (2002) Duchenne muscular dystrophy. *The Journal of the American Academy of Orthopaedic Surgeons*. 10 (2), 138–151.

Taegtmeyer, H., Sen, S. & Vela, D. (2010) Return to the fetal gene program: a suggested metabolic link to gene expression in the heart. *Annals of the New York Academy of Sciences*. 1188191–198.

Taigen, T., De Windt, L.J., Lim, H.W. & Molkentin, J.D. (2000) Targeted inhibition of calcineurin prevents agonist-induced cardiomyocyte hypertrophy. *Proceedings of the National Academy of Sciences of the United States of America*. 97 (3), 1196–1201.

Taimeh, Z., Loughran, J., Birks, E.J. & Bolli, R. (2013) Vascular endothelial growth factor in heart failure. *Nature reviews. Cardiology*. 10 (9), 519–530.

Takahashi, K. & Yamanaka, S. (2006) Induction of pluripotent stem cells from mouse embryonic and adult fibroblast cultures by defined factors. *Cell*. 126 (4), 663–676.

Takahashi, K., Tanabe, K., Ohnuki, M., Narita, M., Ichisaka, T., Tomoda, K. & Yamanaka, S. (2007) Induction of pluripotent stem cells from adult human fibroblasts by defined factors. *Cell*. 131 (5), 861–872.

Takeuchi, F., Yonemoto, N., Nakamura, H., Shimizu, R., Komaki, H., Mori-Yoshimura, M., Hayashi, Y.K., Nishino, I., Kawai, M., Kimura, E. & Takeda, S. (2013) Prednisolone improves walking in Japanese Duchenne muscular dystrophy patients. *Journal of neurology*. 260 (12), 3023–3029.

Takeuchi, J.K., Ohgi, M., Koshiba-Takeuchi, K., Shiratori, H., Sakaki, I., Ogura, K., Saijoh, Y. & Ogura, T. (2003) Tbx5 specifies the left/right ventricles and ventricular septum position during cardiogenesis. *Development*. 130 (24), 5953–5964.

Tamir, Y. & Bengal, E. (1998) p53 protein is activated during muscle differentiation and participates with MyoD in the transcription of muscle creatine kinase gene. *Oncogene*. 17 (3), 347–356.

Tang, Y., Cummins, J., Huard, J. & Wang, B. (2010) AAV-directed muscular dystrophy gene therapy. *Expert opinion on biological therapy*. 10 (3), 395–408.

Tarnopolsky, M. & Martin, J. (1999) Creatine monohydrate increases strength in patients with neuromuscular disease. *Neurology*. 52 (4), 854–857.

Tello, D., Balsa, E., Acosta-Iborra, B., Fuertes-Yebra, E., Elorza, A., Ordóñez, Á., Corral-Escariz, M., Soro, I., López-Bernardo, E., Perales-Clemente, E., Martínez-Ruiz, A., Enríquez, J.A., Aragonés, J., Cadenas, S. & Landázuri, M.O. (2011) Induction of the mitochondrial NDUFA4L2 protein by HIF-1α decreases oxygen consumption by inhibiting Complex I activity. *Cell metabolism*. 14 (6), 768–779.

Thomson, J.A., Itskovitz-Eldor, J., Shapiro, S.S., Waknitz, M.A., Swiergiel, J.J., Marshall, V.S. & Jones, J.M. (1998) Embryonic stem cell lines derived from human blastocysts. *Science*. 282 (5391), 1145–1147.

Thorvaldsdóttir, H., Robinson, J.T. & Mesirov, J.P. (2013) Integrative Genomics Viewer (IGV): high-performance genomics data visualization and exploration. *Briefings in bioinformatics*. 14 (2), 178–192.

Torrente, Y., Belicchi, M., Marchesi, C., Dantona, G., Cogiamanian, F., Pisati, F., Gavina, M., Giordano, R., Tonlorenzi, R., Fagiolari, G., Lamperti, C., Porretti, L., Lopa, R., Sampaolesi, M., Vicentini, L., Grimoldi, N., Tiberio, F., Songa, V., Baratta, P., et al. (2007) Autologous transplantation of muscle-derived CD133+ stem cells in Duchenne muscle patients. *Cell transplantation*. 16 (6), 563–577.

Townsend, D., Yasuda, S., Li, S., Chamberlain, J.S. & Metzger, J.M. (2008) Emergent dilated cardiomyopathy caused by targeted repair of dystrophic skeletal muscle. *Molecular Therapy*. 16 (5), 832–835.

Townsend, D., Yasuda, S., McNally, E. & Metzger, J.M. (2011) Distinct pathophysiological mechanisms of cardiomyopathy in hearts lacking dystrophin or the sarcoglycan complex. *The FASEB Journal*. 25 (9), 3106–3114.

Trollet, C., Athanasopoulos, T., Popplewell, L., Malerba, A. & Dickson, G. (2009) Gene therapy for muscular dystrophy: current progress and future prospects. *Expert opinion on biological therapy*. 9 (7), 849–866.

Tzahor, E. & Evans, S.M. (2011) Pharyngeal mesoderm development during embryogenesis: implications for both heart and head myogenesis. *Cardiovascular research*. 91 (2), 196–202.

Valadares, M.C., Gomes, J.P., Castello, G., Assoni, A., Pellati, M., Bueno, C., Corselli, M., Silva, H., Bartolini, P., Vainzof, M., Margarido, P.F., Baracat, E., Péault, B. & Zatz, M. (2014) Human adipose tissue derived pericytes increase life span in Utrn (tm1Ked) Dmd (mdx) /J mice. *Stem Cell Reviews and Reports*. 10 (6), 830–840.

Van Vliet, P., Wu, S.M., Zaffran, S. & Pucéat, M. (2012) Early cardiac development: a view from stem cells to embryos. *Cardiovascular research*. 96 (3), 352–362.

Vandebrouck, A., Ducret, T., Basset, O., Sebille, S., Raymond, G., Ruegg, U., Gailly, P., Cognard, C. & Constantin, B. (2006) Regulation of store-operated calcium entries and mitochondrial uptake by minidystrophin expression in cultured myotubes. *The FASEB Journal*. 20 (1), 136–138.

Vandebrouck, C., Martin, D., Colson-Van Schoor, M., Debaix, H. & Gailly, P. (2002) Involvement of TRPC in the abnormal calcium influx observed in dystrophic (mdx) mouse skeletal muscle fibers. *The Journal of Cell Biology*. 158 (6), 1089–1096.

Vitiello, L., Bassi, N., Campagnolo, P., Zaccariotto, E., Occhi, G., Malerba, A., Pigozzo, S., Reggiani, C., Ausoni, S., Zaglia, T., Gamba, P., Baroni, M.D. & Ditadi, A.P. (2008) In vivo delivery of naked antisense oligos in aged mdx mice: analysis of dystrophin restoration in skeletal and cardiac muscle. *Neuromuscular Disorders*. 18 (8), 597–605.

Voisin, V., Sébrié, C., Matecki, S., Yu, H., Gillet, B., Ramonatxo, M., Israël, M. & la Porte, de, S. (2005) L-arginine improves dystrophic phenotype in mdx mice. *Neurobiology of disease*. 20 (1), 123–130.

Voit, T., Topaloglu, H., Straub, V., Muntoni, F., Deconinck, N., Campion, G., de Kimpe, S.J., Eagle, M., Guglieri, M., Hood, S., Liefaard, L., Lourbakos, A., Morgan, A., Nakielny, J., Quarcoo, N., Ricotti, V., Rolfe, K., Servais, L., Wardell, C., et al. (2014) Safety and efficacy of drisapersen for the treatment of Duchenne muscular dystrophy (DEMAND II): an exploratory, randomised, placebo-controlled phase 2 study. *Lancet neurology*. 13 (10), 987–996.

Wagner, S., Fueller, T., Hummel, V., Rieckmann, P. & Tonn, J.-C. (2003) Influence of VEGF-R2 inhibition on MMP secretion and motility of microvascular human cerebral endothelial cells (HCEC). *Journal of neuro-oncology*. 62 (3), 221–231.

Wallace, G.Q. & Mcnally, E.M. (2009) Mechanisms of muscle degeneration, regeneration, and repair in the muscular dystrophies. *Annual review of physiology*. 7137–57.

Wang, G.L., Jiang, B.H., Rue, E.A. & Semenza, G.L. (1995) Hypoxia-inducible factor 1 is a basic-helix-loop-helix-PAS heterodimer regulated by cellular O2 tension. *Proceedings of the National Academy of Sciences of the United States of America*. 92 (12), 5510–5514.

Wang, H.G., Pathan, N., Ethell, I.M., Krajewski, S., Yamaguchi, Y., Shibasaki, F., McKeon, F., Bobo, T., Franke, T.F. & Reed, J.C. (1999) Ca2+-induced apoptosis through calcineurin dephosphorylation of BAD. *Science*. 284 (5412), 339–343.

Wang, K., Kim, C., Bradfield, J., Guo, Y., Toskala, E., Otieno, F.G., Hou, C., Thomas, K., Cardinale, C., Lyon, G.J., Golhar, R. & Hakonarson, H. (2013) Whole-genome DNA/RNA sequencing identifies truncating mutations in RBCK1 in a novel Mendelian disease with neuromuscular and cardiac involvement. *Genome medicine*. 5 (7), 67.

Wang, Q., Xu, X., Li, J., Liu, J., Gu, H., Zhang, R., Chen, J., Kuang, Y., Fei, J., Jiang, C., Wang, P., Pei, D., Ding, S. & Xie, X. (2011) Lithium, an anti-psychotic drug, greatly enhances the generation of induced pluripotent stem cells. *Cell research*. 21 (10), 1424–1435.

Wang, Y., Wang, Y., Yang, D., Yu, X., Li, H., Lv, X., Lu, D. & Wang, H. (2015) β_1-adrenoceptor stimulation promotes LPS-induced cardiomyocyte apoptosis through activating PKA and enhancing CaMKII and IκBα phosphorylation. *Critical care (London, England)*. 19 (1), 76.

Wang, Y.X., Dumont, N.A. & Rudnicki, M.A. (2014) Muscle stem cells at a glance. *Journal of Cell Science*. 127 (21), 4543–4548.

Wang, Z., Kuhr, C.S., Allen, J.M., Blankinship, M., Gregorevic, P., Chamberlain, J.S., Tapscott, S.J. & Storb, R. (2007) Sustained AAV-mediated dystrophin expression in a canine model of Duchenne muscular dystrophy with a brief course of immunosuppression. *Molecular Therapy*. 15 (6), 1160–1166.

Watanabe, Y. & Buckingham, M. (2010) The formation of the embryonic mouse heart: heart fields and myocardial cell lineages. *Annals of the New York Academy of Sciences*. 118815–24.

Wehling-Henricks, M., Jordan, M.C., Gotoh, T., Grody, W.W., Roos, K.P. & Tidball, J.G. (2010) Arginine metabolism by macrophages promotes cardiac and muscle fibrosis in mdx muscular dystrophy. *PLoS ONE*. 5 (5), e10763.

Welch, E.M., Barton, E.R., Zhuo, J., Tomizawa, Y., Friesen, W.J., Trifillis, P., Paushkin, S., Patel, M., Trotta, C.R., Hwang, S., Wilde, R.G., Karp, G., Takasugi, J., Chen, G., Jones, S., Ren, H., Moon, Y.-C., Corson, D., Turpoff, A.A., et al. (2007) PTC124 targets genetic disorders caused by nonsense mutations. *Nature*. 447 (7140), 87–91.

Wen, G., Zhang, C., Chen, Q., Luong, L.A., Mustafa, A., Ye, S. & Xiao, Q. (2015) A Novel Role of Matrix Metalloproteinase-8 in Macrophage Differentiation and Polarization. *Journal of Biological Chemistry*. 290 (31), 19158–19172.

Westergren-Thorsson, G., Hernnäs, J., Särnstrand, B., Oldberg, A., Heinegård, D. & Malmström, A. (1993) Altered expression of small proteoglycans, collagen, and transforming growth factor-beta 1 in developing bleomycin-induced pulmonary fibrosis in rats. *Journal of Clinical Investigation*. 92 (2), 632–637.

White, S.M., Constantin, P.E. & Claycomb, W.C. (2004) Cardiac physiology at the cellular level: use of cultured HL-1 cardiomyocytes for studies of cardiac muscle cell structure and function. *American journal of physiology. Heart and circulatory physiology*. 286 (3), H823–9.

Whitehead, N.P., Yeung, E.W. & Allen, D.G. (2006) Muscle damage in mdx (dystrophic) mice: role of calcium and reactive oxygen species. *Clinical and experimental pharmacology & physiology*. 33 (7), 657–662.

Wilhelm, M., Schlegl, J., Hahne, H., Moghaddas Gholami, A., Lieberenz, M., Savitski, M.M., Ziegler, E., Butzmann, L., Gessulat, S., Marx, H., Mathieson, T., Lemeer, S., Schnatbaum, K., Reimer, U., Wenschuh, H., Mollenhauer, M., Slotta-Huspenina, J., Boese, J.-H., Bantscheff, M., et al. (2014) Mass-spectrometry-based draft of the human proteome. *Nature*. 509 (7502), 582–587.

Wilkins, B.J., de Windt, L.J., Bueno, O.F., Braz, J.C., Glascock, B.J., Kimball, T.F. & Molkentin, J.D. (2002) Targeted disruption of NFATc3, but not NFATc4, reveals an intrinsic defect in calcineurin-mediated cardiac hypertrophic growth. *Molecular and cellular biology*. 22 (21), 7603–7613.

Williams, I.A. & Allen, D.G. (2007) Intracellular calcium handling in ventricular myocytes from mdx mice. *American journal of physiology. Heart and circulatory physiology*. 292 (2), H846–55.

Wilschanski, M., Miller, L.L., Shoseyov, D., Blau, H., Rivlin, J., Aviram, M., Cohen, M., Armoni, S., Yaakov, Y., Pugatsch, T., Pugatch, T., Cohen-Cymberknoh, M., Miller, N.L., Reha, A., Northcutt, V.J., Hirawat, S., Donnelly, K., Elfring, G.L., Ajayi, T., et al. (2011) Chronic ataluren (PTC124) treatment of nonsense mutation cystic fibrosis. *The European respiratory journal : official journal of the European Society for Clinical Respiratory Physiology*. 38 (1), 59–69.

Witting, N., Kruuse, C., Nyhuus, B., Prahm, K.P., Citirak, G., Lundgaard, S.J., Huth, von, S., Vejlstrup, N., Lindberg, U., Krag, T.O. & Vissing, J. (2014) Effect of sildenafil on skeletal and cardiac muscle in Becker muscular dystrophy. *Annals of Neurology*. 76 (4), 550–557.

Wood, C.L., Cheetham, T.D., Guglieri, M., Bushby, K., Owen, C., Johnstone, H. & Straub, V. (2015) Testosterone Treatment of Pubertal Delay in Duchenne Muscular Dystrophy. *Neuropediatrics*. (EFirst).

Wozniak, A.C. & Anderson, J.E. (2007) Nitric oxide-dependence of satellite stem cell activation and quiescence on normal skeletal muscle fibers. *Developmental Dynamics*. 236 (1), 240–250.

Wu, B., Cloer, C., Lu, P., Milazi, S., Shaban, M., Shah, S.N., Marston-Poe, L., Moulton, H.M. & Lu, Q.L. (2014) Exon skipping restores dystrophin expression, but fails to prevent disease progression in later stage dystrophic dko mice. *Gene therapy*.

Wu, B., Lu, P., Benrashid, E., Malik, S., Ashar, J., Doran, T.J. & Lu, Q.L. (2010) Dose-dependent restoration of dystrophin expression in cardiac muscle of dystrophic mice by systemically delivered morpholino. *Gene therapy*. 17 (1), 132–140.

Xin, M., Olson, E.N. & Bassel-Duby, R. (2013) Mending broken hearts: cardiac development as a basis for adult heart regeneration and repair. *Nature Reviews Molecular Cell Biology*. 14 (8), 529–541.

Yamaguchi, N., Chakraborty, A., Pasek, D.A., Molkentin, J.D. & Meissner, G. (2011) Dysfunctional ryanodine receptor and cardiac hypertrophy: role of signaling molecules. *AJP: Heart and Circulatory Physiology*. 300 (6), H2187–95.

Yan, W., Wu, F., Morser, J. & Wu, Q. (2000) Corin, a transmembrane cardiac serine protease, acts as a pro-atrial natriuretic peptide-converting enzyme. *Proceedings of the National Academy of Sciences of the United States of America*. 97 (15), 8525–8529.

Yang, Y., Del Re, D.P., Nakano, N., Sciarretta, S., Zhai, P., Park, J., Sayed, D., Shirakabe, A., Matsushima, S., Park, Y., Tian, B., Abdellatif, M. & Sadoshima, J. (2015) miR-206 Mediates YAP-Induced Cardiac Hypertrophy and Survival. *Circulation Research*. 117 (10), 891–904.

Yang, Z., Kyriakides, T.R. & Bornstein, P. (2000) Matricellular proteins as modulators of cell-matrix interactions: adhesive defect in thrombospondin 2-null fibroblasts is a consequence of increased levels of matrix metalloproteinase-2. *Molecular biology of the cell*. 11 (10), 3353–3364.

Yeung, D., Zablocki, K., Lien, C.-F., Jiang, T., Arkle, S., Brutkowski, W., Brown, J., Lochmüller, H., Simon, J., Barnard, E.A. & Górecki, D.C. (2006) Increased susceptibility to ATP via alteration of P2X receptor function in dystrophic mdx mouse muscle cells. *The FASEB Journal*. 20 (6), 610–620.

Yin, H., Price, F. & Rudnicki, M.A. (2013) Satellite cells and the muscle stem cell niche. *Physiological reviews*. 93 (1), 23–67.

Yiu, E.M. & Kornberg, A.J. (2015) Duchenne muscular dystrophy. *Journal of paediatrics and child health*.

Ylä-Herttuala, S. (2012) Endgame: glybera finally recommended for approval as the first gene therapy drug in the European union. *Molecular Therapy*. 20 (10), 1831–1832.

Young, C.N., Sinadinos, A., Lefebvre, A., Chan, P., Arkle, S., Vaudry, D. & Górecki, D.C. (2015) A novel mechanism of autophagic cell death in dystrophic muscle regulated by P2RX7 receptor large-pore formation and HSP90. *Autophagy*. 11 (1), 113–130.

Young, C.N.J., Brutkowski, W., Lien, C.-F., Arkle, S., Lochmüller, H., Zabłocki, K. & Górecki, D.C. (2012) P2X7 purinoceptor alterations in dystrophic mdx mouse muscles: relationship to pathology and potential target for treatment. *Journal of cellular and molecular medicine*. 16 (5), 1026–1037.

Yu, C.-Y., Yuan, Z., Cao, Z., Wang, B., Qiao, C., Li, J. & Xiao, X. (2009) A muscle-targeting peptide displayed on AAV2 improves muscle tropism on systemic delivery. *Gene therapy*. 16 (8), 953–962.

Yue, Y., Pan, X., Hakim, C.H., Kodippili, K., Zhang, K., Shin, J.-H., Yang, H.T., McDonald, T. & Duan, D. (2015) Safe and bodywide muscle transduction in young adult Duchenne muscular dystrophy dogs with adeno-associated virus. *Human Molecular Genetics*.

Zammit, P.S., Partridge, T.A. & Yablonka-Reuveni, Z. (2006) The skeletal muscle satellite cell: the stem cell that came in from the cold. *The journal of histochemistry and cytochemistry : official journal of the Histochemistry Society*. 54 (11), 1177–1191.

Zeng, J., Liu, S., Zhao, Y., Tan, X., Aljohi, H.A., Liu, W. & Hu, S. (2015) Identification and analysis of house-keeping and tissue-specific genes based on RNA-seq data sets across 15 mouse tissues. *Gene*.

Zhang, T., Lu, X., Li, J., Chidiac, P., Sims, S.M. & Feng, Q. (2012) Inhibition of Na/K-ATPase promotes myocardial tumor necrosis factor-alpha protein expression and cardiac dysfunction via calcium/mTOR signaling in endotoxemia. *Basic research in cardiology*. 107 (2), 254–12.

Zhang, X., Azhar, G., Chai, J., Sheridan, P., Nagano, K., Brown, T., Yang, J., Khrapko, K., Borras, A.M., Lawitts, J., Misra, R.P. & Wei, J.Y. (2001) Cardiomyopathy in transgenic mice with cardiac-specific overexpression of serum response factor. *American journal of physiology. Heart and circulatory physiology*. 280 (4), H1782–92.

Zhao, S., Fung-Leung, W.-P., Bittner, A., Ngo, K. & Liu, X. (2014) Comparison of RNA-Seq and microarray in transcriptome profiling of activated T cells. Shu-Dong Zhang (ed.). *PLoS ONE*. 9 (1), e78644.

Zhao, Y., Xu, Y., Zhang, J. & Ji, T. (2014) Cardioprotective effect of carvedilol: inhibition of apoptosis in H9c2 cardiomyocytes via the TLR4/NF-κB pathway following ischemia/reperfusion injury. *Experimental and therapeutic medicine*. 8 (4), 1092–1096.

Zincarelli, C., Soltys, S., Rengo, G. & Rabinowitz, J.E. (2008) Analysis of AAV serotypes 1-9 mediated gene expression and tropism in mice after systemic injection. *Molecular Therapy*. 16 (6), 1073–1080.

Zois, N.E., Bartels, E.D., Hunter, I., Kousholt, B.S., Olsen, L.H. & Goetze, J.P. (2014) Natriuretic peptides in cardiometabolic regulation and disease. *Nature reviews. Cardiology*. 11 (7), 403–412.

Zou, Y., Takano, H., Akazawa, H., Nagai, T., Mizukami, M. & Komuro, I. (2002) Molecular and cellular mechanisms of mechanical stress-induced cardiac hypertrophy. *Endocrine journal*. 49 (1), 1–13.